Development of an efficient method for simulating fixed-bed adsorption dynamics using Ideal Adsorbed Solution Theory

Dissertation

zur Erlangung des akademischen Grades

Doktoringenieur

(Dr.-Ing.)

von M.Sc. Héctor Octavio Rubiera Landa

geb. am 04.01.1977 in Mexiko-Stadt, Mexiko

genehmigt durch die Fakultät für Verfahrens- und Systemtechnik

der Otto-von-Guericke-Universität Magdeburg

Promotionskommission:

Prof. Dr.-Ing. Evangelos Tsotsas (Vorsitz)

Prof. Dr. ir. Joeri Denayer (Gutachter)

Prof. Dr.-Ing. Achim Kienle (Gutachter)

Prof. Dr.-Ing. Andreas Seidel-Morgenstern (Mitglied)

eingereicht am: 08.01.2016

Promotionskolloquium am: 13.05.2016

Declaration of Authorship

I, Héctor Octavio RUBIERA LANDA, MSc., declare herewith that this dissertation,

'' Development of an efficient method for simulating fixed-bed adsorption dynamics using Ideal Adsorbed Solution Theory''

is my own. I confirm that:

- This doctoral dissertation was written entirely while in candidature for the degree of Doctor of Engineering (*Dr.-Ing.* [*Doktoringenieur*]) at Otto-von-Guericke-Universität Magdeburg (Magdeburg, Saxony Anhalt, Federal Republic of Germany) and concurrent tenure as Research Associate for the Physicochemical Foundations Research Group (*PCG*) at Max Planck Institute for Dynamics of Complex Technical Systems (Magdeburg, Saxony Anhalt, Federal Republic of Germany).

- Where I have consulted the published work of others, this is always clearly attributed.

- Where I have quoted from the work of others, the source is always given. With the exception of such quotations, this dissertation is entirely my own work.

- I have properly acknowledged all sources of technical advice and support.

- Where the dissertation is based on work done by myself jointly with others, I have stated exactly what was done by others and what I have contributed myself.

Magdeburg, January 8 $^{\text{th}}$, 2016

Héctor Octavio Rubiera Landa

Master of Science, Chemical & Process Engineering,
Otto-von-Guericke-Universität Magdeburg
Chemical & Systems Engineer (*Ingeniero Químico y de Sistemas*)
I.T.E.S.M., Monterrey, Nuevo León, México

Schriftliche Erklärung

Ich erkläre hiermit, dass ich die vorliegende Arbeit ohne unzulässige Hilfe Dritter und ohne Benutzung anderer als der angegebenen Hilfsmittel angefertigt habe. Die aus fremden Quellen direkt oder indirekt übernommenen Gedanken sind als solche kenntlich gemacht.

Insbesondere habe ich nicht die Hilfe einer kommerziellen Promotionsberatung in Anspruch genommen. Dritte haben von mir weder unmittelbar noch mittelbar geldwerte Leistungen für Arbeiten erhalten, die im Zusammenhang mit dem Inhalt der vorgelegten Dissertation stehen.

Die Arbeit wurde bisher weder im Inland noch im Ausland in gleicher oder ähnlicher Form als Dissertation eingereicht und ist als Ganzes auch noch nicht veröffentlicht.

Magdeburg, 08.01.2016

Héctor Octavio Rubiera Landa

Master of Science, Chemical & Process Engineering
Otto-von-Guericke-Universität Magdeburg
Chemical & Systems Engineer (Ingeniero Químico y de Sistemas)
I.T.E.S.M., Monterrey, Nuevo León, México

Abstract

Development of an efficient method for simulating fixed-bed adsorption dynamics using Ideal Adsorbed Solution Theory

by Héctor Octavio Rubiera Landa, MSc.

A fundamental task to *design, optimize & operate* adsorption-based separation processes consists of correctly understanding and describing the physico-chemical principles governing them. Ongoing research efforts are directed along this line, as innovative adsorptive materials and applications are discovered and state-of-the-art industrial processes are developed and applied to cope with technically demanding *separation & purification* operations of ever-increasing complexity. In this regard, Ideal Adsorbed Solution Theory (IAST) provides a *simple*—albeit *powerful*—alternative to describe multicomponent adsorption equilibria from minimal input information. The principal outcome of this research work is the *development, demonstration & implementation* of a solution approach to solve the equations of IAST, possessing several advantageous features. Theoretical and practical application of this approach are demonstrated by numerous calculation examples. A detailed *proof of concept* on a high-performance liquid chromatography experimental system is provided. Necessary details to *embed* IAST equilibrium calculations into dynamic simulations of fixed-bed adsorbers are given in a practical, simple & useful manner.

Zusammenfassung   *Die Auslegung und Optimierung von adsorptiven Trennprozessen erfordert Kenntnisse der zugrundeliegenden physikalisch-chemischen Grundlagen. Die Theorie der idealen adsorbierten Lösung (IAS-Theorie)* ['Ideal Adsorbed Solution Theory'] *bietet eine einfache Möglichkeit, aus Einzelstoffgleichgewichten die konkurrierende Mehrkomponentenadsorption zu berechnen. Als Hauptergebnis dieser Dissertation wird ein innovativer Lösungsansatz für die IAS-Theorie-Gleichungen abgeleitet, validiert und verwendet. Zahlreiche Anwendungsbeispiele illustrieren sowohl theoretische als auch praktische Aspekten. Anhand eines experimentell untersuchten Systems werden die entwickelten Berechnungsalgorithmen getestet und validiert. Diese Arbeit gibt weiterhin Hinweise, die die Anwendung des obengennanten Gleichgewichtsmodells bei der Berechnung von Adsorbern unterstützen.*

Sinopsis *La comprensión correcta de los fenómenos fisicoquímicos involucrados en los procesos de adsorción permiten utilizárseles para diseñar, optimizar y operar sistemas de separación basados en los mismos. Los esfuerzos de investigación en esta área van encaminados en esta dirección, ya que actualmente se encuentran en desarrollo materiales y procesos novedosos, capaces de atender los requerimientos de sistemas de separación y purificación de cada vez mayor grado de dificultad y complejidad. El resultado principal de este trabajo de investigación consiste en desarrollar, demostrar e implementar de manera práctica un método eficaz y simple para resolver las ecuaciones de la llamada "Teoría de la Solución Ideal Adsorbida" [del inglés: 'Ideal Adsorbed Solution Theory'].* *La aplicación de este novedoso método, así como sus propiedades matemáticas, se ilustra a través de ejemplos detallados. El concepto propuesto es aplicado en su totalidad y evaluado por medio de un sistema experimental de la cromatografía líquida de alta resolución [del inglés: 'High-Performance Liquid Chromatography']. Esta disertación contribuye adicionalmente a presentar los elementos necesarios para aplicar la Teoría de la Solución Ideal Adsorbida en modelos sencillos de columnas de adsorción de lecho empacado, utilizando el método numérico y algoritmos desarrollados.*

Acknowledgements

Contents

List of Figures

List of Tables

Abbreviations

2D	2-Dimensional
AI	Adsorption Isotherm
BET	Brunauer-Emmett-Teller
BTC	Breakthrough Curve
CAS	Computer Algebra System
CCS	Carbon Capture & Storage
CFL	Courant-Friedrichs-Lewy condition
CSP	Chiral Stationary Phase
DBC	Dynamic Breakthrough Curve
D-R	Dubinin-Radushkevich adsorption isotherm
ECP	Elution by Characteristic Point
EOS	Equation Of State
EDM1D	Equilibrium-Dispersive Model in one Dimension
FA	Frontal Analysis
FD	Finite Differences
FVM	Finite Volume Method
GC	Gas Chromatography
GRM	General Rate Model
HETP	Height Equivalent to a Theoretical Plate
HPLC	High-Performance Liquid Chromatography
HTS	High-Throughput Screening
IAST	Ideal Adsorbed Solution Theory
IUPAC	International Union of Pure and Applied Chemistry
IVP	Initial Value Problem
LLE	Liquid-Liquid Equilibria
MSDS	Material Safety Data Sheet
MOC	Method Of Characteristics

MOF	Metal-Organic Framework
MOL	Method Of Lines
MWD	Multiple Wavelength Detector
NTP	Number of Theoretical Plates
ODE	Ordinary Differential Equation
PDE	Partial Differential Equation
PGC	Porous Graphitic Carbon
PSE	Problem Solving Environment
RAST	Real Adsorbed Solution Theory
RI	Refractive Index
RK	Runge-Kutta
RPLC	Reversed-Phase Liquid Chromatography
SMB	Simulated Moving Bed
SSP	Strong Stability Preserving
TMB	True Moving Bed
TVD	Total Variation Diminishing
UDS	Upwind Discretization Scheme
UV	Ultraviolet
VLE	Vapor-Liquid Equilibria
VST	Vacancy Solution Theory

Notation

a	advection velocity [Eq. (8.1), p. 102]
a_i	parameter, component i, several isotherm models [Table 2.2, p. 17]
a_i	activity of component i, $\left[\, \text{mol/m}^3 \,\right]$
a_i^0	surface area occupied by component i in ideal mixture [Eq. (3.5), p. 33]
a_tot	total area occupied by *all* adsorbates in ideal mixture [Eq. (3.5), p. 33]
A	parameter in van Deemter eqn. [Eq. (A10.1), Appendix A10.2, p. 181]
A^a	Helmholtz' free energy of adsorbed phase, a, $\left[\, \text{J} \,\right]$ [Eq. (2.25), p. 28]
A_c	cross-sectional column area, $\left[\, \text{m}^2 \,\right]$ [Eq. (6.7)]
$\mathcal{A}$	adsorbent specific surface area, $\left[\, \text{m}^2/\text{m}^3_\text{ads.} \,\right]$ or $\left[\, \text{m}^2/\text{kg}_\text{ads.} \,\right]$
$\mathfrak{A}$	surface area, $\left[\, \text{m}^2 \,\right]$ [Eq. (2.16a), p. 24]
b	isotherm parameter, several models [Table 2.2, p. 17]
b_L, b_S	BET isotherm parameters [Eq. (2.3i), Table 2.2, p. 17]
B	D-R isotherm parameter [Table 2.2, p. 17]
B	parameter in van Deemter eqn. [Eq. (A10.1), Appendix A10.2, p. 181]
c_i	fluid phase concentration, component i, $\left[\, \text{mol/m}^3 \,\right]$ [Eq. (2.4), p. 17]
c_i^0	fictitious fluid phase concentration, component i, $\left[\, \text{mol/m}^3 \,\right]$
$c_i^\star$	conc. at reference state, component i, $\left[\, \text{mol/m}^3 \,\right]$ [Eq. (3.1), p. 32]
c_in	inlet concentration, $\left[\, \text{mol/m}^3 \,\right]$
$c_{i,\text{inj.}}$	injected concentration, component i, $\left[\, \text{mol/m}^3 \,\right]$
c_tot	total fluid phase concentration, $\left[\, \text{mol/m}^3 \,\right]$
C	arbitrary integration constant [Eq. (9.9b), p. 131
$\mathfrak{C}$	no. of components at equilibrium, in *phase rule* [Eq. (2.22), p. 27]
d	auxiliary notation [Eq. (7.24g), p. 98]
d_0, d_1, d_2, d_3	parameters to fit to empirical functions [Eq. (9.9a), p. 131]
d_c	column diameter, $\left[\, \text{m} \,\right]$, $\left[\, \text{mm} \,\right]$ [Eq. (6.7), p. 81]
d_p	particle diameter, $\left[\, \text{m} \,\right]$, $\left[\, \mu\text{m} \,\right]$ [Assumption VI, Table 6.1, p. 80]
D	parameter in van Deemter eqn. [Eq. (A10.1), Appendix A10.2, p. 181]

D_{app}	apparent dispersion coefficient matrix, $[\mathsf{m^2/s}]$ [Eq. (6.4a), p. 79]
D_{ax}	axial dispersion coefficient, $[\mathsf{m^2/s}]$ [Table A8, Appendix A10, p. 181]
D_L	longitudinal dispersion coefficient, $[\mathsf{m^2/s}]$ [Eq. (6.1), p. 79]
e^T	row vector of ones, size $1 \times N$, [Table 4.1, p. 53]
$e_{\mathrm{c}}^{\mathsf{abs.}}$	*absolute* computational error [Eq. (5.3), p. 67]
$e_{\mathrm{c}}^{\mathsf{rel.}}$	*relative* computational error [Eq. (5.3), p. 67]
eps	*machine epsilon* of employed workstation [Section 5.3, p. 66]
f_i	fugacity, component i [Table 2.2, p. 17]
$\hat{f}_{j+\frac{1}{2}}$	numerical flux at cell boundary $\delta\Omega_{j+\frac{1}{2}}$ [Eq. (7.8), p. 89]
f^T	row vector [Table 4.1, p. 53]
$\mathfrak{f}$	flux function [Eq. (6.15), p. 83]
$\mathfrak{F}$	degrees of freedom specifying intensive state of a phase [Eq. (2.22), p. 27]
$\hat{g}(w)_{j+\frac{1}{2}}$	numerical flux (diffusion) at cell boundary $\delta\Omega_{j+\frac{1}{2}}$ [Eq. (7.18), p. 94]
G^a	Gibbs' free energy of adsorbed phase, a, $[\mathsf{J}]$ [Eq. (2.16d), p. 25]
h_1, h_2	scalars used to compute $[\mathcal{I} + \phi\mathcal{J}]^{-1}$ [Eqs. (7.23c) & (7.23d), p. 96]
$h_{\mathsf{plate},i}$	plate height, component i, $[\mathsf{m}]$ [Section 6.4, p. 82]
$\mathfrak{h}_i$	Henry coefficient, comp. i, $[\mathsf{mol/m^3}_{\mathsf{ads.}} \div \mathsf{mol/m^3}_{\mathsf{sln.}}]$ [Eq. (2.5), p. 18]
$H = H(\lambda)$	matrix used to compute $[\mathcal{I} + \phi\mathcal{J}]^{-1}$ [Eq. (7.23b), Table 7.1, p. 96]
j_{mn}	elements of Jacobian $\mathcal{J}$, $m = 1, \ldots, N$, $n = 1, \ldots, N$ [Fig. 4.3, p. 52]
J	total number of grid cells in FV method [Eq. (7.4), p. 88]
$\mathcal{J}(q(c))$	Jacobian matrix [Eq. (4.9), p. 50]
$\mathcal{I}$	identity matrix, size $N \times N$ [Eq. (4.11), p. 51]
$\mathcal{I} + J_2$	*object* used to compute Jacobian matrix, $\mathcal{J}(q(c))$ [Eq. (4.9), p. 50]
k	$1, 2, \cdots$ [Eq. (3.16f), p. 38]
$k_{\mathsf{C10}}, k_{\mathsf{C11}}$	calib. factors for decylbenzene & undecylbenzene [Section 9.4 p. 123]
$[k], [\ell]$	iteration counters: $1, 2, \cdots$ [Algorithms 3.1 &, p. 41 & 3.2, p. 42]
$K_2 = K_2(\lambda)$	matrix used to obtain $[\mathcal{I} + \phi\mathcal{J}]^{-1}$ [Eq. (7.23e), Table 7.1, p. 96]
$\mathcal{K} = \mathcal{K}(\lambda)$	equivalent of $[\mathcal{I} + \phi\mathcal{J}]^{-1}$ under IAST frame [Eq. (7.24c), p. 97]
$L(\cdot)$	r.h.s. function in SSP-RK integration method [Eq. (7.15), p. 93]
L_{c}	column length, $[\mathsf{m}]$ [Eq. (6.9), p. 81]
m	$1, 2, \ldots$ [Eq. (5.1), p. 62]
m^a	mass of porous solid adsorbent, $[\mathsf{kg}]$ [Fig. 2.4, p. 26]
n_i	moles, component i, $[\mathsf{mol}]$ [Eq. (2.15), p. 24]
n_i^a	moles of component i in adsorbed phase, a, $[\mathsf{mol}]$ [Eq. (2.16a), p. 24]
$n_i^{\mathfrak{c}}$	invariant molar amount of i, $[\mathsf{mol}]$ [Eq. (A4.7), p. 169]
n_i^m	invariant molar amount of i, $[\mathsf{mol}]$ [Eq. (2.27), p. 29]

$\mathfrak{n}$	degree of a *homogeneous* function [Eq. (A3.1), Appendix A3, p. 166]
N	number of adsorbable components [Eq. (2.4), p. 17]
$N_{\mathsf{fr.}}$	number of collected fractions [Table 10.1, p. 146]
$N_{\mathsf{plate},i}$	column plate number, component i [Eq. (6.9), p. 81]
$\mathfrak{P}$	number of phases at equilibrium of studied system [Eq. (2.22), p. 27]
p	pressure, $[\,\mathsf{Pa}\,]$ [Eq. (2.15), p. 24]
p_i	partial pressure, component i, $[\,\mathsf{Pa}\,]$ [Table 2.2, p. 2.2]
q_i	adsorbed phase concentration, component i, $[\,\mathsf{mol/m^3}\,]$ [Eq. (2.1), p. 14]
q_i^0	fictitious concentration of adsorbate i, $[\,\mathsf{mol/m^3}\,]$ [Eq. (3.11), p. 34]
q_i^{sat}	saturation capacity, component i, $[\,\mathsf{mol/m^3}\,]$ [Table 2.2, p. 17]
q_{tot}	total adsorbed phase concentration, $[\,\mathsf{mol/m^3}\,]$ [Eq. (3.11), p. 34]
Q	volumetric flow rate, $[\,\mathsf{m^3/s}\,]$ [Eq. (6.7), p. 81]
$\overline{Q}$	average volumetric flow rate, $[\,\mathsf{m^3/s}\,]$ [Eq. (9.6b), p. (9.6b)]
$r_{j+\frac{1}{2}}$	ratio of differences of consecutive flux function values [Eq. (7.10c)]
s	integration variable [Eq. (3.9), p. 34]
S	entropy, $[\,\mathsf{J/K}\,]$ [Eq. (2.15), p. 24]
S^a	entropy of adsorbed phase, a, $[\,\mathsf{J/K}\,]$ [Eq. (2.16a), p. 24]
S_j	stencil of grid cell j [Eq. (7.7), p. 89]
t	time, $[\,\mathsf{s}\,]$ [Eq. (6.1), p. 79]
t_0	*hold-up* time, $[\,\mathsf{s}\,]$ [Eq. (9.3), p. 124]
t_b	breakthrough time, $[\,\mathsf{s}\,]$ [Eq. (9.8b), p. 130]
t_d	process or equipment dead time, $[\,\mathsf{s}\,]$ [Section 9.4, p. 123]
t_p	peak time, $[\,\mathsf{s}\,]$ [Eq. (9.10), p. 138]
$t_{\mathsf{R},i}$	retention time, component i [Eq. (9.10), p. 138]
T	temperature, $[\,\mathsf{K}\,]$ [Eq. (3.9), p. 34]
u	mobile phase velocity, $[\,\mathsf{m/s}\,]$ [Eq. (6.7), p. 81]
$\mathfrak{u}$	substitution variable for integration [Appendix A6, p. 172]
U	internal energy, $[\,\mathsf{J}\,]$ [Eq. (2.15), p. 24]
$v(c)_j^n$	conserved variable at grid point (j,n) of FD scheme [Eq. (7.1), p. 87]
v_i	generating function, component i [Eq. (4.13h), p. 55]
$\bar{v}_i$	partial molar volume, component i, $[\,\mathsf{m^3/mol}\,]$ [Appendix A4, p. 168]
$\bar{v}_{\mathsf{solv.}}$	partial molar volume of solvent, $[\,\mathsf{m^3/mol}\,,]$ [Appendix A4, p. 168]
V	volume, $[\,\mathsf{m^3}\,]$ [Eq. (2.15), p. 24]
V^a	volume of porous solid adsorbent, $[\,\mathsf{m^3}\,]$ [Eq. (2.16d), p. 25]
V_{c}	column volume, $[\,\mathsf{m^3}\,]$ [Eq. (9.3), p. 124]
$V_{\mathsf{inj.}}$	injected volume, $[\,\mathsf{m^3}\,]$ [Eq. (9.6), p. 126]

$V_{\text{sln.}}$	volume of fluid solution, $[\,\mathsf{m^3}\,]$ [Appendix A4, p. 168]
w	arbitrary conserved variable [Eq. (6.14), p. 83]
w_k	*scaled* reciprocal ads. phase concentration, component k [Table 4.1, p. 53]
W	matrix used in the calculation of $[\,\mathcal{I} + \phi\mathcal{J}\,]^{-1}$ [Table 4.1, p. 53]
$\tilde{W}$	reciprocal of single component ads. phase concentration [Proof 4.3, p. 53]
x_i	mole fraction of species i in ads. phase (Eq. (2.9), [Eq. (3.4),p. 32]
X_i	auxiliary notation for c_i^0 [Proof 4.3, p. 53]
y_i	mole fraction of species i in the fluid phase [Eq. (2.9), p. 19]
z	axial coordinate, $[\,\mathsf{m}\,]$ [Eq. (6.1), p. 79]
z_i	auxiliary notation [Proof 4.3, p. 53]
$\mathfrak{Z}$	N-dimensional *hypersurface* [Eq. (4.7), p. 48]

Greek characters

α_{ij}	selectivity of component i w.r.t. component j [Eq. (2.10), p. 19]
β	parameter in D-R isotherm [Eq. (2.3j), Table 2.2, p. 17]
γ_i	activity coefficient, component i [Eq. (3.3), p. 32]
γ_0, γ	surface tension (*clean*), surface tension, $[\,\mathsf{N/m}\,]$ [Eq. (2.17), p. 25]
δ_k	object used in Proof 7.7 [Eq. (7.24e), p. 97]
Δ	object used in Proof 7.7 [Eq. (7.24e), p. 97]
Δz	size of an equidistant grid cell, j, $[\,\mathsf{m}\,]$ [Fig. 7.2, p 88]
ϵ	total porosity, $[\,-\,]$ [Eq. (6.1), p. 79]
ϵ_{e}	external porosity—i.e., bed *void fraction* [Eq. (6.6), p. 81]
ϵ_{p}	intraparticle porosity [Eq. (6.6), p. 81]
ε_d	constant to avoid divisions by zero, $\varepsilon_d \lesssim 10^{-10}$ [Eq. (7.10c), p. 91]
$\varepsilon_{\text{Tol.}}$	stopping criterium for iterations [Algorithms 3.1 & 3.2, pp. 41, 42]
ζ	integration variable [Eq. (3.16j), p. 38]
ζ_i	variable to obtain Π_i in Redlich-Peterson isotherm [Eq. (5.1), p. 62]
η	parameter in O'Brien & Myers isotherm [Eq. (2.3f), p. 17]
θ	ratio of adsorbed phase concentration to adsorbed phase saturation concentration—i.e., *coverage*—in Tóth isotherm [Eq. (3.16f), p. 38]
κ	parameter in num. interpolation formulæ [Eq. (7.8), p. 89]
λ	arbitrary parameter, Euler's theorem [Eq. (A3.1), Appendix A3, p. 166]
λ	reciprocal of the phase ratio, ϕ [Eq. (7.24a), p. 96]
λ_{UV}	wavelength in UV range of spectrum, $[\,\mathsf{nm}\,]$ [Eq. (9.5), p. 125]
μ_i	chemical potential, component i, $[\,\mathsf{J/mol}\,]$ [Eq. (2.15), p. 24]

μ_i^a	chemical potential of i in ads. phase, $[\,\mathsf{J/mol}\,]$ [Eq. (2.16a), p. 24]
$\mu_i^{\ell,\star}$	chemical potential at standard state, $[\,\mathsf{J/mol}\,]$ [Eq. (3.1), p. 32]
ν	Courant number [Eq. (7.2), p. 87]
ν_i	parameter for several isotherm models, component i [Table 2.2, p. 17]
ξ	integration variable [Eq. (4.6), p. 47]
π	spreading pressure, surface potential, $[\,\mathsf{N/m}\,]$ [Eq. (2.16d), p. 25]
Π_i	*reduced* spreading pressure, component i, $\big[\,\mathsf{mol/m^3_{ads.}}\,\big]$ or $\big[\,\mathsf{mol/kg_{\,ads.}}\,\big]$ [Eq. (3.9), p. 34]
$\Pi^{[k]}$	*reduced* potential, iteration k [Algorithms 3.1 & 3.2, pp. 41, 42]
σ	*scalar* used to compute $\mathcal{J}(q(c))$ [Table 4.1, p. 53]
ϕ	phase ratio, $[\,-\,]$ [Eq. (6.5), p 81]
$\phi(r)$	flux limiter monitor function [Eq. (7.10a), p. 90]
ψ_k	function that expresses dependency of c_k^0 w.r.t. c_1^0 [Eq. (4.2), p. 46]
$\Psi(\xi)$	solution along *orbit* Ψ at ξ_f for given $c = (c_1, \ldots, c_N)^T$ [Fig. 4.1, p. 48]
Ω	spatial domain along coordinate z [Eq. (7.4), p. 88]
Ω_h	discretized spatial domain [Eq. (7.4), p. 88]
Ω_j	cell, spatial partition j with $j = 1, \ldots, J$ [Eq. (7.4), p. 88]

Subscripts

ads.	of adsorbent; pertaining to adsorbent
c	column
feed	of feed; pertaining to feed state
i	component i
inj.	injected; injection
j	component j
k	component k
m	component m
n	component n
sln.	solution; liquid solution
solv.	solvent
tot	total

Superscripts

I, II, ...   numbers of co-existing, distinct, homogeneous phases at equilibrium

a adsorbed phase; adsorbed phase property

abs.   *absolute*

$[k]$ iteration index k, $k = 1, 2, \ldots$ [Eq. (3.18a), p. 41]

ℓ fluid phase property

m denotes a measured, *invariant* property of a solute [Eq. (2.26a), p. 28]

$\mathcal{P}$ total number of phases co-existing at equilibrium [Eq. (2.23), p. 28]

rel.   *relative*

sat   saturated; value at saturation

$(\star)$ particular value, particular solution [Section 4.1, p. 46]

$*$ reference state [Section 3.1, p. 32]

Physical constants, miscellaneous characters & symbols

C8, C10, C11, C12, C13   octyl-, decyl-, undecyl-, dodecyl-, tridecylbenzene

gradPumpSys   injection in HPLC equipment using the dual pump system [Section 9.4, p. 123]

injLoopSys   injection in HPLC equipment using built-in injection loop & auto-sampler system [Section 9.4, p. 123]

Pe_k Péclet number of component k in EDM1D, [Eq. (6.10), p. 81]

$\mathfrak{R}$ universal gas constant, $8.314 \left[\dfrac{\mathsf{J}}{\mathsf{mol}\,\mathsf{K}} \right]$ [Eq. (3.9), p. 34]

$_2\mathsf{F}_1\big[(\cdot,\cdot);\cdot;\cdot\big]$ hypergeometric function

Part I

Adsorption equilibria

Chapter 1

Introduction & scope of work

"Publication is a self-invasion of privacy."

– Marshall McLuhan

1.1 An important industrial technology: adsorption-based separation processes

A DSORPTION is a physicochemical phenomenon of large importance and wide field of application in the transformation industries. In its most simple form, it consists of contacting a homogeneous fluid mixture with a porous material, traditionally possessing large surface area and specific chemical characteristics—i.e., functionalities—allowing a specific physico-chemical interaction to take place, which can be advantageously exploited. The origin and type of surface interactions determine if the process is *reversible*, i.e., physisorption, or *irreversible*, i.e., chemisorption. The focus of this work is the first type, where adsorbed molecules are not chemically modified—i.e., they have a weak, *van der Waals* interaction with the adsorbing material; rather, it is applied to selectively isolate and recover selected compounds from a fluid mixture—i.e., separation operations. Principles and mechanisms behind adsorption-based processes for *separation & purification* are complex, and up to now—astonishingly—only partially understood. Scientists and engineers make a continuing effort to investigate adsorption phenomena, which can naturally lead to optimal design of relevant industrial-scale process operations. These operations can roughly be grouped into three comprehensive categories [1–4]:

3

1. ADSORPTION OPERATIONS;

2. CHROMATOGRAPHY &

3. ION-EXCHANGE OPERATIONS.

Engineering thermodynamics plays a central role to understand, explain and later design these operations [3, 5]. A general overview and description of adsorption-based separation processes can be consulted in [2, 4, 6–12] and numerous references listed therein. An important separation process where adsorption principles need to be understood and applied is PREPARATIVE CHROMATOGRAPHY [4, 13–17]. This motivates the following statement of general character:

> ☆ *The goal of separation science is to isolate target compounds from*
> *homogeneous mixtures, in quantities that are attractive and with*
> *a pre-determined quality specification.*

Adsorption-based separation processes can fulfill this goal for a large number of homogeneous mixtures found in different fluid states of matter: GAS, LIQUID or SUPERCRITICAL FLUID [2–4]. They become an attractive, economically-feasible alternative to conventional, more energy-intensive separation processes such as distillation [3, 4]. Due to their ability to achieve high *separation resolution*, by selectively interacting with the components of a mixture under relatively mild conditions, this kind of processes may be in some cases the only technologically viable alternative to handle particularly challenging separation tasks. An important feature of most adsorption-based separation operations is—in contrast to other separation techniques—their *dynamic character*. This feature poses an additional challenge to describe and understand these processes in order to design and operate them in an economically attractive way.

Fluid mixtures are typically placed in contact with a porous solid phase of large specific surface area or adsorptive capacity*, thus providing the necessary physicochemical interaction between the solid and target substances of interest in the mixture. These interactions are particular for each substance, thus allowing compounds dissolved in the homogeneous fluid mixture to be separated from each other. Furthermore, a particular difficulty arises due to the fact that the description of these interactions depends on:

1. species that constitute the fluid phase;

---

*An example of such are synthetically-manufactured zeolites, as well as other relevant microporous solids.

2. species and functionality of the solid phase; &

3. behavior of the different species once they have adsorbed.

This aspect of adsorption-based separation processes poses difficulties in their description, characterization and understanding. In contrast, generalizations and trends, clearly observed when describing other *simpler* separation processes, are not possible for these reasons. This additional challenge of adsorption-based separations has triggered, in turn, a contemporary approach in the research of materials science that concentrates its attention on developing *tailor-made* adsorbents by, for example, engineering specific porous structures and porous networks—cf. [18], as well as chemically modifying the surface of porous materials with selected functional groups—just to mention two of the currently explored alternatives in this ever-growing field of research [19–24]. All these efforts are pursued with the goal of improving and optimizing industrially relevant separations and discovering novel applications of adsorption principles. A good example of this trend is the design of chiral stationary phases (CSPs) for preparative liquid chromatography applications, which play a fundamental role in manufacturing pharmaceutical and agrochemical products—see e.g., [25–27] and references therein. A second important challenge, currently of high relevance, is the potential application of adsorption technologies for carbon capture & storage (CCS), with significant research effort being led by industrialized nations—see e.g., [28–31].

Porous adsorbents

Materials frequently encountered in adsorption-based processes possess, in general, a large specific surface area with sufficiently high number of adsorption sites, where molecules of adsorbing species are able to interact. A detailed discussion of these interactions is outside the scope of this dissertation; however, it is important to mention that substantial scientific and technical efforts are conducted in order to understand them, as confirmed by the tremendous amount of literature on the topic [32, 33].

For engineering praxis of adsorption, *tailor-made* materials are frequently applied. Standard requirements for these materials are mainly, among others:

1. *high adsorptive capacity* in the form of—but, not restricted to—large specific surface area or large number of *micropores*, *mesopores* & *macropores*, depending on the application and type of molecules to separate;

2. mechanical, chemical and thermal stability; &

3. capacity to interact specifically with either molecules of one type or groups of molecules of the same kind in such a manner that it can be exploited for their separation or purification.

An introductory overview of adsorbents can be found in [19]. Furthermore, the interested reader is referred to [34]; therein, *nanoporous materials* for adsorption applications are specifically addressed.

Table 1.1: Examples of relevant industrial applications of adsorption processes. Adapted from [11, 12, 33, 35].

Application	Adsorbent(s) used
Purification of air	Zeolites, silica gel & activated alumina
Removal of radioactive nuclides from exhaust gas	Activated carbon
Removal of organic components from exhaust air	Activated carbon
Desulfurization	Activated carbon
Purification of methane	Zeolithic molecular sieves, silica gel & activated aluminum oxide
Purification of hydrogen	Zeolithic & carbon molecular sieves
Separation of alkane isomers	Molecular sieves
Water purification	Activated carbon
Separation of non-aqueous substances	Zeolites, silica gel, activated aluminum oxide, & molecular sieves
Separation of close-boiling liquid mixtures, e.g., xylene isomers	Zeolites

Adsorption chromatography

A process technology where principles of adsorption are extensively applied, primarily to design and accomplish difficult separations, is chromatography. Two fundamental physical phenomena govern this process [2, 4, 14, 36]:

1. THERMODYNAMIC EQUILIBRIUM; &

2. MASS TRANSFER KINETICS.

A complete description of the process requires knowledge and understanding of *both*. However, this work focuses on the first aspect due to the fact that in the chosen liquid phase adsorption chromatography experimental system—described in detail in Part III to illustrate *proof of concept*—this is the aspect of the process that needs to be primarily understood in order to describe it [14, 37]. In this respect, a cornerstone idea of this dissertation can be formulated as follows:

> ☆ *The dynamic behavior of highly efficient adsorption chromatography from a liquid phase is fundamentally controlled by the thermodynamic partition—i.e., equilibrium—established between porous stationary phase and adsorbable components contained in the fluid phase. In this case, the chromatographic separation process is* THERMODYNAMICALLY CONTROLLED*, and as such, governed by the functional dependency of the adsorbed phase concentrations (i.e., loadings) w.r.t. their fluid phase concentrations.*

The reader will affirmatively discover in the subsequent chapters of this work well founded arguments that support the statement above.

1.2 State of the art

While it has been 50 years (1965) since Myers & Prausnitz postulated Ideal Adsorbed Solution Theory (IAST) [38]*, it continues to be one of the most popular and widespread predictive multicomponent adsorption equilibrium models, often serving to benchmark

---

*[In order to get an idea of the impact brought about by this publication] According to the scientific references' portal *Web of Science^{TM}* (Thomson Reuters^{TM}) this article has been cited 1234 times! [Consultation conducted on December 1st, 2014.]

alternative, more complex calculation methods—see e.g., Krishna *et al.* [39], Bartholdy *et al.* [40], Swisher *et al.* [41] and the 50th anniversary review by Walton & Sholl [42]. This fact is confirmed by the long list of articles devoted to the subject, with particular emphasis on the solution of its constitutive equations. Recent publications [43, 44], for example, address the possibility to calculate analytical solutions of the model equations, in order to overcome calculation time overheads, and thus facilitating its implementation in numerical codes for dynamic adsorber simulation. In this respect, IAST has also become nowadays a standard option in commercial process simulation environments—e.g., Aspen Plus® [45]. Nevertheless, the continuing task of developing more efficient tools and popularizing IAST at its most basic level is an ongoing effort that will continue for the time to come. The present work should be situated in this context. It is on one hand, a novel alternative contribution to improve algorithmic efficiency of IAST calculations; on the other hand, it describes how IAST can be applied in a practical context to predict competitive equilibria of compounds, which adsorbing alone, display non-trivial adsorption isotherm courses.

1.3 Objectives & highlights of this work

This dissertation features the following Objectives:

1. Introduction, description, proof, & implementation of an efficient approach for multicomponent adsorption equilibria prediction, applying IAST—cf. Chapter 4.

2. Development of analytical formulæ under IAST framework to calculate partial derivatives of adsorbed phase concentrations w.r.t. corresponding fluid phase concentrations at equilibrium, focusing on its application in the numerical simulation of adsorber dynamics—cf. Chapter 7; &

3. Evaluation of IAST as a tool to describe the adsorption behavior of an experimental system to illustrate proof of concept—cf. Chapter 10.

1.4 Sources of information

Books   Several textbooks, monographies, compendia and doctoral theses were consulted in order to acquire the necessary knowledge to develop the ideas presented in the current dissertation. The list of references on the discussed topics is vast. Some of the

classics to the topics, constituted the bases to develop the concepts in this research. The following books are suggested to the reader as general, all-purpose introduction to the topic. For Part I, *Principles of adsorption and adsorption processes* by D. M. Ruthven [46] & *Adsorption Analysis: Equilibria and Kinetics* by D. D. Do [36]; for Part II, *Numerical solution of time-dependent advection-diffusion-reaction equations* by W. Hundsdorfer & Jan G. Verwer [47] and finally for Part III, *Fundamentals of Preparative and Nonlinear Chromatography* by G. Guiochon *et al.* [14].

Scientific articles   A vast number of technical publications from peer-reviewed journals was consulted in order to reach the goals of this work. Although it is difficult to categorize many of them, due to their degree of specialization on a particular topic, they can be divided roughly into three main fields of knowledge: *adsorption fundamentals (thermodynamics & mass transfer)*, *numerical methods (ODEs, PDEs, interpolation & integration)* and *experimental techniques of liquid chromatography (HPLC & adsorption isotherm determination)*. Four articles merit special acknowledgement. The first one is the milestone classic by Myers and Prausnitz, *"Thermodynamics of Mixed-Gas Adsorption" [38]*, which discusses application of solution thermodynamics to describe an adsorbed phase, in an analogous way to the thermodynamic treatment applied in vapor-liquid equilibria (VLE) [48, 49]. The second article is *"Thermodynamics of Multi-Solute Adsorption from Dilute Liquid Solutions" [50]* by Radke & Prausnitz. Herein, the natural extension of the concepts in [38] for the particular case of adsorbates found in dilute liquid solutions is explained. The details of this extension will be presented in Chapter 2 and its importance to liquid adsorption chromatography will be explained in practice in Part III. The third one is *"Adsorption Isotherm and Overloaded Elution Profiles of Phenyldodecane on Porous Carbon in Liquid Chromatography" [51]* by Diack & Guiochon. The peculiar elution behavior of overloaded injections of this compound in the system ACN/PGC is documented, whilst yielding insight into its complex adsorption mechanism. And finally, *"Adsorption Isotherms and Overloaded Elution Profiles of Phenyl-n-alkanes on Porous Carbon in Liquid Chromatography" [52]* again by Diack & Guiochon, this time discussing other phenyl-*n*-alkanes of the homologous series, with different lengths in their alkyl chain, and thus providing a systematic explanation of observed retention times and inflection points along the adsorption isotherm courses. These articles provided the starting basis to develop the present dissertation. Moreover—perhaps needless to stress, *all* articles listed under Bibliography, p. 195, are relevant to different extent to each of the topics herein discussed, and certainly recommended to the interested reader.

Conference proceedings Three important topic-related international conferences—attended by the author—provided valuable information. The first one is the *International Conference on Fundamentals of Adsorption* (FOA), organized by the International Adsorption Society (IAS) and publishing its proceedings in the journal named *Adsorption* (Springer). The second is the *International Symposium, Exhibition & Workshops on Preparative and Process Chromatography, Ion Exchange, Adsorption Processes & Related Separation Techniques* (PREP). And finally, the *International Symposium on Preparative and Industrial Chromatography and Allied Techniques* (SPICA).

Personal communications Important information was conveyed to *the author* in the form of technical discussions with colleagues from the PCG research group and colleagues from external institutions in Germany & Europe as well as other countries of the world while attending high-profile seminars and conferences. These productive contributions, focusing in particular on aspects of liquid chromatography, will be addressed in Part III.

1.5 Published results in peer-reviewed journals

As an important outcome of the partial results obtained in this work, three research articles were published in *peer-reviewed* journals, thus contributing to the studied field of research:

1. *"A Method for Efficiently Solving the IAST Equations with an Application to Adsorber Dynamics"* [53] (main author);

2. *"Use of Adsorbed Solution theory to model competitive and co-operative sorption on elastic ion exchange resins"* [54] (co-author); and

3. *"Evaluating the application of discrete adsorption data to predict competitive equilibria and fixed-bed dynamics using Ideal Adsorbed Solution Theory"* [55] (main author).

Other technical contributions in the form of scientific posters and talks were presented in the respective conferences & meetings attended*.

---

*Conference contributions are listed under "List of Publications" at the back of this thesis.

1.6   Structure of this thesis

In accordance with the dissertation's objectives listed in Section 1.3, this work consists of *eleven* chapters, which are grouped into *four* thematic parts:

Part I: Some notions on adsorption & adsorption equilibria (Chapters 1 - 5)
Chapter 1 introduces the general topic of this work and provides preliminary definitions and concepts necessary in aiding with subsequent chapter presentation. Chapter 2 discusses fundamentals of adsorption. Chapter 3 introduces Ideal Adsorbed Solution Theory (IAST) and reports on different strategies commonly used for its solution. Chapters 4 presents an efficient approach to solve IAST equations; application examples and additional implementation details are discussed in Chapter 5.

Part II: Adsorber dynamics (Chapters 6 - 8)   Chapter 6 presents a basic process description of liquid adsorption chromatography, as well as details of common isothermal models applied to *understand & characterize* it. Chapters 7 & 8 focus on applications of the solution approach of Chapter 4, with emphasis on tubular fixed-bed adsorbers & HPLC columns.

Part III: Experimental demonstration (Chapters 9 - 10)   Chapters 9 & 10 summarize experimental measurement work conducted for practical demonstration and validation of the tools presented in Chapters 4, 5, 6, & 7.

Part IV: Concluding remarks (Chapter 11)   Chapter 11 outlines conclusions of this dissertation and briefly suggests potential workscope along treated lines of research.

The following chapter 2 provides theoretical foundations of this work.

This page intentionally left blank.

Chapter 2

Adsorption isotherms & thermodynamics

"First things first."

– English proverb

Introduction

A discussion of liquid phase adsorption chromatography requires an exposition of fundamental concepts of adsorption & tools that describe adsorption-based separation processes. Adsorption isotherms are therefore the central focus of this chapter. Firstly, an overview of important definitions concerning adsorption phenomena and technical systems is given. Afterwards, discussion continues on aspects of *adsorption thermodynamics* to set the foundation upon which IAST relies, including the classical context postulated by Gibbs [56], which continues to find application today [48, 49, 57]. Finally, a general review on solution thermodynamics of adsorption, presented by Myers [58] and more recently updated by Myers & Monson [59], is briefly introduced and discussed. The definitions and concepts herein addressed are applied throughout the rest of the thesis.

2.1   Single component adsorption isotherm models

In a system consisting of two phases, an adsorbed phase, a, and fluid phase, ℓ, a temperature-dependent partition of solutes, i, indicates their distribution at equilibrium. A natural representation of this equilibrium partition is given by an equation that relates adsorbed phase concentrations, q_i, with corresponding fluid phase concentrations, c_i:

$$q_i = f(c_i, T). \tag{2.1}$$

In order to systematically investigate such a system, temperature, T, is kept constant and partition values, q_i *vs.* c_i, i.e., $\{q_i^{(1)}, c_i^{(1)}\}$, $\{q_i^{(2)}, c_i^{(2)}\}$, etc., are measured after a sufficiently long time[*]. The *ensemble* of partition values constitute the ADSORPTION ISOTHERMS, which can be measured experimentally for single compounds or simultaneously for multiple ones, depending on the applied experimental technique(s)[†]. Figure 2.1
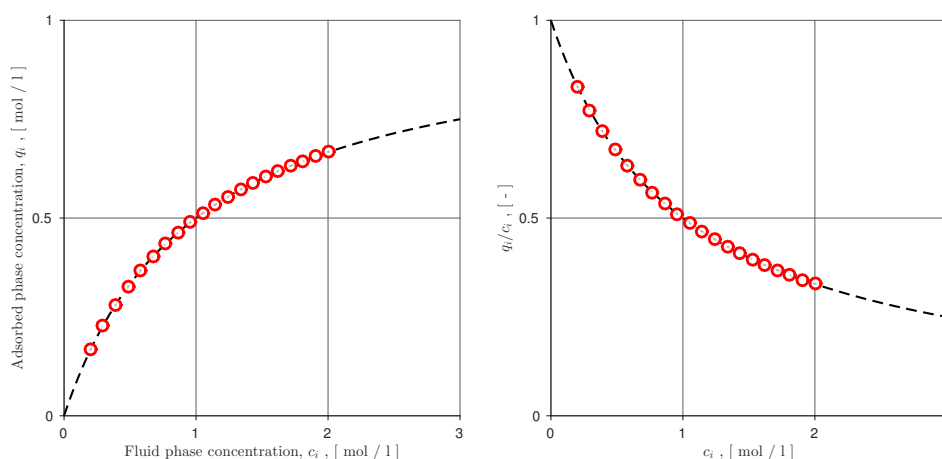
Figure 2.1: Simple example for an adsorption isotherm. Circles (○): measured equilibrium (partition) points, $\{q_i^{(1)}, c_i^{(1)}\}, \{q_i^{(2)}, c_i^{(2)}\}, \ldots$. Dotted line(−−): fitted function, $q_i = f(c_i)$, to equilibrium points shown. The points were generated artificially with the Langmuir isotherm, Equation (2.3a), p. 17 using parameters listed in Table A2, Appendix A2.1, p. 165.

illustrates this simple definition in graphical form for an adsorbate i, including quantities, q_i/c_i—these quotients become relevant in Chapter 3 to implement IAST.

---

[*]Meaning that *enough* time should be given to the system to reach equilibrium. In principle, $\Delta c_i \to 0$ and so $\Delta q_i \to 0$ as $t \to \infty$.

[†]This is addressed in detail in Part III.

2.1.1 Classification criteria

Due to the fact that molecular interactions at high concentrations are complex, a non-linear dependency between equilibrium values in the adsorbed phase, q_i, and fluid phase, c_i, can be established. Elaborate isotherm equations are therefore required for appropriate description over relevant concentration ranges. As a result, a plethora of models, covering a wide spectrum of systems, whilst either justified *theoretically* or *empirically*, are reported in the literature. See among many others [4, 7, 14, 36, 60] and the references therein.

A general classification system introduced by the pioneering work of Brunauer *et al.* [61], later extended by Giles *et al.* [62]—and most recently standardized by the IUPAC [63, 64]—is based on the shape taken by experimental data and fitted adsorption isotherm courses, as illustrated with some examples in Figure 2.2.
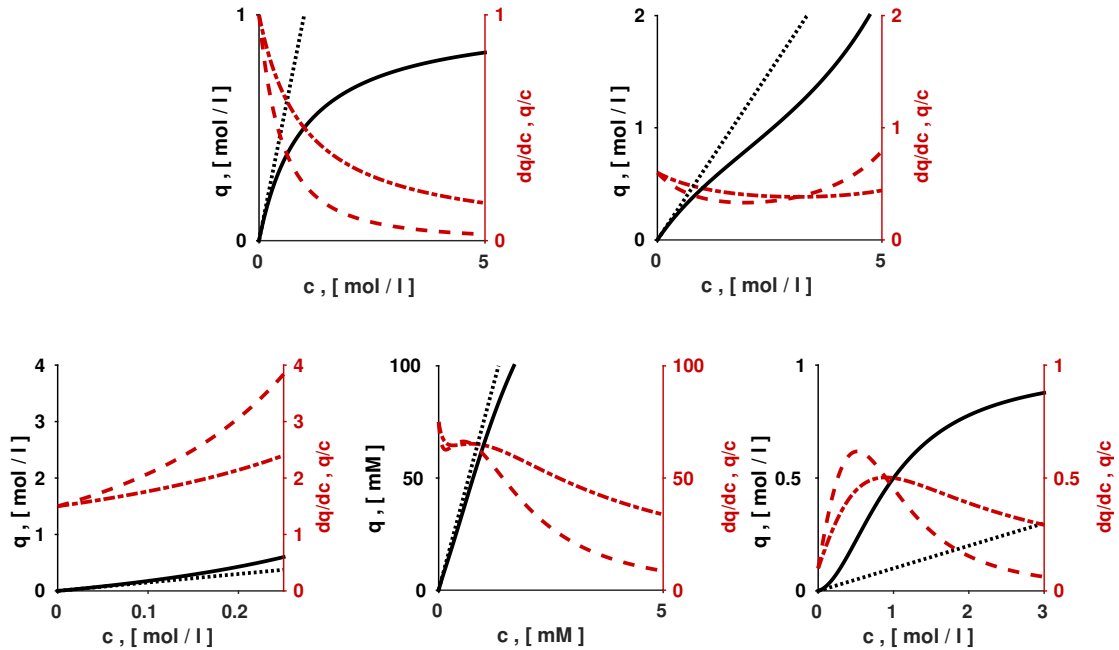
Figure 2.2: Examples of isotherm equations, based on the classification of Brunauer *et al.* [61]. From *left* to *right* & *top* to *bottom*: Langmuir (**Type I**), Eq. (2.3a); BET (**Type II**), Eq. (2.3i); Anti-Langmuir (**Type III**); Quadratic + Langmuir (**Type IV**), Eq. (2.3e); & Quadratic (**Type V**), Eq. (2.3d). (−): $q = f(c)$; (−−): dq/dc; (−·): q/c; & (··): linear limit, applying ɧ. Expressions for q/c, dq/dc and ɧ are listed in Tables 2.3 & 3.3, p. 37. Parameters used to generate these figures can be found in Appendix A2.1, p 165.

Additionally, adsorption equilibrium equations can roughly be grouped into *five comprehensive categories*, in accord with the applied principle used to define and generate them [7, 36, 40]. These categories are listed in Table 2.1. It is important to highlight that several well-known and applied equilibrium models are simple empirical equations,

with sufficient parameters to fit observed experimental behavior. This approach works well over measured concentration ranges, but difficulties can appear when equilibrium is required outside these ranges. Table 2.2 lists important, well-known single component adsorption isotherm model equations[*] Some of these models are addressed in Chapters 5, 8, 9, & 10; the complete list is given to provide an additional guideline and useful references to interested readers.

Table 2.1: Some principles applied to generate adsorption isotherm models.

Founding principle(s)	Examples
1. Kinetics of adsorption & desorption	Langmuir [65], BET [61, 66]
2. Potential Theory, volume filling in micropores [7, 67, 68]	D-R [7, 67, 68], D-A [7]
3. Empirical (*'goodness of fit'*)	Redlich-Peterson [69], Tóth
4. Classical thermodynamics & EOS approach [7, 14, 36, 70–72]	2D van der Waals EOS [7, 70], Virial Mixture Coefficient (VMC) method [72, 73]
5. Statistical thermodynamics, e.g., [74, 75]	Quadratic [43]

A more detailed review of some of the adsorption isotherm models listed in Table 2.2 as well as a discussion on *model linearization & parametrization* can be consulted in [60, 76]. These aspects become useful to perform *model discrimination* from experimentally acquired equilibrium data. It is also important to highlight that some of the equations listed in Table 2.2 are of the general form[†]:

$$q = f(\xi) := \frac{\xi \, \nu'(\xi)}{\nu(\xi)}. \tag{2.2}$$

This applies for example to the Langmuir, Bi-Langmuir, Quadratic, & Quadratic plus Langmuir models, Equations (2.3a), (2.3b), (2.3d), and (2.3e) in Table 2.2, respectively. Equation (2.2), together with the concept of increasing isotherm —i.e., an isotherm equation, $q_i = f(c_i)$, displaying arbitrary increasing values for increasing arguments, c_i, proves its usefulness with regards to the solution principle presented in Chapter 4.

---

[*]The expressions are valid for the two fluid phases considered in this work, *liquid* and *gas*.

[†]This functional form is directly linked to statistical thermodynamics [14].

Table 2.2: Selected single component adsorption isotherm equations, $q_i = f(c_i)$. [a] [b]

Model	Equation	
Langmuir [65]	$q_i = q_i^{\text{sat}} \dfrac{b_i c_i}{1 + b_i c_i}$	(2.3a)
Bi-Langmuir [14]	$q_i = q_{i1}^{\text{sat}} \dfrac{b_{i1} c_i}{1 + b_{i1} c_i} + q_{i2}^{\text{sat}} \dfrac{b_{i2} c_i}{1 + b_{i2} c_i}$	(2.3b)
Freundlich [7, 14]	$q_i = a_i c_i^{\frac{1}{\nu_i}}$	(2.3c)
Quadratic [43]	$q_i = q_i^{\text{sat}} \dfrac{c_i \left[b_{i1} + 2 b_{i2} c_i \right]}{1 + b_{i1} c_i + b_{i2} c_i^2}$	(2.3d)
Quadratic plus Langmuir [51, 52]	$q_i = q_{i1}^{\text{sat}} \dfrac{c_i \left[b_{i1} + 2 b_{i2} c_i \right]}{1 + b_{i1} c_i + b_{i2} c_i^2} + q_{i2}^{\text{sat}} \dfrac{b_{i3} c_i}{1 + b_{i3} c_i}$	(2.3e)
O'Brien & Myers [77]	$q_i = q_i^{\text{sat}} \left[\dfrac{b_i c_i}{1 + b_i c_i} + \sigma_i^2 \dfrac{b_i c_i \left(1 - b_i c_i \right)}{2 \left(1 + b_i c_i \right)^3} \right]$	(2.3f)
Tóth [78, 79]	$q_i = q_i^{\text{sat}} \dfrac{b_i c_i}{\left[1 + \left[b_i c_i \right]^{\nu_i} \right]^{\frac{1}{\nu_i}}}$	(2.3g)
Redlich-Peterson [69, 80]	$q_i = \dfrac{a_i c_i}{1 + b_i c_i^{\nu_i}}$	(2.3h)
BET [14, 44, 66, 81, 82]	$q_i = q_i^{\text{sat}} \dfrac{b_{i\text{S}} c_i}{\left[1 - b_{i\text{L}} c_i \right] \left[1 - b_{i\text{L}} c_i + b_{i\text{S}} c_i \right]}$	(2.3i)
Dubinin-Radushkevich (D-R) [7, 68, 83, 84]	$q_i = q_i^{\text{sat}} \exp \left[-B_i^2 \left(\ln \left[\dfrac{c_i^{\text{sat}}}{c_i} \right] \right)^2 \right], \; B_i := \dfrac{\Re T}{\beta_i E_{i0}}$	(2.3j)
UNILAN [79, 85]	$q_i = \dfrac{q_i^{\text{sat}}}{2 \eta_i} \ln \left[\dfrac{\kappa_i + c_i \exp \left[\eta_i \right]}{\kappa_i + c_i \exp \left[-\eta_i \right]} \right], \; \eta_i \geq 0$	(2.3k)
Sips (Langmuir-Freundlich) [36, 86]	$q_i = q_i^{\text{sat}} \dfrac{\left[b_i c_i \right]^{\frac{1}{\nu_i}}}{1 + \left[b_i c_i \right]^{\frac{1}{\nu_i}}}$	(2.3l)
Fractal BET [87]	$q_i = -q_i^{\text{sat}} \dfrac{b_{i\text{S}} \ln \left[1 - b_{i\text{L}} c_i \right]}{b_{i\text{L}} \left[1 - b_{i\text{L}} c_i + b_{i\text{S}} c_i \right]}$	(2.3m)

a. Parameter notation has been slightly modified in some of the model equations for convenience. Consult the provided reference on each model for further details.

b. For the sake of convenience, fluid phase concentration is expressed as c_i. For the gas phase, c_i should be replaced simply by partial pressure, p_i, if perfect gas behavior is valid, or fugacity, f_i, otherwise.

2.1.2 Henry coefficient and selectivity

Let

$$q_i = f(c_i), \quad i = 1, \dots, N, \qquad \text{at constant } T, \tag{2.4}$$

be a *smooth, continuous* function[*] representing the dependency of the adsorbed phase concentration of a component i, q_i, with respect to the fluid phase concentration, c_i, i.e., an adsorption isotherm model equation. The Henry coefficient for adsorption of component i is thus defined as[†]

$$\mathfrak{h}_i := \lim_{c_i \to 0} \frac{q_i}{c_i} = \lim_{c_i \to 0} \frac{\mathrm{d}q_i}{\mathrm{d}c_i} = f(T). \tag{2.5}$$

Physically this means that at *infinite dilution* of an adsorbable component, i, the coefficient represents a *positively-valued* and *finite equilibrium partition* of an amount of i, established among the fluid and the adsorbed phase, hence

$$q_i \equiv \mathfrak{h}_i\, c_i = f(c_i) \qquad \text{at constant } T. \tag{2.6}$$

This partition is from a practical point of view difficult to quantify experimentally for certain systems. Often extrapolations from a physically attainable low concentration region to the limit $c_i \to 0$ must be assumed, with their corresponding errors. An extrapolation is justified if the gathered data behaves linearly in the measured low concentration range. The limit given by (2.5) is also helpful to test adsorption isotherm model equations for thermodynamic consistency [88, 89]. It will later be observed that for practically relevant adsorption isotherm model equations, the Henry coefficient can either take the value

$$\mathfrak{h}_i = 0 \tag{2.7}$$

e.g., the Dubinin-Radushkevich (D-R) isotherm, Equation (2.3j), Table 2.2, or

$$\mathfrak{h}_i = \infty, \tag{2.8}$$

e.g., Freundlich isotherm, Equation (2.3c), Table 2.2, thus violating the thermodynamic consistency requirement expressed by Equation (2.5)—i.e., positively-valued, finite [88, 89]. For these particular isotherms, strategies have been developed in order to alleviate this drawback, as done for the D-R isotherm, Equation (2.3j) [83, 84, 90–92]. Table 2.3 lists expressions of the Henry coefficient for several isotherms. The Henry coefficient is an important piece of information that allows understanding a limit behavior of adsorption

---

[*]Formally, from the mathematical point of view, this function is C^∞, i.e., *infinitely differentiable*.

[†]The term *Henry coefficient* is adopted in this work in order to remind the reader that it is actually a *temperature-dependent* term. Often the misleading designation «*Henry constant*» is frequently encountered in the chemical engineering literature.

equilibria. It plays a fundamental role in studying the dynamic behavior of certain fixed-bed adsorbers—e.g., packed columns for analytical liquid adsorption chromatography*. Now, let the molar fractions at equilibrium of an adsorbable component, i, in a mixture of N adsorbable components in a diphasic system, consisting of a bulk fluid phase and the adsorbed phase be written as

$$y_i := \frac{c_i}{c_{\text{tot}}} \quad \text{and} \quad x_i := \frac{q_i}{q_{\text{tot}}}, \quad i = 1, \dots, N, \tag{2.9}$$

respectively. The *selectivity*, α, of component i with respect to component j in such a system is defined as

$$\alpha_{ij} := \frac{y_i \, / \, x_i}{y_j \, / \, x_j}, \quad i, j = 1, \dots, N, \quad i \neq j, \tag{2.10}$$

thus indicating the *degree of affinity* or *preference to concentrate* of a particular component with respect to any of the other adsorbable components in the two distinct co-existing phases at equilibrium. This important parameter therefore allows to quickly assess the separation performance of different adsorbents when put in contact with mixtures of adsorbates of interest. Hence, for a given adsorbent, a quantified value of $\alpha_{ij} \to 1$ is to be in general interpreted as a *difficult* separation task, since the equilibrium partition of such a component under this situation does not vary significantly—this naturally implies that there is no particular preference to concentrate in either phase of the system. In contrast, values of $\alpha_{ij} \gg 1$ mean that the affinity of each component i and j to bind with the applied stationary phase is quite different, thus indicating a *potentially undemanding* separation task. Moreover, for diluted systems, the connection with Henry coefficients, $\mathfrak{h}_i$, $\mathfrak{h}_j$, defined by Equation (2.5), is straightforward:

$$\alpha_{ij} = \frac{\mathfrak{h}_j}{\mathfrak{h}_i}. \tag{2.11}$$

The limit behavior expressed by Henry coefficient, Equation (2.5), and used to define selectivity, Equation (2.10), allows only a limited description and understanding of adsorption equilibria—i.e., under *diluted conditions*; it does not suffice to appropriately describe equilibrium partitions covering wider concentration ranges, which are of practical interest for industrial-scale separations and their optimization.

---

*These connections between adsorption theory and the aforementioned liquid adsorption chromatography application are clarified in Part III.

Table 2.3: Henry coefficients, $\mathfrak{h}_i$, and derivatives, dq_i/dc_i, of selected single component isotherm models. [a]

Isotherm	Henry coefficient		Derivative	
Langmuir [65]	$\mathfrak{h}_i = q_i^{\text{sat}} b_i$	(2.12a)	$\dfrac{dq_i}{dc_i} = q_i^{\text{sat}} \dfrac{b_i}{[1+b_i c_i]^2}$	(2.12b)
Bi-Langmuir [14]	$\mathfrak{h}_i = q_{i1}^{\text{sat}} b_{i1} + q_{i2}^{\text{sat}} b_{i2}$	(2.12c)	$\dfrac{dq_i}{dc_i} = q_i^{\text{sat}} \dfrac{b_{i1}}{[1+b_{i1}c_i]^2} + q_{i2}^{\text{sat}} \dfrac{b_{i2}}{[1+b_{i2}c_i]^2}$	(2.12d)
Quadratic [43]	$\mathfrak{h}_i = q_i^{\text{sat}} b_{i1}$	(2.12e)	$\dfrac{dq_i}{dc_i} = q_i^{\text{sat}} \dfrac{b_{i1}+4b_{i2}c_i+b_{i1}b_{i2}c_i^2}{[1+b_{i1}c_i+b_{i2}c_i^2]^2}$	(2.12f)
Quadratic plus Langmuir [51, 52]	$q_{i1}^{\text{sat}} b_{i1} + q_{i2}^{\text{sat}} b_{i3}$	(2.12g)	$\dfrac{dq_i}{dc_i} = q_{i1}^{\text{sat}} \dfrac{b_{i1}+4b_{i2}c_i+b_{i1}b_{i2}c_i^2}{[1+b_{i1}c_i+b_{i2}c_i^2]^2} + q_{i2}^{\text{sat}} \dfrac{b_{i3}}{[1+b_{i3}c_i]^2}$	(2.12h)
O'Brien & Myers [77]	$\mathfrak{h}_i = q_i^{\text{sat}} b_i \left[1 + \dfrac{1}{2}\sigma_i^2 \right]$	(2.12i)	$\dfrac{dq_i}{dc_i} = q_i^{\text{sat}} b_i \dfrac{2+\sigma_i^2+b_ic_i\left[4-4\sigma_i^2+b_ic_i\left[2+\sigma_i^2\right]\right]}{2[1+b_ic_i]^4}$	(2.12j)
Redlich-Peterson [69, 80]	$\mathfrak{h}_i = a_i$	(2.12k)	$\dfrac{dq_i}{dc_i} = a_i \dfrac{1-b_ic_i^{\nu_i}[-1+\nu_i]}{[1+b_ic_i^{\nu}]^2}$	(2.12l)
BET [14, 44, 66]	$\mathfrak{h}_i = q_i^{\text{sat}} b_{iS}$	(2.12m)	$\dfrac{dq_i}{dc_i} = q_i^{\text{sat}} b_{iS} \dfrac{1+b_{iL}[-b_{iL}+b_{iS}]c_i^2}{[-1+b_{iL}c_i]^2[1-b_{iL}c_i+b_{iS}c_i]^2}$	(2.12n)
Tóth [78, 79]	$\mathfrak{h}_i = q_i^{\text{sat}} b_i$	(2.12o)	$\dfrac{dq_i}{dc_i} = \dfrac{q_i^{\text{sat}} b_i}{[1+[b_ic_i]^{\nu_i}]^{-\frac{1+\nu_i}{\nu_i}}}$	(2.12p)
Sips [36, 86]	$\mathfrak{h}_i = \{\infty, \nu_i > 1;\ 0, \nu_i < 1$	(2.12q)	$\dfrac{dq_i}{dc_i} = q_i^{\text{sat}} \dfrac{[b_ic_i]^{\nu_i}\frac{1}{\nu_ic_i}}{[1+[b_ic_i]^{\nu_i}\frac{1}{2}]^2}$	(2.12r)
Dubinin-Radushkevich (D-R) [7, 68, 83] [b]	$\mathfrak{h}_i = 0$	(2.12s)	$\dfrac{dq_i}{dc_i} = \dfrac{1}{c_i^2}\left[q_i^{\text{sat}}\exp\left[-B_i^2\left(\ln\left[\dfrac{c_i^{\text{sat}}}{c_i}\right]\right)^2\right]\cdot\left(-1+2B_i^2\ln\left[\dfrac{c_i^{\text{sat}}}{c_i}\right]\right)\right],\ c_i \in\ ]0,\infty[$	(2.12t)

a. Parameters applied in each model are listed in Table 2.2.
b. Possesses *zeros of higher order* at the origin; a finite, positive value of the slope as defined by (2.5) does not exist.

2.2   Multicomponent adsorption isotherm models

The description provided by single component adsorption equilibrium data and corresponding fit of these data to an adsorption isotherm model equation, covered in Section 2.1, is only useful to a certain extent. The crucial task in developing adsorption-based separations consists of thoroughly understanding adsorption behavior of multiple species, i.e., complex mixtures [14, 93]. It is necessary to recall that *all* adsorbable species in a homogeneous mixture can potentially interact with adsorption sites of the stationary phase and also among themselves once they have adsorbed, leading to complex interactions. These interactions include among several others: *a) competitive be-*
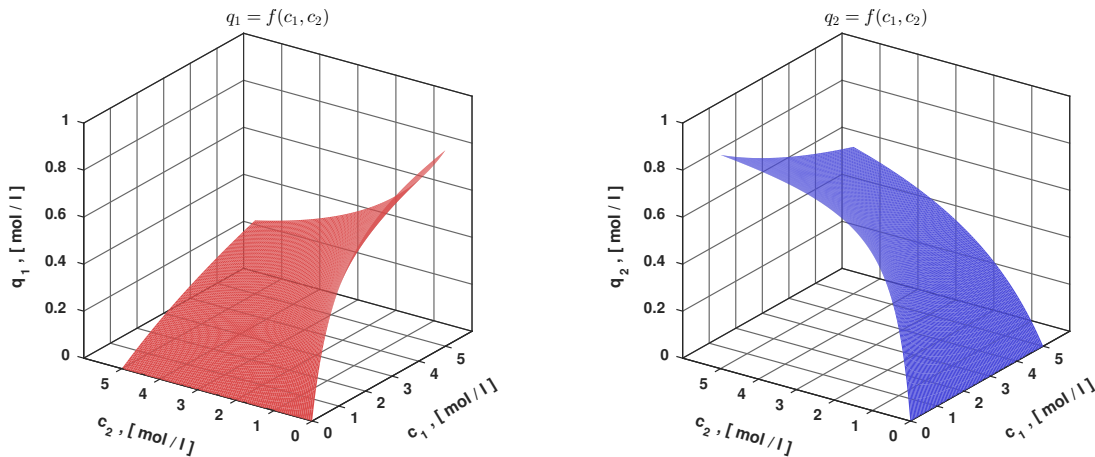
Figure 2.3: Simple competitive binary adsorption isotherms, $q_1 = f(c_1, c_2)$, $q_2 = f(c_1, c_2)$, generated with the competitive Langmuir equation (2.14a) listed in Table 2.4, p. 23. Parameters used to generate the plots are listed in Table A3 of Appendix A2.2, p. 165.

havior for the adsorption sites; and *b) cooperative behavior*, where adsorption of one or more species enhances adsorption of other components in the fluid mixture. These two basic type of interactions amongst adsorbable species are often observed in experimental systems and are in some cases only partially understood. Henceforth, a qualitative and quantitative description of competitive adsorption of multiple species continues to be a challenge to modern research. Already when a few chemically similar species in a mixture are taken into account—for a particular system under investigation—requires a substantially costly and time-consuming experimental effort [94, 95]. A second aspect of fundamental importance is the nature of the adsorbing material used. *Surface heterogeneity* and the different theories behind it—see e.g., [96–98], aim at providing a more detailed picture of adsorption mechanisms, trying to reconcile physical observations with applied models in a better fashion.

Recent advances in high-throughput screening (HTS) and high-throughput experimental

platform design have become one important alternative aimed at tackling the cumbersome task of experimentally measuring multicomponent, competitive adsorption equilibria; they are particularly useful in several biotechnological and biopharmaceutical applications, as explained in [99–103]. This empirical approach seems to be increasing in popularity in separation science overall. Nonetheless, the classical approach, whereby thermodynamics' principles are applied in order to predict multicomponent adsorption based on single component adsorption equilibria, continues to be an important and useful tool due to three factors:

1. it is of general validity;

2. it is simple to apply and usually not cost-demanding; &

3. a comprehensive amount of reported *single component* adsorption equilibrium data on commercial adsorbents of industrial relevance is readily available—see e.g., [79]; in turn, this information can be employed to predict multicomponent behavior.

2.2.1 Classification criterium for multicomponent isotherms

A simple way to group multicomponent adsorption isotherm models reported in the literature is by considering whether a given equation is expressed EXPLICITLY as a function of arguments $c_1, \ldots, c_N$, or expressed by an IMPLICIT equation of more general character. First practical attempts to provide explicit expressions for mixtures by extending the Langmuir model to several components can be traced back to the work of Markham & Benton [104]. This model, together with other common examples for explicit models, are listed in Table 2.4. Mathematically, in analogy to Equation (2.4) for a single adsorbable component, a competitive multicomponent adsorption isotherm model consisting of N adsorbable species is given in explicit form by

$$q_i = f(c_1, \ldots, c_N), \quad i = 1, \ldots, N \qquad (2.13)$$

at constant temperature, T. For specific application in liquid chromatography—the focus of Part III, explicit expressions exist for many systems—see e.g., [105, 106]. The choice of applying either an explicit, algebraically simple equation, or an implicit model to describe multicomponent adsorption equilibria is important from a practical point of view, e.g., when the calculation of these equilibria have to be carried out *millions of times*—cf. Chapter 7, p. 85. Quite often, however, serious limitations in the usage of these explicit equations, such as those listed in Table 2.4, become evident when these

Table 2.4: Examples of explicit—algebraically *simple*—competitive adsorption isotherm models, given by an equation of the form $q_i = f(c_1, \ldots, c_N)$, for $i = 1, \ldots, N$ components.

Model	Equation	
Multicomponent Langmuir [104]	$q_i = q_i^{\text{sat}} \dfrac{b_i c_i}{1 + \sum\limits_{j=1}^{N} b_j c_j}$	(2.14a)
Two component bi-Langmuir [14, 107]	$q_i = q_{i1}^{\text{sat}} \dfrac{b_{i1} c_i}{1 + b_{11}c_1 + b_{12}c_2} +$ $q_{i2}^{\text{sat}} \dfrac{b_{i2} c_i}{1 + b_{21}c_1 + b_{22}c_2}, \ i = 1,2$	(2.14b)
Multicomponent Tóth [14, 108]	$q_i = q^{\text{sat}} \dfrac{b_i c_i}{\left[1 + \left[\sum\limits_{j=1}^{N} b_j c_j \right]^{\nu_i} \right]^{\frac{1}{\nu_i}}}$	(2.14c)
Multicomponent Sips [4, 7, 36] [a]	$q_i = q_i^{\text{sat}} \dfrac{b_i c_i^{\frac{1}{\nu_i}}}{1 + \sum\limits_{j=1}^{N} b_j c_j^{\frac{1}{\nu_j}}}$	(2.14d)

a. Sometimes referred to as *Loading Ratio Correlation*, 'LRC' [7].

models are applied to describe actual measured mixture equilibrium data. Mixtures of components, which adsorbing alone display complex adsorption courses, require either a more sophisticated approach, or a mixture equation with sufficient number of parameters for a satisfactory and useful description. Determining these parameters, in turn, requires a careful and comprehensive experimental plan, which is quite often difficult to realize for several reasons—e.g., costs, availability of materials, etc.

Table 2.5: Examples of non-explicit multicomponent adsorption models.

Model	Reference(s)
Ideal Adsorbed Solution Theory (IAST)	[38, 50]
Vacancy Solution Theory (VST)	[109]
Real Adsorbed Solution Theory (RAST)	[110, 111]
Spreading Pressure Dependent Equation (SPD)	[112]
Predictive Read Adsorbed Solution Theory (PRAST)	[113]
Multicomponent Potential Adsorption Theory (MPTA)	[40, 114–116]
Segregated Ideal Adsorbed Solution Theory (SIAST)	[41]
Generalized Predictive Adsorbed Solution Theory (GPAST)	[117]

Table 2.5 lists several *non-explicit* multicomponent adsorption isotherm models that have been developed, studied and implemented during the last 50 years, with IAST as the pioneering work in this regard. Classical theories based on solution thermodynamics'

principles are an important alternative for multicomponent adsorption calculation and prediction.

2.3 Thermodynamics of an adsorbed phase

As stated in Section 2.2, equilibrium expressions of practical application can be generated with the appropriate conceptual framework [58].

A starting point of general character to analyze separation processes is the FUNDAMENTAL PROPERTY RELATION—see among many others [38, 46, 48, 57, 118], relating at least *seven* thermodynamic variables, used to describe a *homogeneous**, bulk phase of volume V in an *open*, well-defined, homogeneous system:

$$\mathrm{d}U = T\,\mathrm{d}S - p\,\mathrm{d}V + \sum_{i=1}^{N} \mu_i\,\mathrm{d}n_i, \tag{2.15}$$

whereby, $U = f(T, S, p, V, \mu_1, \ldots, \mu_N, n_1, \ldots, n_N)$. This expression basically condenses two universal postulates: the First Law and Second Law of Thermodynamics—see among many others [4, 46, 48]. By adopting a *Gibbsian view* [56, 118] of a two dimensional adsorbed phase, a, Equation (2.15) needs to be modified, since now a surface, $\mathfrak{A}$, needs to be taken into account, in addition to volume, V^a, so it is conveniently re-cast as [98, 119]

$$\mathrm{d}U^a = T\,\mathrm{d}S^a - p\,\mathrm{d}V^a - \pi\,\mathrm{d}\mathfrak{A} + \sum_{i=1}^{N} \mu_i^a\,\mathrm{d}n_i^a. \tag{2.16a}$$

Equivalent expressions to (2.16a)—also *Fundamental Relations*—can be written by applying the definitions of:

$$\text{(Enthalpy)} \quad H^a = U^a + pV^a + \pi\mathfrak{A},$$

$$\text{(Helmholtz free energy)} \quad A^a = U^a - TS^a \quad \text{and}$$

$$\text{(Gibbs free energy)} \quad G^a = H^a - TS^a = U^a + pV^a - TS^a + \pi\mathfrak{A},$$

---

*Meaning that the phase has the same physical composition & state of matter in all its constituent parts [56].

therefore arriving by differentiation at:

$$\mathrm{d}H^a = T\,\mathrm{d}S^a + V^a\,\mathrm{d}p + \mathfrak{A}\,\mathrm{d}\pi + \sum_{i=1}^{N}\mu_i^a\,\mathrm{d}n_i^a, \tag{2.16b}$$

$$\mathrm{d}A^a = -S^a\,\mathrm{d}T - p\,\mathrm{d}V^a - \pi\,\mathrm{d}\mathfrak{A} + \sum_{i=1}^{N}\mu_i^a\,\mathrm{d}n_i^a \quad \text{and} \tag{2.16c}$$

$$\mathrm{d}G^a = -S^a\,\mathrm{d}T + V^a\,\mathrm{d}p + \mathfrak{A}\,\mathrm{d}\pi + \sum_{i=1}^{N}\mu_i^a\,\mathrm{d}n_i^a. \tag{2.16d}$$

Hereby $\pi\,\mathrm{d}\mathfrak{A}$ should be understood, in the classical sense discussed, as a *surface work term*, with state variable, π [46], having a clear *physical* definition [38, 50, 95, 118, 119]:

$$\pi \equiv \gamma_0 - \gamma, \tag{2.17}$$

where γ_0 and γ represent surface tensions of the fluid film in contact with the adsorbent, *before* adsorbing and *after* desorbing, respectively, and given the term *spreading pressure* [118].

In a broader sense, π is treated as a *surface potential* of the adsorbing material*, independent of the particular *morphology* it might possess. This is due to the fact that for certain types of adsorbents, the concept of *surface* is rather *ambiguous*—e.g., zeolites & microporous materials [58, 59, 119]. As a consequence, the Fundamental Relation written for adsorbed phase, a, Equation (2.16), has general application to a wide class of adsorbents and is employed to:

1. establish a relationship between surface potential, π and chemical potentials of *adsorbed* species,

$$\mu_i^a,\ i = 1,\ \dots,\ N;$$

2. provide a general formulation, from which an *ideal adsorbed solution* can be defined [36, 38].

---

*Sometimes also referred to as *surface energy*. Already in the seminal papers by Hill [119–121], a *formal suggestion* is made to refer to this term as a *potential* of the adsorbent, abandoning the—somehow restrictive—concept of *area*.
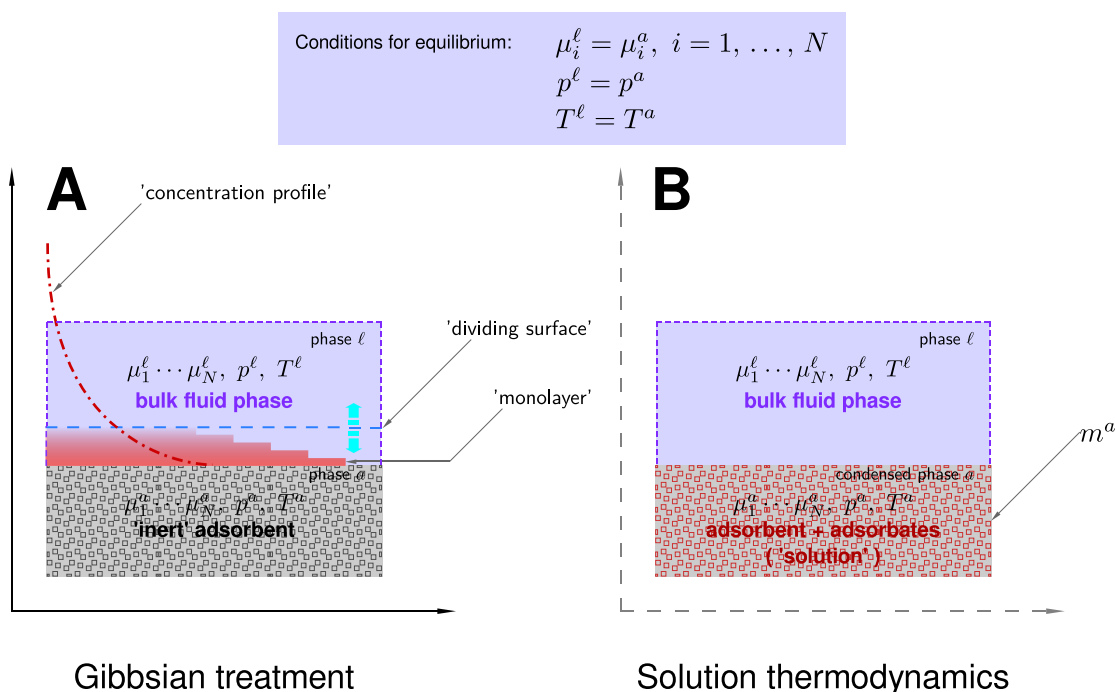
Figure 2.4: Conceptual picture of thermodynamics applied to adsorption [48, 56, 59], depicting two theoretical treatments used to describe phases a & ℓ under equilibrium—cf. Equation (2.23). (**A**): *Gibbsian* treatment with an *inert* adsorbent plus layers of adsorbed phase and used in this work; (**B**): solution thermodynamics treatment, suited better for adsorbed phases for which the concept of surface is ambiguous, e.g., zeolites, metal-organic frameworks (MOFs), etc.

Derivation of Gibbs' adsorption isotherm

The Fundamental Relation (2.16d), restricted to constant temperature, T, pressure, p, and potential, π, can be integrated by applying *Euler's homogeneous function theorem*—refer to Appendix A3 for details, so that

$$G^a = \sum_{i=1}^{N} \mu_i^a\, n_i^a. \tag{2.18}$$

The total differential of Equation (2.18), $\mathrm{d}G^a$, is therefore

$$\mathrm{d}G^a = \sum_{i=1}^{N} \mu_i^a\, \mathrm{d}n_i^a + \sum_{i=1}^{N} n_i^a\, \mathrm{d}\mu_i^a \tag{2.19}$$

to express differential changes in Gibbs' energy of the adsorbed phase. Substracting Eq. (2.19) from Equation (2.16d) yields the GIBBS-DUHEM equation for the adsorbed phase, thus establishing a central relationship between *state property*, π, and *component*

properties, μ_i^a [46, 120]:

$$- S^a \, \mathrm{d}T + V^a \, \mathrm{d}p + \mathfrak{A} \, \mathrm{d}\pi = \sum_{i=1}^{N} n_i^a \, \mathrm{d}\mu_i^a. \tag{2.20}$$

Additionally, restricting to constant T and p holds:

$$- \mathfrak{A} \, \mathrm{d}\pi + \sum_{i=1}^{N} n_i^a \, \mathrm{d}\mu_i^a = 0. \tag{2.21}$$

Equation (2.21) is GIBBS' ADSORPTION ISOTHERM; it plays a central role in adsorption thermodynamics, because it establishes a direct relationship between the surface potential, π, and the chemical potentials of all species i in the adsorbed phase. Further details of its application are provided in Chapter 3.

Phase rule for adsorption

In contrast to VLE, in order to fix the *intensive state* of an adsorbed phase—i.e., give a complete description of the *condition* of a homogeneous phase and *all* its constituents, an additional intensive variable, π, was taken into account in Fundamental Relations (2.16). Therefore, the following phase rule applies [48, 59]

$$\mathfrak{F} = \mathfrak{C} - \mathfrak{P} + 3, \tag{2.22}$$

whereby, $\mathfrak{F}$ denotes the number of *degrees of freedom*—i.e., independent variables—that fix the state of the system; $\mathfrak{C}$ indicates the number of components and $\mathfrak{P}$ represents the number of phases at equilibrium, which for the *two-phase systems* considered in this work means $\mathfrak{P} = 2$.

Conditions for equilibrium

By definition, a system consisting of two or more distinct phases is found at *equilibrium* when [4, 48, 49, 56, 57, 118, 122]: *a)* it is found at constant temperature, T; *b)* it is found at constant pressure, p; and *c)* the *chemical potential* of each species i in any

co-existing phase does not change and is the same. These *conditions* are expressed as:

$$T^{\mathrm{I}} = T^{\mathrm{II}} = \cdots = T^{\mathcal{P}-1} = \mu_i^{\mathcal{P}}, \quad i = 1, \ldots, N, \tag{2.23a}$$

$$p^{\mathrm{I}} = p^{\mathrm{II}} = \cdots = p^{\mathcal{P}-1} = p^{\mathcal{P}} \ \text{ and} \tag{2.23b}$$

$$\mu_i^{\mathrm{I}} = \mu_i^{\mathrm{II}} = \cdots = \mu_i^{\mathcal{P}-1} = \mu_i^{\mathcal{P}}, \tag{2.23c}$$

for $\mathrm{I}, \mathrm{II}, \cdots, \mathcal{P}$ co-existing phases at equilibrium. For analysis of adsorption-based separations, two distinct phases, fluid phase, ℓ, and adsorbed phase, a, are typically identified, so that

$$\mu_i^{\ell} = \mu_i^a, \quad i = 1, \ldots, N \tag{2.24}$$

at constant temperature, T, and constant pressure, p [46, 48, 118]. This is illustrated schematically in Figure 2.4. Equation (2.24) is *crucial* to obtain working equations that link the theoretical concepts presented above to application. This will be described in more detail in Chapter 3 in order to derive the equations of IAST.

2.4 Adsorption from dilute liquid solutions

Special emphasis is given now to the case of adsorption from dilute liquid solutions, because it is required to describe IAST as applied to liquid phase adsorption chromatography, the focus of discussion in Part III. Adsorption from *dilute liquid solution* is a special case of adsorption of liquid adsorbates in mixtures*. Following Radke & Prausnitz [50], with ideas put forward earlier by Rowley & Innes [125–127], the *Fundamental Relation*, expressed in terms of Helmholtz free energy of adsorbed phase, A^a, Equation (2.16c), is written as:

$$\mathrm{d}A^a = -S^a \,\mathrm{d}T - p \,\mathrm{d}V^a - \pi \,\mathrm{d}\mathfrak{A} + \mu_{\mathsf{solv.}} \,\mathrm{d}n_{\mathsf{solv.}} + \sum_{i=1}^{N} \mu_i^a \,\mathrm{d}n_i^a, \tag{2.25}$$

with $A^a = f(S^a, T, p, V^a, \pi, \mathfrak{A}, \mu_{\mathsf{solv.}}, \mu_1, \cdots, \mu_N, n_{\mathsf{solv.}}, n_1^a, \cdots, n_N^a)$. The fact that a *condensed phase*—i.e., a liquid mixture—is put in contact with the adsorbent is taken into account by quantifying the moles of solvent, $n_{\mathsf{solv.}}$, and each solute, n_i^a. At constant temperature, T, equivalently to Equation (2.21), holds

$$\mathfrak{A} \,\mathrm{d}\pi = \sum_{i=1}^{N} n_i^m \,\mathrm{d}\mu_i^a, \tag{2.26a}$$

---

*One important historical reference is e.g., Ostwald & de Izaguirre [123] and the book by Kipling [124].

where

$$n_i^m \approx V_{\text{sln.}} \Delta c_i \tag{2.26b}$$

is an *invariant* adsorbed phase molar amount*, m, measured experimentally. This basically means that a known mass of adsorbent is put in contact—i.e., *immersed* or *flooded*—with a known volume of liquid solution and concentration of solutes; after equilibrium is established, differences in bulk liquid concentrations, Δc_i, can be quantified, providing an approximation of molar amounts of solutes, n_i^m, in the adsorbed phase. In this way, further specification of location of a *dividing surface* between adsorbed and bulk phases is conveniently avoided[†]. Due to the *indirect* character of n_i^m, an additional relationship involving actual adsorbed quantities, n_i^a, is established formally as [50]

$$n_i^m := n_i^a - \frac{c_i}{c_{\text{solv.}}} n_{\text{solv.}}^a. \tag{2.27}$$

Appendix A4 provides necessary details to understand Equation (2.27). In contrast to adsorption of gases, now two *condensed phases* are put in contact under controlled conditions to reach equilibrium. Even for the case of a single solute diluted in a solvent, molecules of both substances have access to adsorption sites, with the solute preferentially binding onto the solid matrix, and thus, displacing solvent molecules in the process.

In the case of dilute liquid solutions, therefore, the solvent is treated as INERT, which means that Equation (2.26a) is in reality of *approximate character only*, in light of the rigorous theoretical derivation discussed.

Considerations applicable to liquid adsorption chromatography It becomes necessary to reconcile the concepts of solution thermodynamics described in the previous sections with the adsorption equilibria measurement methods performed in liquid adsorption chromatography—e.g, those obtained with an HPLC equipment, as explained in Part III.

The papers of Wang *et al.* [129], Riedo & sz. Kováts [130], Eltekov *et al.* [131], Kazakevich & McNair [132], Fornstedt [133], and Vajda & Guiochon [134] provide ample information and *bridge the gap* between these equilibrium concepts and the intrinsically dynamic chromatographic techniques. The main outcome of the investigations of these authors confirms that the thermodynamic framework discussed in this section can

---

[*]Meaning that it is *invariant* w.r.t. the position of Gibbs' dividing surface—cf. Figure 2.4.

[†]Consult the books by Kipling [124] & Rouquerol *et al.* [128] for a useful explanation about Gibbs' dividing surface (GDS).

be applied to liquid adsorption chromatography systems measured experimentally, as explained in Part III of this work, under the considerations mentioned before.

Summary

While most of the adsorption equilibrium models presented in this chapter were originally developed to characterize adsorption from the gas phase, many of the models can also be used for bulk liquids and dilute liquid solutions, with careful use and interpretation of the constituent model parameters [14]. IAST, an application of solution thermodynamics—cf. Table 2.5, is the only multicomponent adsorption equilibrium model that uses *exclusively* information about adsorption equilibrium of INDIVIDUAL COMPONENTS in a *thermodynamically consistent fashion*. This is one of the main reasons for its widespread application.

A possibility that has been explored for adsorption from a gaseous mixture is the application of a two-dimensional EQUATION OF STATE (EOS)—see e.g., Hoory & Prausnitz [70], Talu *et al.* [135] and Appel *et al.* [72].

In the particular case of liquid adsorption chromatography, well-established models to describe non-ideality, commonly applied to other equilibrium tasks, e.g., VLE and LLE, are *emulated* with model parameters being fitted to experimentally observed adsorption equilibrium data in order to apply RAST. Examples of this empirical approach have been documented in [136] and [111]. Other models, such as NRTL EQUATION [137] and WILSON EQUATION [138], with minor modifications to fulfill thermodynamic consistency, have also been implemented.

Chapter 3

Ideal Adsorbed Solution Theory[*]

"...All theories have strengths and weaknesses ..."

– Sofie Bartholdy *et al.* in [40]

Introduction

$\mathbf{A}$TTENTION is now focused on Ideal Adsorbed Solution Theory (IAST) [38], a predictive multicomponent adsorption equilibrium model, originally developed to treat gas phase adsorption, which is thermodynamically consistent [38, 139], and later extended to address dilute liquid solutions [50]. Discussion of its derivation, starting from basic equations of thermodynamics introduced in Chapter 2, follows in the next section.

---

[*]CHAPTER DISCLAIMER. Partial contents of this chapter have been reported in: *"A Method for Efficiently Solving the IAST Equations with an Application to Adsorber Dynamics"* [53]. The information is presented as part of this dissertation and it is an original published contribution to the field in a peer-reviewed journal. There is none whatsoever intention of self-plagiarism; the information serves rather as complementary content to this dissertation. Furthermore, the publishing company has granted partial reproduction of the contents in the article mentioned above. [License No.: **3743030164049**, requested and obtained on Nov. 6$^{\text{th}}$, 2015 from John Wiley & Sons, Inc. through Copyright Clearance Center.]

3.1 Model description & assumptions made

Equilibrium between fluid & adsorbed phases The conditions for equilibrium given by Equations (2.23), in particular

$$\mu_i^\ell = \mu_i^a, \quad i = 1, \ldots, N, \tag{2.24}$$

are applied in order to establish a relationship between concentrations in the fluid phase, ℓ, and adsorbed phase, a. The chemical potential of species, i, in a *dilute solution* is given by [4, 48, 50, 118]:

$$\mu_i^\ell = g_i^*(T) + \Re T \ln \frac{c_i}{c_i^*}. \tag{3.1}$$

Likewise, the chemical potential of component, i, in the adsorbed phase is written as [38]:

$$\mu_i^a = g_i^*(T) + \Re T \ln c_i^0(T, \pi) + \Re T \ln \left[\gamma_i^a x_i \right]. \tag{3.2}$$

The reference state applied, indicated by $*$, is the same for both phases. The second summand in (3.2) contains *hypothetical* fluid phase concentrations, c_i^0, at constant temperature, T, and spreading pressure, π, of the mixture. x_i is the molar fraction of species i in the adsorbed phase. Substitution of (3.1) and (3.2) in condition (2.24) yields the equilibrium expression

$$c_i = c_i^0(T, \pi) \, \gamma_i^a \, x_i, \quad i = 1, \ldots, N, \tag{3.3}$$

whereby $\gamma_i^a = f(T, \pi, x_1, \cdots, x_N)$ are activity coefficients in the adsorbed phase that describe deviations from ideal behavior [38, 122].

Definition of an ideal adsorbed phase Firstly, an equation applicable to the concept of *ideal adsorbed solution* is obtained by taking (3.3) and allowing each adsorbed phase activity coefficient, $\gamma_i^a \to 1$, which produces an expression analogous to Raoult's law:

$$c_i = c_i^0(T, \pi) \, x_i. \tag{3.4}$$

Secondly, in an ideal adsorbed phase, molecules of all adsorbates $i = 1, \ldots, N$, interact with each other in such a way that they occupy the same surface area, a_i^0, as if they would have separately adsorbed and equilibrated *alone* with the same concentration at the same temperature, T, and spreading pressure, π, of the considered mixture—an expression of the two-dimensional variant of Amagat's law for volumes [38]. Henceforth

holds:

$$a_{\text{tot}} = \sum_{i=1}^{N} a_i^0 x_i, \tag{3.5}$$

where a_{tot} represents the total area occupied by species, $i = 1, \ldots, N$, in direct proportion to their molar fractions in the adsorbed phase, x_i—i.e., an *ideal mixture*. Table 3.1 summarizes the model assumptions taken into account in IAST.

Table 3.1: IAST competitive adsorption model assumptions.

No.	Assumption
I	Ideal mixing of the adsorbates within the adsorbent, i.e., *excess energy of mixing* of the adsorbates is *zero*.
II	Ideal fluid phase.

In many real systems the description given above for an *ideal solution* does not apply, as two neglected aspects play a fundamental role in competitive adsorption [14, 46]: *a) adsorbate-adsorbate* interactions, crucial if multi-layer adsorption takes place—cf. BET isotherm, Table 3.4, p. 38, Equation (2.3i); & *b)* adsorbent *surface heterogeneities*—see e.g., [96, 98]. These aspects in turn, can lead to well-known, but complicated phenomena, such as *selectivity reversal* and *azeotropic behavior*—see e.g., [140].

Surface potential, π   Additional relations are required to complete the model due to state variable, π. At equilibrium

$$\pi = \pi_1(c_1^0) \overset{!}{=} \cdots \overset{!}{=} \pi_N(c_N^0) \tag{3.6}$$

holds, where each of the $i = 1, \ldots, N$ adsorbable components, i.e., adsorbates, exerts a spreading pressure, π_i, proportional to *fictitious*[*] fluid phase concentrations, c_i^0, i.e., the concentration that would be required by an adsorbate *alone* to generate the surface potential, π, possessed by the mixture. Further, hypothetical fluid phase concentrations, c_i^0, appearing in (3.4), need to be calculated to satisfy Equation (3.6). With the help of Gibbs' adsorption isotherm (2.21) for a single species i and equilibrium condition (2.24)

---

[*]The term *fictitious* is used interchangeably with the term *hypothetical*.

written in differential form, $\mathrm{d}\mu_i^a = \mathrm{d}\mu_i^\ell$, holds:

$$- \mathfrak{A}\,\mathrm{d}\pi_i + n_i^a\,\mathfrak{R}T\,\mathrm{d}\ln c_i = 0. \tag{3.7}$$

Introducing $\mathcal{A} \equiv \mathfrak{A}/V^a$ and $q_i^0 \equiv n_i^a/V^a$ to refer to the volume of adsorbent, V^a, yields*

$$- \mathcal{A}\,\mathrm{d}\pi + \mathfrak{R}T\,\frac{q_i}{c_i}\,\mathrm{d}c_i = 0, \tag{3.8}$$

which upon integration, establishes the direct dependency of *state variable* π_i w.r.t. measurable single component equilibria, $q_i^0 = f(c_i^0)$, by

$$\Pi_i = f(c_i^0) \equiv \frac{\mathcal{A}}{\mathfrak{R}T}\pi_i(c_i^0) = \int\limits_0^{c_i^0} \frac{q_i^0}{s}\,\mathrm{d}s, \tag{3.9}$$

whereby, Π_i, the *reduced* spreading pressure—reduced potential—is introduced for convenience. It has units $\left[\mathsf{mol/m^3_{ads.}}\right]$ or $\left[\mathsf{mol/kg_{ads.}}\right]$, following the applied definitions of $\mathcal{A}$ and q_i^0 above. The adsorbed phase molar fractions, x_i, fulfill the mass balance

$$\sum_{i=1}^N x_i = \sum_{i=1}^N \frac{c_i}{c_i^0} = 1, \tag{3.10}$$

thus completing the relationship between hypothetical fluid phase concentrations, c_i^0 and surface potential, π. The total adsorbed concentration, q_{tot}, is given by

$$q_{\mathrm{tot}} = f(c, c^0) = \left[\sum_{i=1}^N \frac{x_i}{q_i^0}\right]^{-1} = \left[\sum_{i=1}^N \frac{1}{q_i^0}\frac{c_i}{c_i^0}\right]^{-1}, \tag{3.11}$$

in accord with the description of an *ideal adsorbed phase* given by Equation (3.5). The concentrations c_i^0 are therefore KEY VARIABLES in the calculation of this model. According to Equation (3.9), each c_i^0 should be such, that it *builds-up* the necessary surface potential, π, in order to fulfill equilibrium condition (3.6). These quantities can become quite large for low values of x_i, i.e., $c_i^0 \gg c_i$, which is in particular probable for *less adsorbed* compounds, as exemplified by re-casting Equation (3.4) as

$$c_i^0 = \frac{c_i}{x_i}, \quad i = 1, \ldots, N. \tag{3.4'}$$

---

*Under the assumption that V^a is *invariant* throughout the adsorption process.

Finally, adsorbed phase concentrations are calculated directly from Equation (3.11):

$$q_i = f(c, c^0) = q_{\text{tot}}\, x_i, \quad i = 1, \ldots, N. \tag{3.12}$$

Table 3.2 summarizes the model equations of IAST.

Table 3.2: Summary of IAST equations [38, 50].

Description	Equation	
Raoult's law (adsorption)	$c_i = c_{\text{tot}}\, y_i = c_i^0(T, \pi)\, x_i$	(3.4)
Equilibrium condition	$\Pi \equiv \Pi_1 \overset{!}{=} \cdots \overset{!}{=} \Pi_N$	(3.6)
Spreading pressure	$\Pi_i = f(c_i^0) \equiv \dfrac{\mathcal{A}}{\mathfrak{R}\,T}\pi_i(c_i^0) = \displaystyle\int_0^{c_i^0} \dfrac{q_i^0}{s}\,\mathrm{d}s$	(3.9)
Closure	$\displaystyle\sum_{i=1}^{N} x_i = \sum_{i=1}^{N} \dfrac{c_i}{c_i^0} = 1$	(3.10)
Total adsorbed phase concentration	$q_{\text{tot}} = \left[\displaystyle\sum_{i=1}^{N} \dfrac{x_i}{q_i^0}\right]^{-1} = \left[\displaystyle\sum_{i=1}^{N} \dfrac{1}{q_i^0}\dfrac{c_i}{c_i^0}\right]^{-1}$	(3.11)
Adsorbed phase concentration, component i	$q_i = q_{\text{tot}}\, x_i, \quad i = 1, \ldots, N$	(3.12)

3.2 Consistency of single component adsorption isotherms & limit behavior of solutions

The *input information* provided to IAST needs to fulfill a *consistency requirement*; this means basically that equations—i.e., models—describing single component adsorption isotherms:

1. possess a *well-established* Henry limit as discussed in Section 2.1.2; &

2. may be integrated, at least in principle, for $c_i^0 \to \infty$, $i = 1, \ldots, N$.

These two requirements become clear by inspection of the integral expression of Gibbs' adsorption isotherm, Equation (3.9). In practice, data are difficult to gather close to the lower bound of the theoretically available concentration range, $[0, \infty)$, while the upper

bound is only a mathematical *construct* or *aid*, not related to the physical system, as binding of adsorbates is in reality finite, and as such, bounded.

IAST equilibrium calculations are in particular prone to error for the *lower* concentration range, since, for *general increasing isotherms*, this is the region where changes in equilibrium values and therefore in surface potential, Π, occur more suddenly, especially for data with steep slopes at low concentration values, near the origin—cf. Table 2.3, p. 20. This fact can also be observed in Figure 2.2, p. 15, by inspecting the behavior of $\mathrm{d}q_i/\mathrm{d}c_i$ for several isotherm types.

A second aspect of *physical consistency* has to do with the limit behavior of N-component solutions. By assumption of existence of an IAST solution, $q = f(c)$, whereby

$$q = [\, q_1, \, \ldots, \, q_N \,]^T ; \ \ q_i = f(c_1, \, \ldots, \, c_N), \ \ i = 1, \, \ldots, N,$$

let an arbitrarily chosen component $c_j \to 0$; consequently, $q_j \to 0$, i.e., *j vanishes*. When this limit situation occurs, the $(N-1)$-component IAST equilibria should be recovered.

3.3 Methods of solution for IAST equations

3.3.1 Difficulties encountered when solving IAST equations

The main difficulty encountered stems from the fact that Gibbs' adsorption isotherm, Equation (3.9), has an upper limit of integration, c_i^0, which is unknown. Furthermore, the equations for the total adsorbed phase concentration, q_{tot}, and the components' concentrations, q_i, have explicit expressions depending on c_i^0. Even for known upper integration limit, c_i^0, Equation (3.9) provides the functional dependency

$$\Pi = \Pi_i = f(c_i^0), \tag{3.13}$$

whereas its inverse,

$$c_i^0 = f^{-1}(\Pi), \tag{3.14}$$

is actually what is required for the solution. These difficulties, which shall be addressed again in Chapter 4, are summarized in the following items:

ITEM 1: Integration of Equation (3.9)—performed via an analytical expression for q_i^0/c_i^0— cf. Table 3.3—or via truncation of a series expansion; calculated numerically otherwise.

ITEM 2: Inversion of $\Pi_i = f(c_i^0)$—performed analytically when possible, numerically otherwise.

ITEM 3: Initialization of the numerical method to solve specific nonlinear algebraic equations, i.e., provide suitable starting *guess* values—in the case it may be required by the applied numerical method.

Table 3.3: Expressions for quotients, q_i^0/c_i^0, of selected isotherm models, cf. Table 2.2, p. 17.

Isotherm	Quotient	
Langmuir [65]	$q_i^{\text{sat}} \dfrac{b_i}{1 + b_i c_i^0}$	(3.15a)
Bi-Langmuir [14]	$q_{i1}^{\text{sat}} \dfrac{b_{i1}}{1 + b_{i1} c_i^0} + q_{i2}^{\text{sat}} \dfrac{b_{i2}}{1 + b_{i2} c_i^0}$	(3.15b)
Freundlich [7, 14]	$a_i\, c_i^{0\,\frac{1-\nu_i}{\nu_i}}$	(3.15c)
Quadratic [43]	$q_i^{\text{sat}} \dfrac{b_{i1} + 2\, b_{i2} c_i^0}{1 + b_{i1} c_i^0 + b_{i2} c_i^{0\,2}}$	(3.15d)
Quadratic plus Langmuir [51, 52]	$q_{i1}^{\text{sat}} \dfrac{b_{i1} + 2\, b_{i2} c_i^0}{1 + b_{i1} c_i^0 + b_{i2} c_i^{0\,2}} + q_{i2}^{\text{sat}} \dfrac{b_{i3}}{1 + b_{i3} c_i^0}$	(3.15e)
O'Brien & Myers [77]	$q_i^{\text{sat}} \left[\dfrac{b_i}{1 + b_i c_i^0} + \dfrac{\sigma_i^2\, b_i\,(1 - b_i c_i^0)}{2\,(1 + b_i c_i^0)^3} \right]$	(3.15f)
Tóth [78, 79]	$q_i^{\text{sat}} \dfrac{b_i}{\left[1 + \left[\, b_i c_i^0 \,\right]^{\nu_i} \right]^{\frac{1}{\nu_i}}}$	(3.15g)
Redlich-Peterson [69, 80]	$\dfrac{a_i}{1 + b_i c_i^{0\,\nu_i}}$	(3.15h)
BET [14, 44, 66]	$q_i^{\text{sat}} \dfrac{b_{i\text{S}}}{\left[1 - b_{i\text{L}} c_i^0 \right]\left[1 - b_{i\text{L}} c_i^0 + b_{i\text{S}} c_i^0 \right]}$	(3.15i)
Sips [36, 86]	$q_i^{\text{sat}} \dfrac{b_i^{\frac{1}{\nu_i}}\, c_i^{0\,\frac{1-\nu_i}{\nu_i}}}{1 + \left[\, b_i c_i^0 \,\right]^{\frac{1}{\nu_i}}}$	(3.15j)

Table 3.4: *Reduced* potentials, $\Pi_i = f(c_i^0)$, obtained with Equation (3.9).

Model	Result	
Langmuir [65]	$\Pi_i = q_i^{\text{sat}} \ln \left[1 + b_i c_i^0 \right]$	(3.16a)
Bi-Langmuir [14]	$\Pi_i = q_{i1}^{\text{sat}} \ln \left[1 + b_{i1} c_i^0 \right] + q_{i2}^{\text{sat}} \ln \left[1 + b_{i2} c_i^0 \right]$	(3.16b)
Quadratic [43]	$\Pi_i = q_i^{\text{sat}} \ln \left[1 + b_{i1} c_i^0 + b_{i2} c_i^{0\,2} \right]$	(3.16c)
Quadratic plus Langmuir [51, 52]	$\Pi_i = q_{i1}^{\text{sat}} \ln \left[1 + b_{i1} c_i^0 + b_{i2} c_i^{0\,2} \right] + q_{i2}^{\text{sat}} \ln \left[1 + b_{i3} c_i^0 \right]$	(3.16d)
O'Brien & Myers [77]	$\Pi_i = q_i^{\text{sat}} \left[\ln \left[1 + b_i c_i^0 \right] + \dfrac{\sigma_i^2 b_i c_i^0}{2 \left[1 + b_i c_i^0 \right]^2} \right]$	(3.16e)
Tóth [78, 79] [a]	$\Pi_i = \theta_i - \dfrac{\theta_i}{\nu_i} \ln \left[1 - \theta_i^{\nu_i} \right] - \displaystyle\sum_{k=1}^{\infty} \dfrac{\theta_i^{k\nu_i + 1}}{k\nu_i \left[k\nu_i + 1 \right]},$ $\qquad \theta_i \equiv \dfrac{q_i^0}{q_i^{\text{sat}}}, \ q_i^0 = f(c_i^0)$	(3.16f)
Redlich-Peterson [69, 80] [b]	$\Pi_i = a_i c_i^0 \cdot {}_2\mathsf{F}_1 \left[1, \dfrac{1}{\nu_i}, 1 + \dfrac{1}{\nu_i}, -b_i c_i^{0\,\nu_i} \right]$	(3.16g)
BET [14, 44, 66]	$\Pi_i = -\dfrac{q_i^{\text{sat}} \ln \left[1 - b_{i\mathsf{L}} c_i^0 \right]}{b_{i\mathsf{L}}} + \dfrac{q_i^{\text{sat}} \ln \left[1 - b_{i\mathsf{L}} c_i^0 + b_{i\mathsf{S}} c_i^0 \right]}{b_{i\mathsf{L}} - b_{i\mathsf{S}}}$	(3.16h)
Dubinin-Radushkevich (D-R) [7, 83, 84, 92] [c]	$\Pi_i = q_i^{\text{sat}} \exp \left[-\dfrac{1}{4B_i^2} \right]$ $\qquad + q_i^{\text{sat}} \dfrac{\sqrt{\pi}}{2B_i} \left[\mathsf{erf} \left[\dfrac{1}{2B_i} \right] - \mathsf{erf} \left[B_i \ln \left[\dfrac{c_i^{\text{sat}}}{c_i^0} \right] \right] \right]$	(3.16i)
UNILAN [79]	$\Pi_i = \dfrac{q_i^{\text{sat}}}{2\eta_i} \displaystyle\int_{-\eta_i}^{\eta_i} \ln \left[1 + \left(\dfrac{c_i^0}{\kappa_i} \right) \exp \zeta \right] \, d\zeta, \ \eta_i > 0$	(3.16j)
Sips [36, 86]	$\Pi_i = \nu_i \, q_i^{\text{sat}} \ln \left[1 + \left[b_i c_i^0 \right]^{\frac{1}{\nu_i}} \right]$	(3.16k)
Fractal BET [87] [d]	$\Pi_i = q_i^{\text{sat}} \dfrac{b_{i\mathsf{S}}}{b_{i\mathsf{L}}} \left[\begin{array}{l} \ln \left[1 - b_{i\mathsf{L}} c_i^0 \right] \ln \left[\dfrac{b_{i\mathsf{L}} \left(1 - b_{i\mathsf{L}} c_i^0 + b_{i\mathsf{S}} c_i^0 \right)}{b_{i\mathsf{S}}} \right] + \\[2mm] \mathsf{Li}_2 \left[b_{i\mathsf{L}} c_i^0 \right] + \mathsf{Li}_2 \left[\dfrac{\left[b_{i\mathsf{L}} - b_{i\mathsf{S}} \right] \left[b_{i\mathsf{L}} c_i^0 - 1 \right]}{b_{i\mathsf{S}}} \right] \end{array} \right]$	(3.16l)

a. $q_i^0 = f(c_i^0)$ from isotherm expression, Eq. (2.3g).
b. Uses the 4-argument hypergeometric function ${}_2\mathsf{F}_1[(\cdot, \cdot); \cdot; \cdot]$.
c. In the second summand of the r.h.s., $\pi = 3.14 \cdots$.
d. Employs the single argument polygeometric function $\mathsf{Li}_2[\cdot]$. Computed with MATHEMATICA $^{\circledR}$ [141].

By inspection of the IAST equations a standard approach for their solution would be as follows. Single component isotherm models, i.e., algebraic equations, are introduced in Equation (3.9) that fit well to experimental measurements. IAST has the flexibility that the best suitable single component adsorption isotherm model for each of the independently measured experimental data sets should be used. It is necessary to keep in mind though, that the IAST prediction is particularly sensitive to the accuracy of the

equilibrium data in the low concentration region, because this defines the starting point to *build-up* in spreading pressure—i.e., surface potential—by integration of (3.9). These integrals can be computed either in closed form, as listed in Table 3.4, or approximated numerically. In general, this procedure yields a nonlinear algebraic system.

3.3.2 Analytical solutions

Taylor series expansions of LeVan & Vermeulen [142]   These authors developed successive expansions to approximate the functional relationship $\Pi = f(c_1, c_2)$; the number of terms in the expansion determines the achievable computational accuracy. These are *cheap* to evaluate and provide an analytical approximation $q_i = f(c_1, c_2)$, $i = 1, 2$ when the single component isotherms are either expressed by Langmuir (2.3a) or Freundlich (2.3c) equations. They suggest the possibility to apply their technique to any type of single component isotherm for which the explicit expression, $c_i^0 = f^{-1}(\Pi)$ exists—cf. ITEM 1 & ITEM 2.

Padé approximants of Frey & Rodrigues [143]   Two ideas to perform IAST calculations are suggested by these authors. A *Padé approximant* can be used to represent $c_i^0 = f^{-1}(\Pi)$. As a result, an explicit substitute representation, $q_i = f(c)$, $i = 1, \ldots, N$, is obtained, as done by LeVan & Vermeulen [142]. The accuracy of the expression depends on the kind of approximant employed. An important idea presented in this publication is to fit the *equivalent* Padé representation *directly* to experimental equilibrium data. One pitfall that can be quickly identified with this method is related to the ability of the Padé approximation to represent the equilibrium data accurately over sufficiently wide concentration ranges, as required for IAST calculations, in general—cf. Equation (3.4′) and Section 3.2.

Solution for competitive binary mixtures with the Quadratic model [43]   Ilić *et al.* published an analytical solution where *each* single component adsorption isotherm is expressed by the Quadratic isotherm model, Equation (2.3d); the problem in essence solves a cubic polynomial, whose solution can be obtained using the ansatz devised by Nickalls [144] via reformulation of the analytical formulæ of Cardano [145].

Solution for competitive binary mixtures of Tarafder *et al.* [44]   A general approach for binary mixtures of compounds exhibiting either BET (Equation (2.3i)),

Langmuir (Equation (2.3a)) or Quadratic (Equation (2.3d)) isotherm courses was proposed and demonstrated by these researchers.

It is interesting to observe that up to now, the task to obtain closed form solutions to IAST equations has focused almost exclusively on competitive binary mixtures, i.e., $N = 2$. The general case with arbitrary, $N \geq 3$, components seems at this point intractable[*]. Despite of this, closed form solutions for two components are a *fundamental tool* for preliminary calculation and validation of solutions for IAST equations, particularly valuable to analyze errors of numerically obtained estimations—this is addressed again in connection with the developed solution approach in Chapter 5.

3.3.3 Numerical solutions

Two widely applied *strategies*, designated as **Case I** and **Case II**—presented below in detail—are described by Do [36] and were originally presented by Myers & Valenzuela [78, 79]. The strategy selection basically depends on whether c_i^0 can be expressed as a function of Π or not—cf. ITEM 1 & ITEM 2, p. 36.
Recently Mangano *et al.* [146] have presented a detailed analysis of the convergence of *these* general solution methods. Their contribution corrects possible shortfalls in providing adequate starting values to these NEWTON-TYPE algorithms. Additional concepts worth mentioning, which aim at speeding up IAST calculations, were also presented recently by Santos *et al.* [147] and Santori *et al.* [148].

Case I The simplest calculation is performed in two steps:

1. Each equation, $\Pi = f(c_i^0)$, $i = 1, \ldots, N$, is *integrated directly*—cf. ITEM 1; Table 3.4 provides some examples of this result for several isotherm models.

2. Each of the equations $\Pi = f(c_i^0)$ is now *analytically inverted* to provide explicit functions in Π, i.e. $c_i^0 = f^{-1}(\Pi)$, $i = 1, \ldots, N$—cf. ITEM 2.

These expressions in turn, are substituted in Equation (3.10), yielding the nonlinear algebraic equation

$$\mathcal{F}(\Pi) := \sum_{i=1}^{N} \frac{c_i}{c_i^0} - 1 = 0, \quad i = 1, \ldots, N, \tag{3.17}$$

---

[*]This is most likely to change in the near future, as interest in IAST is perpetuated.

which possesses the single unknown Π. An iterative procedure to treat Equation (3.17) is given in detail in Algorithm 3.1, using the Newton-Raphson method—see e.g., [36, 149–152].

1: **procedure** IAST_CASE1$(c = [c_1, \ldots, c_N]^T)$ ▷ Get equilibrium values $q = f(c)$

2:      $\Pi^{[0]} \leftarrow \Pi^{\mathsf{guess}}$

3:      **while** $|\Pi^{[k+1]} - \Pi^{[k]}| \leq \varepsilon_{\mathsf{Tol.}}$ **do**   ▷ Stopping criterium

4:         $\Delta\Pi^{[k+1]} \leftarrow -\dfrac{\mathcal{F}(\Pi^{[k]})}{\mathcal{F}'(\Pi^{[k]})}$

5:         $\Pi^{[k+1]} \leftarrow \Delta\Pi^{[k+1]} + \Pi^{[k]}$

6:         $\Pi^* \leftarrow \Pi^{[k+1]}$

7:      **end while**

8:      **return** Π^* ▷ Π^* is the sought after *root*

9:      $c_i^{0,*} \leftarrow f(\Pi^*); \; i = 1, \ldots, N$

10:      $q_i^{0,*} \leftarrow f(c_i^{0,*})$

11:      $q_i \leftarrow \left[\sum\limits_i^N \dfrac{1}{q_i^{0,*}} \dfrac{c_i}{c_i^{0,*}} \right]^{-1} \left[\dfrac{c_i}{c_i^{0,*}} \right]; \; i = 1, \ldots, N$

12:      $q \leftarrow [q_1, \ldots, q_N]^T$

13: **end procedure**

Algorithm 3.1: IAST calculation for Case I; see among others [36, 78, 79].

Case II   If *integration & inversion* are not available in closed form, a *second iteration loop* has to be embedded in the computation given by Algorithm 3.1.

$$\Pi^{[k+1]} = \Pi^{[k]} - \frac{\mathcal{F}^{[k]}}{\mathcal{F}'^{[k]}} \tag{3.18a}$$

where

$$\mathcal{F}' \equiv \frac{\mathrm{d}\mathcal{F}}{\mathrm{d}\Pi} = \sum_{i=1}^{N} \frac{\partial \mathcal{F}}{\partial c_i^0} \frac{\partial c_i^0}{\partial \Pi}. \tag{3.18b}$$

The terms $\partial c_i^0 / \partial \Pi$ in Equation (3.18b) are computed with Gibbs adsorption isotherm, Equation (3.9), written in differential form:

$$\frac{\partial c_i^0}{\partial \Pi} = \frac{c_i^0}{q_i^0}. \tag{3.18c}$$

In this case an outer iteration loop is required to estimate Π and an inner loop to obtain $c_i^0(\Pi)$, as listed in Algorithm 3.2. So suitable starting values, Π^{guess} & $c^{0,\mathsf{guess}}$, are required for each of these iteration loops.

1: **procedure** $\text{IAST\_CASE2}(c = [\,c_1,\,\ldots,\,c_N\,]^T)$ ▷ Get equilibrium values $q = f(c)$

2:     $\Pi^{[0]} \leftarrow \Pi^{\text{guess}}$

3:     **while** $|\Pi^{[k+1]} - \Pi^{[k]}| \leq \varepsilon_{\text{Tol.}}$ **do**   ▷ Stopping criterium, *outer loop*

4:        **for** $i \leftarrow 1, N$ **do**

5:           $c_i^{0[0]} \leftarrow c_i^{0,\,\text{guess}}$

6:           **while** $|c_i^{0[\ell+1]} - c_i^{0[\ell]}| \leq \varepsilon_{\text{Tol.}}$ **do**   ▷ Stopping criterium, *inner loop*

7:              $\Delta c_i^{0[\ell+1]} \leftarrow -\dfrac{\mathcal{G}(c_i^{0[\ell]})}{\mathcal{G}'(c_i^{0[\ell]})}$

8:              $c_i^{0[\ell+1]} \leftarrow \Delta c_i^{0[\ell+1]} + c_i^{0[\ell]}$

9:              $c_i^{0,*} \leftarrow c_i^{0[\ell+1]}$

10:           **end while**

11:           **return** $c_i^{0,*}$

12:        **end for**

13:        $c^{0,*} \leftarrow \left[\,c_1^{0,*},\,\ldots,\,c_N^{0,*}\,\right]^T$

14:        $\Delta\Pi^{[k+1]} \leftarrow -\dfrac{\mathcal{F}(\Pi^{[k]}(c^{0,*}))}{\mathcal{F}'(\Pi^{[k]}(c^{0,*}))}$

15:        $\Pi^{[k+1]} \leftarrow \Delta\Pi^{[k+1]} + \Pi^{[k]}$

16:        $\Pi^{*} \leftarrow \Pi^{[k+1]}$

17:     **end while**

18:     **return** $\Pi^{*},\ c^{0,*}$ ▷ $\Pi^{*},\ c^{0,*}$ are the sought after *roots*

19:     $q_i^{0,*} \leftarrow f(c_i^{0,*});\ i = 1,\,\ldots,\,N$

20:     $q_i \leftarrow \left[\displaystyle\sum_i^N \dfrac{1}{q_i^{0,*}}\dfrac{c_i}{c_i^{0,*}}\right]^{-1}\left[\dfrac{c_i}{c_i^{0,*}}\right];\ i = 1,\,\ldots,\,N$

21:     $q \leftarrow [\,q_1,\,\ldots,\,q_N\,]^T$

22: **end procedure**

Algorithm 3.2: IAST calculation for Case II; see among others [36, 78, 79].

Method of O'Brien & Myers [77, 153]   This is the last method to be addressed in detail, since it is closely related to the solution method developed in Chapter 4. These authors looked closely at Equation (3.6) and realized that it can be expressed as a series

of equalities

$$\Pi_1(c_1^0) = \Pi_2(c_2^0), \tag{3.19a}$$

$$\Pi_2(c_2^0) = \Pi_3(c_3^0), \tag{3.19b}$$

$$\vdots$$

$$\Pi_{N-2}(c_{N-2}^0) = \Pi_{N-1}(c_{N-1}^0), \tag{3.19c}$$

providing $N-1$ equations, whereby *only* fictitious concentrations, c_i^0, $i = 1, \ldots, N$, appear. Equation

$$\sum_{i=1}^{N} \frac{c_i}{c_i^0} = 1, \tag{3.10}$$

completes system (3.19), so that it is *properly* determined—i.e., N equations for N unknowns. This approach has significant and important advantages to other methods:

1. it conveniently exploits the structure of IAST equations by emphasizing that obtaining $c^0 = \begin{bmatrix} c_1^0, \ldots, c_N^0 \end{bmatrix}^T$ is a KEY ASPECT to solve the problem, since the rest of IAST equations, viz. Equation (3.11) & Equations (3.4), can be expressed as functions of c^0 ONLY;

2. furthermore, equalities (3.19) can be re-cast as [153]

$$\Pi_1(c_1^0) = \Pi_N(c_N^0), \tag{3.20a}$$

$$\Pi_2(c_2^0) = \Pi_N(c_N^0), \tag{3.20b}$$

$$\vdots$$

$$\Pi_{N-1}(c_{N-1}^0) = \Pi_N(c_N^0), \tag{3.20c}$$

significantly reducing the computational cost needed to solve the resulting nonlinear algebraic system of equations via application of NEWTON-RAPHSON method, due to the particular structure of (3.20).

Just as in other iterative methods presented before—cf. Algorithm 3.1 & 3.2, successful calculation with this method relies on provision of suitable starting values, $c^{0,\,\text{guess}}$, to perform iterations. Moreover, this method presumes construction of (3.20), which means that if *integration*— ITEM 1—of Equation (3.9) is not available in closed form, for *any* of the single component adsorption isotherms involved, the method does not work.

Summary

The derivation of the IAST model was explained, starting from the definition of an ideal adsorbed solution and subsequently applying the equations of thermodynamics, discussed in Sections 2.3 & 2.4. Several established solution strategies were outlined, and most importantly, acknowledging three factors, viz. ITEM 1, ITEM 2 & ITEM 3, p. 36, which are crucial to propose and implement a novel solution principle, the subject addressed in depth in Chapter 4.

It is also important to mention some PRACTICAL DIFFICULTIES, encountered when IAST is applied to gathered experimental data, including:

1. limited availability of equilibrium data in the low concentration range, i.e., $c_i^0 \to 0$;

2. limited accuracy of measured data;

3. reliable extrapolations from measured data, beyond the highest measured equilibrium value;

4. fitted adsorption isotherm equations to single component equilibria; &

5. existence of actual saturation limits or solubility limits for specific adsorbate/adsorbent systems—thus reinforcing the concept of fictitious (hypothetical) fluid phase concentrations.

Dealing with these practical difficulties is *essential* for correct application of the model. While the assumption of an ideally-behaved adsorbed phase seems rather restrictive, it has been proven to work in many practical cases. One of the key reasons behind this has to do with the fact that no actual restrictions are imposed on the *shape* of the single component equilibria, $q_i^0 = f(c_i^0)$. Moreover, an ideal adsorbed solution can be considered a *limit case* for real adsorbed phases.

Chapter 4

Efficient approach to solve IAST equations[*]

". . . Good. That's what I wrote them [the papers] *for, so people could use them."*

– Shivaji Sircar at FOA 11, Baltimore, MD, USA

Introduction

MODEL equations for IAST have been introduced and explained in detail in Chapter 3. Standard, documented techniques for solving the model were explained and discussed as well. Now attention is set on an efficient approach that can incorporate a large number of single component isotherm models in a thermodynamically consistent way. The method is *accurate, robust, efficient*, and *easy to implement*; its derivation and justification, together with its mathematical features, are explained next.

---

[*]CHAPTER DISCLAIMER. Partial contents of this chapter have been reported in: *"A Method for Efficiently Solving the IAST Equations with an Application to Adsorber Dynamics"* [53]. The information is presented as part of this dissertation and it is an original published contribution to the field in a peer-reviewed journal. There is none whatsoever intention of self-plagiarism; the information serves rather as complementary content to this dissertation. Furthermore, the publishing company has granted partial reproduction of the contents in the article mentioned above. [License No.: **3743030164049**, requested and obtained on Nov. 6th, 2015 from John Wiley & Sons, Inc. through Copyright Clearance Center.]

4.1 Solution method

If a closer look is taken at the equilibrium condition given by Equation (3.6), it is easily observed that it can be formulated as $N - 1$ equalities:

$$\Pi_1(c_1^0) = \Pi_2(c_2^0),$$
$$\Pi_1(c_1^0) = \Pi_3(c_3^0),$$
$$\vdots$$
$$\Pi_1(c_1^0) = \Pi_N(c_N^0),$$

supplemented with

$$\frac{c_1}{c_1^0} + \frac{c_2}{c_2^0} + \cdots + \frac{c_N}{c_N^0} = 1$$

(4.1)

to yield a well determined system of size N in the $c^0 = \left[\, c_1^0, \ldots, c_N^0 \,\right]^T$ unknowns. This starting point was already documented by O'Brien & Myers for their calculation method [153], as explained in Section 3.3.3, p. 40.

Now, it can be inferred further that if equalities in (4.1) hold true, then

$$c_k^0 = \psi_k(c_1^0), \quad k = 1, \ldots, N \tag{4.2}$$

also holds.

> ☆ *The solution principle, as expressed by the—simple—function ψ_k*
> *in (4.2), is the core of this dissertation.*

With help of Equation (4.2), *implicit differentiation*[*] can be applied *directly* to the $N-1$ equalities (4.1), so that

$$\Pi_k'(\, c_k^0(c_1^0)\,) \, \frac{\mathrm{d}}{\mathrm{d}c_1^0} c_k^0(c_1^0) = \Pi_1'(c_1^0), \quad k = 1, \ldots, N \tag{4.3}$$

and the following *decoupled, non-autonomous* initial value problem (IVP)[†] can be formulated

$$\frac{\mathrm{d}c_k^0}{\mathrm{d}c_1^0} = \frac{\Pi_1'(c_1^0)}{\Pi_k'(c_k^0)} = \frac{q_1^0(c_1^0)/c_1^0}{q_k^0(c_k^0)/c_k^0}. \tag{4.4a}$$

This initial value problem can be integrated with *initial condition*

$$c_k^0(0) = 0, \quad k = 1, \ldots, N, \tag{4.4b}$$

---

[*]See among many others [154].
[†]See for example [155, 156], among many other standard texts on fundamentals of ODEs.

which holds true and is *physically correct*, because when the adsorbent is clean—i.e., free of adsorbable components, $q_k = 0$, there are no changes in the interfacial tension of pure fluid phase alone in contact with the adsorbent, and therefore no changes in spreading pressure—surface potential, π, occur. This in turn means that the hypothetical fluid phase concentrations, c_i^0, must be zero; this *reference state* is clearly stated by the lower limit of integral (3.9).

The solution principle (4.2) reduces the amount of problem unknowns by one, substantially simplifying the problem to be solved by exploiting its structure.

It is important to underline that the choice of writing c_1^0 as the independent variable in (4.2) is completely arbitrary; the problem formulation is also valid when any of the other c_k^0, $k \neq 1$, is chosen as independent variable.

In order to carry out the integration of (4.4), it is only necessary that

$$\frac{\mathrm{d}q_i^0}{\mathrm{d}c_i^0}(0) > 0 \tag{4.5a}$$

is fulfilled for *increasing* single component adsorption isotherms, $q_i^0 = f(c_i^0)$, with the property

$$\Pi_i(c_i^0) \to \infty \quad \text{for} \quad c_i^0 \to \infty, \quad i = 1, \dots, N. \tag{4.5b}$$

If a trivial, independent variable, ξ, is introduced to proceed with the integration of initial value problem (4.4), so that

$$\frac{\mathrm{d}c_k^0}{\mathrm{d}\xi} = \frac{q_1^0 \, / \, c_1^0}{q_k^0 \, / \, c_k^0}, \tag{4.6a}$$

$$c_k^0(\xi = 0) = 0, \quad k = 1, \dots, N, \tag{4.6b}$$

a solution in the *positive octant of an N-dimensional space*, of coordinates $c_1^0, \dots, c_N^0$, is computed. For $k = 1$—of course—this is trivial, as $\mathrm{d}c_1^0/\mathrm{d}\xi = 1$, and therefore $c_1^0 \equiv \xi$. The result obtained with (4.6) is just $\psi_k(c_1^0)$, Equation (4.2). It can be proven that the solution in this space exists and is unique [53] for single component adsorption isotherms that fulfill the condition (4.5a). To this matter, it is important to stress once more, that certain single component adsorption isotherm equations do not provide *consistent* expressions for the zero concentration limit requirement of condition (4.5a). For these isotherm models the solution method does not work—cf. Table 2.3, p. 20.

Particular solutions, $c^{0,\star}$ The integration of (4.4) yields an *orbit* that provides the general solution of the form (4.2). In order to locate any required particular solution,
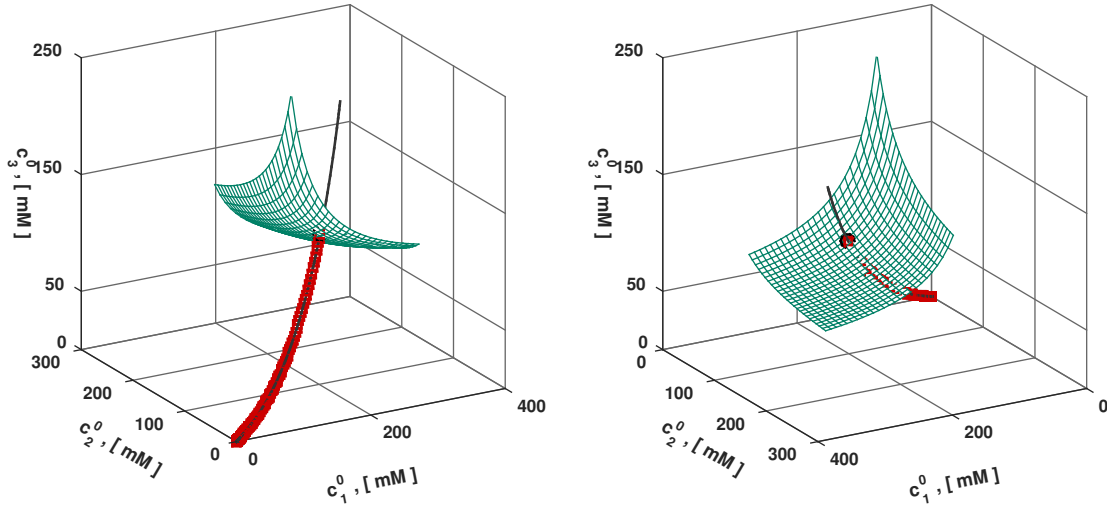
Figure 4.1: Geometric representation of applied solution principle for $N = 3$ adsorbates. Solution orbit, $\psi(\xi)$, which projects towards the interior of the *positive octant* defined by c^0, cuts *hypersurfaces* $\mathfrak{Z}$—cf. Equation (4.7), *transversely*. Each *hypersurface* is uniquely defined by input fluid phase concentrations c. Component 1: *octylbenzene* (C8); component 2: *decylbenzene* (C10); & component 3: *undecylbenzene* (C11). Input fluid phase concentrations: $c = \{50, 50, 50\}[\mathsf{mM}]$. *Fictitious* fluid phase concentrations at equilibrium: $c^0 = \{236.05, 144.97, 112.80\}[\mathsf{mM}]$. Exerted reduced spreading pressure: $\Pi = 829.48 [\mathsf{mmol/l_{ads.}}]$. Adsorbed phase concentrations at equilibrium: $q = \{61.49, 100.13, 128.69\}[\mathsf{mM}]$. Applied single component isotherm parameters are listed in Table A4, Appendix A8, p 174.

$c_i^{0,\star}(c_1^{0,\star})$, for fluid phase concentrations, $c^\star = [\,c_1^\star, \cdots, c_N^\star\,]^T$—given as *input information* of the equilibrium calculation, integration proceeds up to the point where closure condition (3.10) is fulfilled; at that point, *orbit* (4.6) *cuts transversely* the N-dimensional *hypersurface* defined as

$$\mathfrak{Z}^{(\star)} := \left[\sum_{i=1}^{N} \frac{c_i^\star}{c_i^0} - 1 \right] = f(c_1^0, \ldots, c_N^0, c_1^\star, \ldots, c_N^\star), \tag{4.7}$$

and the integration stops—this hypersurface lives in the positive *octant*, $c_i^0 > 0$, $\forall i$. The inclusion of (4.7) in computations is done with the aid of piecewise-defined function 'cut', leading to the *autonomous* IVP

$$\frac{\mathrm{d}c_k^0}{\mathrm{d}\xi} = \mathsf{cut}\, \frac{q_1^0 \,/\, c_1^0}{q_k^0 \,/\, c_k^0}, \tag{4.8a}$$

$$c_k^0(0) = 0, \quad k = 1, \ldots, N, \tag{4.8b}$$

with

$$\mathsf{cut} := f(c_1^0, \cdots, c_N^0, c_1^\star, \cdots, c_N^\star) = \begin{cases} 1, & \left[\prod_{j=1}^N c_j^0 \right] \left[\sum_{i=1}^N \frac{c_i^\star}{c_i^0} - 1 \right] > 0, \\ \\ 0, & \text{otherwise.} \end{cases} \tag{4.8c}$$

Stationary values—sought solution, $c^{0,\star}$, are subsequently applied in Equations (3.11) & (3.12) to obtain $q^\star$ at equilibrium.

> ☆   *Advantages of this approach become clear when looking at the simplicity of IVP formulation* (4.8)*; difficulties in computing solutions described by* ITEM 1*,* ITEM 2 *&* ITEM 3*, p. 36, are satisfactorily overcome.*

4.2   Physical interpretation of the solution approach

Integration of IVP (4.8) from $c_i^0(0)$, $i = 2, \dots, N$ to a positive, finite value $c_i^{0,\star} = \psi_i(\xi)$ is *equivalently* represented by integration of the area under the curve of $q_i^0/c_i^0 = f(c_i^0)$; this integral is simply $\Pi_i = f(c_i^0)$—cf. Equation (3.9), p. 34. Expressions for these reduced surface potentials are listed in Table 3.4 for typical isotherm models. This is illustrated in Figure 4.2. Moving along the solution orbit, $\Psi(\xi)$, is analogous to simultaneously
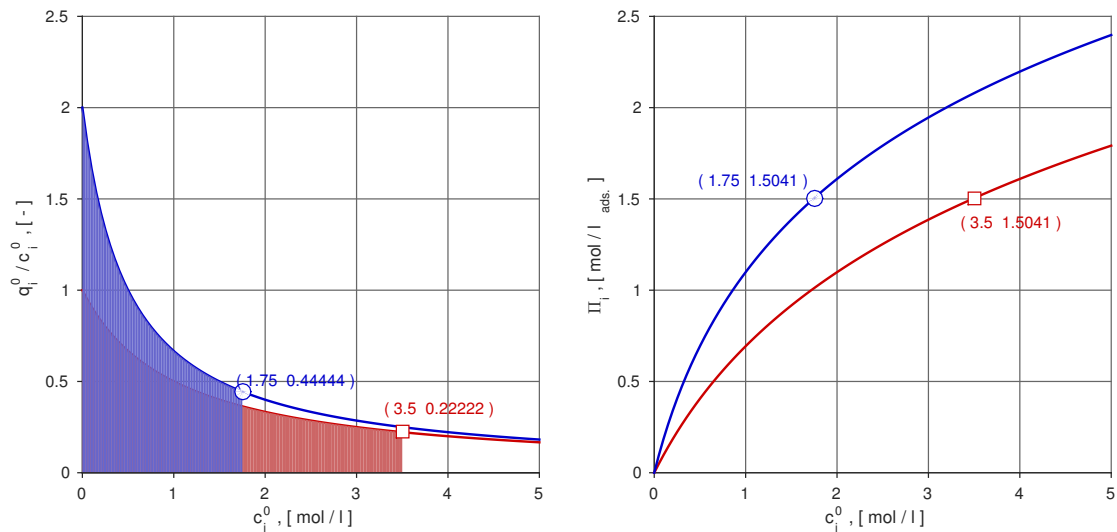
Figure 4.2: Representation of *build-up* in reduced surface potential, i.e., spreading pressure, Π for particular given liquid phase concentrations, $c_i^\star = \{0.5, 1.5\}\,[\mathsf{mol/l}]$, applying IAST with single component Langmuir isotherms, Equation (2.3a). Spreading pressure value, $\Pi = 1.5041\,[\mathsf{mol/l_{ads.}}]$ was obtained directly with Equation (3.16a), Table 3.4, p. 38. Parameters used to generate the plots are listed in Table A3, Appendix A2.2, p. 165.

increasing/decreasing the reduced potential values, Π_i, $i = 1, \ldots, N$, thus moving from one equilibrium point to the next. This, in turn, translates to changes in adsorbed phase concentration values, q_i, expressed by Equation (3.12). This is *congruent* with the expected physical behavior when the adsorbed phase is considered ideal.

4.3   Jacobian of q under IAST framework

For various purposes it is beneficial to compute derivatives of adsorption isotherms, $q = f(c)$, with respect to arguments, c, efficiently—cf. Section 6.4, Kvaalen *et al.* [157, 158] and Rhee *et al.* [159, 160]. In the case of competitive adsorbed phase concentrations,

$$q_i = f(c_1, \ldots, c_N), \quad i = 1, \ldots, N,$$

the matrix of partial derivatives of $q(c)$, i.e., Jacobian matrix $\mathcal{J}(q(c))$ of size $N \times N$, is defined as

$$\mathcal{J}(q(c)) := \begin{pmatrix} \dfrac{\partial q_1}{\partial c_1} & \cdots & \dfrac{\partial q_1}{\partial c_N} \\ \vdots & \ddots & \vdots \\ \dfrac{\partial q_N}{\partial c_1} & \cdots & \dfrac{\partial q_N}{\partial c_N} \end{pmatrix}. \tag{4.9}$$

For implementation, it is of significant advantage to compute these derivatives directly, preferably with explicit, analytical formulæ that can yield accurate results. In the case of some multicomponent adsorption models this is trivial. For example, the *multicomponent Langmuir* isotherm,

$$q_i = f(c) = q_i^{\text{sat}} \frac{b_i \, c_i}{1 + \sum\limits_{k=1}^{N} b_k \, c_k}, \ i = 1, \ldots N \tag{2.14a}$$

—Table 2.4, p. 23, has the following Jacobian for N adsorbates:

$$
\mathcal{J}(q(c)) =
\begin{cases}
i = j, \quad \dfrac{\partial q_i}{\partial c_j} = \dfrac{q_i^{\mathrm{sat}}\, b_i \left[1 + \sum\limits_{k=1}^{N} b_k\, c_k \right] - b_i\, q_i^{\mathrm{sat}}\, b_i\, c_i}{\left[1 + \sum\limits_{k=1}^{N} b_k\, c_k \right]^2}, \\[3em]
i \neq j, \quad \dfrac{\partial q_i}{\partial c_j} = -\dfrac{q_i^{\mathrm{sat}}\, b_j\, b_i\, c_i}{\left[1 + \sum\limits_{k=1}^{N} b_k\, c_k \right]^2}; \quad i = 1, \ldots, N, \text{ and } j = 1, \ldots, N.
\end{cases}
\tag{4.10}
$$

When closed form expressions such as (4.10) are not available, $\mathcal{J}(q(c))$ must be approximated numerically; this usually results in costly algorithms from the computational point of view—see e.g., Tolsma & Barton [161]. Henceforth, two *crucial* reasons to try to obtain closed form expressions for $\mathcal{J}(q(c))$ are *a*) ACCURACY; and *b*) COMPUTATIONAL COST —thus motivating their attainment.

The fact that single component isotherms considered, $q_i^0 = f(c_i^0)$, fulfill conditions (4.5a) & (4.5b) and have a representation of the form given by Equation (2.2), p. 16, gives way to explicit, analytical formulæ for this Jacobian, written in *compact* form as [53]

$$
\mathcal{J}(q(c)) \equiv [\mathcal{I} + J_2]\, \mathsf{diag}\left[\dfrac{q_{\mathrm{tot}}}{c_i^0} \right],
\tag{4.11a}
$$

with $\mathcal{I} + J_2$ expressed by *objects*—i.e., *simple* vector and matrix products, so that

$$
\mathcal{I} + J_2 := \left(\mathcal{I} - \left[x w^T \right] \right) \left(\mathcal{I} - \left[W x e^T \right] \right) - \sigma \left[x e^T \right];
\tag{4.11b}
$$

and thus yielding the *working formula*[*]:

$$
\mathcal{J}(q(c)) = \left[\left(\mathcal{I} - \left[x w^T \right] \right) \left(\mathcal{I} - \left[W x e^T \right] \right) - \sigma \left[x e^T \right] \right] \mathsf{diag}\left[\dfrac{q_{\mathrm{tot}}}{c_i^0} \right],
\tag{4.11c}
$$

given in terms of a *rank-2 perturbation* of the *identity matrix*, $\mathcal{I}$. Equivalently holds

$$
\mathcal{J}(q(c)) = \left(\mathcal{I} + [x, y] \begin{bmatrix} f^T \\ -e^T \end{bmatrix} \right) \mathsf{diag}\left(\dfrac{q_i}{c_i} \right)
\tag{4.11d}
$$

---

[*]By the term *working formula* it is meant to emphasize that this expression is directly applicable in computations.
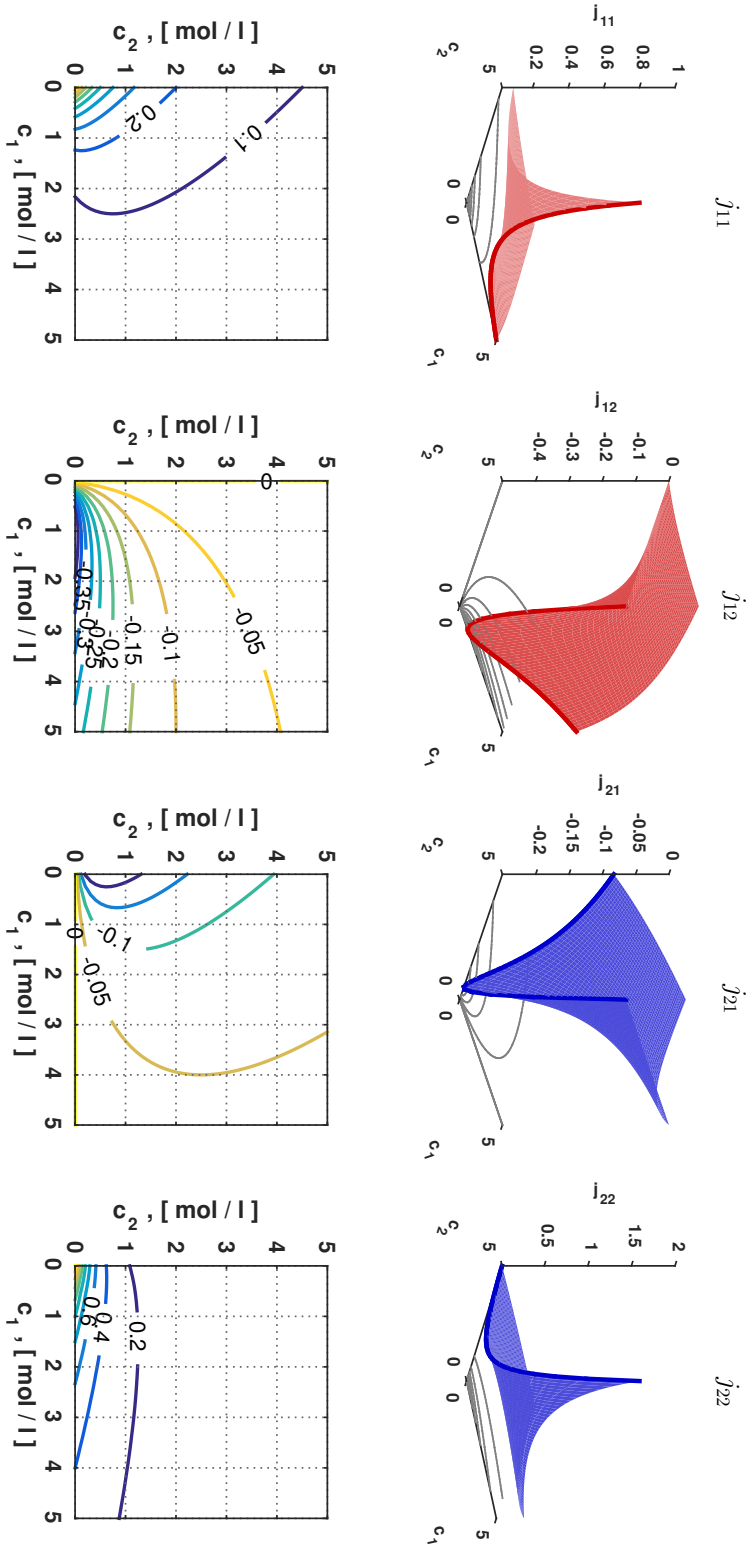
Figure 4.3: Graphical illustration of $\mathcal{J}(q)$ for binary, competitive Langmuir model, Equation (4.10), corresponding to $q = f(c)$ illustrated in Figure (2.3). $j_{11} \equiv \partial q_1/\partial c_1$; $j_{12} \equiv \partial q_1/\partial c_2$; $j_{21} \equiv \partial q_2/\partial c_1$; & $j_{22} \equiv \partial q_2/\partial c_2$. Parameters used to generate the plots are listed in Table A3, Appendix A2.2, p. 165.

after a suitable factorization. Table 4.1 lists *objects' definitions* used throughout expressions (4.11). These are computed with $c = [\, c_1, \, \ldots, \, c_N \,]^T$ and the corresponding $c^0 = [\, c_1^0, \, \ldots, \, c_N^0 \,]^T$ at equilibrium.

It should be acknowledged that fictitious fluid phase concentrations, c^0, can be computed with *any* of the IAST calculation methods described before—cf. Section 3.3, p. 36, as well as the IVP approach described in Section 4.1.

Justification of Jacobian formula (4.11).

The validity of $\mathcal{J}(q)$, Equation (4.11), was prepared by Flockerzi [162] and follows below[*].

Table 4.1: Definitions of objects required for computation of $\mathcal{J}(q)$; $k = 1, \, \ldots, \, N$.

Object	Expression	
Scaled reciprocal adsorbed phase concentrations	$w_k := \dfrac{q_{\text{tot}}}{q_k^0}, \; w = \mathsf{col}(w_k), \; W = \mathsf{diag}(w_k)$	(4.12a)
Column vector of adsorbed phase mole fractions	$x_k := \dfrac{c_k}{c_k^0}, \; x = \mathsf{col}(x_k), \; X = \mathsf{diag}(x_k)$	(4.12b)
Column vector of fluid phase mole fractions	$y_k := \dfrac{q_k}{c_k^0}, \; y = \mathsf{col}(y_k), \; Y = \mathsf{diag}(y_k)$	(4.12c)
Scalar σ	$\sigma := \displaystyle\sum_{k=1}^{N} w_k \, c_k \, q_{\text{tot}} \; \dfrac{\mathrm{d}}{\mathrm{d}c_k^0} \dfrac{1}{q_k^0}$	(4.12d)
Row vector of *ones* of size $1 \times N$	$e^T = (\, 1, \, \cdots, \, 1 \,)$	(4.12e)
Row vector f^T	$f^T := \left[w^T W x - \sigma \right] e^T - w^T$	(4.12f)

Proposition 4.3.1. *Under the frame of IAST, Equation* (4.11) *is a valid representation of* $\mathcal{J}\big(q(c)\big)$.

Proof. Let the following substitutions apply in order to simplify the notation: $Q_i \equiv q_i$; $q \equiv q_{\text{tot}}$; $x_i \equiv c_i$; $X_i \equiv c_i^0$; and $z_i \equiv x_i / X_i$. Further, the proof will be completed in stepwise fashion, thus clearly illustrating some supplementary features.

---

[*]In this proof *standard* column vector & matrix notations are used, unless otherwise specified.

Step 1 Equation (3.12) in p. 35, is written in vector form, so that

$$
\begin{pmatrix} Q_1 \\ \vdots \\ Q_N \end{pmatrix} = q \begin{pmatrix} z_1 \\ \vdots \\ z_N \end{pmatrix}, \quad z \equiv \begin{pmatrix} x_1/X_1 \\ \vdots \\ x_N/X_N \end{pmatrix} \quad \therefore \ Q = qz. \tag{4.13a}
$$

Hereby, the following expression, obtained by re-writing the *scalar* (3.11), becomes significantly useful throughout this proof:

$$
\frac{1}{q} \equiv \left(\frac{1}{q_1^0} z_1 + \cdots + \frac{1}{q_N^0} z_N \right) = \left(\tilde{W}_1 z_1 + \cdots + \tilde{W}_N z_N \right) = \tilde{W}^T z, \tag{4.13b}
$$

whereby reciprocals $\tilde{W}_i \equiv 1/q_i^0$ have been introduced for a more compact notation. An expression for the Jacobian, $\mathcal{J}(Q)$, is obtained by application of the Chain Rule to (4.13a), yielding

$$
\mathcal{J}(Q) = z \left[\partial_z q \, z_x + \partial_X q \, X_x \right] + q z_x. \tag{4.13c}
$$

Step 2 Now, appropriate expressions for each of the terms in Equation (4.13c) need to be addressed. The partial derivatives $\partial_z q$ and $\partial_X q$ are given by

$$
\partial_z q = -q^2 \left(\frac{1}{q_1^0}, \cdots, \frac{1}{q_N^0} \right) = -q^2 \left(\tilde{W}_1, \cdots, \tilde{W}_N \right) = -q^2 \tilde{W}^T \quad \text{and} \tag{4.13d}
$$

$$
\partial_X q = -q^2 \left(z_1 \left(\frac{1}{q_1^0} \right)', \cdots, z_N \left(\frac{1}{q_N^0} \right)' \right) = -q^2 \left(z_1 \tilde{W}_1', \cdots, z_N \tilde{W}_N' \right), \tag{4.13e}
$$

respectively. In deriving expressions (4.13d) & (4.13e), it is only necessary to keep in mind that $q_i^0 = f(X_i)$, $\forall i$.

Recalling the solution approach, proposed in Section 4.1, z_i are functions of X_i and '*parameters*' $x_1, \cdots, x_N$, so that

$$
z_i = f\left(x_i, X_i(x_1, \ldots, x_N) \right), \ i = 1, \ldots, N. \tag{4.13f}
$$

Step 2a In Equation (4.13c), the Jacobian z_x is required, so this is computed first for each component i. For example, for component 1 holds $z_1 = f\left(x_1, X_1(x_1, \ldots, x_N) \right)$; since, $z_1 = x_1/X_1$, then

$$
z_{1x_1} \equiv \frac{\partial z_1}{\partial x_1} = \frac{X_1 - x_1 X_1'}{X_1^2} = \frac{1}{X_1} - \frac{z_1}{X_1} \frac{\partial X_1}{\partial x_1}.
$$

Therefore,

$$
z_x = \begin{pmatrix} \dfrac{1}{X_1} & 0 & \cdots & 0 \\ 0 & \ddots & & \vdots \\ \vdots & & \ddots & 0 \\ 0 & & 0 & \dfrac{1}{X_N} \end{pmatrix} - \begin{pmatrix} \dfrac{z_1}{X_1}\dfrac{\partial X_1}{\partial x_1} & \dfrac{z_1}{X_1}\dfrac{\partial X_1}{\partial x_2} & \cdots & \dfrac{z_1}{X_1}\dfrac{\partial X_1}{\partial x_N} \\ \dfrac{z_2}{X_2}\dfrac{\partial X_2}{\partial x_1} & \dfrac{z_2}{X_2}\dfrac{\partial X_2}{\partial x_2} & \cdots & \dfrac{z_2}{X_2}\dfrac{\partial X_2}{\partial x_N} \\ \vdots & \vdots & & \vdots \\ \dfrac{z_N}{X_N}\dfrac{\partial X_N}{\partial x_1} & \dfrac{z_N}{X_N}\dfrac{\partial X_N}{\partial x_2} & \cdots & \dfrac{z_N}{X_N}\dfrac{\partial X_N}{\partial x_N} \end{pmatrix},
$$

whereby factorizing its rightmost matrix leads to the *compact* form

$$
z_x = \mathsf{diag}\left(\frac{1}{X_i}\right) - \mathsf{diag}\left(\frac{z_i}{X_i}\right) X_x, \quad i = 1, \ldots, N. \tag{4.13g}
$$

Step 2b   In order to compute the Jacobian X_x in Equation (4.13c) and (4.13g), it is necessary to turn now to the original system of equations to solve, expressed in terms of GENERATING FUNCTIONS, v_k, $k = 1, \ldots, N$—see Appendix A6 for details on these functions. The system of equations to consider is therefore

$$
v_1(X_1) - v_2(X_2) = 0, \ v_1(X_1) - v_3(X_3) = 0, \ \cdots
$$
$$
v_1(X_1) - v_N(X_N) = 0, \tag{4.13h}
$$
$$
\frac{x_1}{X_1} + \cdots + \frac{x_N}{X_N} - 1 = 0.
$$

Differentiating (4.13h) with respect to parameters x yields

$$
v_1'(X_1)(X_1)_x - v_2'(X_2)(X_2)_x = 0, \ v_1'(X_1)(X_1)_x - v_3'(X_3)(X_3)_x = 0, \ \cdots
$$
$$
v_1'(X_1)(X_1)_x - v_N'(X_N)(X_N)_x = 0,
$$
$$
\frac{1}{X_1} - \frac{x_1(X_1)_{x_1}}{X_1^2} - \frac{x_2(X_2)_{x_1}}{X_2^2} - \cdots = 0, \ -\frac{x_1(X_1)_{x_2}}{X_1^2} + \frac{1}{X_2} - \frac{x_2(X_2)_{x_2}}{X_2^2} - \cdots = 0, \ \cdots
$$
$$
- \cdots + \frac{1}{X_N} - \frac{x_N(X_N)_{x_N}}{X_N^2} = 0,
$$
$$
\tag{4.13i}
$$

with column vectors $(X_k)_x \equiv [\,(X_k)_{x_1}, \cdots, (X_k)_{x_N}\,]^T$, $k = 1, \ldots, N$. From the structure of (4.13i), it is easy to observe that re-arranging terms allows a factorization of the

form:

$$
\begin{pmatrix}
v_1'(X_1) & -v_2'(X_2) & 0 & 0 & \cdots \\
v_1'(X_1) & 0 & -v_3'(X_3) & 0 & \cdots \\
\cdots & \cdots & \cdots & \cdots & \cdots \\
\frac{x_1}{X_1^2} & \frac{x_2}{X_2^2} & \frac{x_3}{X_3^2} & \frac{x_4}{X_4^2} & \cdots
\end{pmatrix}
X_x =
\begin{pmatrix}
0 & 0 & \cdots & \cdots & \cdots \\
0 & 0 & \cdots & \cdots & \cdots \\
\cdots & \cdots & \cdots & \cdots & \cdots \\
\frac{1}{X_1} & \frac{1}{X_2} & \cdots & \cdots & \cdots
\end{pmatrix}.
\tag{4.13j}
$$

Whilst (4.13j) may seem *cumbersome*, it can be re-written in a very simple and useful manner, because a representation of the Jacobian X_x is sought *at equilibrium*; in other words, holds:

$$
v_1 \overset{!}{=} v_2, \; v_1 \overset{!}{=} v_3, \; \cdots, \; v_1 \overset{!}{=} v_N,
\tag{4.13k}
$$

which, together with the fact that (4.13j) is *rank-deficient*, gives way to factorization

$$
X_x = \frac{1}{\mu}
\begin{pmatrix}
\frac{1}{v_1'} \\
\vdots \\
\frac{1}{v_N'}
\end{pmatrix}
\left(\frac{1}{X_1}, \; \cdots, \; \frac{1}{X_N} \right).
\tag{4.13l}
$$

In light of property

$$
q_k^0 = f(\xi) = \xi \frac{v_k'(\xi)}{v_k(\xi)} = \frac{1}{\tilde{W}_k},
\tag{2.2}
$$

p. 16—repeated here for completeness, a useful computation results:

$$
p_k = \frac{1}{X_k v_k'} = \frac{\tilde{W}_k}{v_k},
\tag{4.13m}
$$

obtained simply by re-arranging terms. The *scalar* μ in Equation (4.13l) is defined as

$$
\mu := \sum_{i=1}^{N} \frac{x_i}{X_i^2 v_i'} = \sum_{i=1}^{N} \frac{x_i}{X_i} \frac{1}{X_i v_i'} = \sum_{i=1}^{N} \frac{z_i}{X_i v_i'} = \sum_{i=1}^{N} z_i p_i.
\tag{4.13n}
$$

With the help of the p_k in (4.13m), the object

$$
\alpha := \frac{1}{p^T z}
\begin{pmatrix}
z_1 p_1 \\
\vdots \\
z_N p_N
\end{pmatrix}
\tag{4.13o}
$$

can be defined; each α_k is expressed as

$$\alpha_k = \frac{z_k}{\sum_j p_j z_j / p_k} = \frac{z_k}{\sum_j \frac{\tilde{W}_j}{v_j} z_j / \frac{\tilde{W}_k}{v_k}} = \frac{z_k \tilde{W}_k}{\sum_j \tilde{W}_j z_j} = \frac{1}{\tilde{W}^T z} \tilde{W}_k z_k = q \, \tilde{W}_k z_k, \qquad \text{(4.13p)}$$

herewith effectively canceling the v_k!

Step 2c With the help of (4.13o), it is possible to re-write Equation (4.13g) as:

$$
\begin{aligned}
z_x &= \mathsf{diag}\left(\frac{1}{X_i}\right) - \alpha \left(\frac{1}{X_1}, \cdots, \frac{1}{X_N}\right) \\
&= \mathsf{diag}\left(\frac{1}{X_i}\right) - \alpha \, \mathsf{diag}\left(\frac{1}{X_i}\right) e^T \\
&= \mathsf{diag}\left(\frac{1}{X_i}\right) \left[\mathcal{I} - \alpha e^T\right];
\end{aligned}
\qquad \text{(4.13q)}
$$

and as it becomes evident from (4.13p), z_x is now given in terms of X_i and x_i only!

Step 3 With the computational details explained throughout **Step 2**, it is now possible to substitute suitable terms in (4.13c). With the help of (4.13d), (4.13e) and (4.13q) holds

$$
\begin{aligned}
q^{-2} \mathcal{J}(Q) &= -z \left[\tilde{W}^T z_x + \left(z_1 \tilde{W}_1', \cdots, z_N \tilde{W}_N'\right) X_x \right] + \tilde{W}^T z \, z_x \\
&= \tilde{W}^T z \left(\mathcal{I} - \frac{1}{\tilde{W}^T z} z \tilde{W}^T\right) z_x - z \left(z_1 \tilde{W}_1', \cdots, z_N \tilde{W}_N'\right) X_x \\
&= \tilde{W}^T z \left(\mathcal{I} - \frac{1}{\tilde{W}^T z} z \tilde{W}^T\right) \mathsf{diag}\left(\frac{1}{X_i}\right) \left[\mathcal{I} - \alpha e^T\right] \\
&\qquad\qquad\qquad - z \left(z_1 \tilde{W}_1', \cdots, z_N \tilde{W}_N'\right) X_x.
\end{aligned}
\qquad \text{(4.13r)}
$$

Step 3a In order to conveniently handle the terms $\tilde{W}_1', \cdots, \tilde{W}_N'$ in (4.13r), the *scalar*

$$\beta := \sum_{i=1}^N \alpha_i \left[\tilde{W}_i' X_i\right] = \frac{\sum_{i=1}^N \left[z_i \tilde{W}_i' X_i p_i\right]}{p^T z} = \frac{1}{\mu} \sum_{i=1}^N \left[z_i \tilde{W}_i' X_i p_i\right] \qquad \text{(4.13s)}$$

is defined by application of (4.13n). Since it can be established that

$$\mathsf{diag}\left(\frac{1}{X_i}\right) \beta z e^T = z \left(z_1 \tilde{W}_1', \cdots, z_N \tilde{W}_N'\right) X_x, \qquad \text{(4.13t)}$$

Equation (4.13r) becomes

$$
\begin{aligned}
q^{-2}\mathcal{J}(Q) &= -z\left[\tilde{W}^T z_x + \left(z_1 \tilde{W}_1', \cdots, z_N \tilde{W}_N'\right) X_x\right] + \tilde{W}^T z\, z_x \\
&= \tilde{W}^T z\left(\mathcal{I} - \frac{1}{\tilde{W}^T z} z \tilde{W}^T\right) z_x - z\left(z_1 \tilde{W}_1', \cdots, z_N \tilde{W}_N'\right) X_x \\
&= \tilde{W}^T z\left(\mathcal{I} - \frac{1}{\tilde{W}^T z} z \tilde{W}^T\right) \mathsf{diag}\left(\frac{1}{X_i}\right)\left[\mathcal{I} - \alpha e^T\right] \\
&\qquad\qquad\qquad\qquad\qquad - \mathsf{diag}\left(\frac{1}{X_i}\right) \beta z e^T.
\end{aligned}
\tag{4.13u}
$$

Step 3b   Finally, Equation (4.13u) can be re-arranged to arrive at the form of Equation (4.11). With (4.13b) the $\tilde{W}^T z$ term is substituted by q, so that

$$
q^{-2}\mathcal{J}(Q) = \frac{1}{q}\left(\mathcal{I} - q\, z\tilde{W}^T\right)\mathsf{diag}\left(\frac{1}{X_i}\right)\left[\mathcal{I} - \alpha e^T\right] - \mathsf{diag}\left(\frac{1}{X_i}\right)\beta z e^T;
\tag{4.13v}
$$

solving for $\mathcal{J}$, factorizing $\mathsf{diag}\left(\frac{1}{X_i}\right)$ and re-arranging yields

$$
\mathcal{J}(Q) = \left[\left[\mathcal{I} - q\, z\tilde{W}^T\right]\left[\mathcal{I} - \alpha e^T\right] - q\beta z e^T\right]\mathsf{diag}\left[\frac{q}{X_i}\right].
\tag{4.13w}
$$

Finally, to write (4.13w) in terms of the scaled objects listed in Table 4.1, substitutions: $w^T \equiv q\tilde{W}^T$, $\sigma \equiv q\beta$ and $Wx \equiv \alpha$ are applied, so that

$$
\mathcal{J} = \left[\left[\mathcal{I} - xw^T\right]\left[\mathcal{I} - Wxe^T\right] - \sigma x e^T\right]\mathsf{diag}\left[\frac{q_{\mathrm{tot}}}{c_i^0}\right].
\tag{4.11}
$$

This completes the proof. $\qquad\qquad\qquad\qquad\qquad\qquad\qquad\qquad\qquad\qquad\qquad\square$

The particular structure of (4.11) is not *arbitrary*; it is specifically designed to address potential computational issues and therefore warrants certain degree of *robustness*, needed for its later application. Moreover, this is an essential feature if the calculation of $\mathcal{J}(q)$ is embedded in fixed-bed adsorber calculations—cf. Section 7.7, p. 96.

The scalar object

$$
\sigma := \sum_{k=1}^{N} w_k\, c_k\, q_{\mathrm{tot}}\, \frac{\mathrm{d}}{\mathrm{d}c_k^0}\frac{1}{q_k^0}
\tag{4.12d}
$$

is of *fundamental importance* when computing the Jacobian $\mathcal{J}(q)$ with Equation (4.11); it contains

$$
\frac{\mathrm{d}}{\mathrm{d}c_k^0}\frac{1}{q_k^0}, \quad k = 1, \ldots, N,
\tag{4.14}
$$

i.e., derivatives of the *reciprocals* of single component isotherms, $q_i^0 = f(c_i^0)$, which are easily obtained in closed form[*]. Table 4.2 lists some examples of them.

Table 4.2: Selected expressions of the derivatives of reciprocals of adsorbed phase concentrations, $\mathrm{d}\left(1/q_k^0\right)/\mathrm{d}c_k^0$. For *physically relevant* $c_i^0 \in [0, \infty)$, the expressions always yield a negative σ.

Isotherm	Expression [a]	
Langmuir	$$\frac{\mathrm{d}}{\mathrm{d}c_i^0}\frac{1}{q_i^0} = -\frac{1}{q_i^{\mathrm{sat}}\,b_i\,c_i^{0^2}}$$	(4.15a)
Quadratic	$$\frac{\mathrm{d}}{\mathrm{d}c_i^0}\frac{1}{q_i^0} = -\frac{b_{i1} + 4\,b_{i2}\,c_i^0 + b_{i1}\,b_{i2}\,c_i^{0^2}}{q_i^{\mathrm{sat}}\,c_i^{0^2}\,[\,b_{i1} + 2\,b_{i2}\,c_i^0\,]^2}$$	(4.15b)
Quadratic + Langmuir	$$\frac{\mathrm{d}}{\mathrm{d}c_i^0}\frac{1}{q_i^0} = -\frac{\begin{aligned}&q_{i1}^{\mathrm{sat}}\,\left[\,1 + b_{i3}c_i^0\,\right]^2\,\left[\,b_{i1} + 4b_{i2}c_i^0 + b_{i1}b_{i2}c_i^{0^2}\,\right] + \\ &\quad q_{i2}^{\mathrm{sat}}\,b_{i3}\,\left[\,1 + b_{i1}c_i^0 + b_{i2}c_i^{0^2}\,\right]^2\end{aligned}}{\left[\begin{aligned}&q_{i1}^{\mathrm{sat}}\,c_i^0\,\left[\,b_{i1} + 2b_{i2}c_i^0\,\right]\,\left[\,1 + b_{i3}c_i^0\,\right] + \\ &\quad q_{i2}^{\mathrm{sat}}\,b_{i3}c_i^0\,\left[\,1 + b_{i1}c_i^0 + b_{i2}c_i^{0^2}\,\right]\end{aligned}\right]^2}$$	(4.15c)
Redlich-Peterson	$$\frac{\mathrm{d}}{\mathrm{d}c_i^0}\frac{1}{q_i^0} = \frac{-1 + b_i\,[\,-1 + \nu_i\,]\,c_i^{0\,\nu_i}}{a_i\,c_i^{0^2}}$$	(4.15d)

a. Verified with MATHEMATICA [®] [141].

---

[*]It is usually a good idea to verify these expressions with a CAS, e.g., MATHEMATICA [®] [141].

Summary

Two central contributions have been presented in detail in this chapter:

1. A method to solve the equations of IAST, developed for generally increasing single component adsorption isotherms, possessing a *positive* and *finite* initial slope—cf. Equation (4.5). Many isotherm models fulfill this requirement—see Table 2.2; the method does not work when it is not fulfilled. However, additional *manipulations* of single component isotherm expressions can be applied in some cases to alleviate this minor pitfall—e.g., as suggested by Seidel & Gelbin [163] for extrapolation from experimentally acquired data of organic solutes dissolved in water, adsorbed by activated carbon; and Linders [84] & Linders *et al.* [92], whereby a *repair* to Dubinin-Radushkevich, Equation (2.3j), and Dubinin-Astakhov equations is proposed and applied to obtain *formal* Henry limit values for these isotherms at the origin.
   A crucial feature of the method consists of illustrating and succintly explaining the relationship amongst all problem variables involved—i.e., concentrations, thus providing some insight to their physical meaning; this is possible due to the generation of a complete solution—*orbit*—for prescribed fluid phase concentration ranges. *Particular solutions* are thereafter sought along this computed functional dependency. In this sense, the complete solution may be calculated '*once and for all*' to be later embedded in applications, e.g., fixed-bed adsorber calculations—cf. Chapters 6 & 7. The method is *a*) FAST; *b*) ROBUST; *c*) ACCURATE; and *d*) EASY TO IMPLEMENT. These aspects are illustrated in detail by practical examples and benchmarking against other well-established calculation methods in Chapter 5.

2. Analytical formulæ to obtain *directly* Jacobian of adsorbed phase concentrations, $\mathcal{J}(q)$, using hypothetical fluid phase concentrations, c^0, in turn obtained by solving the IAST equilibrium problem *a priori*.
   These formulæ have several *important* applications; two of them are addressed in Chapters 6 and 8.

Chapter 5

Practical aspects of the proposed solution approach*

"The purpose of computing is insight, not numbers."

– Richard Hamming

Introduction

ADVANTAGEOUS features of the solution method [53] introduced in Chapter 4 are now discussed in detail through several examples, thus illustrating the potential of the solution approach and its elemental features, as well as conveying insight concerning its practical implementation.

5.1 Simplicity of implementation

The calculation of adsorption equilibria becomes a simple, straightforward task by means of problem re-formulation into an IVP, as already explained in Chapter 4. The IVP

---

*CHAPTER DISCLAIMER. Partial contents of this chapter have been reported in: *"A Method for Efficiently Solving the IAST Equations with an Application to Adsorber Dynamics"* [53]. The information is presented as part of this dissertation and it is an original published contribution to the field in a peer-reviewed journal. There is none whatsoever intention of self-plagiarism; the information serves rather as complementary content to this dissertation. Furthermore, the publishing company has granted partial reproduction of the contents in the article mentioned above. [License No.: **3743030164049**, requested and obtained on Nov. 6$^{\text{th}}$, 2015 from John Wiley & Sons, Inc. through Copyright Clearance Center.]

possesses an analytical solution for specific types of single-component isotherm models, $q_i^0 = f(c_i^0)$, and number of adsorbable components, N. In the general case, however, the integration of Equation (4.4) cannot be computed in closed form and therefore should be performed numerically. This is not an issue, however, as the current *state of the art* in numerical solution of ODEs allows for an uncomplicated implementation in practical terms, with flexible user-defined specification of solution accuracy [156, 164–166]. Table 3.3, p. 37, provides already a list of quotients q_i^0/c_i^0 for some isotherm models, required to implement the method.

Predicting competitive equilibria with Redlich-Peterson single component isotherms

A well-known adsorption isotherm is the one proposed by Redlich & Peterson [69], cf. Table 2.2, p. 17—repeated here for completeness:

$$q_i^0 = f(c_i^0) = \frac{a_i\, c_i^0}{1 + b_i\, c_i^{0\,\nu_i}}, \quad i = 1, \ldots, N. \tag{2.3h}$$

Despite of the simplicity of (2.3h)—i.e., three adjustable empirical parameters only, it possesses a non-trivial expression for reduced potential, Π, as listed in Table 3.4, Equation (3.16g), p. 38, whereby the hypergeometric function*, ${}_2\mathsf{F}_1\,[\,\cdot,\cdot,\cdot,\cdot\,]$, is used. Alternatively, a closed-form formula presented in [80]

$$\Pi(c_i^0) = \frac{a_i/\nu_i}{b_i^{\,1/\nu_i}} \left[\frac{\pi}{\sin(\pi/\nu_i)} + \sum_{m=1}^{\infty} (-1)^m \, \frac{\zeta_i^{\,m-(1/\nu_i)}}{m - (1/\nu_i)} \right], \tag{5.1}$$

with $\dfrac{1}{\nu_i} \notin \mathbb{N}$, $\pi = 3.14 \cdots$, $\zeta_i := \dfrac{1}{b_i\, c_i^{0\,\nu_i}} < 1$, can be applied to obtain $\Pi^{\dagger}$.
The solution orbit, i.e., $\xi \mapsto \Psi(\xi)$, defining the equilibrium relation, $c_2^0 = \psi_2(c_1^0)$, is

---

*See among others Abramowitz & Stegun [145] for a formal definition.

†This solution should be applied carefully, since $c_i^0 \in \left(1/b_i^{1/\nu_i}, \infty \right)$ must be considered for the series in formula (5.1) to converge.

obtained directly with (2.3h), by integrating IVP

$$\frac{\mathrm{d}c_1^0}{\mathrm{d}\xi} = 1, \tag{5.2a}$$

$$\frac{\mathrm{d}c_2^0}{\mathrm{d}\xi} = \frac{a_1}{a_2} \frac{\left[1 + b_2\, c_2^{0\,\nu_2}\right]}{\left[1 + b_1\, c_1^{0\,\nu_1}\right]}, \tag{5.2b}$$

$$c_i^0(0) = 0, \quad i = 1, 2, \tag{5.2c}$$

in accord with the solution principle described in Section 4.1, in particular Equation (4.6), p. 47. Figure 5.1 illustrates the solution orbit, $c_2^0 = \psi_2(\xi)$, obtained by numerical integration of (5.2), applying in this particular example the single component equilibria parameters reported by Seidel *et al.* [167] and listed in Table 5.1.

Table 5.1: Single component adsorption isotherm parameters for Redlich-Peterson model—cf. Eq. (2.3h), p. 17—of two organic solutes in H_2O/activated carbon system at $20\,°C$, as reported by Seidel *et al.* [167].

Compound	Parameters		
	a_i	b_i	ν_i
	$[\mathsf{l/g}]$	$[\mathsf{l/mmol}]^{\nu_i}$	$[-]$
phenol (component 1)	524	329	0.78
indol (component 2)	2378	1128	0.86

The particular form of the computed orbit is influenced by the r.h.s. of ODE system (5.2) and applied parameters. The orbit computation—i.e., integration—stops at equilibrium values: $c_1^{0,\star} = 16.9305\,[\mathsf{mmol/l}]$, $c_2^{0,\star} = 2.2679\,[\mathsf{mmol/l}]$, corresponding to input fluid phase concentration values: $c_1^\star = 2.0\,[\mathsf{mmol/l}]$, $c_2^\star = 2.0\,[\mathsf{mmol/l}]$. These values yielded a reduced spreading pressure at equilibrium, $\Pi^\star = 11.8771\,[\mathsf{mmol/g_{ads.}}]$, which was independently verified by the above mentioned alternatives to compute its value, viz. *a*) applying formula (5.1); *b*) numerical integration of the corresponding q_i^0/c_i^0 up to obtained integration limits, $c_i^{0,\star}$; and *c*) applying formula (3.16g) from corresponding single component isotherm information—cf. Table 5.1. All three calculations yielded an identical result. The same *exercise* may be conducted for *any* value lying along $c_2^0 = \psi_2(\xi)$, in order to obtain corresponding reduced potential values at equilibrium.
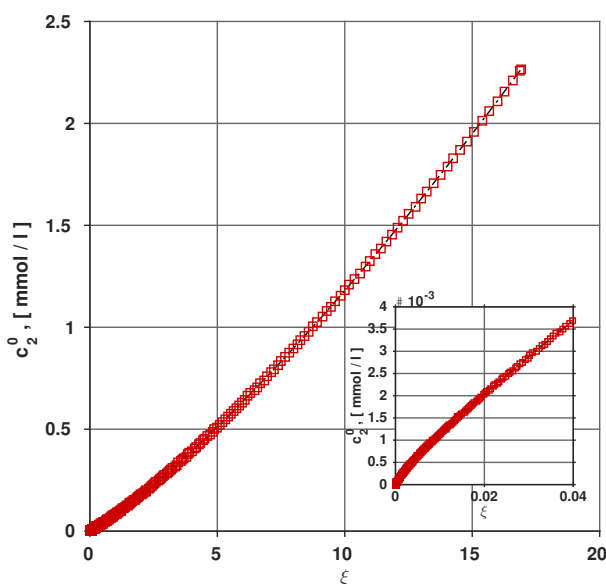
Figure 5.1: Solution orbit, $\psi_2(\xi)$, obtained by integration of the IVP (5.2), applying parameters in Table 5.1. The computation was performed with the general-purpose numerical integrator `ode15s` in MATLAB $^{\circledR}$ [168], at user-defined error tolerance values: $\mathsf{RelTol} = 10^{-7}$ & $\mathsf{AbsTol} = 10^{-8}$, and selecting numerical differentiation formulæ (NDF) as integration algorithm.

5.2 Efficiency

The application of any calculation method for IAST demands *computational efficiency.* One common criterium of efficiency dictates that calculations should be performed as *fast* as possible, with *minimal* computational effort—e.g., storage, number of elementary processor operations, etc.

IAST equilibria prediction for a system with five compounds

A direct measure of computational efficiency is the time required to compute equilibrium values. This was verified by solving a *five* component problem documented by Moon & Tien [169] and O'Brien & Myers [153], which has become a benchmark to test published IAST calculation methods [53, 146, 169]*. Single component adsorption equilibria are described by isotherm equation (2.3f)—Table 2.2, p. 17, which possesses explicit reduced spreading pressure expression (3.16e)—Table 3.4, p. 38, obtained by integration of quotient (3.15h)—Table 3.3, p. 37. The applied parameters are listed in Table 5.2.

---

*The *ten* component problem of the same series originally published by Moon & Tien [169] has been throughly addressed as a benchmark task by several authors, including: O'Brien & Myers [153], Rubiera Landa *et al.* [53] and Mangano *et al.* [146].

Table 5.2: Single component adsorption isotherm parameters for O'Brien & Myers model—cf. Eq. (2.3f), p. 17—of five components, as reported by O'Brien & Myers [153].

Compound	Parameters		
	q_i^{sat}	b_i	σ_i
	$[\,\mathsf{mol/kg}\,]$	$[\,\mathsf{kPa}^{-1}\,]$	$[-]$
Component 1	5.0	0.01	1.2
Component 2	2.0	0.006	1.1
Component 3	3.0	0.0009	0.8
Component 4	7.0	0.1	0.9
Component 5	2.0	0.06	1.0

Figure 5.2 illustrates individual *orbits*, $\psi_k(\xi)$, $k = 1, \ldots, 5$, obtained with the proposed approach, stopping the integration at fictitious partial pressures, $p^{0,\star} = \{0.0255, 6.4513, 2.7253, 0.0009, 0.6452\} \times 10^5 \, [\,\mathsf{kPa}\,]$, in equilibrium with prescribed gas phase molar fractions, $y^\star = \{60, 60, 60, 90, 30\}$ at $p^\star = 300 \, [\,\mathsf{kPa}\,]$. The resulting adsorbed phase concentrations at equilibrium are: $q^\star = \{0.1424, 0.0006, 0.0013, 5.9154, 0.002860\} \, [\,\mathsf{mol/kg}\,]$. Reduced surface potential *build-up* is also illustrated, stopping at equilibrium, $\Pi^\star = 16.5233 \, [\,\mathsf{mol/kg}_{\mathsf{ads.}}\,]$.

In order to compare efficiency as described above, the task was also computed with Algorithm 3.2 and FastIAS [153]. Resulting calculation times are listed in Table 5.3. In all cases where the new solution approach was applied, the results were correct *at least* to one decimal; accuracy improved as the tolerance specification became more *stringent*, at a higher computational cost, as listed in the results. It can therefore be concluded that several ODE integrators available in commercial software packages, as the one herein employed, should provide adequate results, which is an aspect of *robutstness* discussed in Section 5.4 below.

This example also illustrates the ability of the IVP approach to handle competitive multicomponent IAST equilibrium predictions easily, with any arbitrary number of adsorbable components, N. Two possibilities to improve efficiency further include: *a)* storing the computed orbit in the form of an *interpolant* that may be *cheap* to evaluate—for example a polynomial function or a B-spline representation—and then seeking for particular solutions with a *root-bracketing* technique, such as Brent's method or other [149, 151, 170, 171]; & *b)* attempt an implementation of an ODE solver in *vectorized form*—see e.g., Shampine [172].
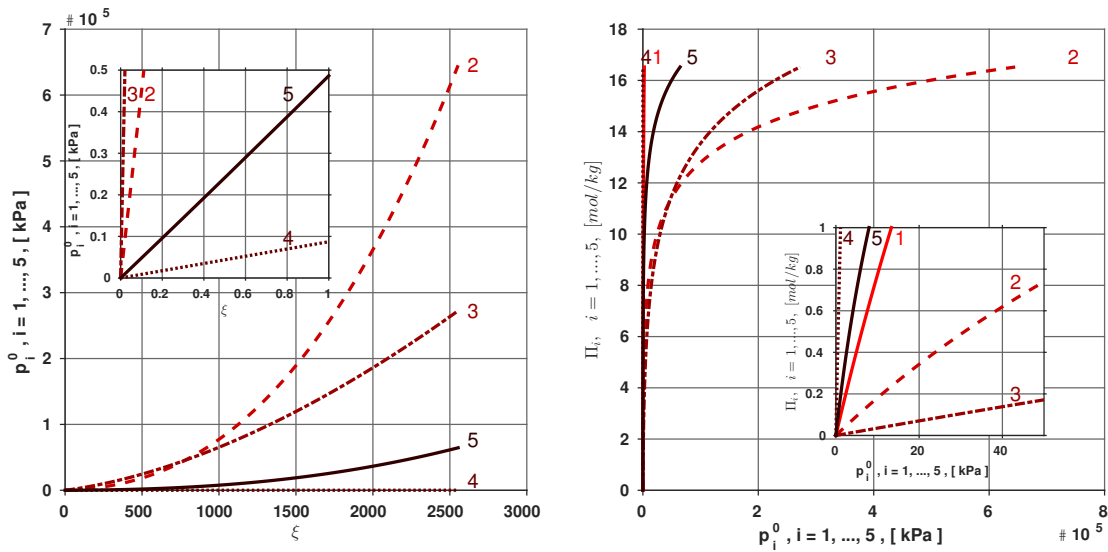
Figure 5.2: Solution, $\Psi(\xi)$, for five component problem. $(-)$: component 2; $(--)$: component 3; $(-\cdot)$: component 4; & $(\cdot\cdot)$: component 5. The computation was performed with the general-purpose numerical integrator **ode45** in MATLAB $^{\circledR}$ [168], at user-defined error tolerance values: RelTol $= 10^{-7}$ & AbsTol $= 10^{-8}$—cf. Appendix A1 for software details. This method employs the adaptive time-stepping Runge-Kutta 4(5) pair developed by Dormand & Prince [173].

5.3 Accuracy

As has been mentioned above, the solution approach provides a direct accuracy control through the specification of a suitable ODE integrator. Error control specifications are usually available in common *state of the art* integrators*, such as those provided by MATHEMATICA $^{\circledR}$ [141] and MATLAB $^{\circledR}$ [168]. A simple comparison between equilibrium calculations, performed with available analytical solution methods briefly discussed in Chapter 4 and the same calculations using the proposed solution approach, serves three key purposes: *a*) validation of the adsorption equilibrium calculations; *b*) evaluation of the attainable values of accuracy, according to numerical integrator specifications; & *c*) Test for limit cases, e.g., behavior of the solution when the concentration of an arbitrary component in the mixture vanishes, $c_i \to 0$—cf. Section 3.2.

---

*Consult e.g., Gear [174] and Hairer *et al.* [164, 166] for information about error control in ODE numerical integration.

Table 5.3: Computational performance of different IAST calculation methods for five compound task.

Calculation method	Tolerance [a]	Statistics [b] [c]	Execution time [d]
		Steps / Evaluations	[s]
IVP w/ ode23	*default*	30 / 91	0.09
	stringent	373 / 1120	0.12
	very stringent	35860 / 107581	9.99
IVP w/ ode45	*default*	21 / 127	0.02
	stringent	73 / 439	0.05
	very stringent	1036 / 6217	0.48
IVP w/ ode15s	*default*	47 / 114	0.05
	stringent	156 / 243	0.11
	very stringent	1110 / 2296	0.64
Algorithm 3.2	$\varepsilon_{\mathsf{Tol.}} = 10^{-10}$	n/a	0.17
O'Brien & Myers (FastIAS) [e]	$\varepsilon_{\mathsf{Tol.}} = 10^{-4}$	n/a	0.02

a. Tolerance values, absolute (absTol) / relative (relTol): '*default*': $10^{-3}/10^{-6}$; '*stringent*': $10^{-7}/10^{-8}$; & '*very stringent*': $10^{-13}/10^{-13}$.

b. Refers to number of computed steps yielded as output of the integration and number of r.h.s. function evaluations required.

c. n/a: "not applicable" for this method.

d. Refer to Appendix A1, p. 163 for specifics about the software applied in these calculations.

e. Using FastIAS [153]; implementation by Do [36].

Comparing IVP approach against analytical solution of Ilić *et al.* [43]

An analytical solution for a binary competitive case where single component adsorption isotherms are given by the Quadratic model—cf. Equation (2.3d) in Table 2.2, p. 17—was published by Ilić *et al.* [43], as summarized in Section 3.3.2, p. 39. By definition of error terms

$$e_{\mathsf{c}}^{\mathsf{abs.}} := |q_i - \hat{q}_i| \qquad \text{and} \qquad e_{\mathsf{c}}^{\mathsf{rel.}} := \frac{q_i - \hat{q}_i}{q_i}, \tag{5.3}$$

on the adsorbed phase concentration values at equilibrium, q_i, $i = 1, \ldots, N$, an assessment of the computational accuracy can be attained for the approach explained in Chapter 4 by comparing with this analytical solution. Table 5.4 provides applied single component isotherm parameters.

Figure 5.3 illustrates the obtained equilibria and the effect of inflection points of individual isotherms on competitive equilibria predictions applying IAST. The corresponding

Table 5.4: Single component adsorption isotherm parameters for Quadratic model—cf. Eq. (2.3d), p. 17—of two components. Values are *similar* to those reported by Ilić *et al.* [43], but modified slightly to *enhance* the effect of the inflection point along each isotherm course, as displayed in Figure 5.3.

Compound	Parameters		
	q_i^{sat} $[\,\mathrm{g/l}\,]$	b_{i1} $[\,\mathrm{l/g}\,]$	b_{i2} $[\,\mathrm{l^2/g^2}\,]$
Component 1	0.5	0.2	1.0
Component 2	0.5	0.3	3.0
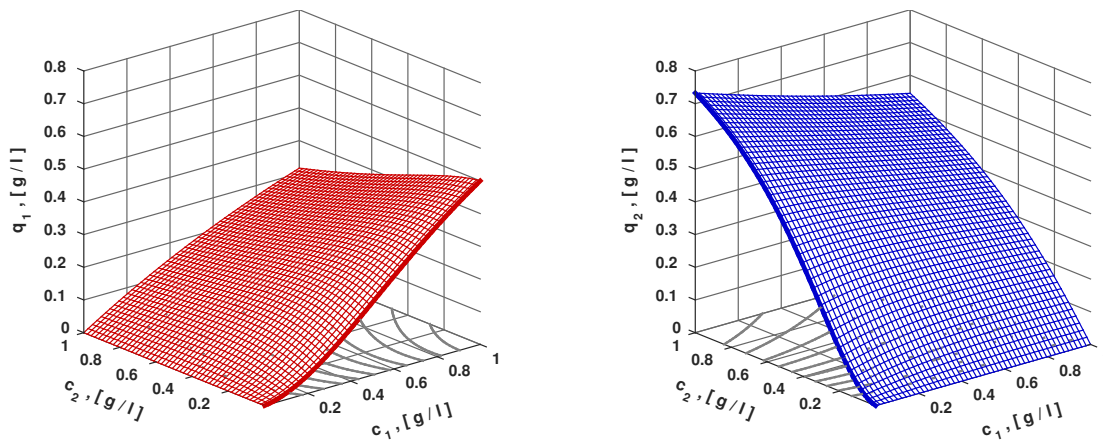
Figure 5.3: Adsorbed phase concentrations, $q_1 = f(c_1, c_2)$, $q_2 = f(c_1, c_2)$, obtained with IAST employing single component Quadratic isotherms. Parameters listed in Table 5.4.

Jacobian functions, $\mathcal{J}(q)$, are depicted in Figure 5.4. The inflection points of single component equilibria produce the shapes observed, and differ to those introduced previously in Figure 4.3, p. 52, whereby the binary competitive Langmuir equation was applied[*]. In order to verify the validity and solution behavior, an independent calculation of $\mathcal{J}(q)$ via *direct numerical differentiation* of adsorbed phase concentrations, $q = f(c)$—cf. Figure 5.3, was performed; the analytical solution displayed in Figure 5.4 was recovered as the calculation grid was refined, and thus, validating Jacobian formulæ (4.11).

Table 5.5 documents values of maximum errors incurred, as defined by formulas (5.3). These calculations of q_i at equilibrium were performed on an equidistant grid of 50×50

---

[*]Appendix A5 demonstrates that this explicit multicomponent equation is *equivalent* to IAST—cf. Equation (A5.4).
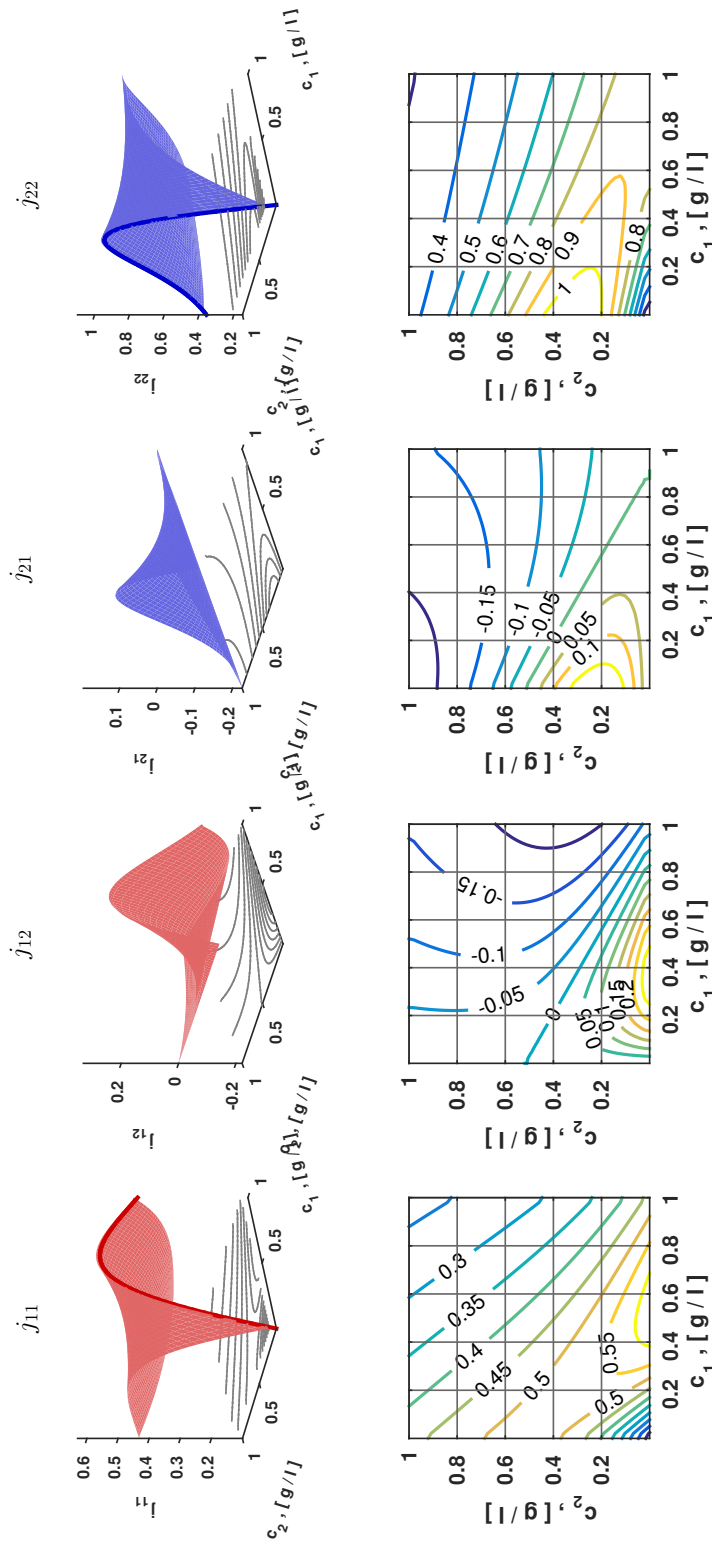
Figure 5.4: Jacobian of adsorbed phase concentrations, q_i, obtained with IAST employing single component Quadratic isotherms. $j_{11} \equiv \partial q_1/\partial c_1$; $j_{12} \equiv \partial q_1/\partial c_2$; $j_{21} \equiv \partial q_2/\partial c_1$; & $j_{22} \equiv \partial q_2/\partial c_2$. Parameters used to generate the plots are listed in Table 5.4.

values, spanning concentration ranges, $c_i \in \left[10^{10} \cdot \mathsf{eps}, 1\right] \; [\,\mathsf{g/l}\,]^*$.

Table 5.5: Maximum absolute & relative errors—Equation (5.3)—computed with the IVP solution approach and other standard methods. Calculations performed with MATLAB $^®$; see Appendix A1 for software details.

Calculation method	Errors on q_1		Errors on q_2		Execution time ^{a}
	$e_\mathrm{c}^{\mathsf{abs.}}$	$e_\mathrm{c}^{\mathsf{rel.}}$	$e_\mathrm{c}^{\mathsf{abs.}}$	$e_\mathrm{c}^{\mathsf{rel.}}$	
	$[\,\mathsf{g/l}\,]$	$[\,-\,]$	$[\,\mathsf{g/l}\,]$	$[\,-\,]$	$[\,\mathsf{s}\,]$
Analytical ^{b}	n/a	n/a	n/a	n/a	0.00004
IVP w/ ode23	3.3×10^{-7}	3.4×10^{-7}	1.4×10^{-6}	4.3×10^{-6}	0.0124
IVP w/ ode45	1.5×10^{-7}	1.6×10^{-7}	1.1×10^{-5}	1.3×10^{-5}	0.0085
IVP w/ ode15s	3.6×10^{-6}	3.7×10^{-6}	3.9×10^{-4}	2.6×10^{-4}	0.0292
Algorithm 3.2	1.1×10^{-8}	1.1×10^{-8}	2.5×10^{-6}	3.4×10^{-6}	0.0004
O'Brien & Myers ^{c}	1.0×10^{-12}	6.4×10^{-12}	8.8×10^{-11}	3.4×10^{-6}	0.0005

a. Average execution time of a *single* equilibrium calculation.
b. Reported by Ilić *et al.* [43].
c. Using FastIAS [153]; implementation by Do [36].

As can be concluded from these results, the *attainable accuracy* strongly depends on the type of integration technique, proportionally to the execution time; typically, the more sophisticated the integrator, the longer it takes to compute. The three tested integrators yielded comparable results under *mildly stringent* tolerance specifications of $\mathsf{absTol} = 10^{-5}$ and $\mathsf{relTol} = 10^{-7}$, thus proving that the IVP approach reproduces the analytical calculation accurately, with reasonable execution times.

$^*\mathsf{eps} = 2.2204 \times 10^{-16}$ refers to the *machine epsilon* of the employed workstation.

5.4 Robustness

A principal feature of the IVP solution approach is its *independence* from a suitable provision of guess values, $c^{0,\text{guess}}$, in contrast to initializing iteration loops when solving IAST tasks in their standard algebraic form, i.e., with the methods of Chapter 3.

IAST equilibria prediction for binary mixture of adsorbates using Quadratic plus Langmuir single component isotherms

As explained previously in Chapter 2, explicit multicomponent equations, while desirable, are often not available. Such is the case when *complex behavior*, displayed in the form of inflections along the isotherm courses, is observed—a experimental system possessing these characteristics is addressed in detail in Part III.

A single component isotherm equation, capable to describe these inflections is the Quadratic plus Langmuir model (2.3e), listed in Table 2.2, p. 17. Equipped with this single component information, and application of the IVP approach holds

$$\frac{\mathrm{d}c_1^0}{\mathrm{d}\xi} = 1, \tag{5.4a}$$

$$\frac{\mathrm{d}c_2^0}{\mathrm{d}\xi} = \frac{q_{11}^{\text{sat}} \dfrac{b_{11} + 2b_{12}c_1^0}{1 + b_{11}c_1^0 + b_{12}c_1^{0^2}} + q_{12}^{\text{sat}} \dfrac{b_{13}}{1 + b_{13}c_1^0}}{q_{21}^{\text{sat}} \dfrac{b_{21} + 2b_{22}c_2^0}{1 + b_{21}c_2^0 + b_{22}c_2^{0^2}} + q_{22}^{\text{sat}} \dfrac{b_{23}}{1 + b_{23}c_2^0}}, \tag{5.4b}$$

$$c_i^0(0) = 0, \quad i = 1, 2. \tag{5.4c}$$

A solution orbit, illustrated in Figure 5.5, is easily obtained by application of parameters listed in Table A4 of Appendix A8, p. 174, for compounds, phenyl-*n*-octane (C8), component 1, and phenyl-*n*-decane (C10), component 2. To the extent of the author's knowledge, there is no analytical solution for this example. However, a reference solution to compare with can be generated by computing with *very stringent* tolerances' specification, using the IVP approach and selecting the higher-order ODE integration method. The solution displayed in Figure 5.5 and computed with less stringent tolerances matches this reference solution. Additional evidence of *correct* solution behavior is observed when computing the orbit in the limit $\xi \to 0$, for which

$$c_2^0 \approx \frac{\mathfrak{h}_1}{\mathfrak{h}_2}\xi = \frac{\mathfrak{h}_1}{\mathfrak{h}_2}c_1^0 \tag{5.5}$$
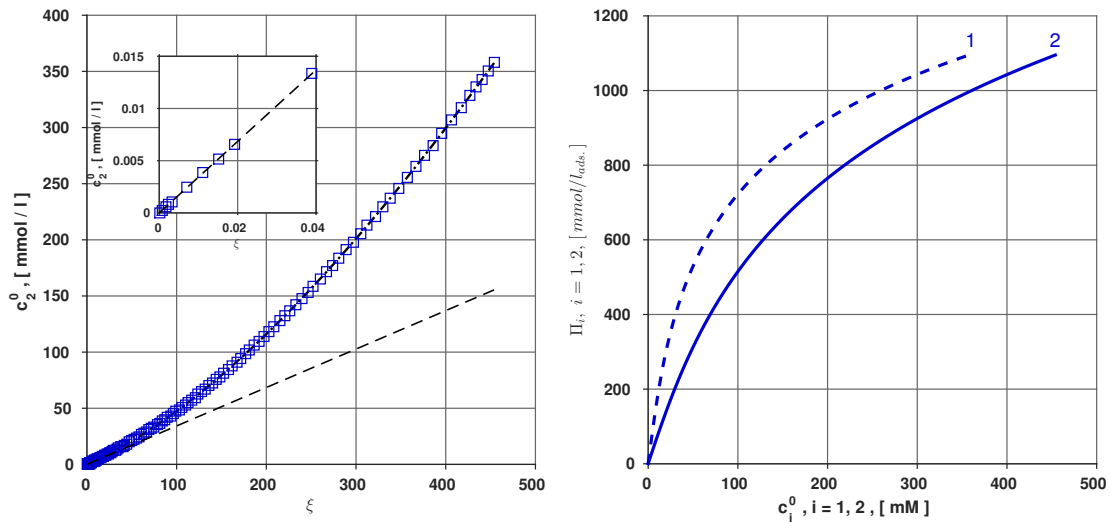
Figure 5.5: Solution orbit, $\psi_2(\xi)$, obtained by integration of the IVP (5.4), applying parameters in Table A4 of Appendix A8, p. 174. Component 1: *octylbenzene* (C8); component 2: *decylbenzene* (C10). The computation was performed with the general-purpose numerical integrator ode15s in MATLAB $^{\circledR}$ [168], at user-defined error tolerance values: RelTol $= 10^{-7}$ & AbsTol $= 10^{-8}$, and selecting numerical differentiation formulæ (NDF) as integration algorithm.

from inspection of IVP (5.4). The solution orbit converges to Equation 5.5, as also illustrated in the figure for very low concentrations. Figure 5.6 illustrates computed competitive isotherms, whereas Figure 5.7 displays the Jacobian approximations, analogous to the example applying Langmuir isotherms, Figure 4.3, p. 52 and Figure 5.4 for the Quadratic isotherms' example for comparison. Once more, the occurrence of inflection points in the individual isotherms determines the shape of these functions, which translates into particular dynamics of adsorption processes where competitive equilibria are described by these type of isotherms. This is addressed in detail in Part II.
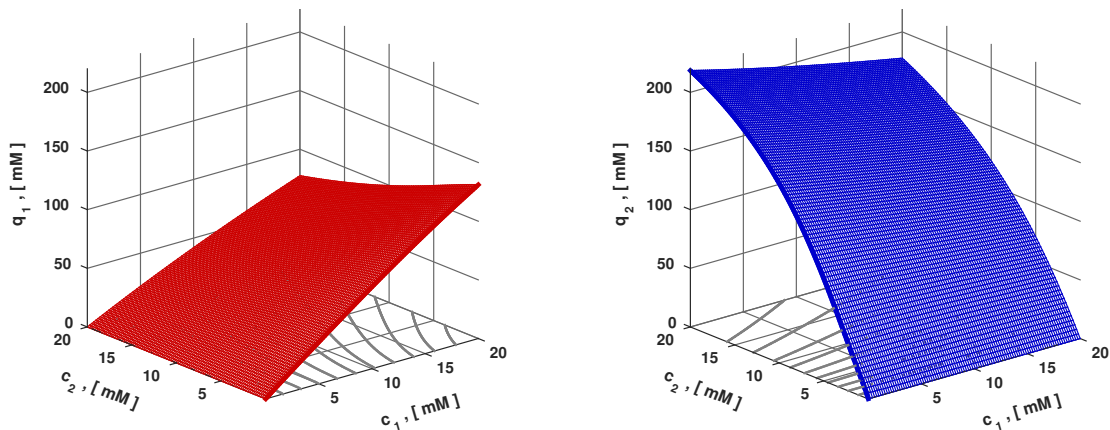
Figure 5.6: Adsorbed phase concentrations, $q_1 = f(c_1, c_2)$, $q_2 = f(c_1, c_2)$, obtained with IAST employing single component Quadratic plus Langmuir isotherms. Parameters listed in Table A4 of Appendix A8, p. 174.
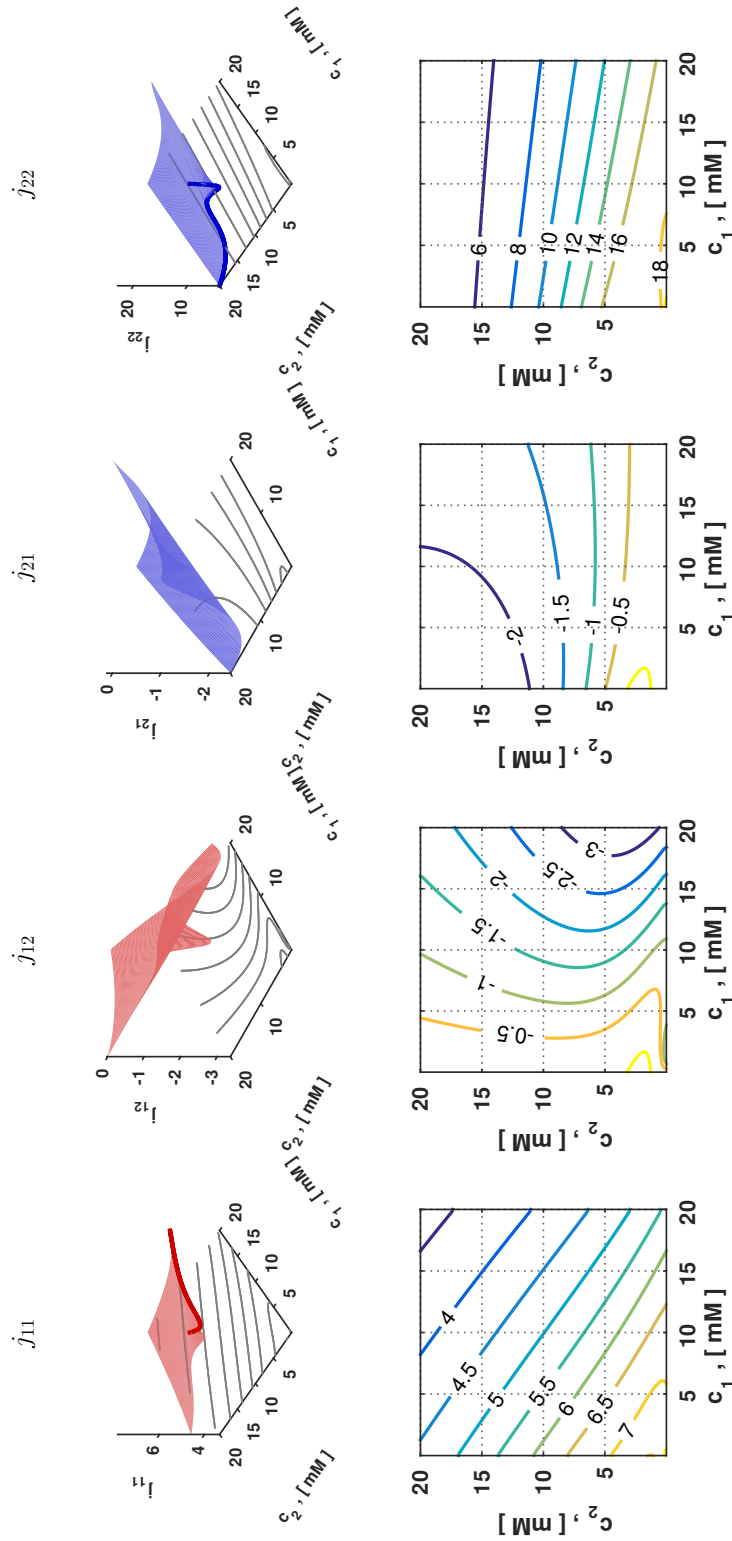
Figure 5.7: Jacobian of adsorbed phase concentrations, q_i, obtained with IAST employing single component Quadratic plus Langmuir isotherms. $j_{11} \equiv \partial q_1/\partial c_1$; $j_{12} \equiv \partial q_1/\partial c_2$; $j_{21} \equiv \partial q_2/\partial c_1$; & $j_{22} \equiv \partial q_2/\partial c_2$. Parameters used to generate the plots are listed in Table A4 of Appendix A8, p. 174.

Summary

Four fundamental aspects: *a*) SIMPLICITY; *b*) EFFICIENCY; *c*) ACCURACY; & *d*) RO-BUSTNESS, for the IVP solution principle presented in Chapter 4, were explained and illustrated by means of examples—relevant to the context of this work, viz. isotherms with *inflection points* along their functional relationships.

The method was successfully validated for typically encountered single component adsorption isotherm equations, demonstrating *flexibility* and *ample range of application.*

Advantages & disadvantages of the solution approach   While the proposed solution principle—with naturally extended Jacobian formulæ—is not *universal*, i.e., does not work for *every* single component adsorption isotherm model, it constitutes a reliable computation tool for IAST, designed for incorporating IAST equilibria into dynamic modeling of a class of adsorption-based operations, which will be the topic of Part II.

Two important *disadvantages* to keep in mind are: *a*) calculation times are similar to those of numerical quadrature approximations, comparable to Algorithm 3.2, p. 42; and *b*) inability to use *directly* single component isotherm equations that are not well-defined at the origin to estimate multicomponent equilibria. Despite of these *shortcomings*, every commonly encountered aspect discussed in Section 3.3.1, p. 36, is dealt with in a sound and advantageous manner. Moreover, it should be kept in mind that *input information* to the solution approach, the fluid phase concentrations, $c = [\, c_1, \, \ldots, \, c_N \,]^T$, should follow the PHYSICALLY CORRECT property, $c \geq 0$, i.e., positive, finite. This aspect will be addressed again when implementing the IVP solution approach to compute fixed-bed adsorber dynamics in Part II.

Part II

Adsorber dynamics

Chapter 6

Dynamic modeling of packed-bed adsorbers*

"Science is a differential equation. Religion is a boundary condition."

– Alan Turing

Introduction

$\mathbf{M}$ANY adsorption-based separation operations consist of tubular columns packed with adsorbents in order to process fluid mixtures. A classical—i.e., *deterministic*—mathematical description for a *class* of fixed-bed adsorbers, used in liquid chromatography, is presented in this chapter†. This description consists of partial differential equations (PDEs), requiring the application of suitable numerical techniques to obtain their solution. While the discussion of this chapter is centered primarily around liquid chromatography, due to the experimental demonstration presented in Part III, it is nonetheless useful for other adsorption-based separation processes as well. Knowledge of adsorption equilibria is an essential ingredient to describe the dynamic behavior of

---

*CHAPTER DISCLAIMER: Partial contents of this chapter have been reported in: *"A Method for Efficiently Solving the IAST Equations with an Application to Adsorber Dynamics"* [53]. The information is presented as part of this dissertation and it is an original published contribution to the field in a peer-reviewed journal. There is none whatsoever intention of self-plagiarism; the information serves rather as complementary content to this dissertation. Furthermore, the publishing company has granted partial reproduction of the contents in the article mentioned above. [License No.: **3743030164049**, requested and obtained on Nov. 6 th, 2015 from John Wiley & Sons, Inc. through Copyright Clearance Center.]

†Other modeling approaches such as e.g., stochastic models [175], are not considered.

fixed bed adsorbers. Throughout Part I, IAST has been discussed and a novel solution approach for its constitutive equations was introduced in Chapters 4 and 5. Along this line of thought, it is desired to *incorporate* IAST equilibrium calculations into models that describe the *intrinsic* dynamic behavior of fixed-bed adsorption columns. Before addressing this topic, an appropriate mathematical model to describe fixed-bed adsorption from the liquid phase is discussed next.

6.1 Overview of one-dimensional models

Mathematical models used to describe adsorption-based packed column processes, including liquid adsorption chromatography columns—e.g., HPLC columns, can be *roughly* classified into two comprehensive families [2, 4, 13, 14, 46, 176]:

1. Models that account *exclusively* for ADSORPTION THERMODYNAMICS, for example: *a*) ideal model—a.k.a. (local) Equilibrium Theory [4, 14, 46]; & *b*) equilibrium-dispersive model [14, 46, 176].

2. Models that account for both THERMODYNAMICS & MASS-TRANSFER KINETICS, among others: *a*) lumped-kinetic models [14, 46]; *b*) lumped-pore model [14, 46]; *c*) General Rate Model (GRM) [4, 14, 177–180]; & *d*) under consideration of additional mechanisms, such as kinetics of adsorption/desorption or chemical reactions, the *versatile* model of Berninger *et al.* (VERSE-LC model) [181, 182].

In HPLC of readily soluble, *small* molecules and packed columns with *small* particle sizes, mass-transfer effects are usually *fast*. This is typically confirmed in practice by measuring plate numbers—i.e., equivalent, theoretical number of separation stages, $N_{\mathsf{plate}, i}$, $i = 1, \ldots, N$, of investigated substances. A high plate number is as a rule an indication of fast mass-transfer kinetics of the column packing and usually translates to *high* separation efficiency in the column. In this particular situation, applying the family of *equilibrium-based* models is justified. Mass-transfer effects, on the other hand, usually become relevant in systems with *large* particle sizes and specific diffusion and adsorption mechanisms—see e.g., [183] among many others. A good example of such systems is competitive adsorption of *bulky* protein molecules in columns packed with ion-exchange resins, where, in addition, *steric hindrance* needs to be accounted for—see e.g., [184, 185] and references listed therein.

6.2   Macroscopic mass balance equation

A *time-dependent* macroscopic mass balance performed on a column packed with porous particles where adsorption occurs and without chemical reaction is written as [2, 4, 14, 186]

$$\frac{\partial[\epsilon c]}{\partial t} + \frac{\partial}{\partial t}\big[\,[\,1-\epsilon\,]\,q\,\big] + \frac{\partial[\,u\epsilon c\,]}{\partial z} = \frac{\partial}{\partial z}\left[D_L\,\frac{\partial[\,\epsilon c\,]}{\partial z}\right].\tag{6.1}$$

Equation (6.1) is a second order parabolic PDE, thus requiring *two* boundary conditions and an initial condition to be completely described [186]. Typical boundary conditions were given by Danckwerts [187]—thus defining particular solutions of (6.1).

Model assumptions considered   Without sacrificing the description of salient features of the model, given by Equation (6.1), Table 6.1 lists general assumptions commonly encountered in modeling of fixed-bed adsorption columns—see e.g., Wankat [2].

The mass balance equation (6.1) is simplified by the application of the model assumptions listed in Table 6.1 to

$$\epsilon\frac{\partial c}{\partial t} + (1-\epsilon)\,\frac{\partial q}{\partial t} + \epsilon\,\frac{\partial[uc]}{\partial z} = \epsilon\,\frac{\partial}{\partial z}\left[D_{\text{app}}\,\frac{\partial c}{\partial z}\right].\tag{6.2}$$

Moreover, by application of assumptions V, VI & VII, Equation (6.2) becomes

$$\epsilon\frac{\partial c}{\partial t} + (1-\epsilon)\,\frac{\partial q}{\partial t} + \epsilon u\frac{\partial c}{\partial z} = \epsilon\,\frac{\partial}{\partial z}\left[D_{\text{app}}\,\frac{\partial c}{\partial z}\right]\tag{6.3}$$

for constant velocity, *u*. In Sections 6.4 & 6.3, two *equilibrium-based* models are described in detail, whereby Equation (6.3) is the starting point for their derivation.

6.3   Equilibrium-Dispersive Model

Application of assumptions listed in Table 6.1 leads to a frequently applied model, viz. the simple, one parameter, one-dimensional Equilibrium Dispersive Model (EDM1D) [4, 14, 46, 176]:

$$\frac{\partial c}{\partial t} + \phi\,\frac{\partial q}{\partial t} + u\,\frac{\partial c}{\partial z} = D_{\text{app}}\,\frac{\partial^2 c}{\partial z^2}\;,\tag{6.4a}$$

Table 6.1: Assumptions made to implement *equilibrium-based* models, as applied in modeling liquid chromatography.

No.	Assumption
I	Isothermal process operation conditions—i.e., T remains constant. As a result, the energy balance equation is omitted, as heat transfer mechanisms, e.g., *conduction & convection* inside the packed bed, as well as *heat generation by adsorption*, are neglected.
II	Adsorption isotherms, $q = f(c)$—cf. Chapter 2, p. 13, suffice to describe equilibria of adsorbates; pressure effects on equilibria are neglected.
III	Inert, chemically-stable and non-degradable porous particles *without* chemical reaction.
IV	Fully-reversible, physisorption mechanism, i.e., no chemisorption.
V	Incompressible mobile—fluid—phase; the mobile phase percolates through the bed at a constant velocity and viscosity.
VI	Rigid porous particles of uniform size, d_{p}, are considered; neither *swelling* nor *shrinkage* of porous particles occur, i.e., total bed porosity, ϵ, is therefore assumed *constant*—see e.g., [54, 188–193] among others, for models considering these effects.
VII	Non-deformable, uniform pore structure of the particles, which translates to constant total porosity, ϵ, intraparticle porosity, ϵ_{p} & interparticle porosity, ϵ_{e}, with uniformly packed column—i.e., neither *channeling* nor *fingering* within *porous media* take place.
VIII	Neither *axial* nor *radial* variations in the total porosity are displayed, i.e., $\epsilon \neq f(z, r)$ homogeneously packed porous media—see e.g., [194] for radially-distributed HPLC column modeling.
IX	Kinetics of adsorption & desorption are *fast*.

with Danckwerts' boundary conditions [187]

$$\textbf{(inlet:)} \quad u\,c(t, z = 0) - D_{\mathrm{app}}\left.\frac{\partial c}{\partial z}\right|_{z=0} = u\,c_{\mathrm{in}}(t), \qquad (6.4\mathrm{b})$$

$$\textbf{(outlet:)} \quad \left.\frac{\partial c}{\partial z}\right|_{z=L} = 0\,, \qquad (6.4\mathrm{c})$$

and initial condition

$$c_0 = c(t = 0, z). \qquad (6.4\mathrm{d})$$

Equations (6.4) are written compactly with vector variables

$$c = (c_1, \ldots, c_N)^T, \quad c_{\mathrm{in}} = (c_{1,\mathrm{in}}, \ldots, c_{N,\mathrm{in}})^T, \quad q = (q_1, \ldots, q_N)^T$$

to express liquid phase concentrations, inlet—i.e., *injected*—concentrations and adsorbed phase concentrations, respectively. The parameter

$$\phi := \frac{1 - \epsilon}{\epsilon}, \tag{6.5}$$

is the *phase ratio*, i.e., the column volume occupied by the solid phase with respect to the column volume occupied by the liquid phase, which accounts for the "bulk" *interparticle* volume plus the *intraparticle* volume, so that the following expression relating the *interparticle* voidage, ϵ_e, and *intraparticle* porosity, ϵ_p, to *total* porosity, ϵ, in the fixed-bed can be written [4, 14]:

$$\epsilon = \epsilon_e + \epsilon_p \left[1 - \epsilon_e \right]. \tag{6.6}$$

The mobile phase velocity is defined as:

$$u := \frac{Q}{\epsilon A_c} = \frac{4\,Q}{\epsilon \pi d_c^2}, \tag{6.7}$$

where Q is the volumetric flow rate and A_c is the cross-sectional area of the column. All the effects causing band profile diffusion are lumped together onto apparent diffusion coefficients,

$$D_{app} = \mathsf{diag}\left(D_{app,1}, \ldots, D_{app,N}\right). \tag{6.8}$$

These apparent diffusion coefficients can be estimated by means of a suitable correlation—Chung & Wen [195], Guiochon & Lin [196]—or directly estimated from experimental measurements—Meyer [197]. Since they are directly related to mass-transfer kinetics' effects, they are functions of the mobile phase velocity, u, and the plate number, $N_{\mathsf{plate},k}$:

$$D_{app,k} = \frac{1}{2} \frac{u\,L_c}{N_{\mathsf{plate},k}}, \quad k = 1, \ldots, N. \tag{6.9}$$

Quite often an *apparent* PÉCLET number [186], defined as the ratio of *convective transport*, $u\,L_c$, to *diffusive transport*, D_{app}, along spatial coordinate, z, is introduced to be able to compare among systems. In accord with Equation (6.9),

$$\mathsf{Pe}_k := \frac{u\,L_c}{D_{app,k}} = 2\,N_{\mathsf{plate},k}. \tag{6.10}$$

Values of this parameter indicate if the system is *convection-dominated* [4, 198, 199]. This is also closely related to numerical methods applied to solve model equations (6.4), as will be explained in Chapter 7.

For the term $\partial q(c)/\partial t$ in Equation (6.4a) holds

$$\frac{\partial q_i(c)}{\partial t} = \sum_{k=1}^{N} \frac{\partial q_i}{\partial c_k} \frac{\partial c_k}{\partial t}, \quad i = 1, \ldots, N \tag{6.11}$$

by applying the Chain Rule, since adsorption equilibrium prevails. Details to employ IAST in the dynamic column modeling are given in Chapter 7, Section 7.7. The expressions $\partial q_i/\partial c_i$ are simply the Jacobian elements discussed in Section 4.3, p. 50, under the frame of IAST.

6.4 Ideal model: local Equilibrium Theory

The *hypothetical situation* of an infinite mass transfer rate, i.e., $h_{\text{plate}} \to 0$, is now considered—cf. Assumption IX, Table 6.1. In this way, process dynamics are governed exclusively by adsorption equilibria, i.e., it entirely becomes THERMODYNAMI-CALLY CONTROLLED; therefore, the following mass balance holds:

$$\frac{\partial c}{\partial t} + \phi \frac{\partial q(c)}{\partial t} + u \frac{\partial c}{\partial z} = 0. \tag{6.12}$$

Equation (6.12) is simplified with Equation (6.11), as explained before. The partial derivatives in (6.11) are just elements of the Jacobian matrix, $\mathcal{J}(q(c))$, already discussed in Section 4.3, in particular Equation (4.9), p. 50. As a result, Equation (6.12) is written formally as

$$[\mathcal{I} + \phi \mathcal{J}] \frac{\partial c}{\partial t} + u \frac{\partial c}{\partial z} = 0. \tag{6.13}$$

The *elegance* and usefulness of Equation (6.13) lies in the fact that it is a system of *N first order, quasilinear equations*, whose solution in the time-space plane* can be determined by applying the METHOD OF CHARACTERISTICS (MOC)—see e.g., [159, 160, 200][†]. Abundant literature where this approach is applied and discussed in the context of liquid chromatography is available, among many others, [159, 160, 200, 203–209]. However, with this approach, only a few fully analytical solutions have been developed and reported.

---

*This is often regarded as *'distance-time'* plane in the literature; it is simply the space defined by the *Cartesian product* $[0, L] \times [0, t]$ where the solution of $c(t, z)$ lives.

[†]Some *historical* references on this topic include the works of Wilson [201] and DeVault [202].

Hyperbolic conservation law

Equation (6.13) belongs to a larger class of equations known in the physical sciences as *conservation laws.* The following proof confirms this statement.

Proposition 6.4.1. *Equation* (6.12) *can be written in conservation form—see among others* [159, 210–213].

Proof. Take Equation (6.12) and introduce the *conservation* variable

$$w := c + \phi\, q, \quad \text{with flux defined as} \quad \mathfrak{f} \equiv uc. \tag{6.14}$$

Equation (6.12) can therefore be written as

$$\frac{\partial w}{\partial t} + \frac{\partial \mathfrak{f}}{\partial z} = 0. \tag{6.15}$$

Further, if $\partial q/\partial c$ exists, for *smooth* $q = f(c)$, then $\partial q/\partial t = (\partial q/\partial c)\,(\partial c/\partial t)$ holds for equilibrium-based models—cf. Equation (6.11). Under these considerations and using conservation variable, w,

$$\frac{\partial}{\partial t}\,[\,c + \phi\, q\,] + \frac{\partial \mathfrak{f}}{\partial z} = 0. \tag{6.16}$$

Equations (6.12) and (6.16) are *equivalent.* $\qquad\square$

With this proof it is also possible to write Equation (6.13) as:

$$\frac{\partial c}{\partial t} = [\,\mathcal{I} + \phi\, \mathcal{J}\,]^{-1}\,(-u)\,\frac{\partial c}{\partial z}. \tag{6.17}$$

This mathematical feature of the equations of chromatography lead *naturally* to methods commonly applied in the numerical approximation of hyperbolic conservation laws, in general [213, 214].

The Equilibrium-Dispersive Model (EDM1D) (6.4) can also be written in conservation form. As explained in Chapter 7, numerical methods applied for computing solutions of hyperbolic conservation laws *may* be applied in some cases to solve convection-diffusion equations of the type expressed by this model.

Summary

A brief overview of standard models applied in one-dimensional modeling of packed bed adsorbers was presented and explained. Special emphasis was set on *equilibrium-based* models, which, despite of their *simplicity*, can be applied under appropriate assumptions to a number of technically relevant processes, e.g.,

1. liquid chromatography under dilute conditions; &

2. gas chromatography of dilute gases without *significant* changes in local gas velocity, i.e., negligible *sorption effect* & pressure drop along the fixed-bed.

Analytical solutions are unfortunately limited to simple cases only. Henceforth, Chapter 7 provides necessary details to solve numerically the equilibrium-based models considered in this work, emphasizing the framework of IAST.

Chapter 7

Numerical simulation of packed-bed adsorber models[*]

> *"(...). It is not necessary to study this routine in detail in order to understand the major point: building efficient reliable programs, even for simple tasks, requires careful engineering combined with computer understanding."*

> – David Kahaner, Cleve Moler & Stephen Nash in [149]

Introduction

THE equilibrium-dispersive model, introduced in Section 6.3, has an analytical solution only for *simple* boundary conditions, adsorption isotherms—e.g., linear and Langmuir isotherm—to represent adsorption equilibria and number of adsorbable components, N [14, 46]. The general case, Equation (6.4), consisting of Danckwerts' boundary conditions and competitive local equilibrium model—e.g., IAST, for arbitrary

---

[*]CHAPTER DISCLAIMER: Partial contents of this chapter have been reported in: *"A Method for Efficiently Solving the IAST Equations with an Application to Adsorber Dynamics"* [53]. The information is presented as part of this dissertation and it is an original published contribution to the field in a peer-reviewed journal. There is none whatsoever intention of self-plagiarism; the information serves rather as complementary content to this dissertation. Furthermore, the publishing company has granted partial reproduction of the contents in the article mentioned above. [License No.: **3743030164049**, requested and obtained on Nov. 6th, 2015 from John Wiley & Sons, Inc. through Copyright Clearance Center.]

number of adsorbable components, N, requires a reliable numerical approximation*, as closed form solutions are limited.

7.1 Numerical methods for equilibrium-based models

There are several approaches to numerically solve second order, parabolic PDEs—cf. [215–218], such as the equilibrium-dispersive model in one dimension, Equation (6.4). Two domains, spatial, z, and temporal, t, may be discretized, so two widely applied strategies arise. The first alternative, FULL DISCRETIZATION, consists of partitioning *both* domains. The kind of partition is defined by the numerical method itself. In the second strategy, only one of the domains is discretized, while the remaining one is given a *continuous* treatment; it is therefore given the name METHOD OF LINES†. An ODE system arises after its application. Figure 7.2 illustrates the discretization approach. Development of numerical methods to solve PDEs has considerably gained relevance in the last 40 years. In the framework of method of lines, three well-known kinds of discretization are traditionally applied, viz. finite differences (FD), finite elements (FE) and finite volume methods (FV)—see e.g., [14, 196, 217]. Consequently, a wide palette of numerical techniques have been developed and are readily available. A *fundamental premise* to consider when selecting a discretization method is the following:

> ☆ *Liquid chromatography is governed by laws of conservation (mass, energy & momentum). Therefore, numerical schemes used to simulate this process should mimic applicable conservation principles.*

With this idea in mind, a sound choice of numerical discretizations can be undertaken, in the hope that they possess the following—desirable—*monotonicity* properties [47]: *a*) POSITIVITY; *b*) TOTAL-VARIATION-DIMINISHING SATISFYING; and *c*) MAXIMUM-PRIN-CIPLE SATISFYING. In this work, two *conservative* schemes that are monotone are addressed. First, a classical numerical scheme, of wide application in liquid chromatography, is explained. Secondly, a third order upwind-biased scheme is explained.

---

*An important assumption is made in this case, inasmuch as solutions obtained by applying the numerical scheme approximate & *converge* to actual PDE solution. *Rigorous* proofs are up to this date difficult and in general not available [14, 46].

†This second method is popular in chemical engineering due to its ease of implementation; see e.g., Schiesser [219] and Saucez *et al.* [220].

7.2 Conservative Finite Difference scheme (FD)

Rouchon *et al.* [211, 212] applied the scheme of Godunov—see e.g., [213, 214]—to solve the hyperbolic conservation law expressed by the equilibrium model (6.15)*. The differentials in time and space of conservation law (6.15) are approximated by simple first order finite differences, so that

$$u\frac{c_{j+1}^n - c_j^n}{\Delta x} + \frac{v(c)_j^n - v(c)_j^{n-1}}{\Delta t} = 0, \tag{7.1}$$

with discrete conserved variables, $v(c)_j^n \equiv c_j^n + \phi\, q_j^n$. Further, since local equilibrium prevails, $q_j^n = f(c_j^n)$. Figure 7.1 geometrically represents the computational *molecule* [221] of Equation (7.1). Since the scheme is only first order accurate, its discretization error,
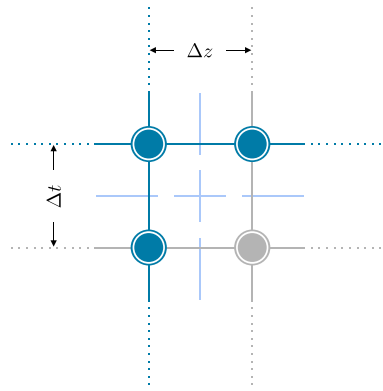
Figure 7.1: Computational *molecule* used in conservative finite differences.

in the form of *numerical dispersion*, is proportional to the refinement—i.e., number of grid points, J—of spatial coordinate, x. This numerical dispersion—the *leading term* of the error in the approximation (7.1) of mathematical model, Equation (6.4a), p. 79—can be efficiently adapted to the apparent axial diffusion term, $D_{\mathrm{app}}\dfrac{\partial^2 c}{\partial x^2}$, of equilibrium-dispersive model (6.4) by adjustment of Δx.

The finite difference scheme (7.1) is stable for COURANT number [14, 221]:

$$\nu > 1. \tag{7.2}$$

---

*The discretization is often referred to as *Rouchon algorithm* in the liquid chromatography community.

7.3   Finite Volume Method (FVM)

Application of the finite volume method to solve the PDEs of the packed column model, Equation (6.4), yields the exact *conservation form* formulation—see e.g., [213, 214]:

$$\int_{\Omega_j} \frac{\partial}{\partial t} w(x,t)\, \mathrm{d}x + \left((f(w))_{j+\frac{1}{2}} - (f(w))_{j-\frac{1}{2}} \right) = 0. \tag{7.3}$$

$w(x,t)$ is a conserved variable—cf. proof given in Section 6.4. The flux function $(f(w))_{j+\frac{1}{2}}$ is evaluated at the corresponding coordinate of the cell boundary, $\partial\Omega_{j+\frac{1}{2}}$. The *discretized* spatial domain, Ω_h, approximates Ω and consists of *non-overlapping, equidistant cells*, Ω_j, so that

$$\Omega \approx \Omega_h \equiv \bigcup_{j=1}^{J} \Omega_j = \{\, \Omega_1, \cdots, \Omega_{j-1}, \Omega_j, \Omega_{j+1}, \cdots, \Omega_J \,\}. \tag{7.4}$$

The Ω_j are numbered in ascending order, in the direction of flow, i.e., '*from left to right*', as shown schematically in Figure 7.2. A key ingredient of Equation (7.3) is precisely
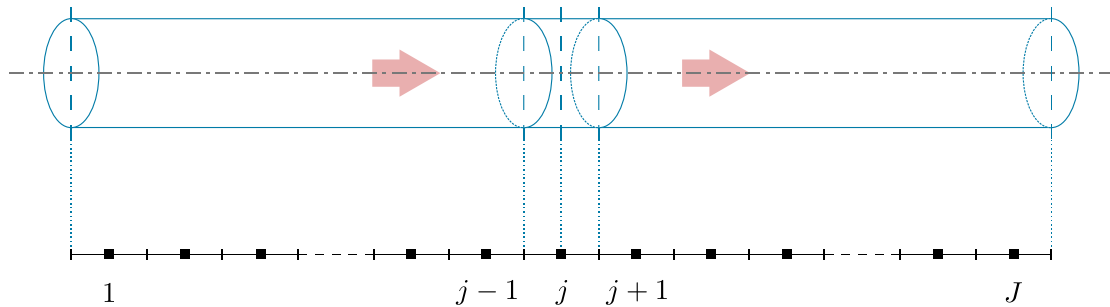
Figure 7.2: Graphical illustration of the discretized spatial domain, partitioned into equidistant grid cells of size Δz. Arrows indicate flow direction, i.e., '*from left to right*'. [Shown for illustration ONLY; actual physical dimensions vary!]

the evaluation of the flux functions, $(f(w))_{j+\frac{1}{2}}$, albeit computed state variables—i.e., *unknowns*, are located at cell centers, x_j, of the grid cells, $\Omega_j{}^*$. This is referred to as *cell-centered* discretization, as shown in Figure 7.2, and is the one used in this work—a *vertex-centered* formulation may be defined as well [47]. A further noteworthy aspect of the method is contained in the first term of Equation (7.3), as it indicates the integral of the conserved state variable over cell domain, Ω_j. In its simplest form, this term may be represented by the *average value* of $w(x,t)$ over the interval $]x_{j-\frac{1}{2}}, x_{j+\frac{1}{2}}[\equiv \Omega_j$. In order to apply Equation (7.3), flux functions $(f(w))_{j+\frac{1}{2}}$ need an approximation, which defines

---

*Equation (7.3) is *exact*; it is simply the integral form equivalent of Equation (6.4).

the implemented FV technique. This *reconstruction step* [47, 213, 214] is performed with information of cell averages, w, at each grid cell, Ω_j, and is explained next.

7.4 Spatial discretization

There are many alternatives to approximate flux functions $\left(f(w)\right)_{j-\frac{1}{2}}$ and $\left(f(w)\right)_{j+\frac{1}{2}}$ in Equation 7.3. In order to simplify the notation in what follows, let

$$f_{j-\frac{1}{2}} \equiv \left(f(w)\right)_{j-\frac{1}{2}} \quad \text{and} \quad f_{j+\frac{1}{2}} \equiv \left(f(w)\right)_{j+\frac{1}{2}}. \tag{7.5}$$

The simplest way—and perhaps best-known, approximates values at the cell faces, $\partial\Omega_{j+\frac{1}{2}}$, by *upwinding* values of f_j, which are evaluated at cell averages, w_j, so that

$$\hat{f}_{j+\frac{1}{2}} = f_j. \tag{7.6}$$

It is therefore known as UPWIND SCHEME (UDS)—see e.g., LeVeque [213] and Toro [214]. A more sophisticated possibility to compute $f_{j+\frac{1}{2}}$ would include values of several adjacent cells around Ω_j, by means of a *compact stencil*

$$S_j := \left\{ \cdots, f_{j-1}, f_j, f_{j+1}, \cdots \right\}. \tag{7.7}$$

In this way, a *higher order interpolation* formula can be applied on S_j to provide a *higher order approximation*, $\hat{f}_{j+\frac{1}{2}}$ to flux functions, $f_{j+\frac{1}{2}}$. In essence it is consequently expected that including more state variables, i.e., extending the stencil (7.7), should improve this approximation. Generally speaking, the success of the FV technique depends upon two main factors: *a)* the amount of cells, J, used in the discretization; *b)* the degree and type of approximation—e.g., interpolation—applied to compute $\hat{f}_{j+\frac{1}{2}}$. In order to obtain a useful FV approximation for this work, a THIRD ORDER, UPWIND-BIASED SCHEME, reported by Koren, *et al.* [222, 223], with numerical flux functions approximated by the interpolation formula

$$\hat{f}_{j+\frac{1}{2}} = f_j + \frac{1+\kappa}{4}\left(f_{j+1} - f_j\right) + \frac{1-\kappa}{4}\left(f_j - f_{j-1}\right), \tag{7.8}$$

was implemented, tested and validated against two numerical techniques: *a)* upwind scheme—cf. Equation (7.6) & *b)* orthogonal collocation on finite elements (OCFE)—see e.g., [198, 199, 224]. The parameter κ in Equation (7.8) is assigned a value in the interval $[-1, 1]$. The value $\kappa = \frac{1}{3}$ is optimal, providing the desired high order interpolation

polynomial on the *three-valued* stencil

$$S_j = \{f_{j-1}, f_j, f_{j+1}\} \tag{7.9}$$

for *smooth* parts of the solution; see Figure 7.3. However, in the presence of *discontinu-*
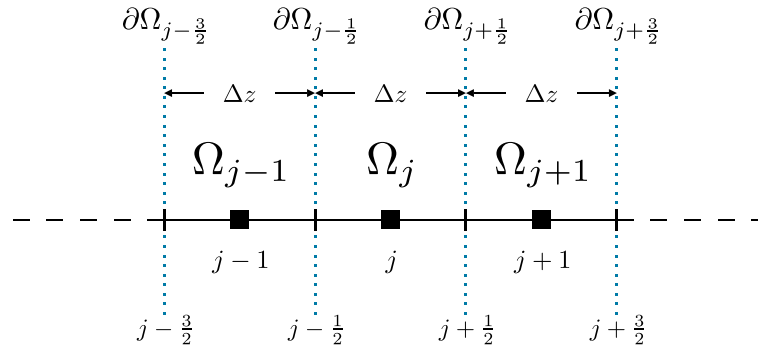
Figure 7.3: Graphical illustration of the applied stencil, S_j, partitioned into equidistant grid cells, Ω_j, of size Δz.

ities of the computed solution as it is evolved in time, suppression of *spurious, physically unrealistic oscillations* that may eventually appear can be accomplished using a *flux limiter technique*—see e.g. [213, 214] for details. A flux limiter *monitor function*, $\phi(r)$, keeps the scheme *monotone*. An abundance of flux monitor formulæ have been published—see e.g., Kemm [225] and references therein.

The flux monitor expression used in this work, proposed by Koren *et al.* [222, 223] is:

$$\phi(r) = \mathsf{max}\left[0, \mathsf{min}\left[2r, \mathsf{min}\left[\frac{1}{3} + \frac{2}{3}r, 2\right]\right]\right], \tag{7.10a}$$

satisfying the *monotonicity domain* of Sweby [226]; *in principle* this monitor function should be able to: *a)* guarantee 3rd order accurate spatial approximation to sought-after solutions; & *b)* resolve different types of discontinuities that may appear in the computed solution with *high resolution*. Figure 7.4 illustrates the monitor function (7.10a), thus explaining graphically the internal operation of this higher-order scheme. The flux
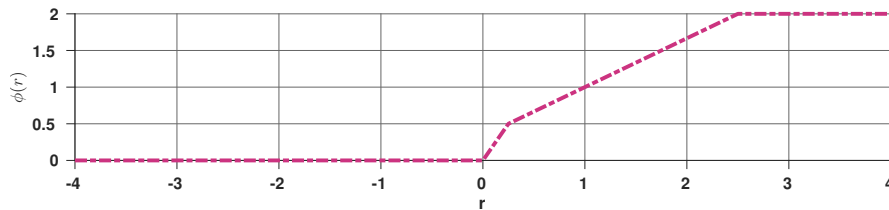
Figure 7.4: Flux limiter monitor function, $\phi(r)$, expressed by Equation (7.10a).

function approximations are

$$\hat{f}_{j+\frac{1}{2}} = f_j + \frac{1}{2}\phi\left(r_{j+\frac{1}{2}}\right)(f_j - f_{j-1}),$$ (7.10b)

whereby the limiter function (7.10a) is evaluated for arguments $r_{j+\frac{1}{2}}$ defined as

$$r_{j+\frac{1}{2}} := \frac{f_{j+1} - f_j + \varepsilon_d}{f_j - f_{j-1} + \varepsilon_d},$$ (7.10c)

applying a small positive constant, ε_d, to avoid divisions by zero when the computation is performed [222, 223].

Treatment of boundary conditions

Due to the employed stencil (7.9), a strategy of adding *ghost cells* at the inlet, and outlet was applied [47, 213].

Inlet BC   In order to compute flux $\hat{f}_{\frac{1}{2}}$, the inlet boundary condition, Equation (6.4b), p. 80, is applied *directly*; the value w_{in} is then extrapolated to the *leftmost* ghost cell variable, $\bar{w}_0$, in order to obtain $\hat{f}_{\frac{3}{2}}$ with Equation (7.10b).

Outlet BC   For the flux $\hat{f}_{J+\frac{1}{2}}$ the *linear extrapolation* formula

$$\hat{f}_{J+\frac{1}{2}} = \hat{f}_J + \frac{1}{2}\left[\hat{f}_J - \hat{f}_{J-1}\right]$$ (7.11)

was employed.

Figure 7.5 illustrates the applied BC treatment[*]. An example illustrating the implementation of this spatial discretization is given in Appendix A7.

---

[*]The adopted BC treatment proved to be stable for every numerical simulation & considered operational scenarios—i.e., process conditions. For multicolumn implementation, different formulæ to treat the boundaries may be necessary.
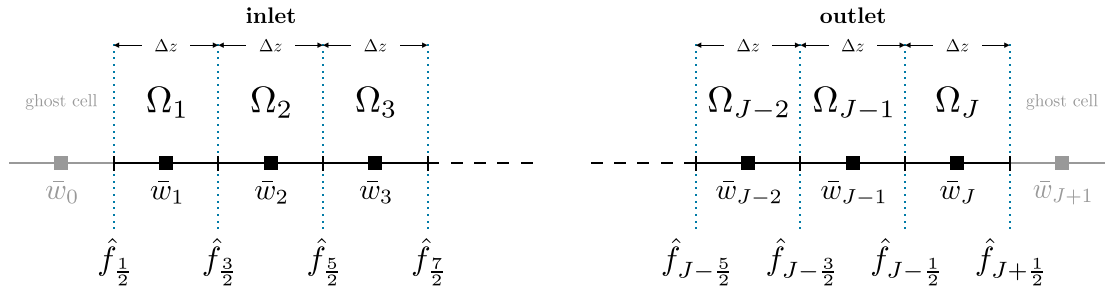
Figure 7.5: Graphical illustration of applied stencil, S_j, at $z = 0$ and $z = L$, including *leftmost* and *rightmost* ghost cells, viz. 0 and $J + 1$, added to the discretized domain to implement inlet and outlet boundary conditions.

7.5 Time integration

As mentioned before—cf. Section 7.1, application of the method of lines to Equation (7.3) yields approximation

$$\int_{\Omega_j} \frac{\partial}{\partial t} w(x, t) \, \mathrm{d}x \approx (\Delta x)_j \frac{\mathrm{d}}{\mathrm{d}t} \bar{w}_j(t) \tag{7.12}$$

for its leftmost term; in conjuction with *numerical flux functions*, $\hat{f}_{j+\frac{1}{2}}$, Equation (7.10b), leads to semi-discrete form

$$(\Delta x)_j \frac{\mathrm{d}}{\mathrm{d}t} \bar{w}_j(t) + \left(\hat{f}_{j+\frac{1}{2}} - \hat{f}_{j-\frac{1}{2}} \right) = 0, \tag{7.13}$$

written *formally* as

$$\frac{\mathrm{d}}{\mathrm{d}t} \bar{w}_j(t) = -\frac{1}{(\Delta x)_j} \left(\hat{f}_{j+\frac{1}{2}} - \hat{f}_{j-\frac{1}{2}} \right), \quad j = 1, \ldots, J. \tag{7.14}$$

Equation (7.14) provides the necessary FV approximation to the sought solution.

Strong-Stability-Preserving Runge-Kutta Methods

Equation (7.14) is a system of *coupled* ODEs of size J, which in theory can be integrated by any appropriate method, as long as certain stability requirements are guaranteed— see e.g., [164, 166]. However, as mentioned at the start of the chapter, not only stability is critical, but also properties: *a*) POSITIVITY; *b*) BOUNDEDNESS; & *c*) TVD PROPERTY—in one dimension. The applied limited κ-scheme for the spatial domain discretization *already* warrants these properties under certain conditions [222, 223]. When evolving the solution of ODE system (7.14) in time, t, an integration method should

be applied that also fulfills these properties—see Hundsdorfer & Verwer [47]. Enforcing *positivity*—i.e., non-negativity, for example, is difficult to realize for standard ODE methods readily found in commercial codes [227].

A *strong stability preserving* Runge-Kutta method (SSP-RK) is designed specifically to enforce the required monotonicity properties listed above. Among the one-step integration methods of this class, popularized by Shu and co-workers [228–230], the *explicit, one-step* third order method (SSP-RK3)

$$u^{(1)} = u^n + \Delta t \, L(u^n), \tag{7.15a}$$

$$u^{(2)} = \frac{3}{4}u^n + \frac{1}{4}u^{(1)} + \frac{1}{4}\Delta t \, L(u^{(1)}), \tag{7.15b}$$

$$u^{n+1} = \frac{1}{3}u^n + \frac{2}{3}u^{(2)} + \frac{2}{3}\Delta t \, L(u^{(2)}). \tag{7.15c}$$

is a suitable choice for the tasks at hand. A SSP-RK method is in essence a *convex combination* of Euler steps. This means that (7.15) is *stable* under *CFL condition**

$$\nu := \frac{\Delta t}{\Delta x} \left| f'(w) \right|; \quad \nu \leq 1, \tag{7.16}$$

therefore restricting somehow the performance of integration scheme (7.15), in comparison to e.g., *adaptive time-stepping* methods, often popular in commercial, technical computing software packages [165, 231, 232]. Nonetheless, the main goal is to preserve the TVD property—i.e., ensuring solution positivity, together with highly accurate solution approximations of equilibrium-dispersive model (6.4). The selection of this particular time discretization should become clear in Section 8.1, p. 102; therein, a comparison between a *classical* Runge-Kutta scheme and the SSP-RK method to compute a particular solution is discussed in detail. Moreover, Appendix A7 provides a simple example, whereby application of spatial discretization discussed in Section 7.4 yields an ODE system after implementing the *method of lines*—cf. Section 7.1; these ODEs can be integrated *explicitly* with time discretization (7.15).

Special emphasis has been given in this section to application of spatial discretizations and time-marching schemes that preserve NON-NEGATIVITY of computed solutions for dynamic fixed-bed adsorber models. This is an additional constraint, essential to incorporate IAST equilibria predictions into corresponding numerical schemes, as the equilibrium model requires *input information $c \geq 0$*.

---

*Courant-Friedrichs-Lewy condition; see e.g. [210, 213, 214] & abundant references therein listed.

7.6 Application of limited κ-scheme to obtain solution approximations of EDM1D

In analogous manner to Koren *et al.* [222, 223], *convection-dominated* problems[*], with *moderately high* to *high* Péclet numbers, can also be treated with the κ-scheme described in Section 7.4. For diffusion operator

$$\frac{\partial}{\partial z}\left(D_{\text{app}}\frac{\partial w}{\partial z}\right), \tag{7.17}$$

a central difference can be defined on stencil (7.7) as well. Assuming constant D_{app}, yields

$$\frac{\partial}{\partial z}\left(D_{\text{app}}\frac{\partial w}{\partial z}\right) \approx D_{\text{app}}\frac{1}{\Delta z}\left(\left(\frac{\partial w}{\partial z}\right)_{j+\frac{1}{2}} - \left(\frac{\partial w}{\partial z}\right)_{j-\frac{1}{2}}\right). \tag{7.18}$$

The differentials $\left(\frac{\partial w}{\partial z}\right)_{j+\frac{1}{2}}$ and $\left(\frac{\partial w}{\partial z}\right)_{j-\frac{1}{2}}$ are, in addition, approximated by simple backward differences, so

$$\left(\frac{\partial w}{\partial z}\right)_{j+\frac{1}{2}} \approx \frac{\bar{w}_{j+1} - \bar{w}_j}{\Delta z} \quad \text{and} \quad \left(\frac{\partial w}{\partial z}\right)_{j-\frac{1}{2}} \approx \frac{\bar{w}_j - \bar{w}_{j-1}}{\Delta z}, \tag{7.19}$$

providing finally the desired approximation

$$\left(D_{\text{app}}\frac{\partial^2 w}{\partial z^2}\right)_j \approx D_{\text{app}}\frac{\bar{w}_{j+1} - 2\bar{w}_j + \bar{w}_{j-1}}{\Delta z^2}, \tag{7.20}$$

which is also *congruent* with stencil (7.9). For computation of the advective fluxes, the procedure already outlined in Section 7.4 is applied. If diffusion is significant or dominant, a strategy that may deal with each term *separately* is encouraged for the purpose of numerical efficiency and stability—see e.g., Hundsdorfer & Verwer [47]. A reason for this is that stability condition (7.16) seriously constraints the allowable time step size of the explicit integration scheme (7.15), rendering it inefficient. Hereby, the class of IMEX (implicit-explicit) integration methods are an applied alternative when diffusion becomes *dominant*—see e.g., [47].

---

[*]By this term it is meant a convection-diffusion equation, whereby convection is the dominant transport mechanism—i.e., small diffusion coefficients.

Treatment of boundary conditions (BCs) for diffusive terms

In this case *one-sided* second order finite difference approximations are applied[*].

Inlet BC   For this boundary holds

$$\left(D_{\text{app}}\frac{\partial^2 w}{\partial z^2}\right)_{\frac{1}{2}} \approx D_{\text{app}}\frac{-8w_{\text{in}} + 9\bar{w}_1 - \bar{w}_2}{3\Delta x}. \tag{7.21}$$

Outlet BC   The equation

$$\left(D_{\text{app}}\frac{\partial^2 w}{\partial z^2}\right)_{J+\frac{1}{2}} \approx D_{\text{app}}\frac{8\bar{w}_{J+1} - 9\bar{w}_J + \bar{w}_{J-1}}{3\Delta x} \tag{7.22}$$

is applied. Hereby, $\bar{w}_{J+1}$ stands for the state variable of the rightmost ghost cell, Ω_{J+1}, as shown in Figure 7.5.

---

[*]Other approximations to these derivatives are possible; since the formula for the approximation at the interior—Equation (7.20)—is at most second order accurate, a second order approximation at the boundaries is justified as well.

7.7 Incorporating IAST equilibria into equilibrium-based fixed-bed adsorber models

Hyperbolicity of dynamic model equations

An equilibrium-based model can be written as [53]:

$$\frac{\partial c}{\partial t} = [\mathcal{I} + \phi \mathcal{J}]^{-1} (-u) \frac{\partial c}{\partial z}. \tag{6.17}$$

Recall the formulation to calculate the Jacobian discussed in Chapter 4. Due to the *properties* of the computation of $\mathcal{J}$, the natural question remains open, whether or not it may be possible to compute *directly* the inverse shown on the r.h.s. of Equation (6.17). Its accompanying matrix, $[\mathcal{I} + \phi \mathcal{J}]^{-1}$, should be such that *hyperbolicity* of (6.17) is not lost[*]. The following proof, developed by Flockerzi [162], analyzes this fundamental requirement to solve (6.17).

Proposition 7.7.1. *The matrix $[\mathcal{I} + \phi \mathcal{J}]^{-1}$ is hyperbolic with N real distinct eigenvalues for strictly increasing q_k^0, $k = 1, \ldots, N$.*

Table 7.1: Definitions of additional objects applied to compute $\mathcal{K}(\lambda)$.

Object	Expression	
Diagonal matrix $D = D(\lambda)$	$D = \mathsf{diag}(d_k), \; d_k := \dfrac{q_{\mathrm{tot}}}{\lambda c_k^0 + q_{\mathrm{tot}}}$	(7.23a)
Matrix $H = H(\lambda)$	$H := D\,x\,f^T - D\,W\,x\,e^T$	(7.23b)
Scalar $h_1 = h_1(\lambda)$	$h_1 := 1 + \mathsf{tr}\,[\,H\,]$	(7.23c)
Scalar $h_2 = h_2(\lambda)$	$h_2 := \mathsf{det}\,[\,\mathcal{I} + H\,]$	(7.23d)
Matrix $K_2 = K_2(\lambda)$	$K_2 := \dfrac{1}{h_2}\left[\,h_1\,H - H^2\,\right]$	(7.23e)

Proof. Let

$$\lambda \equiv \frac{1}{\phi} \tag{7.24a}$$

—i.e., the reciprocal of column model parameter ϕ in Equation (6.5), employing the substitutions: $x_i \equiv c_i$ and $X_i \equiv c_i^0$. With additional objects defined in Table 7.1 and

---

[*]The phenomenon of *loss of hyperbolicity*, i.e., *degeneracy*, is up to date not completely understood; it is an active research area of PDEs. See e.g., Keyfitz & Kranzer [233] and Keyfitz [234].

Jacobian representation (4.11), p. 51, holds

$$[\lambda\mathcal{I} + \mathcal{J}]^{-1} = [\mathcal{I} + \phi\mathcal{J}]^{-1} = \frac{1}{\phi}\mathcal{K}\left(\frac{1}{\phi}\right) = \lambda\mathcal{K}(\lambda), \qquad (7.24\text{b})$$

obtained with the SHERMAN-MORRISON-WOODBURY formula—see e.g., Hager [235] and Golub & Van Loan [236]. The matrix $\mathcal{K}$ is therewith defined as

$$\mathcal{K}(\lambda) := \mathsf{diag}\left(\frac{c_i^0}{q_{\text{tot}}}\right)\left[\mathcal{I} - K_2(\lambda)\right]\mathsf{diag}\left(\frac{q_{\text{tot}}}{\lambda\, c_i^0 + q_{\text{tot}}}\right), \quad i = 1, \ldots, N, \qquad (7.24\text{c})$$

with K_2 given by Equation (7.23e), listed in Table 7.1.

Real eigenvalues / Symmetrization The starting point consists of

$$\lambda\mathcal{I} + \mathcal{J}(q) \;=\; D^{-1}(\lambda)\left(\mathcal{I} + H(\lambda)\right)\Delta \;=\; D^{-1}(\lambda)\,\Delta + H(0)\,\Delta, \qquad (7.24\text{d})$$

with objects

$$\Delta = \mathsf{diag}(\delta_k); \quad \delta_k := \frac{q_{\text{tot}}}{c_k^0}. \qquad (7.24\text{e})$$

$H(0)$ in (7.24d) above can be factorized as:

$$\begin{aligned}
H(0)\,\Delta &= X\left((e^T W^2 x - \sigma)e^T - w^T\right)\Delta - Wxe^T\,\Delta && (7.24\text{f})\\
&= X\left((e^T W^2 x - \sigma)ee^T - ew^T - we^T\right)\Delta \\
&= (X\Delta^{-1})^{1/2}\big[(\Delta X)^{1/2}\left((e^T W^2 x - \sigma)ee^T - ew^T - we^T\right)(\Delta X)^{1/2}\big]\\
&\quad \times (X\Delta^{-1})^{-1/2}.
\end{aligned}$$

Since Equation (7.24f) is similar to a *symmetric matrix*, it possesses N real eigenvalues with N linearly independent eigenvectors.

Positive eigenvalues It is important to acknowledge that $\lambda\mathcal{I} + \mathcal{J}(q)$ needs to be *invertible*, which in turn implies that $\mathcal{J}(q)$ has only *positive eigenvalues*, since, per definition (7.24a), $\lambda \geq 0$. A direct consequence of this fact, following (7.24f), is a *nonzero* determinant, $\mathsf{det}\left(\mathcal{I} + H(\lambda)\right)$. Introducing

$$f^T D = (w^T W x - \sigma)d^T - w^T D = (e^T W^2 x - \sigma)d^T - d^T W,$$

with the auxiliary notation, $d \equiv \text{col}\,(d_k)$,

$$
\det\,(\mathcal{I} + H) \;=\; \det \begin{bmatrix} 1 - e^T DW x & -e^T Dx \\ f^T DW x & 1 + f^T Dx \end{bmatrix} \tag{7.24g}
$$

$$
= \; 1 - e^T DW x + f^T Dx - e^T DW x \cdot f^T Dx + e^T Dx \cdot f^T DW x
$$

$$
= \; 1 - d^T W x + d^T \left[(e^T W^2 x - \sigma)\,\mathcal{I} - W \right] \left[x + (d^T x)\,W x - (d^T W x)\,x \right]
$$

$$
= \; 1 - d^T W x + d^T \left[(e^T W^2 x)\,\mathcal{I} - W \right] \left[x + (d^T x)\,W x - (d^T W x)\,x \right] - \sigma\,d^T x
$$

$$
= \; 1 - 2 d^T W x + e^T W^2 x \cdot d^T x - d^T x \cdot d^T W^2 x + (d^T W x)^2 - \sigma\,d^T x
$$

$$
= \; (1 - d^T W x)^2 + d^T x (e^T - d^T) W^2 x - \sigma\,d^T x
$$

is obtained. Each of the summands in the last line of Equation (7.24g) is *positive*, since

$$
\sigma := \sum_{k=1}^{N} w_k\,c_k\,q_{\text{tot}}\,\frac{\mathrm{d}}{\mathrm{d}c_k^0}\,\frac{1}{q_k^0}, \tag{4.12d}
$$

for required strictly increasing single component isotherms, $q_i^0 = f(c_i^0)$, is *always negative*—cf. selected examples considered in Table 4.2, p. 59.

This completes the proof. $\qquad\qquad\qquad\qquad\qquad\qquad\qquad\qquad\square$

An outstanding feature of formula (7.24c) consists of its direct application to dynamic model (6.17), thus additionally avoiding the intermediate computation of $\mathcal{J}(q(c))$. Just as in the case of Jacobian, $\mathcal{J}$—explained in Section 4.3, p. 50, only c^0 at equilibrium, for prescribed c, are needed. A simple application of the *objects* in Table 7.1 and that should clarify the calculation workflow is presented in Algorithm 7.1.

Applying $\mathcal{K}(\lambda)$ in EDM1D

The application of $\mathcal{K}(\lambda)$ also holds for equilibrium-dispersive model (6.4). Henceforth, Equation (7.24c) is used directly with this model, so that

$$
\frac{\partial c}{\partial t} = [\mathcal{I} + \phi \mathcal{J}]^{-1} \left[-u\,\frac{\partial c}{\partial z} + D_{\text{app}}\,\frac{\partial^2 c}{\partial z^2} \right]
$$

$$
= \lambda\,\mathcal{K}(\lambda) \left[-u\,\frac{\partial c}{\partial z} + D_{\text{app}}\,\frac{\partial^2 c}{\partial z^2} \right], \tag{7.25}
$$

1: **procedure** Use_$\mathcal{K}(c = [c_1, \ldots, c_N]^T, \lambda)$ ▷ Compute $\mathcal{K}$ given c, λ

2:     **procedure** IAST_CALC$(c = [c_1, \ldots, c_N]^T)$ ▷ Obtain $c^{0,*}$ at equilibrium

3:     **end procedure**

4:     $\lambda^* \leftarrow \lambda$

5:     $q_i^{0,*} \leftarrow f(c_i^{0,*}); \ i = 1, \ldots, N$

6:     $q_{\text{tot}}^* \leftarrow \left[\sum_i^N \dfrac{c_i}{q_i^{0,*} c_i^{0,*}} \right]^{-1}$

7:     $K_2^* \leftarrow D^*, H^*, h_1^*, h_2^* \leftarrow q_{\text{tot}}^*, c_i^{0,*}, \lambda^*$ ▷ Evaluate *objects* in Table 7.1

8:     $\mathcal{K}^* \leftarrow c_i^{0,*}, q_{\text{tot}}^*, K_2^*, \lambda^*$

9:     $[\mathcal{I} + \phi \mathcal{J}]^{-1} \leftarrow \lambda^*, \mathcal{K}^*$

10: **end procedure**

Algorithm 7.1: Application of $\mathcal{K}(\lambda)$, using *objects* listed in Table 7.1 with fictitious fluid phase concentrations, c^0, obtained *a priori* from *any* of the IAST solution methods explained in Chapters 3 and 4.

holds. Application of the method of lines yields finally the ODE system [53]

$$
\begin{aligned}
\frac{\mathrm{d}\bar{c}(t)_j}{\mathrm{d}t} &= \left([\mathcal{I} + \phi \mathcal{J}]^{-1} \right)_j \left[\begin{array}{c} -\dfrac{1}{\Delta z} \left(\hat{f}_{j+\frac{1}{2}} - \hat{f}_{j-\frac{1}{2}} \right) \\[2mm] + D_{\text{app}} \dfrac{\bar{c}_{j+1} - 2\bar{c}_j + \bar{c}_{j-1}}{\Delta z^2} \end{array} \right] \\[4mm]
&= \left(\lambda \, \mathcal{K}(\lambda) \right)_j \left[\begin{array}{c} -\dfrac{1}{\Delta z} \left(\hat{f}_{j+\frac{1}{2}} - \hat{f}_{j-\frac{1}{2}} \right) \\[2mm] + D_{\text{app}} \dfrac{\bar{c}_{j+1} - 2\bar{c}_j + \bar{c}_{j-1}}{\Delta z^2} \end{array} \right], \quad j = 1, \cdots, J,
\end{aligned}
\tag{7.26}
$$

which approximates the solution of (7.25). Numerical fluxes, expressed in this case as $\hat{f}_{j+\frac{1}{2}} \equiv u\hat{c}_{j+\frac{1}{2}}$, are calculated with Equation (7.10b), as explained previously.

Summary

In this chapter two numerical techniques: *a)* finite difference method (FD); & *b)* finite volume method (FVM) were presented in detail, with an emphasis on their practical application to approximate solutions of fixed-bed adsorber models applicable to liquid chromatography.

Due to the nature of PDEs that describe these dynamic models, numerical methods of solution that fulfill mathematical properties, which are naturally compatible with the physics of modeled variables—i.e., *concentrations*, were selected.

A way to *embed* IAST as local equilibrium model was developed and discussed, exploiting the structure of equilibrium-based model equations and properties of $\mathcal{J}(q(c))$—cf. Chapter 4—by introduction of $\mathcal{K}(\lambda)$, thus realizing a FLEXIBLE and COMPUTATIONALLY EFFICIENT simulation tool.

Chapter 8

Dynamic simulations[*]

*"...do we use a low-order method on a fine mesh
or a high-order method on a coarse mesh? ..."*

– Eleuterio Toro

Introduction

A theoretical prediction of dynamic behavior of fixed-bed adsorbers in one dimension can now be performed with the numerical simulation tools developed in Chapter 7. Firstly, details concerning performance of these tools are addressed; more specific computation tasks, similar to those required for Part III are explained afterwards. A discussion of some of these results follows, serving as basis for the evaluation of experimentally acquired data, which will be presented in Chapter 10.

---

[*]CHAPTER DISCLAIMER. Partial contents of this chapter have been reported in: *"A Method for Efficiently Solving the IAST Equations with an Application to Adsorber Dynamics"* [53]. The information is presented as part of this dissertation and it is an original published contribution to the field in a peer-reviewed journal. There is none whatsoever intention of self-plagiarism; the information serves rather as complementary content to this dissertation. Furthermore, the publishing company has granted partial reproduction of the contents in the article mentioned above. [License No.: **3743030164049**, requested and obtained on Nov. 6th, 2015 from John Wiley & Sons, Inc. through Copyright Clearance Center.]

8.1 Relevant aspects of applied numerical discretizations for selected fixed-bed column models

Convergence to analytical solution of a step change in concentration of a single adsorbate

A simple validation and verification of the numerical tools developed for column models (6.4), p. 79 and (6.12), p. 82 is now considered. *Convergence* is an important property to ensure that computed results approximate the sought-after solutions correctly. This property can be demonstrated by considering the applied discretization scheme to approximate solutions to an equilibrium-based model, whereby a single component possessing a linear isotherm, defines local adsorption equilibrium:

$$q_i = \mathfrak{h}_i\, c_i. \tag{2.6}$$

A simple analytical solution is available to compare with the numerical approximations. This task is equivalent to solving the linear advection equation with constant velocity, a^*,

$$w_t + a w_z = 0. \tag{8.1}$$

By identifying

$$w \equiv c_i \quad \text{and} \quad a \equiv \frac{u}{1 + \phi\,\mathfrak{h}_i}, \tag{8.2}$$

the single component linear chromatography equation

$$\frac{\partial c_i}{\partial t} = -\frac{u}{1 + \phi\,\mathfrak{h}_i}\,\frac{\partial c_i}{\partial z}, \tag{8.3}$$

is recovered, in analogy to Equation (6.17), p. 83. Figure 8.1 illustrates the concentration breakthrough curve that results when a step change in the inlet concentration, $c_{\mathrm{in}}(t)$, is effected on an initially *clean*, column—i.e., free of adsorbate. This is defined by boundary and initial conditions

$$c_{i,\,\mathrm{in}}(t) = c_i(t, z = 0) = c_{i,\,\mathrm{feed}}, \quad t \geq 0 \quad \text{and} \tag{8.4a}$$

$$c_{i0} = c_i(t = 0, z) = 0. \tag{8.4b}$$

---

*Despite of the *apparent* simplicity of Equation (8.1), it is a classical benchmark for the class of numerical schemes herein considered.

Both analytical solution and numerical approximations are displayed in this figure. The approximations were computed with the method of lines, applying the limited third order upwind-biased spatial discretization described in Section 7.4. The resulting ODE system is listed in Appendix A7, p. 173.

A *refinement* of the spatial grid, i.e., increasing the number of cells, J, causes the numerical approximation to converge progressively to the analytical solution, thus confirming the behavior expected from the applied spatial discretization—consult Koren [222] and Hundsdorfer *et al.* [223] for details. Additional tests with different types of inlet boundary condition values yielded similar results as those illustrated with this simple example, thus confirming an acceptable performance of this numerical approximation and its adequacy to approximate solutions to the investigated equilibrium-based models. Values between $J = 200$ and $J = 800$ cells were found to be adequate for the applied numerical approximations.
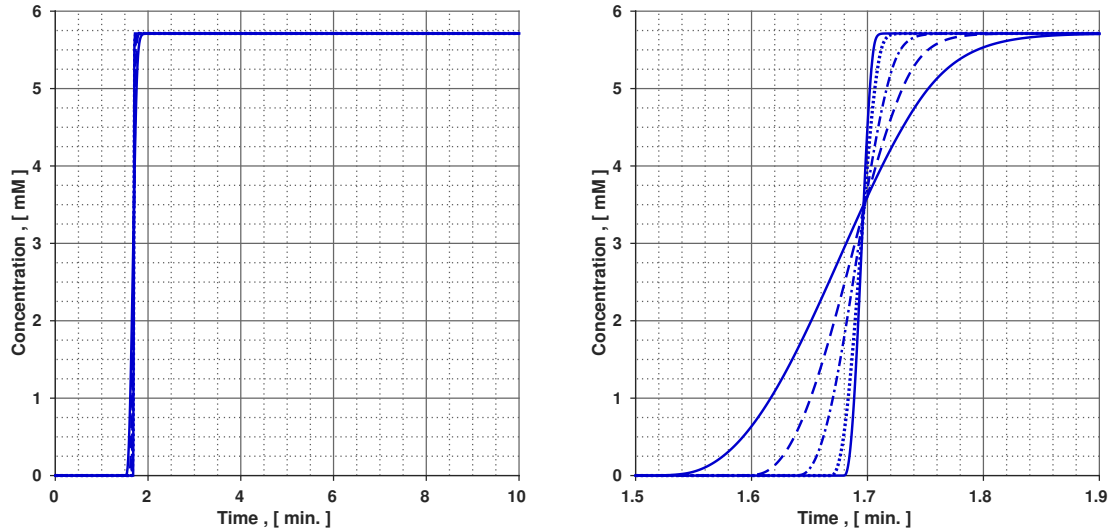
Figure 8.1: Convergence to analytical solution of the ideal model for a step change in concentration from 0 to $c_{\text{feed}} = 5.712\,[\text{mM}]$ at the inlet boundary given by Equation (8.4), using the third order upwind-biased scheme on *coarse* grids with equidistant number of cells, J. (−): $J = 50$; (−−): $J = 100$; (−·): $J = 200$; (··): $J = 500$; (−): $J = 1000$. Applied ODE integration method: 3rd order SSP-RK scheme (7.15) of Section 7.5, p. 93.

Numerical integration schemes

In the application of the method of lines discussed above, the time integration was assumed to be computed *exactly**. The temporal approximation to the resulting ODE system should therefore guarantee at least the same order of accuracy as the applied

---

*Therefore the term *lines*: continuous.

discretization along axial coordinate, z, thus contributing only with minimal errors to the overall approximation. Here, however, caution is recommended. General purpose, *'out-of-the-box'* integration packages can cause numerical difficulties. This is clearly illustrated in Figure 8.2. Herein, an example of instability known as *ringing* is displayed— refer to Hairer *et al.* [164, 166] for details. This type of phenomenon *pollutes* the computed approximation, but may be conveniently avoided by application of a SSP-RK integration scheme such as (7.15), as discussed previously, in order to preserve the physically correct bounds of the solution. This is achieved at expense of longer computation times, since no adaptive time-stepping was performed when this integration scheme was applied.
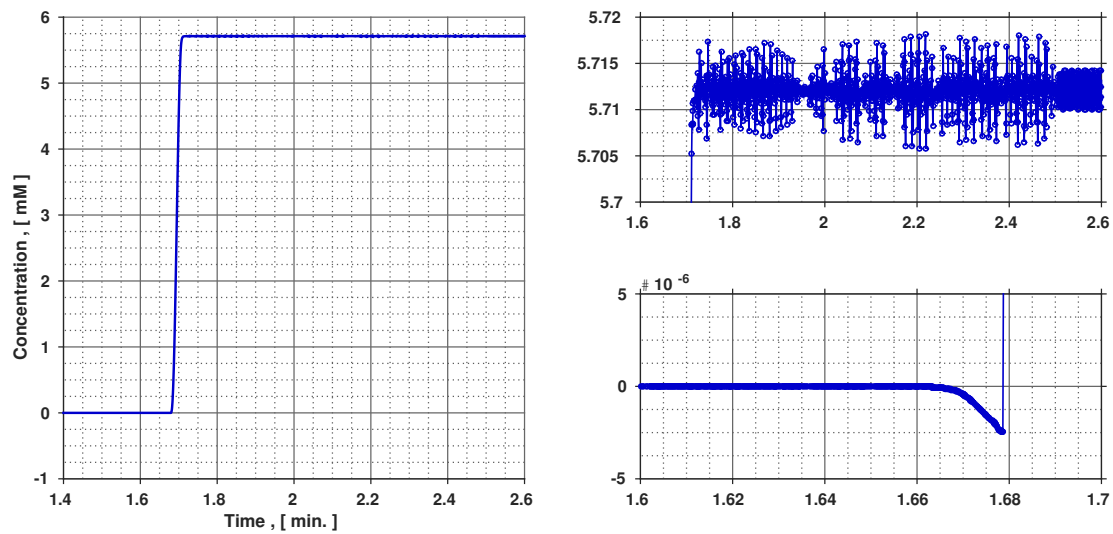
Figure 8.2: Illustration of the *ringing* phenomenon, observed for the approximation (−): $J = 1000$, displayed in Figure 8.1. Applied ODE integration method: `ode45`, Dormand & Prince [173], at default error tolerances. Due to this numerical instability, the solution becomes unbounded, potentially leading to a solution blow-up.

When IAST equilibrium calculations are applied to model fixed-bed dynamics, using the approach developed in Chapter 4, the considerations discussed above should be taken into account in order to approximate the solutions correctly.

8.2 Performance of proposed IAST approach in dynamic column simulations

Elution profiles of narrow rectangular plug injections

A common calculation task of numerical modeling for liquid chromatography consists of reproducing small volume injections of mixtures of solutes, which in the case of competitive adsorption behavior between them, produce elution profiles that differ from standard, *gaussian-like* peaks, observed when adsorption competition is absent. The former situation is often encountered when the concentrations of solutes in the injected mixtures are *high* or when the injected volumes are *large*—i.e., column *overloading* [14]. In order to simulate these injections, the boundary condition at the inlet

$$c_{i,\,\mathrm{in}}(t) = \begin{cases} c_{i,\,\mathrm{inj.}}, \ 0 \leq t \leq t_{i,\,\mathrm{inj.}}, \\ 0, \ t_{\mathrm{inj.}} \leq t, \end{cases} \qquad i = 1, \ldots, N \qquad (8.5)$$

is commonly applied to provide an approximation of actual injection profiles.

Figure 8.3 illustrates results of numerical simulations for a liquid chromatography column, whereby the inlet condition (8.5) was applied in EDM1D (6.4), p. 79, with initial condition $c_0 = c(t = 0, z) = 0\,[\mathsf{mmol/l}]$. This numerical solution was obtained with the third order upwind-biased scheme described in Section 7.4, p. 89, using IAST to model competitive equilibria between the solutes. An approximation to the *equilibrium model* solution is also depicted in the figure for comparison. This approximation was obtained with the same numerical scheme by assigning $D_{\mathrm{app},k} \to 0\,[\,\mathsf{cm^2/min.}\,]$—cf. Equation (6.9).

Due to strong competitive effects, a significant displacement of the less-adsorbed compound, C8, whose peak apex substantially exceeds the injected concentration values, $c_{i,\,\mathrm{inj.}} = 80\,[\,\mathsf{mmol/l}\,]$, can be observed, as predicted by IAST equilibria. The trailing edge of the more-adsorbed compound, C10, displays the characteristic desorption curve observed under the presence of inflection points along its single component isotherm course. The numerical scheme approximates the solutions satisfactorily on coarse spatial grids, as evidenced by the excellent resolution of the trailing edges of both C8 and C10 peaks.
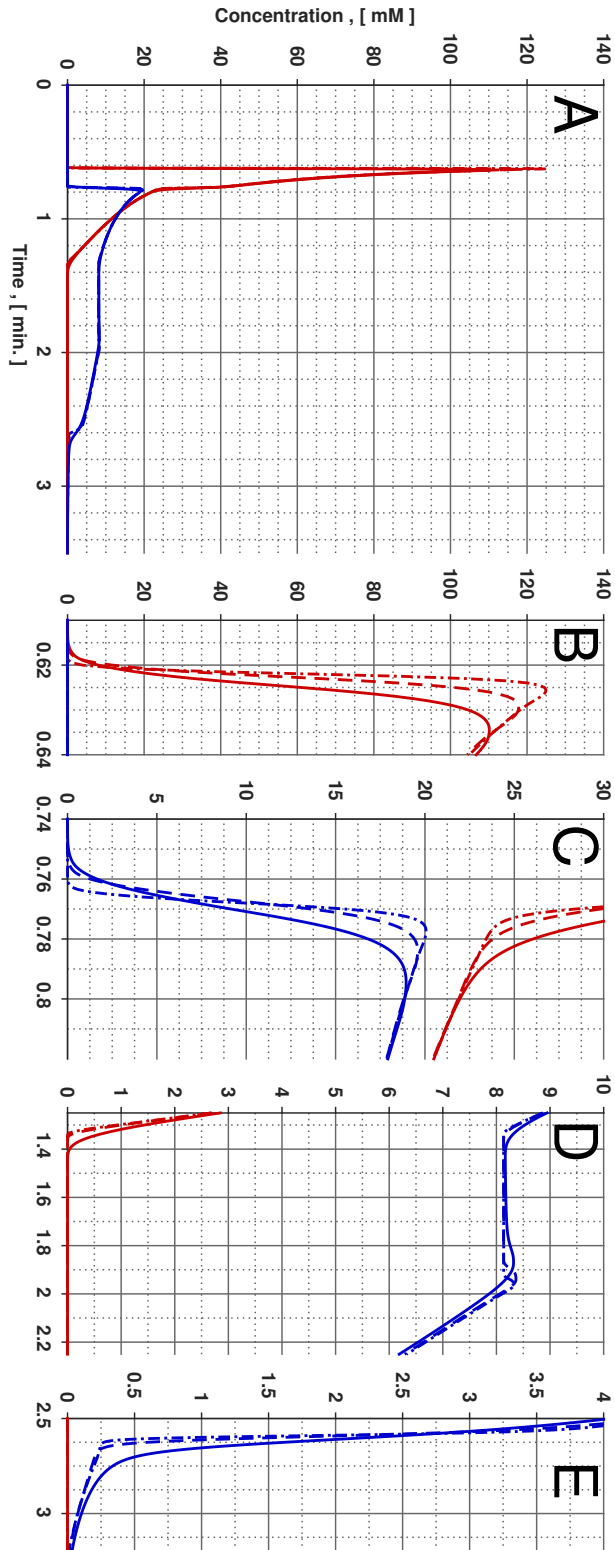
Figure 8.3: Numerical approximations to ideal equilibrium model and EDM1D for a narrow rectangular inj. *plug* of an equimolar mixture of octylbenzene (C8) & decylbenzene (C10), $t_{i,\,inj.} = 0.2\,[\,min.\,]$, with concentrations $c_{1,\,inj.} = c_{2,\,inj.} = [\,mmol/l\,]$. $(-\cdot-)$: approx. to ideal model with $J = 400$, $\Delta t = 5 \times 10^{-4}\,[\,min.\,]$; $(--)$: approx. to ideal model with $J = 200$, $\Delta t = 5 \times 10^{-4}\,[\,min.\,]$; $\&$ $(-)$: approx. to EDM1D with $J = 100$, $\Delta t = [\,min.\,]$. Competitive adsorption equilibria was computed using IAST with IVP approach presented in Chapter 4, using single component Quadratic plus Langmuir model for each compound. Applied isotherm and simulation parameters are listed in Appendix A8, Tables A4, p. 174 & A5, p. 175, respectively, **(A)**: resulting competitive elution profiles; **(B)**: breakthrough of less-adsorbed C8 peak, displaced strongly by C10; **(C)**: breakthrough of C10; **(D)**: intermediate plateau of C10, illustrating effect of inflection points; & **(E)**: desorption of C10, alone, with a sharp trailing profile, followed by smooth desorption for concentration values below its first inflection point.

Comparison of calculations obtained with different numerical schemes

A useful comparison of the computational performance of the numerical schemes presented in Chapter 7 is obtained when *a*) the dynamic model—i.e., Equation (6.4) & *b*) the embedded equilibrium model—i.e., IAST Equations, Table 3.2, p. 35, are benchmarked *simultaneously.*

For this purpose, a column dynamics task is solved with the two discretizations discussed in detail before to approximate EDM1D solutions: *a*) Finite Difference scheme, Section 7.2, p. 87; & *b*) Finite Volume Method, Section 7.3, p. 88, using $\mathcal{K}(\lambda)$ presented in Section 7.7, p. 96.

Figure 8.4 illustrates elution profiles computed with both discretization schemes. The more pronounced *smearing* of the elution profiles computed with FD scheme is to be expected, since this type of discretization is only first order accurate [213, 214]. This yielded the depicted *shock layers*, which, despite of numerical dispersion, are estimated to elute at their corresponding breakthrough times correctly. This is the expected behavior of *conservative schemes* [47, 213].

On the other hand, the higher order discretization provides a more accurate approximation, with less numerical diffusion. Due to its inherent nonlinearity, it was observed that in most of the analyzed calculations the scheme was more computationally demanding, as documented by the recorded average calculation times listed in Table 8.1.

All in all, this example provides, once more, comparable numerical results for two radically different solution strategies, therefore demonstrating that the proposed IVP approach, in particular application of Equation (7.24c), p. 97, computes IAST solutions correctly, thus *validating* it.

Table 8.1: Calculation times obtained for numerical simulations applying FD scheme and FVM discretization, applying IAST as competitive equilibrium model.

Num. scheme / IAST solution method	Execution time [a] [s]
FD, Section 7.2 / modified FastIAS [153] [b]	164
FVM, Section 7.3 / modified FastIAS [153] [b]	3473
FVM, Section 7.3 / IVP approach [c], Chapter 4	63307

a. Values were obtained by computing num. approximations w/ MATLAB [168]—cf. Appendix A1.

b. Computed w/ implementation by Do [36].

c. Computed w/ `ode45` at default error tolerances.

It is important to highlight some features of the applied schemes that explain the numbers reported in Table 8.1. Firstly, in the case of the applied FD scheme, the IAST equilibrium values, i.e., adsorbed phase concentrations at equilibrium, $q = f(c)$, are applied *directly* into the computation—recall Equation (7.1), p. 87. In contrast, the FV discretization with the method of lines yields an ODE system of size J, which is subsequently integrated in time. The matrix $\mathcal{K}(\lambda)$ then *operates* on the r.h.s. of this ODE system, cf. Equation (7.26), p. 99. This matrix requires the IAST solution approach to generate the required values of c^0 at equilibrium for its computation. As a result, the r.h.s. of ODE system (7.26) is intrinsically nonlinear. Further, the calculation of the solution in time, t, is more *costly* due to internal function evaluations of the applied numerical integrator. For example, applying the SSP-RK method (7.15) requires the calculation of two internal stages, $u^{(1)}$, $u^{(2)}$, in order to advance the solution one time step as explained before. Therefore, it can be stated in general, that improvements in solution accuracy come at the cost of performing a larger number of function evaluations, which in this particular example translate into longer calculation times, as documented in Table 8.1.

Secondly, the difference in calculation times for column dynamics among the numerical schemes is expected from the computational performance already documented for different IAST solution approaches—cf. Table 5.5 of Section 5.3, p. 70—used to obtain the IAST equilibrium values. These equilibrium calculations represent a significant amount of the overall computational cost.

Lastly, recalling Chapter 3, it is important to keep in mind that in this example, it has been possible to compute IAST solutions with modified FastIAS because the single component Quadratic plus Langmuir isotherms possess an analytical formula for Π—cf. Equation (3.16d) in Table 3.4, p. 38. In the case this is not fulfilled, and this IAST solution method can not be applied, longer calculation times as reported in Table 8.1, should be expected.

One important reason that motivates computing the solution approximations with the best attainable accuracy—i.e., with the higher order scheme—is that, for problems with complex adsorption equilibria, features of the computed elution profiles, such as the appearance of shock layers, are easier to identify and analyze. This likely occurs when inflections along the isotherm courses are present.
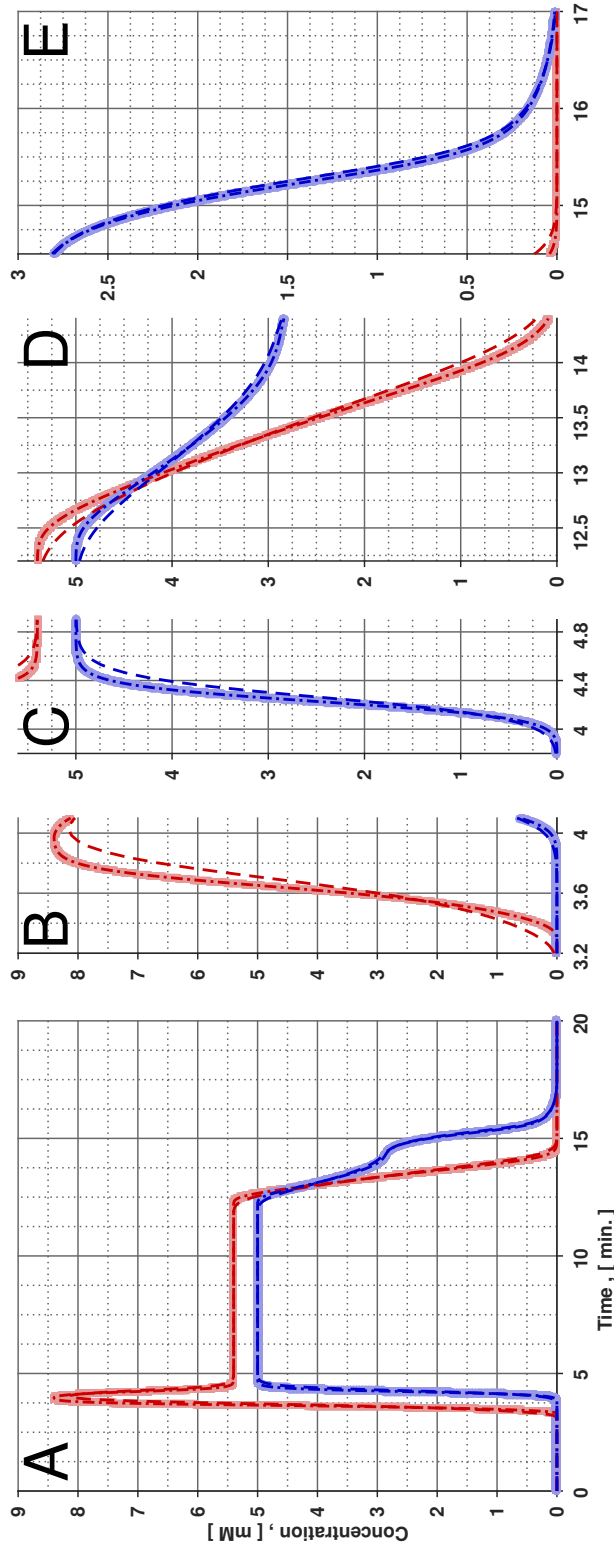
Figure 8.4: Numerical approximations to EDM1D for a wide, rectangular inj. *plug* of a mixture of decylbenzene (C10) & undecylbenzene (C11). $t_{i,\,\text{inj.}} = 10\,[\text{min.}]$, with concentrations $c_{\text{C10, inj.}} = 5.4\,[\text{mM}]$ & $c_{\text{C11, inj.}} = 5.0\,[\text{mM}]$. $(-\cdot)$: limited 3rd order upwind-biased discretization, IAST computed numerically w/ modified FastIAS; $(--)$: FD scheme, IAST computed numerically w/ modified FastIAS; & $(-)$: limited 3rd order upwind-biased discretization, IAST computed numerically w/ IVP approach. Calculation times required for each simulation are listed in Table 8.1. Applied isotherm and simulation parameters are listed in Appendix A8, Tables A4, p. 174 & A5, p. 175, respectively, (A): resulting competitive elution profiles; (B): breakthrough of C11; (C): breakthrough of less-adsorbed C10, displaced by C11; (D): simultaneous, coherent desorption of C10 & C11; & (E): desorption of the more-retained C11, alone.

8.3 Simulation of *chromatographic cycles*

A typical task in adsorption-based separation processes consists of computing the so-called CHROMATOGRAPHIC CYCLE, which consists basically of two steps:

1. an *adsorption step* from an initial, uniform equilibrium state at every point of the column, i.e., $c_0 = c(t = 0, z)$, to a feed state, which is attained by supplying the column with a solution of the adsorbates with concentrations $c_{i,\text{feed}}$ until a new equilibrium condition is reached; &

2. a *desorption step*, whereby, the column, which was equilibrated completely with feed concentrations, $c_{i,\text{feed}}$, is subsequently brought back to the initial state concentrations—those prevailing in the column before the adsorption step was effected—thus the name *'cycle'*.

Henceforth, the cycle is modeled by applying two step changes in the feed concentrations of the system at the inlet boundary, $z = 0$. If the ideal model—Section 6.4, p. 82—is applied with this simple boundary condition, and a solution can be computed analytically, a particularly useful tool for optimization of adsorption-based separations is obtained[*]. The task can also be computed numerically with the schemes presented in Chapter 7. Moreover, approximate solutions of the ideal model may be obtained by setting $D_{\text{app},k} \to 0$ in EDM1D, as shown in the examples of Section 8.2.

An important advantage of operating the adsorption process cyclically is that it offers the opportunity to investigate adsorption equilibria from dynamic operation as will be demonstrated in Chapter 10.

Chromatographic cycle of a *pre-loaded* column

Figure 8.5 illustrates simulation results of a cycle obtained for a pre-loaded column, whereby a binary case with C10 and C11 is considered. Four equilibrium points are identified with lowercase letters: 'a', 'b', 'c' and 'd'. Breakthrough shock layers and *smooth* trailing edges connect these equilibrium points. The shape of these transitions is completely defined by adsorption equilibria, $q = f(c)$, and thus, a direct consequence of applying single component adsorption isotherms with inflection points along their courses to compute competitive equilibria with IAST for this particular example. The

---

[*]Refer to the sources listed in Section 6.4.
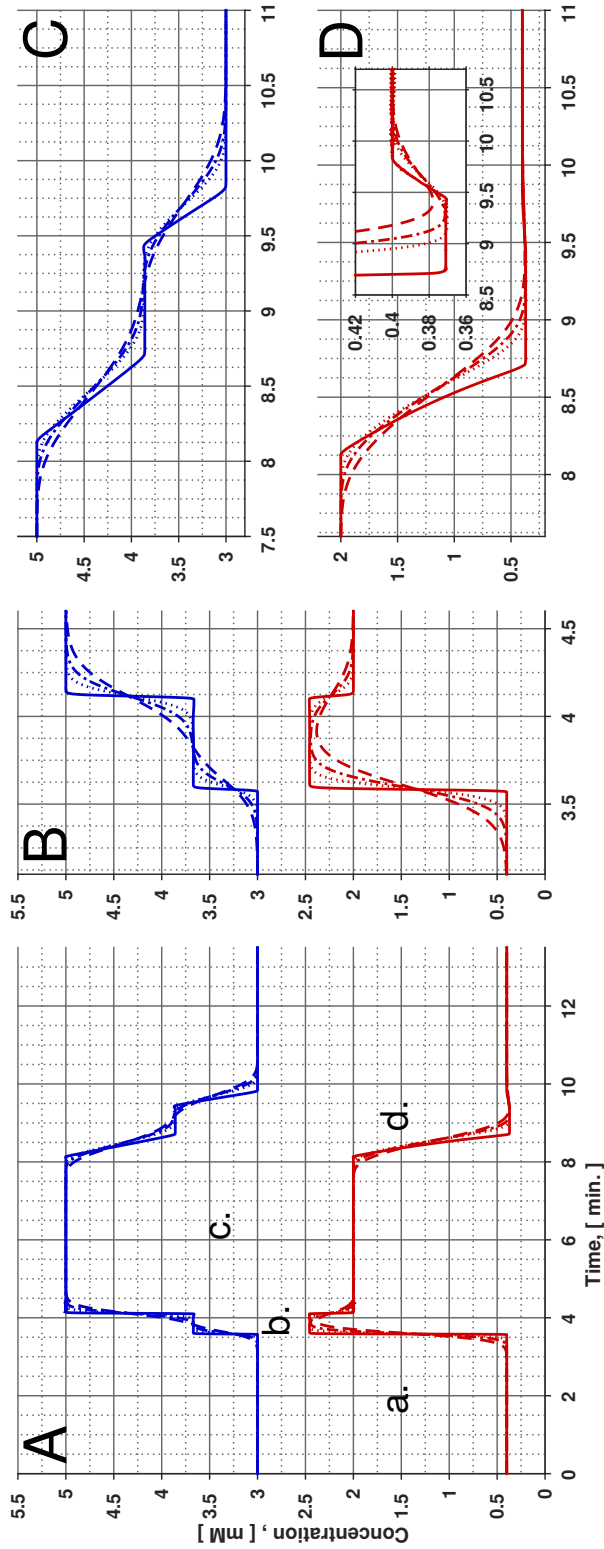
Figure 8.5: Chromatographic cycle illustration for a *pre-loaded* column. (**A**): elution profiles, featuring the following equilibrium *states*: (**a.**): initial state w/ $c_{1,0} = 0.4\,[\text{mM}]$ & $c_{2,0} = 3.0\,[\text{mM}]$; (**b.**): displacement plateau of *less-adsorbed* component w/ $c_1 = 2.45\,[\text{mM}]$ & $c_2 = 3.67\,[\text{mM}]$; (**c.**): feed state, $c_{1,\text{feed}} = 2.0\,[\text{mM}]$ & $c_{2,\text{feed}} = 5.0\,[\text{mM}]$; and (**d.**): intermediate plateau during desorption step, $c_1 = 0.371\,[\text{mM}]$ & $c_2 = 3.858\,[\text{mM}]$. (**B**): breakthrough shock layers & displacement plateaux. (**C**): desorption back to the initial concentration for the less-adsorbed component, C10. (**D**): desorption back to the initial concentration for the more-adsorbed component, C11. (**–**): ideal model approximated numerically with limited third order upwind-biased scheme; (**– –**): FD scheme with $N_{\text{plate},k} = 250$; (**– ·**): FD scheme with $N_{\text{plate},k} = 1000$; & (**· ·**): FD scheme with $N_{\text{plate},k} = 2000$. Applied simulation parameters are listed in Table A5 of Appendix A8, p. 175.

figure also reveals the excellent approximation obtained by performing the calculation with the higher order discretization. For comparison, as before, solutions of EDM1D computed with the FD scheme are also given. The higher order discretization resolves features of the solution on a coarse grid that are difficult to see with the FD scheme solution at low plate numbers, caused by numerical dispersion. This can be clearly observed at the intermediate plateau, 'd', that appears during the desorption step— figure inset 'D'. This confirms once more that the higher order scheme can be used advantageously to obtain approximations for the ideal model (6.12).

Chromatographic cycle of a *fully regenerated* column

The more frequently encountered case in liquid chromatography, wherein a stationary phase is completely equilibrated with a solution of known concentration and regenerated afterwards with pure solvent, is illustrated in Figure 8.6. This is expressed by an initial state $c_0 = c(t = 0, z) = 0$.

Numerical approximations for different values of column efficiency, computed by varying the apparent diffusion coefficient, $D_{\mathrm{app},k}$, are illustrated for comparison. At the applied feed concentrations, $c_{i,\mathrm{feed}}$, a particularly strong displacement is predicted by IAST, even for the case with the largest apparent diffusion coefficient, corresponding to $N_{\mathsf{plate}} = 200$. Competitive adsorption equilibria calculated with IAST, at the considered concentration ranges, i.e., $c_{i,\mathrm{feed}} = 15\,[\,\mathsf{mM}\,]$, are responsible for the magnitude of this displacement. The trailing edges of the elution profiles reveal an incipient reversal in the elution order from the feed state concentration up to a value of $\approx 5\,[\,\mathsf{mM}\,]$.
While the smallest applied diffusion coefficient is not particularly close to the limit case, $D_{\mathrm{app},k} \to 0$, which corresponds to an ideal, local equilibrium model solution, the computation with this value provides already a good approximation of this limit case.

Complete chromatographic cycles, as described above, will be further explored in Chapter 10 in order to estimate multicomponent equilibria calculations from experimental measurements by its application.
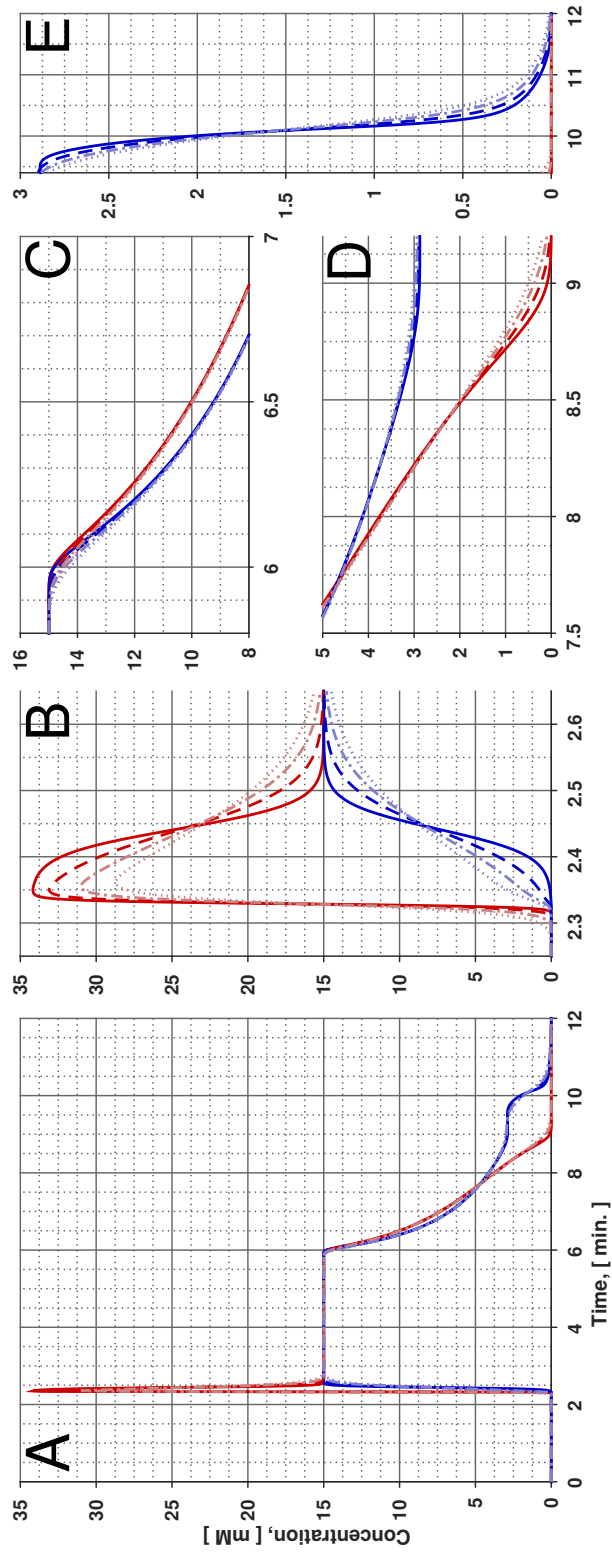
Figure 8.6: Illustration of a chromatographic cycle with an initially *clean* column calculated with EDM1D. Initial state: $c_0(t, z) = 0$ & $q_0(t, z) = 0$. Feed state: $c_{i,\,\text{feed}} = 15\,[\text{mM}]$. Applied plate numbers: (–): $N_{\text{plate}} = 1000$; (–): $N_{\text{plate}} = 500$; (–·): $N_{\text{plate}} = 300$; & (··): $N_{\text{plate}} = 200$. Employed simulation parameters are listed in Table A5 of Appendix A8, p. 175. Applied isotherm parameters are listed in Table A14, p. 187.

Summary

A suitable *strategy* to approximate solutions of the ideal model and the equilibrium-dispersive model (EDM1D) for multiple competing adsorbates under IAST, exemplified by typical liquid chromatography tasks, was validated and its computational performance was tested. The applied numerical tools offer the following advantages: *a) accuracy*; *b) robustness*; and *c) efficiency.* Moreover, the approximations can be performed on coarse grids, which makes them particularly efficient, reducing computational cost. As a bonus—albeit not implemented, parallelization of the algorithm should be straightforward, which could help to overcome minor pitfalls of possible computational performance due to stringent, high accuracy calculation requirements imposed in the equilibrium calculation—cf. Section 5.3, p. 66.

Throughout this chapter a variety of calculation methods have been proposed:

1. two strategies to solve the PDEs of fixed-bed equilibrium-based adsorber models, which can be extended easily to handle more detailed models, such as those mentioned in Section 6.1, p. 78; &

2. strategies that allow the application of IAST to describe competitive adsorption phenomena inside the column which are advantageous and that exploit the solution approach explained in Chapters 4 and 5.

These methods have illustrated the potential of the IVP approach to incorporate IAST equilibrium calculations in simple dynamic column models as well as relevant aspects to be considered for a reliable implementation.

Part III

Experimental demonstration performing a High-Performance Liquid Chromatography investigation

Chapter 9

Adsorption equilibria of alkylbenzenes in the acetonitrile/PGC system

"The devil *is in the detail."*

– English proverb

Introduction

In order to apply and verify the tools described in Part I & II, an experimental system from liquid phase adsorption chromatography was investigated in detail. Firstly, a description of the system is provided. Secondly, a detailed account of performed experimental procedures is given. Lastly, the obtained single component adsorption equilibria, necessary as *input information* for IAST implementation, are presented.

9.1   System description

The experimental system that has been investigated for a proof of the concepts presented in Parts I & II, consists of phenyl-*n*-alkanes—i.e., benzyl rings with attached alkyl chains, as illustrated in Figure 9.1. These compounds dissolved in acetonitrile adsorb onto porous graphitic carbon (PGC) stationary phases. High purity, HPLC-grade quality acetonitrile (ACN) was used as solvent to prepare solutions of phenyl-*n*-alkanes and employed as mobile phase for *carry-through, displacement & column regeneration* in the HPLC apparatus. In this system, reported and investigated by Diack & Guiochon [51, 52], complex adsorption behavior of phenyl-*n*-alkanes is documented. In their work, elution profiles of overloaded injections of a homologous series of these compounds were recorded, viz. phenyl-*n*-octane (*octylbenzene*, 'C8'), phenyl-*n*-decane (*decylbenzene*, 'C10'), phenyl-*n*-undecane (*undecylbenzene*, 'C11'), phenyl-*n*-dodecane (*dodecylbenzene*, 'C12'), and phenyl-*n*-tridecane (*tridecylbenzene*, 'C13'). They observed an *atypical behavior* of the elution bands while progressively increasing injected concentrations and volumes—i.e., column *overloading.* Single component adsorption isotherms were recorded for each compound using Frontal Analysis (FA). Fitted parameters to the measured adsorption equilibrium data, using the Quadratic plus Langmuir isotherm model—cf. Equation (2.3e), p. 17, were estimated. The system is particularly interesting because the adsorption isotherm courses of these compounds exhibit inflection points at certain temperatures and concentration ranges. These inflection points demand a careful and methodical approach to estimate and describe the adsorption equilibria.
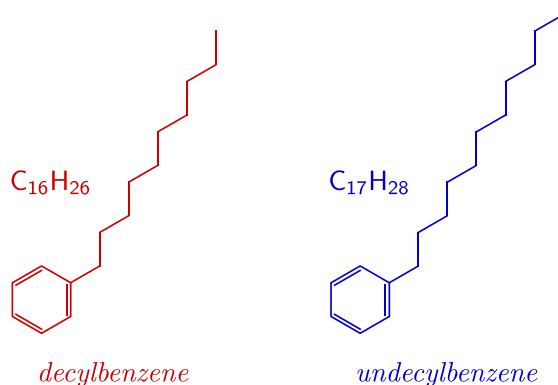
Figure 9.1: Structural formulas of decylbenzene (C10) [237] & undecylbenzene (C11) [238].

Origin & nature of inflection points   The effect of inflection points along adsorption isotherm courses in overloaded elution profiles has been analyzed both theoretically—see e.g., [239]—and experimentally, in connection with complex liquid phase adsorption

mechanisms observed in specific RPLC systems—see e.g., [37, 76, 240–244]*. Already in the earlier publication of Brunauer *et al.* [61] a rational explanation is provided for **Type III** behavior—cf. Chapter 2, Section 2.1.1, p. 15. Therein, predominantly stronger *cohesive forces* between molecules of adsorbate, organized in layers above a monolayer in contact with the adsorbent surface, are attributed for *cooperative behavior* in the experimental systems they analyzed. A delicate balance between *adhesive & cohesive forces* is therefore, in principle, responsible for observed behavior. It seems plausible that this idea applies to the alkylbenzenes/ACN/PGC system of this study as well, as pointed out by Diack & Guiochon [52], since interactions of alkyl chains of neighboring adsorbed molecules seem to favor cooperative behavior. The orientation of the benzyl ring for homologous alkylbenzenes, albeit with shorter alkyl chains and branches, was investigated for analytical concentrations using a methanol/water mobile phase on Hypercarb$^{\text{TM}}$ column by De Matteis *et al.* [246, 247]. Their findings aimed at establishing a relationship between *retention behavior* and *structural & steric conformations* of adsorbed alkylbenzene molecules. Length of alkyl chain seems to determine preferred conformations, which translated to particular retention mechanisms. They supported their experimental findings with molecular simulation studies.

All in all, the more relevant and challenging task of estimating adsorption equilibrium of *multicomponent mixtures* of phenyl-*n*-alkanes in the ACN/PGC system becomes particularly difficult using an explicit isotherm equation—cf. Table 2.4, p. 23, in contrast to e.g., a *simpler* system, consisting only of compounds characterized by Langmuir adsorption isotherms—extensively studied and well understood, whereby adsorbate-adsorbate interactions are not taken into account.

The *prediction* of competitive adsorption equilibria is quite demanding when single component isotherms already display inflection points along their courses—see e.g., [76]. An possibility to tackle this task consists of applying a THERMODYNAMICALLY CONSISTENT PRINCIPLE that employs *exclusively* measured single component adsorption isotherms, such as IAST, whilst assessing its suitability to describe the adsorption system of interest.

As explained in Chapters 3 and 4, input information for IAST are adsorption isotherms of each compound obtained *individually* in the selected fluid/adsorbent system, ACN/PGC, at the same investigated temperature, T, for which the behavior of the *mixture* needs to be described. The following sections provide technical details pertaining the acquisition of this information for the experimental system described above.

---

*Strictly speaking, adsorption on PGC, should be neither categorized as *reversed phase*, nor as *normal phase*, though it displays *reversed-phase behavior* [245].

9.2   Equipment description & technical assembly details

High-performance liquid chromatography device

An Agilent 1260 Infinity analytical instrument, purchased from Agilent Technologies, was used to perform the measurements. Table 9.1 lists its constituent modules & corresponding part numbers for reference, whilst Figure 9.2 illustrates its setup; actual pictures of the equipment are documented in Appendix A9. Further, this device is controlled automatically and programmed with the equipment manufacturer's software ChemStation and its maintenance software utilities [248].

Table 9.1: Modules of Agilent 1260 Infinity HPLC equipment. Pictures of these modules are displayed in Figure A1, Appendix A9, p. 176.

Module (manufacturer's ID-tag)	Id., Fig. 9.2 & Fig. A1, p. 176
Degasser (1260 Degasser)	B
Dual pump module (1260 Bin Pump)	C
Sample injection module (1260 ALS)	D
Column compartment & oven (1260 TCC)	E
Multiple wavelength UV detector (1260 MWD VL)	F
Refractive index (RI) detector module (1260 RID)	G
Analytical-scale fraction collector	J

Flow rate meter

A volumetric flow rate meter from DURATEC* was installed downstream the HPLC station in order to precisely measure the flow rate delivered by the HPLC pumping module. Small deviations of around 1.5 - 2.0 % were observed between selected volumetric flow rate set-point and actual recorded values. Monitoring of the volumetric flow rate is essential for precise adsorption equilibrium determination using FA [14, 94]—cf. Equation (9.7). Calibration sheet(s) for this device can be found in Appendix A9.

---

*DURATEC Analysentechnik GmbH. Rheinauer Strasse 4, D-68766 Hockenheim, Germany. http://www.duratec.de.
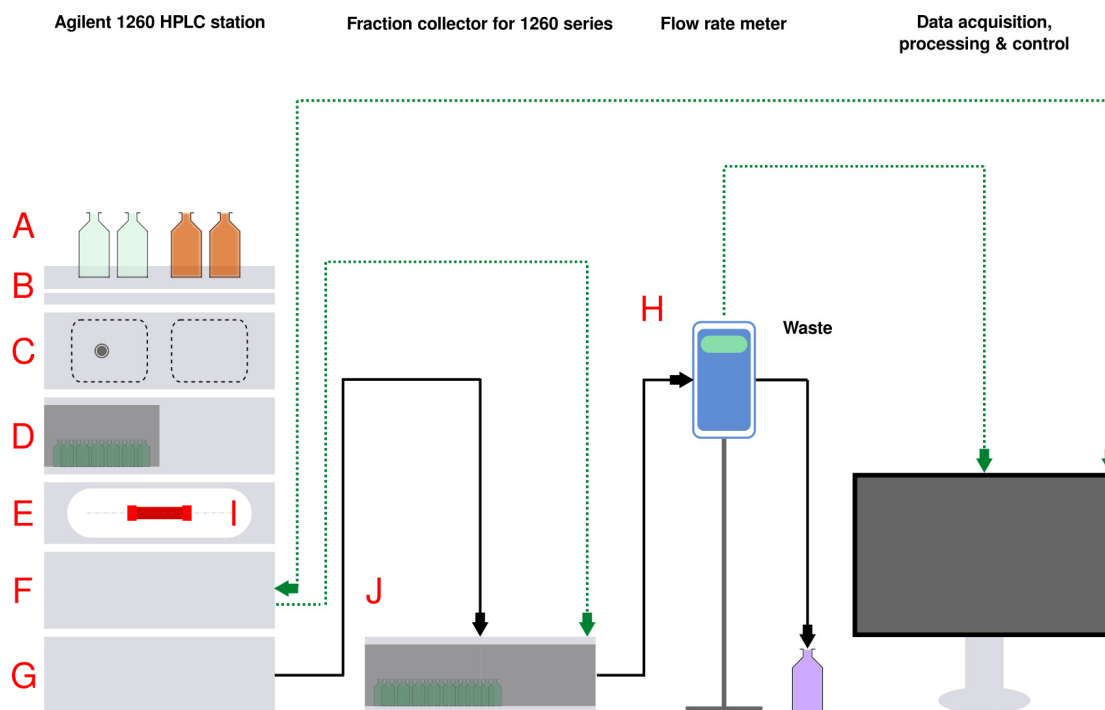
Figure 9.2: Schematic representation of employed equipment setup. Pictures of the measurement devices are displayed in Figure A1, Appendix A9, p. 176. Refer to Figure 9.4 for a picture of the employed HPLC column. ($-$): physical tubing connections; ($\cdot\cdot$): I/O and e-control signals.

9.3   Applied materials & methods

Chemicals[*]

HPLC-grade acetonitrile was purchased from VWR/BDH Prolabo[†] to prepare injected solutions and samples, as well as *mobile phase* for the HPLC measurements. Investigated chemical compounds were purchased from Tokyo Chemical Industry Co., Ltd. (TCI Deutschland GmbH), and Sigma-Aldrich®, with a purity specification of 97 %—as measured by the manufacturer. Table 9.2 lists the CAS Registry Numbers—'CAS numbers'—of applied chemicals for easy identification.

While specification of purity of purchased chemicals is *high*—97 %, small discrepancies in elution behavior amongst chemicals' suppliers were noticed. Figure 9.3 illustrates this point for *undecylbenzene* (C11). Under the same operating conditions—temperature, T, volumetric flow rate, Q, PGC stationary phase, and HPLC-grade solvent, the recorded

---

[*]Names of companies & commercial brands are mentioned for the sole purpose of clarity in the exposition and proper documentation of the conducted academic, non-commercial research study.

[†]Product designation: «Acetonitril HiPerSolv CHROMANORM®, gradient grade für die HPLC ».

Table 9.2: CAS Registry Numbers of applied chemicals to facilitate their identification; molecular weights & densities.

Chemical compound	CAS Registry No.	Molecular weight [g/mol]	Density [b] [g/ml]
acetonitrile (ACN) [a]	75-05-8	41.05	0.7820
octylbenzene (C8)	2189-60-8	190.32	0.8560
decylbenzene (C10)	104-72-3	218.38	0.8575
undecylbenzene (C11)	6742-54-7	232.40	0.8550
dodecylbenzene (C12)	123-01-3	246.43	0.8555
tridecylbenzene (C13)	123-02-4	260.46	0.8845

a. HPLC-grade quality.
b. Measured at $20\,^{\circ}$C.

elution profiles vary. The explanation behind this lies most likely in potential impurities of the chemicals. Precaution was taken to work every experimental run with compounds from the same manufacturer to avoid this problem. This is certainly critical when determining adsorption equilibria for a particular substance. Best practice is to use *analytical standards*, although these may not be readily available commercially for some compounds[*].
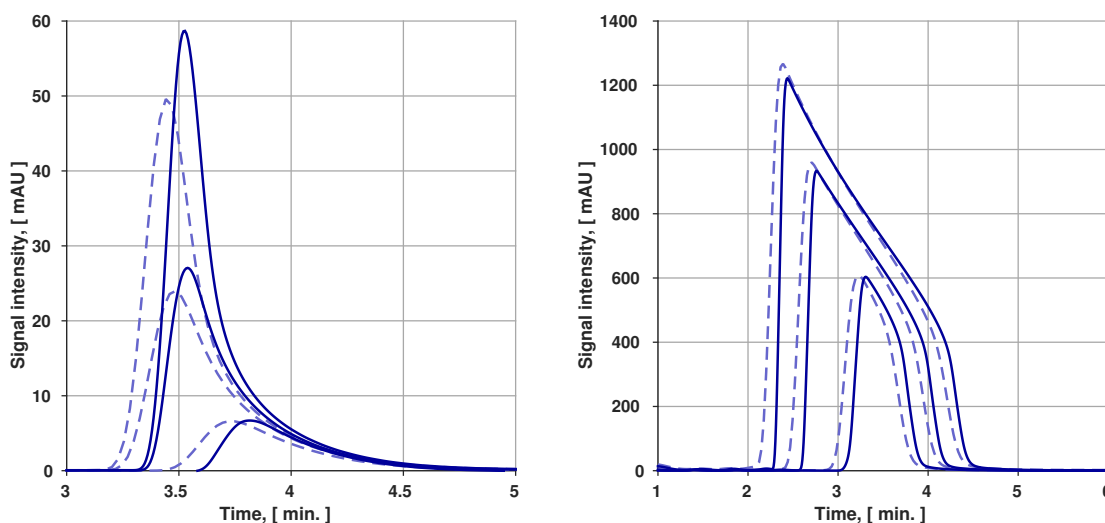
Figure 9.3: Comparison of injections of undecylbenzene (C11) supplied by two different vendors: ($-$): TCI (Tokyo Chemical Industry Co., Ltd.); ($--$): Acros Organics (Thermo Fisher Scientific), employing in both sets a 30×4.6 [mm] Hypercarb$^{\text{TM}}$ column, under *identical* HPLC operating conditions. Injected volumes, $V_{\text{C11, inj.}}$: 1, 3, 5 [μl] (*left*); 100, 300, 500 [μl] (*right*). Volumetric flowrate $\overline{Q} = 1.0$ [ml/min.]. Temperature, $T = 323$ K. Signals were recorded at $\lambda_{\text{UV}} = 254$ [nm].

---

[*]At the time these measurements were conducted, only the analytical standard for *decylbenzene* (C10) was available for purchase in the market. The author decided to proceed with the '*impure*' chemicals herein documented anyhow, without further purification steps.

Stationary phase

A porous graphitic carbon (PGC) HPLC column of dimensions $L_c = 50\,[\mathsf{mm}]$ and diameter $d_c = 4.6\,[\mathsf{mm}]$—commercialized under the name Hypercarb$^{\mathrm{TM}*}$—was acquired for the measurements. Specific details related to the retention mechanisms and structural characteristics of this stationary phase can be consulted from the manufacturer in Pereira [249]. An extensive literature exists on applications of PGC as stationary phase in liquid chromatography, see among many others [245–247, 250–254]. Appendix A9 contains a copy of the manufacturer's certificate for the column used in this study, while Figure 9.4 presents a picture of this column.
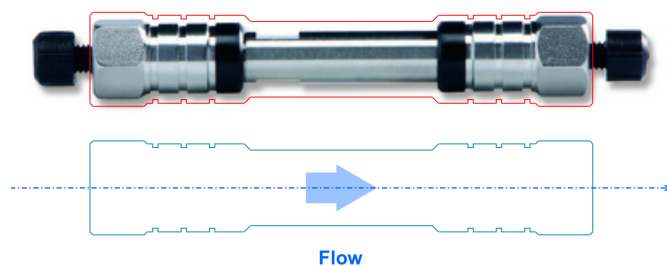
Figure 9.4: Picture of a Hypercarb$^{\mathrm{TM}}$ column of dimensions $L_c = 50\,[\mathsf{mm}]$ and diameter $d_c = 4.6\,[\mathsf{mm}]$ used in the experimental study. The corresponding certificate of the employed column can be consulted in Appendix A9.2, p. 177.

9.4 Preliminary measurement procedures & preparation

Estimation of plant dead times, t_d

Two types of dead time can be identified in the equipment, depending on the operation mode required for a particular measurement. The operation modes have been identified as follows:

1. injLoopSys. This is the *standard* operation mode of the HPLC instrument, where the sample injection is performed by the automatic sampler module of the device—cf. Table 9.1. This mode was applied in Section 9.5 for single compound injections of different concentrations and also in Section 10.2, p. 144 to perform analysis of

---

*A brand of Thermo Fisher Scientific, Inc.

samples obtained by fraction collection. In this mode the dead volume, $V_{d,\,\mathsf{injLoopSys}}$, yields the dead time

$$t_{d,\,\mathsf{injLoopSys}} = \frac{V_{d,\,\mathsf{injLoopSys}}}{\overline{Q}}, \tag{9.1}$$

whereby $\overline{Q}$ denotes the average volumetric flow rate.

2. $\mathsf{gradPumpSys}$. Measurement of the dead time of the system when operating through the gradient pump operation for sample injection was verified with an step change in concentration effected by switching to channel B at a fixed time and recording the response. The automatic sampler module is *bypassed* when the equipment is operated in this manner. As a bonus, one can determine the hydrodynamic dispersion of the internal capillaries of the instrument alone, since the column is removed from the system for this measurement. The actual dispersion observed in the recorded chromatograms is, therefore, a lumped or combined effect of all dispersion sources in the system, e.g., capillaries, internal connectors, junctions, and valves. This operation mode was employed for Frontal Analysis measurements described in Section 9.6. Its corresponding dead time is

$$t_{d,\,\mathsf{gradPumpSys}} = \frac{V_{d,\,\mathsf{gradPumpSys}}}{\overline{Q}}. \tag{9.2}$$

Estimation of total porosity, ϵ

This parameter is important to: *a*) quantify reported experimental results; & *b*) apply this value in the numerical simulations of EDM1D, cf. Chapter 6. A simple procedure was used for its quantification, see e.g., Meyer [197]. Two measurements of a non-adsorbable chemical compound, compatible with the solvent/adsorbent system at hand, are required. A small volume of a few microliters of a sufficiently *small molecule* of a non-retained chemical is injected with the installed HPLC column, recording the eluted peak time, t_0'; the column is afterwards removed and a second injection is performed to estimate the deadtime of the injection loop system, from this second recorded peak, $t_{d,\,\mathsf{injLoopSys}}$. Applying the following expression

$$\epsilon = \frac{\overline{Q}\,t_0}{V_{\mathrm{c}}} \quad \text{with} \quad t_0' = t_0 + t_{d,\,\mathsf{injLoopSys}}, \tag{9.3}$$

the total porosity, ϵ, is obtained—recall Equation (6.6), p. 81. The employed hold-up time, t_0, is corrected with $t_{d,\,\mathsf{injLoopSys}}$. For the applied Hypercarb$^{\mathrm{TM}}$ column, total

porosity was estimated to be $\epsilon = 0.745$, which falls within manufacturer's specification—consult Pereira [249]. Further details on estimation of this parameter for the employed column can be consulted in the work of Kusian [255].

Calibration curves to quantify concentrations of alkylbenzenes

Two types of CALIBRATION CURVES were prepared to conduct analysis of recorded chromatograms—see Meyer [197] for further details:

1. Peak areas operating in the injLoopSys mode—displayed in Figure 9.5. The resulting *linear* calibration factors

$$k_{C10} = 153.9 \left[\frac{\mathsf{mAU \cdot s}}{\mathsf{mM}} \right] \quad \text{and} \quad k_{C11} = 148.1 \left[\frac{\mathsf{mAU \cdot s}}{\mathsf{mM}} \right] \tag{9.4}$$

   were obtained from the linear regressions displayed in Figure 9.5 for decylbenzene (C10) and undecylbenzene (C11), respectively. These factors were applied to analyze the samples of the different solutions employed. The factors are valid for injected volumes of 1 $[\mu l]$ and $\lambda_{UV} = 220 \, [\mathsf{nm}]$. They were also used to analyze the collected fractions of overloading experiments described in Chapter 10.

2. Application of *direct* detector signal calibration, whereby

$$\lambda_{UV} = \{ 220; 225; 230; 235; 240; 245; 250; 254 \} \, [\mathsf{nm}] \tag{9.5}$$

   were the recorded absorption wavelengths; these were selected by considering the recorded UV spectra of the two alkylbenzenes, in the range $\lambda_{UV} \in [190, 400] \, [\mathsf{nm}]$, documented in Appendix A11. The corresponding calibration points were obtained from FA measurements explained in Section 9.6.

Estimation of column plate, N_{plate} & column axial dispersion, D_{ax} from a non-retained compound

The efficiency of the employed Hypercarb$^{\mathrm{TM}}$ column was verified also by Kusian [255] under *analytical conditions* with distilled water $(\mathsf{H_2O})^*$ as a non-retained molecule, in

---

*Generated with a milliQ $^{\circledR}$ instrument available in the laboratory.
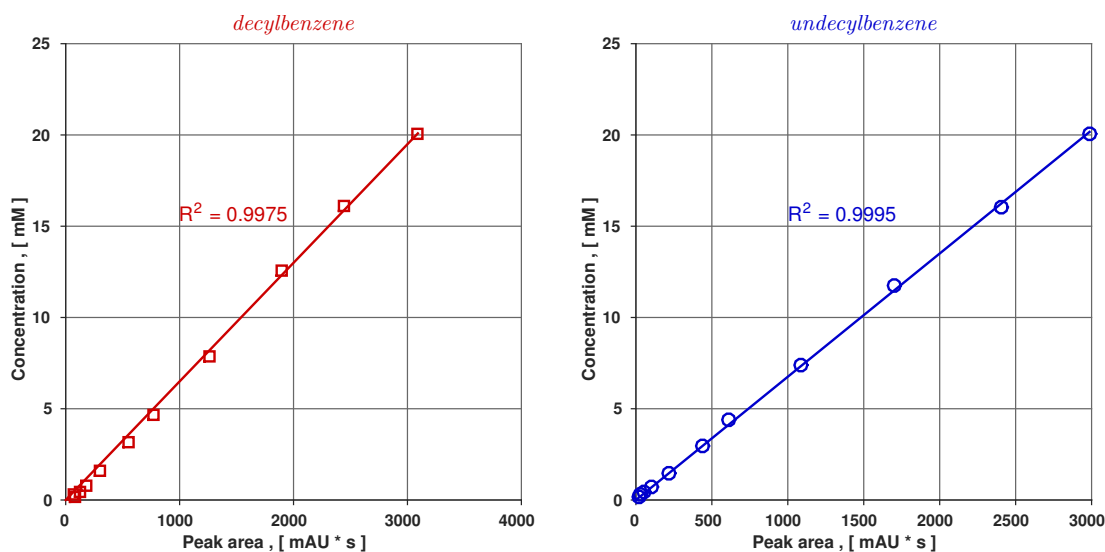
Figure 9.5: Calibration curves for collected fractions' analysis at $\lambda_{\mathsf{UV}} = 220 \, [\,\mathsf{nm}\,]$ for *decylbenzene* ($\mathsf{C10}$) & *undecylbenzene* ($\mathsf{C11}$). Plotted values are listed in Table A6, Appendix A10.1, p. 179, from solutions of various concentrations of $\mathsf{C10}$ & $\mathsf{C11}$ in ACN, documented in Table A7 in Appendix A10, p. 180.

analogy to the description provided with the column's certificate—documented in Appendix A9.2, p. 177. The resulting plate number measurements of this non-retained analyte are documented in Appendix A10.2, p. 181.

9.5 Preliminary injections of single compounds

In analogous manner to Diack & Guiochon [51, 52], elution profiles were recorded employing a commercial PGC stationary phase, confirming the behavior observed and documented by these researchers for the alkylbenzenes/ACN/PGC system. A series of elution profiles with increasing injection volumes, $V_{i,\,\mathrm{inj.}}$, for each compound is presented in Figure 9.6. The trailing portion of the elution profiles of these injections were used to establish approximate concentration ranges where the inflection points along the isotherm courses are located. This range lies *roughly* between $0 - 5 \, [\,\mathsf{mM}\,]$ for both compounds. This preliminary information was useful to organize the Frontal Analysis program execution, discussed in Section 9.6.

Verification of elution profiles & injected amounts   A useful equation to evaluate the elution profiles is:

$$n_{i,\,\mathrm{inj.}} = c_{i,\,\mathrm{inj.}} \, V_{\mathrm{inj.}}, \ \text{ where } V_{\mathrm{inj.}} \equiv V_{\mathsf{injLoopSys}}, \tag{9.6a}$$
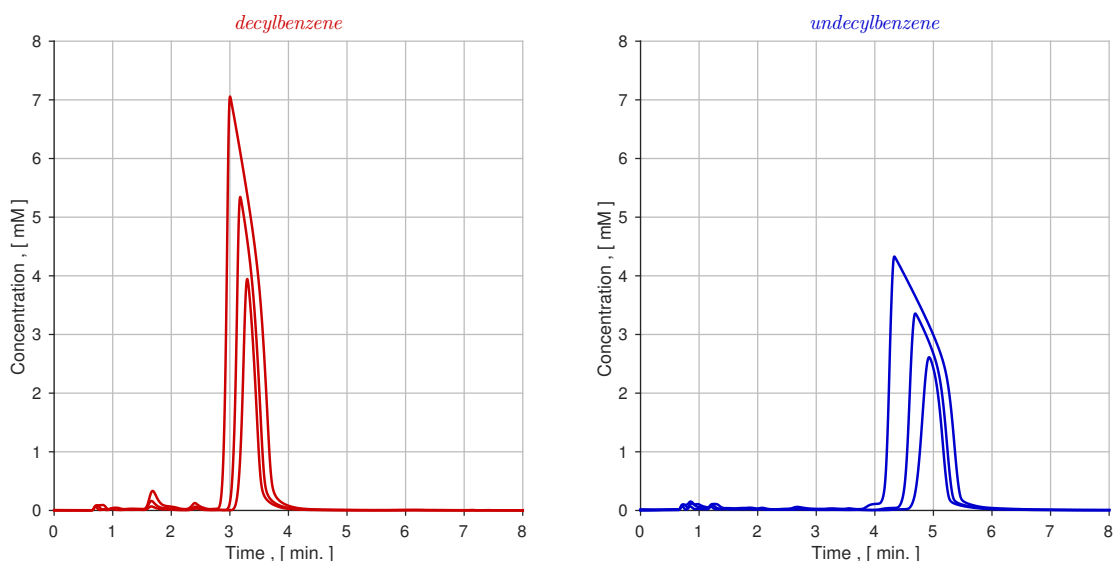
Figure 9.6: Elution profiles of injections of investigated alkylbenzenes, `C10` and `C11`. Displayed injected volumes, $V_{\text{inj.}}$: 50, 100 & 200 $[\mu\text{l}]$ of prepared solutions with concentrations, $c_{i,\text{inj.}}$: 20.06 $[\text{mM}]$ & 20.02 $[\text{mM}]$, respectively—cf. Table A7 in Appendix A10, p. 180.

whereby, the injected concentrations, $c_{i,\text{inj.}}$ are known. Alternatively, since mass is conserved in the process,

$$\overline{Q} \int\limits_{t_1}^{t_2} c_{i,\text{inj.}}(t) \; \mathrm{d}t \leftarrow n_{i,\text{inj.}} = \overline{Q} \int\limits_{t_1}^{t_2} c(t, z = L) \; \mathrm{d}t. \tag{9.6b}$$

Hereby, $\overline{Q}$ denotes an average value of the recorded volumetric flowrate—cf. Section 9.2. Equation (9.6b) is simply a mass balance over *any* component i in the column. Comparison of (9.6a) and (9.6b) was frequently applied to verify the validity and accuracy of the reported experimental results.

9.6 Frontal Analysis of single compounds

Several techniques are available to determine adsorption isotherms. Classical, well-known techniques are thoroughly described and documented in books and technical publications [14, 94, 128, 256, 257]. Mainly, techniques can be classified in two groups: STATIC & DYNAMIC—see e.g., [258]. These designations refer to the type of experimental procedure used to obtain adsorption equilibrium information.

In STATIC METHODS, a known concentration of an adsorbable substance is put in contact with a fixed amount of solid stationary phase [128]. Mass transport from mobile phase to solid phase will occur under controlled experimental conditions, i.e., temperature and

pressure, in order for the—closed—system to attain thermodynamic equilibrium. Driving force for this mass transfer is the difference in chemical potential between the two phases [2, 46]. After a sufficiently long time, a mass balance is calculated in order to determine concentrations in both phases. The procedure is repeated for different amounts of substance in the fluid phase, i.e., solute concentrations. Each of these provides an adsorption equilibrium point, which is subsequently marked in a *q vs. c* diagram, thus providing complete equilibrium information at constant temperature, T, within the investigated concentration range. Static methods are usually very time-consuming, but provide adequate accuracy.

DYNAMIC METHODS, on the other hand, are standard practice of semi-preparative & preparative scale liquid-phase adsorption chromatography [14, 94]. It can be unarguably stated that they are the *workhorse* to quantify adsorption equilibrium for these types of separation processes. Additional information can be obtained from these techniques, e.g., mass transfer mechanism information, elution profile behavior and process conditions themselves. Frontal Analysis (FA) belongs to the class of dynamic measurement methods—see e.g., [14, 129, 259]. Specific aspects addressing FA method accuracy, compared to other dynamic methods, are discussed in [260]. A thorough review of the technique for both single component and competitive mixture isotherm measurement can be found in [94]. Many interesting examples of its application have been documented—see e.g., Lisec [261].

Advantages & disadvantages of FA technique

Just like any other experimental technique for adsorption equilibria measurement, FA displays attractive features, whilst suffering of some drawbacks as well; these are listed in Table 9.3.

Table 9.3: Frontal Analysis (FA) technique: advantages & disadvantages.

ADVANTAGES	DISADVANTAGES
1. *accurate*; applicable on low-efficiency columns;	1. additional control & monitoring of volumetric flow rate needed;
2. requires only *simple* mass balances—*capacity* equations;	2. prone to error propagation in *stepwise, staircase* modality; &
3. provides detector calibration *directly*; &	3. requires large amounts of investigated chemicals—i.e., costly; *time-consuming.*
4. applicable to *simultaneous* competitive equilibria measurement, too.	

Despite of the listed *disadvantages*, the technique is well-established and it is ideally suited to gain thorough insight of adsorption behavior of the investigated experimental system.

Method description and working equations

A solution of an adsorbable compound*, i, of known concentration, $c_{i,\text{feed}}$, is injected to an initially *clean*—i.e., non-loaded—column, packed with the adsorbent of interest and kept at a constant temperature, T, in order to effect a step change in concentration of the fluid phase flowing through the column. The concentration is thus kept constant at the inlet. After a determined amount of time, this concentration value is registered at the column outlet by the instrument's detector. This is typically observed as a sharp, sigmoid-like curve in the signal. An indication that the stationary phase has reached completely an equilibrium concentration, $c_i^{(\text{II})}$, corresponding to the injected concentration, $c_{i,\text{feed}}$, occurs when the detector signal remains constant, i.e., the step change concentration has been attained and thus marks the point in time at which it is in equilibrium with its corresponding adsorbed phase concentration. In general, these step changes in concentration are applied for any starting value at equilibrium, $c_i^{(\text{I})}$. In this way, it becomes possible to progressively introduce step changes in the concentration, as illustrated in Figure 9.7. The *uptake* of compound i by the stationary phase is therefore obtained from a mass balance for the column, referred to as *capacity* equation:

$$\Delta n_i = n_i^{(\text{II})} - n_i^{(\text{I})} = \overline{Q} \left[\Delta c_i^{(\text{I·II})} \left(t_2 - t_1 \right) - \int_{t_1}^{t_2} c_i(t) \, \mathrm{d}t \right], \qquad (9.7\text{a})$$

whereby Δn_i represents the amount of solute adsorbed by the stationary phase when a concentration step change of the fluid phase, $\Delta c_i^{(\text{I·II})} \equiv c_i^{(\text{II})} - c_i^{(\text{I})}$, is exerted on the column. The lower integration limit is set by

$$t_1 = t_{\text{step}}^{(\text{I·II})} + t_{d,\text{gradPumpSys}} + t_0; \quad t_2 > t_1, \qquad (9.7\text{b})$$

taking into account the dead volume of the instrument when injecting the solution using the gradient pump modality described before—cf. Equation (9.2). The upper limit, t_2, is selected by noticing the point in time when the recorded concentration signal is stable, and does not vary as a result of the effected step change. The adsorbed phase

---

*This compound is often referred to as *eluate* or *solute* in the chromatography jargon.

concentration at equilibrium is calculated with

$$\Delta q_i = q_i^{(\mathrm{II})} - q_i^{(\mathrm{I})} = \frac{\Delta n_i}{(1-\epsilon)V_{\mathrm{c}}}, \quad \text{therefore,} \quad q_i^{(\mathrm{II})} = q_i^{(\mathrm{I})} + \Delta q_i. \tag{9.7c}$$

The set of equilibrium values obtained from subsequent application of several concentration steps are then plotted in a *q vs. c* diagram—i.e., the adsorption isotherm curve $q_i = f(c_i)$.

A slightly different approach also applied to evaluate the FA concentration steps is the so-called *'equal-area'* method [14, 176]. Since time of injection and solution concentration are known, a *mass balance* for compound i can be established also in the form:

$$t_{\mathrm{b},i}\,\overline{Q}\Delta c_i = \epsilon V_{\mathrm{c}}\Delta c_i + (1-\epsilon)\,V_{\mathrm{c}}\Delta q_i, \tag{9.8a}$$

whereby, $\Delta q_i = q_i^{(\mathrm{II})} - q_i^{(\mathrm{I})}$ and $\Delta c_i = c_i^{(\mathrm{II})} - c_i^{(\mathrm{I})}$, yielding

$$q_i^{(\mathrm{II})} = q_i^{(\mathrm{I})} + \frac{t_{\mathrm{b},i}\,\overline{Q} - \epsilon V_{\mathrm{c}}}{(1-\epsilon)\,V_{\mathrm{c}}}\left[c_i^{(\mathrm{II})} - c_i^{(\mathrm{I})}\right]. \tag{9.8b}$$

The breakthrough time, $t_{\mathrm{b},i}$, signalizes the concentration change from $c_i^{(\mathrm{I})}$ to $c_i^{(\mathrm{II})}$. It is determined by *equalizing* graphically the two areas around the applied concentration step generated by a vertical line drawn at $t_{\mathrm{b},i}$ that *cuts* through the step curve. This also defines in a precise way the amount of solute i adsorbed by the column from (9.8b).
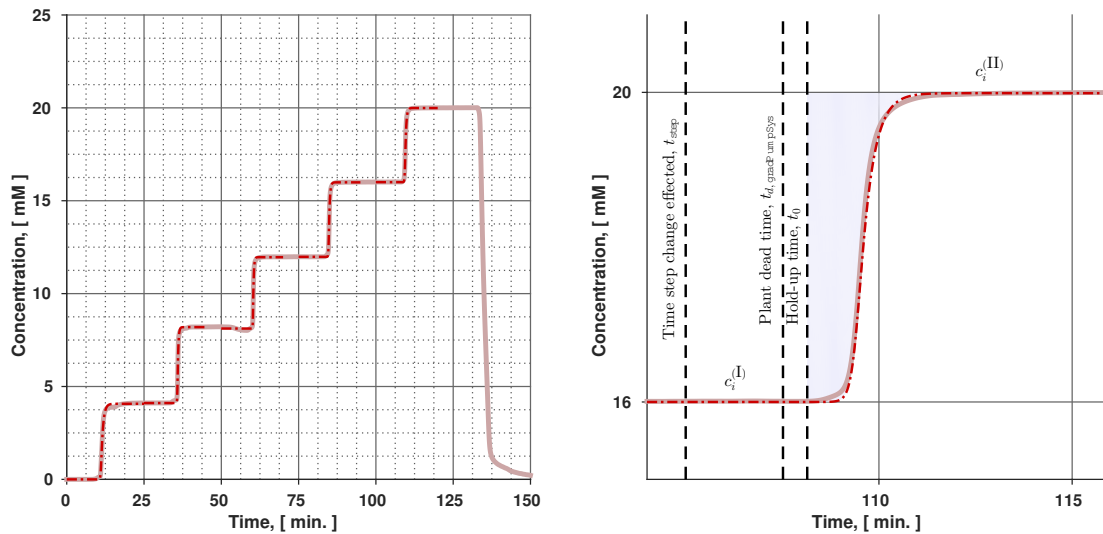
Figure 9.7: Illustration of a typical FA elution profile for decylbenzene (C10). $(-\cdot)$: *post-processed* steps via sigmoidal function (9.9a), in order to evaluate adsorptive capacity with Equation (9.7). The resulting equilibrium values are listed in Table A11, Appendix A10, p. 184.

The results of the *'equal-area'* method, Equation (9.8) and the *'capacity'* method, Equation 9.7 are therefore equivalent, since they are based on a mass balance of adsorbate i in the column, using the recorded elution concentration profile that results from bringing the system from an initial state of equilibrium, (I), to a new one, (II).

Post-processing of experimental elution profiles from FA measurements

Data post-processing operations typically applied to the *raw data* include: *a) re-scaling*; *b) baseline offset correction*; *c) drift correction*; *d) noise filtering*; and *e) smoothing*. An explanation for these terms, as well as further technical details regarding signal post-processing can be consulted in e.g., Felinger [262] and Meyer [197].
An alternative to post-process the recorded signals and compute the *adsorptive capacities* of FA measurements is achieved by fitting the elution profiles of the concentration steps to appropriate *step functions*. In this way, the experimental noise in the measured signals is eliminated and a *smooth*, accurate representation of the concentration steps is achieved. For this purpose, the five-parameter formula

$$y = f(x) = d_0 + \frac{d_1 - d_0}{\left[1 + \exp\left[d_2\left[x - d_3 \right] \right] \right]^{d_4}}, \tag{9.9a}$$

with *lower* asymptote, d_1 and *upper* asymptote, d_0, was employed to fit each step change of the FA concentration profile. Formula (9.9a) possesses, in turn, the *indefinite* integral

$$y = \int f(x)\,\mathrm{d}x = \frac{1}{d_2 d_4}\left[1 + \exp\left[d_2\left[x - d_3 \right] \right] \right]^{-d_4}.$$

$$\left[\begin{array}{l} d_0 d_2 d_4\left[1 + \exp\left[d_2\left(x - d_3 \right) \right] \right]^{d_4} x \\[2mm] + \left[d_0 - d_1 \right]\left[1 + \exp\left[d_2\left(x - d_3 \right) \right] \right]^{d_4} \\[2mm] {}_2\mathsf{F}_1\left[d_4, d_4, 1 + d_4, -\exp\left[d_2\left[x - d_3 \right] \right] \right] \end{array} \right] + C, \tag{9.9b}$$

which was applied to evaluate adsorptive capacities from Equation (9.7)—Guiochon *et al.* [14]. Figure 9.7 illustrates an example of a fitted step function using formula (9.9a).

Resulting single component adsorption isotherms of decylbenzene (C10) and undecylbenzene (C11) at $323\,\mathrm{K}$ ($50\,°\mathrm{C}$)

Application of the post-processing tools and evaluation of the FA results with the *capacity* method described previously, using formulas (9.9), yielded single component adsorption isotherms, $q_i^0 = f(c_i^0)$, $i = 1, 2$, for decylbenzene (C10) and undecylbenzene (C11) as illustrated in Figures 9.8 and 9.9. Additionally, the resulting quotients q_i^0/c_i^0 are also displayed in order to apply IAST—cf. Chapter 3; these are particularly useful to confirm the *presence of inflections points* in the isotherm courses and estimate with accuracy the concentration values at which these occur.
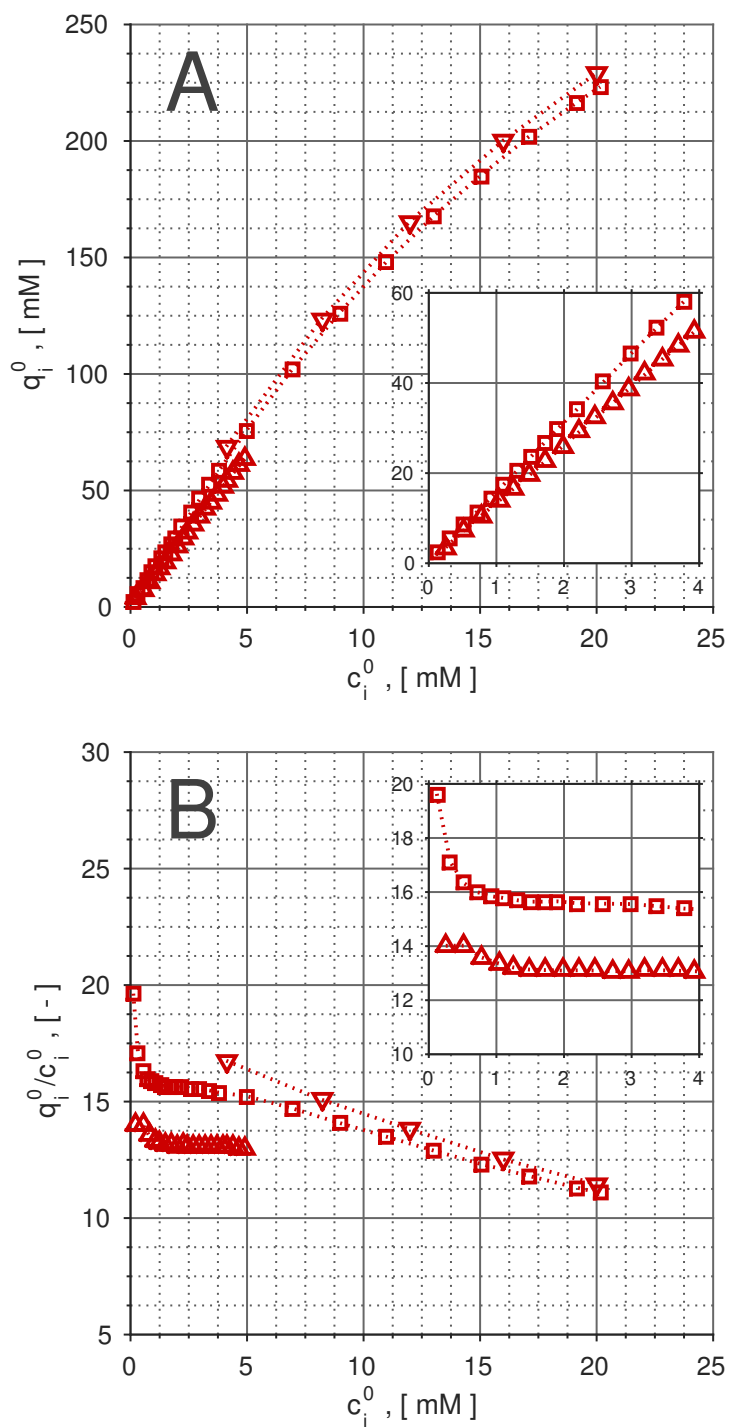
Figure 9.8: (**A**): adsorption isotherms of decylbenzene ($C10$) dissolved in ACN at $323.15\,K$ ($50\,^{\circ}C$), measured with a $50 \times 4.6\,[\,mm\,]$ Hypercarb^{TM}column—cf. Appendix A9.2. ($\square$): 24 pts. in conc. range $0 - 20\,[\,mM\,]$, Table A9, p. 182; ($\triangledown$): 5 pts in conc. range $0 - 20\,[\,mM\,]$; ($\triangle$): 20 pts. in conc. range $0 - 5\,[\,mM\,]$, Table A10, p. 183. (**B**): corresponding quotients, q_i^0/c_i^0, obtained from equilibrium points illustrated in (**A**).
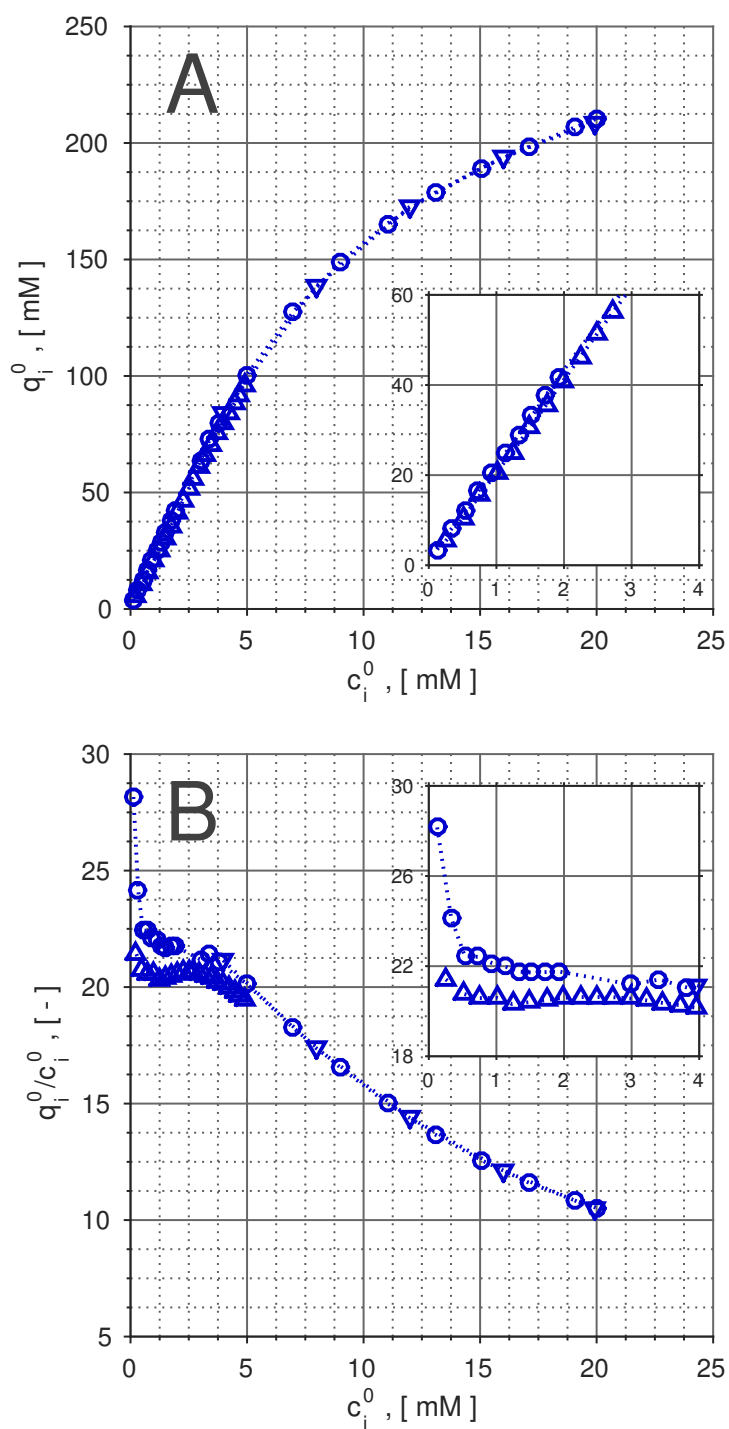
Figure 9.9: (**A**): adsorption isotherms of undecylbenzene ($C11$) dissolved in ACN at $323.15\,K$ ($50\,°C$), measured with a $50 \times 4.6\,[\text{mm}]$ Hypercarb^{TM}column—cf. Appendix A9.2. ($\square$): 24 pts. in conc. range $0 - 20\,[\text{mM}]$, Table A9, p. 182; ($\triangledown$): 5 pts in conc. range $0 - 20\,[\text{mM}]$; ($\triangle$): 20 pts. in conc. range $0 - 5\,[\text{mM}]$, Table A10, p. 183. (**B**): corresponding quotients, q_i^0/c_i^0, obtained from equilibrium points illustrated in (**A**).

Effect of temperature[*]

Figure 9.10, illustrates the effect of temperature on the elution of peaks of C10 and C11. Breakthrough times were shortened as temperature was increased. This is the expected behavior, since preference to adsorb is favored at lower temperatures, resulting in longer peak retention times, as shown in the figure.
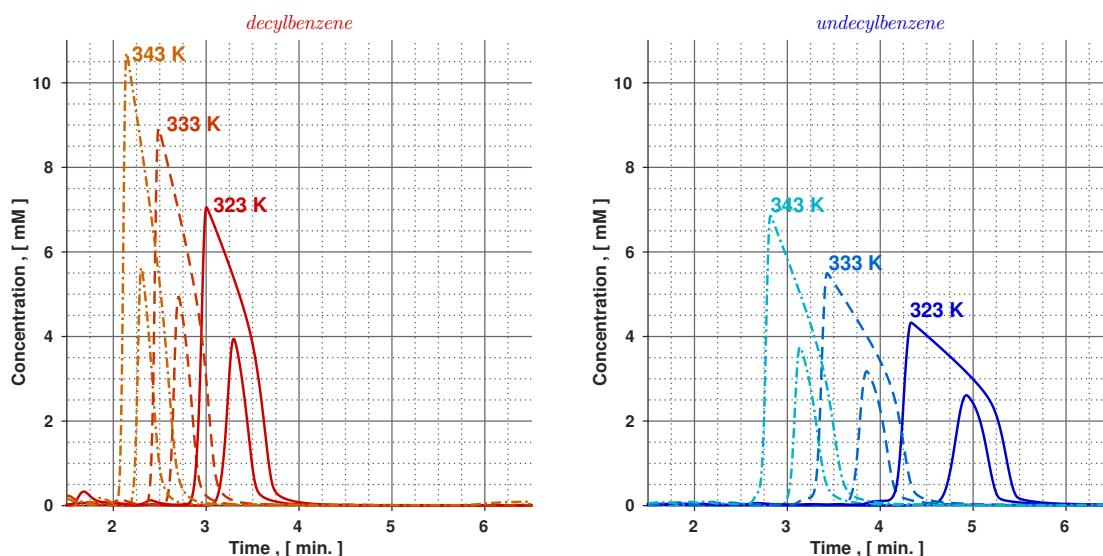
Figure 9.10: Injections of decylbenzene (C10) and undecylbenzene (C11) at different temperatures. $(-)$: 323 K (50 °C); $(--)$: 333 K (60 °C); & $(-\cdot)$: 343 K (70 °C). Injected volumes, $V_{i,\,\text{inj.}}$: 50 [μl] and 200 [μl] of solutions with concentration $c_{i,\,\text{inj.}} = 20$ [mM].

The adsorption equilibria of the alkylbenzenes was quantified by measuring single component FA at three different temperatures: 323.15 K (50 °C), 333.15 K (60 °C) and 343.15 K (70 °C). The results are illustrated in Figures 9.11 and 9.12 for measurements in the ranges $0 - 20$ [mM] and $0 - 5$ [mM], respectively. These measurements helped to verify the reasoning given in Section 9.1, regarding origin of inflections along isotherm functions, since it can be observed that the inflection points become less pronounced as temperature is increased. Further calorimetric studies were not pursued, as it was sufficient for the experimental implementation and demonstration of this study to work with enough gathered data at 323.15 K (50 °C). At this temperature, the effect of the inflection points was clearly observed in the performed measurements, at a flow rate set point of $Q = 1.0$ [ml/min.].

---

[*]Preliminary results of this section were presented at the PREP Conference in 2013—cf. Appendix 7.
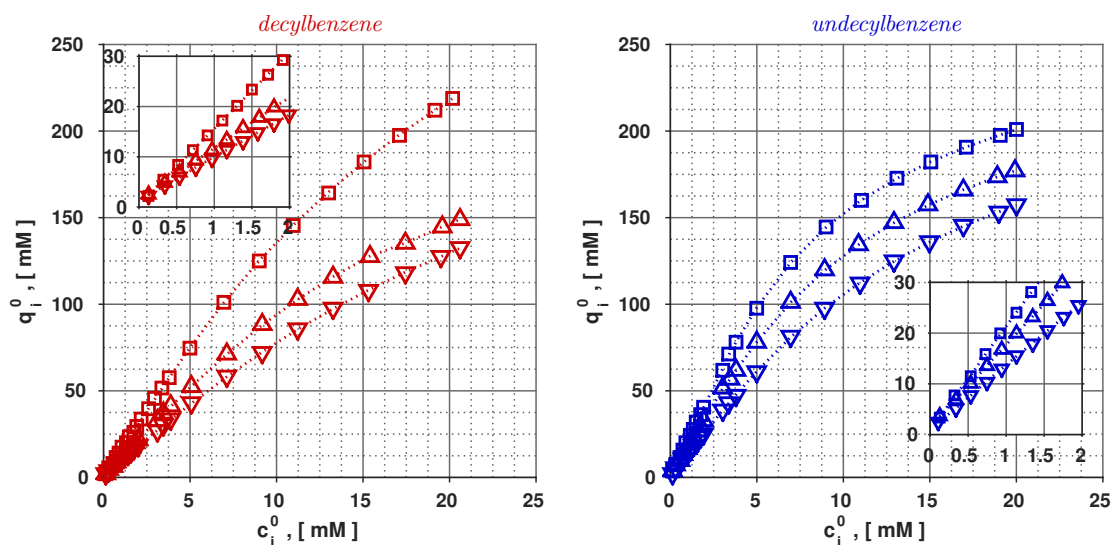
Figure 9.11: Decylbenzene & undecylbenzene adsorption equilibria measured by FA at 323 K (□,□), 333 K (△,△) & 343 K (▽,▽). Plotted data points are reported in Table A12, Appendix A10.4, p. 185.
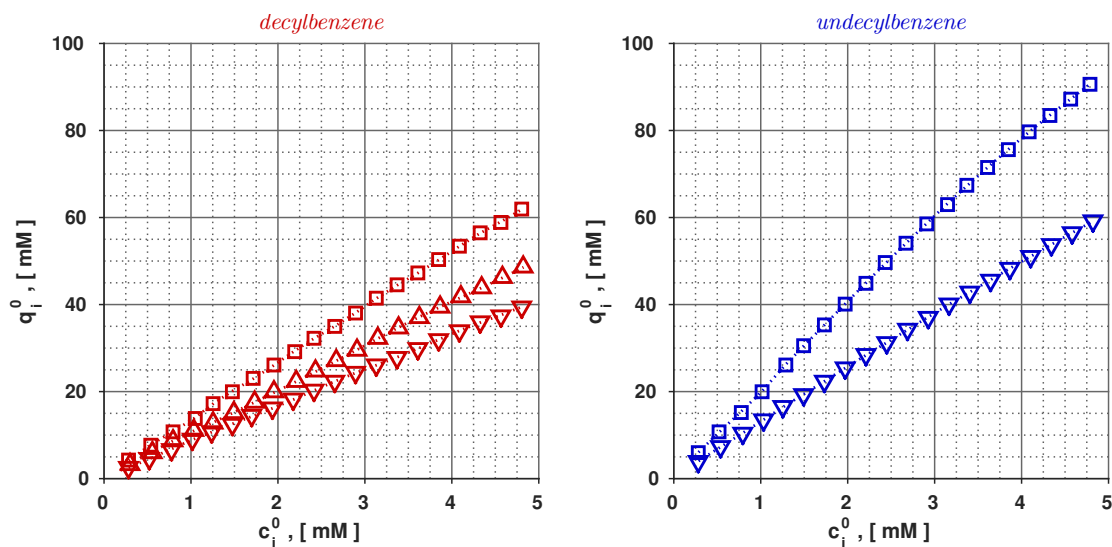
Figure 9.12: Decylbenzene & undecylbenzene adsorption equilibria measured by FA at 323 K (□,□), 333 K (△) & 343 K (▽,▽). Plotted data points are reported in Table A13, Appendix A10.4, p. 186.

9.7 Fitting of measured adsorption isotherms to Quadratic plus Langmuir model

Evaluation of the single component FA runs produced the adsorption isotherms, i.e., equilibrium points, illustrated in Figure 9.8 for decylbenzene (`C10`) and Figure 9.9 for undecylbenzene (`C11`).

These equilibrium points were fitted to the five-parameter Quadratic plus Langmuir isotherm

$$q_i = q_{i1}^{\mathrm{sat}} \frac{c_i \left[b_{i1} + 2b_{i2}c_i \right]}{1 + b_{i1}c_i + b_{i2}c_i^2} + q_{i2}^{\mathrm{sat}} \frac{b_{i3}c_i}{1 + b_{i3}c_i}, \ i = \mathsf{C10}, \mathsf{C11}, \tag{2.3e}$$

in analogous manner to the work of Diack & Guiochon [51, 52]. This model is capable of describing the observed presence of two inflection points along the courses, under certain parameter value constellations.

Parameter values were obtained by using the optimization toolboxes and `Curve Fitting Tool` available in MATLAB® [168]—see Appendix A1, p. 163, for further software details. Special attention was set on the qualitative behavior of model (2.3e) with the obtained parameter values for the q_i^0/c_i^0 functions illustrated in Figures 9.8 and 9.9, as this is essential for applying IAST. From elution profiles of peaks of small injected
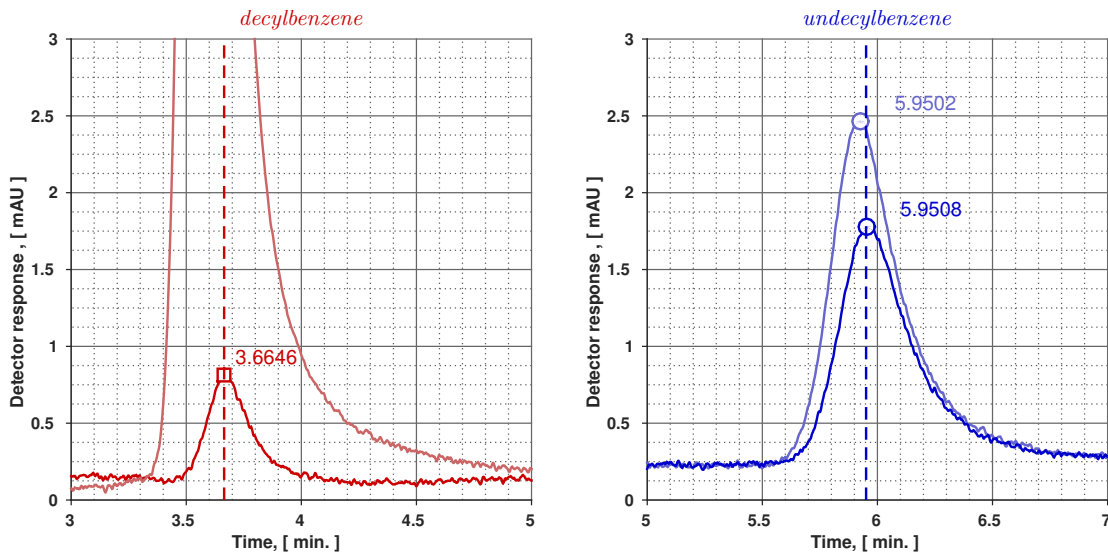
Figure 9.13: Elution profiles to estimate Henry coefficients, $\mathfrak{h}_i$, of investigated alkylbenzenes in ACN/PGC system from peak times under analytical conditions. Temperature $T = 323\,\mathrm{K}$. Volumetric flow rate set-point: $1.0\,[\mathsf{ml/min.}]$.

volumes, $V_{\mathrm{inj.}}$, it was possible to establish experimentally Henry limit values, $\mathfrak{h}_i$, for each alkylbenzene, as illustrated in Figure 9.13. In the linear region of the adsorption

isotherms—i.e., *Henry region*, Equation (2.5), p. 18—holds

$$t_{\mathrm{p},i} \approx t_{\mathrm{R},i} = t_0 \left[1 + \phi \, \mathfrak{h}_i \right] \quad \text{or} \quad \mathfrak{h}_i = \frac{1}{\phi} \left[\frac{t_{\mathrm{R},i}}{t_0} - 1 \right] = \frac{\epsilon}{1 - \epsilon} \left[\frac{t_{\mathrm{R},i}}{t_0} - 1 \right], \qquad (9.10)$$

thus obtaining the values $\mathfrak{h}_{\mathsf{C10}} = 13.8$ and $\mathfrak{h}_{\mathsf{C11}} = 24.6$ after correcting for the instrument's dead time, which was found to be $t_{d,\,\mathsf{injLoopSys}} = 0.057\,[\,\mathsf{min.}\,]$. These Henry limit values may be applied to establish *constraints* on the values of the parameters of the applied isotherm equation under analytical conditions, because in accord with Equation (2.12g)—Table 2.3, p. 20,

$$\mathfrak{h}_i = q_{i1}^{\mathrm{sat}} \, b_{i1} + q_{i2}^{\mathrm{sat}} \, b_{i3}. \qquad (2.12\mathrm{g})$$

Furthermore, the theoretical saturation limit for the Quadratic plus Langmuir model

$$q_i^{\infty} = 2 q_{i1}^{\mathrm{sat}} + q_{i2}^{\mathrm{sat}}, \qquad (9.11)$$

was employed. A simple starting guess value for q_i^{∞} may be obtained from a *Langmuirian* fit to the gathered FA data points. The values $q_{\mathsf{C10}}^{\infty} = 370\,[\,\mathsf{mM}\,]$ and $q_{\mathsf{C11}}^{\infty} = 267\,[\,\mathsf{mM}\,]$ were applied. *Positively-valued* equation parameters were also enforced. Firstly, on the grounds of physical definition, saturation capacities, q_{i1}^{sat} & q_{i2}^{sat}, are positive and finite. Secondly, the constraint, b_{i1}, b_{i2}, $b_{i3} \geq 0$ was employed for convenience. *Zeros* in the denominators of these terms in Equation (2.3e), produced by assuming negative parameter values, could limit its range of applicability. For IAST, single component isotherms should be available, in principle, in the entire concentration range $c_i^0 \in [0, \infty)$, cf. Section 3.2, p. 35.

Quadratic plus Langmuir isotherm parameters obtained from FA measurements at 323 K

Figures 9.14 and 9.15 illustrate the resulting single component isotherm fits and the experimental points obtained by FA for comparison for decylbenzene ($\mathsf{C10}$) and undecylbenzene ($\mathsf{C11}$), respectively.

The estimated parameter values are listed in Table A14 of Appendix A10.5, p. 187.
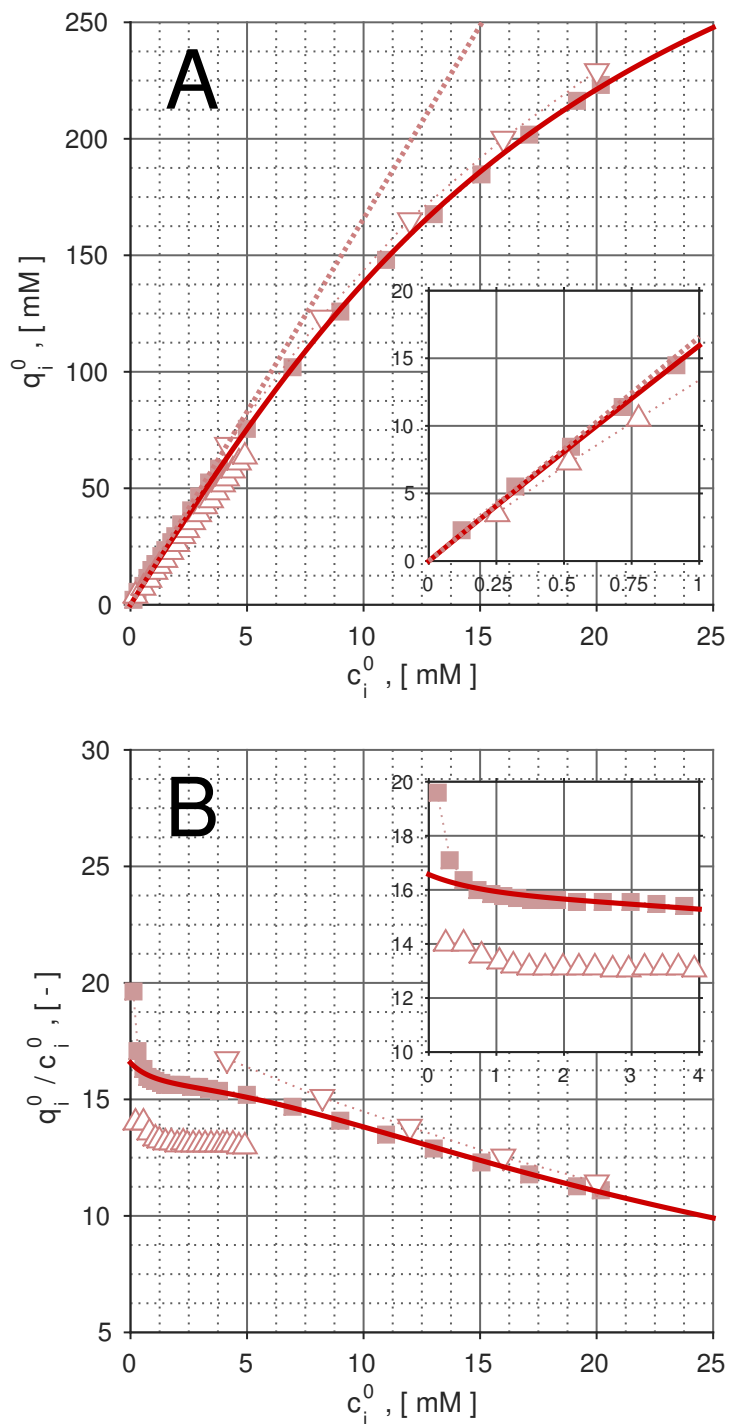
Figure 9.14: Adsorption isotherms of decylbenzene (C10), described by the Quadratic plus Langmuir model (2.3e), obtained by parameter fitting. ($-$): fit to FA points. $\triangledown$: points from 5-step FA program; ■: points from *long* FA program, $0-20$ [mM], Table A9, p. 182; $\triangle$: points from *long* FA program, $0-5$ [mM], Table A10, p. 183.
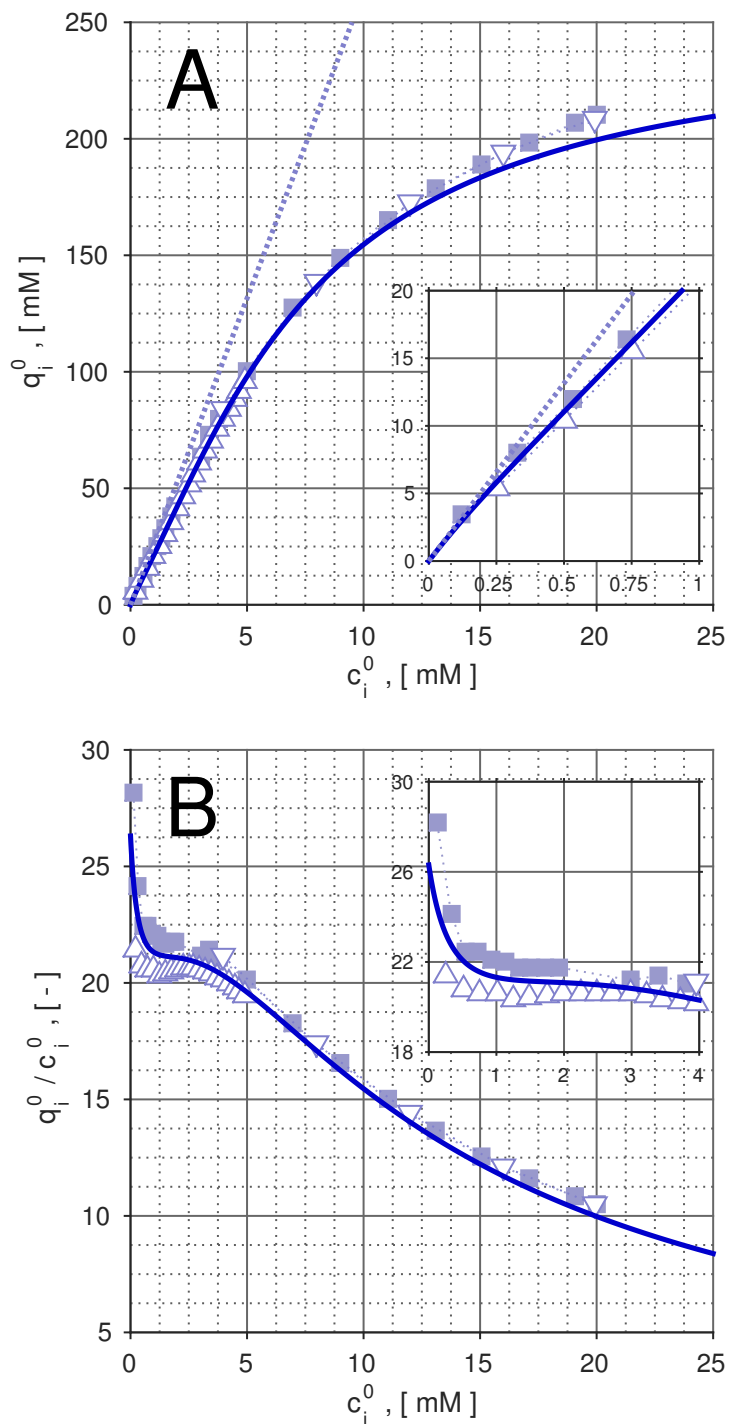
Figure 9.15: Adsorption isotherms of undecylbenzene (C11), described by the Quadratic plus Langmuir model (2.3e), obtained by parameter fitting. (−): fit to FA points. ▽: points from 5-step FA program; ■: points from *long* FA program, $0 - 20$ [mM], Table A9, p. 182; △: points from *long* FA program, $0 - 5$ [mM], Table A10, p. 183.

Summary

In this chapter a experimental system consisting of alkylbenzenes dissolved in acetonitrile, adsorbing onto a commercial porous graphitic carbon (PGC) stationary phase was introduced and described briefly. Hereby selected adsorbates featured inflection points along their adsorption isotherm courses in the solvent/adsorbent system chosen. The adsorption isotherms of selected compounds were measured with the classical experimental procedure of Frontal Analysis (FA). Therefore, the main piece of information required to implement IAST calculations—i.e., single component adsorption isotherms, $q_i^0 = f(c_i^0)$, was obtained.

Parameter values for the Quadratic plus Langmuir single component isotherm were estimated from FA results for the investigated alkylbenzenes, viz. C10 and C11. These values are listed in Table A14.

Further application of the experimental results herein reported will be presented in Chapter 10.

Addendum: Practical recommendations

The following important items should be taken into account to perform adsorption equilibria measurements, using the methods explained throughout this chapter:

- For compounds displaying inflection points along the adsorption equilibrium courses, a precise and numerous collection of data points is strongly recommended, particularly at concentration values where these inflections occur—*wheresoever & whensoever* feasible.

- Variations in physical properties amongst stationary phases, even in the case of materials supplied by the same manufacturer, should be expected. An example was presented whereby two of the Hypercarb columns employed in this study, differing from each other only in their column length, L_c, exhibited different values of total porosity, ϵ, albeit estimated values were found to be within the manufacturer's specification [249].

- The same applies to purchased chemicals; an example was illustrated in Figure 9.3, whereby different elution behavior of *undecylbenzene* from two different suppliers was observed for the same type of measurement, hardware and HPLC operation conditions. In practice however, these chemicals may be difficult to obtain commercially as high purity analytical standards.

This page intentionally left blank.

Chapter 10

Predicting competitive elution behavior of alkylbenzenes in the acetonitrile/PGC system

"In theory there is no difference between theory and practice. In practice there is."

– Yogi Berra

Introduction

In this chapter the ability of IAST to describe mixtures of the experimental system, presented in detail considering the adsorption of the single compounds in Chapter 9, is tested. Firstly, a series of overloaded injections of mixtures of the same alkylbenzenes, `C10` and `C11`, are performed and analyzed. Since individual adsorption isotherm information has been acquired previously, it can be applied directly in a second step together with a *simple* fixed-bed column model to predict competitive adsorption dynamics using IAST. Lastly, the obtained predictions can be compared to corresponding experimental elution profiles.

10.1 Applied methodology

A *simple workflow* is implemented in order to assess the ability of IAST to reproduce measured binary, competitive elution profiles of the experimental system described in Chapter 9—Section 9.1, p. 118, under overloaded conditions. It consists of a series of steps, required to test IAST or any other multicomponent prediction model with actual measured data from an adsorption-based separation unit, regardless of its size, i.e., it is applicable to lab-scale HPLC columns, as well as large packed columns used for industrial adsorption, following the model assumptions for the process listed in Table 6.1, Section 6.2, p. 79.

This METHODOLOGY consists of the following STEPS, which brings together concepts, tools and information presented throughout the previous chapters:

1. obtain single component isotherms with an accurate measurement method—cf. Chapter 9, Section 9.6, p. 127;

2. measure competitive multicomponent elution profiles—this chapter, Section 10.2;

3. apply IAST using the estimated single component isotherms with the solution approach of Chapter 4 in conjuction with a suitable dynamic fixed-bed adsorber model, described in Chapters 6 and 7; &

4. assess the capability of IAST to predict the measured multicomponent profiles by comparison of *experimental* results and *theoretical* predictions— as will be explained in Section 10.3.

10.2 Overloaded injections of binary mixtures of alkylbenzenes

Several overloaded injections of binary mixtures of decylbenzene ($C10$) and undecylbenzene ($C11$) in solutions of various concentrations were fed to the column described in Section 9.2, p. 120.

Preliminary measurements to understand system behavior

A set of three preliminary injections was performed with a solution of equimolar concentration of $20\,[mM]$ $C10$: $20\,[mM]$ $C11$—consult Table A7, p. 180 for details regarding

the preparation of this solution. Large injection volumes of $V_{i,\,\mathrm{inj.}} = 5\,[\,\mathsf{ml}\,]$ were applied to the system for equimolar injections of 5, 10 and 15 $[\,\mathsf{mM}\,]$ using the gradPumpSys mode, explained in Section 9.4, p. 123. These injections can not be performed with the standard injLoopSys mode because the built-in injection loop has a maximum capacity of 1000 $[\,\mu\mathsf{l}\,]$. The recorded elution profiles are illustrated in Figure 10.1.
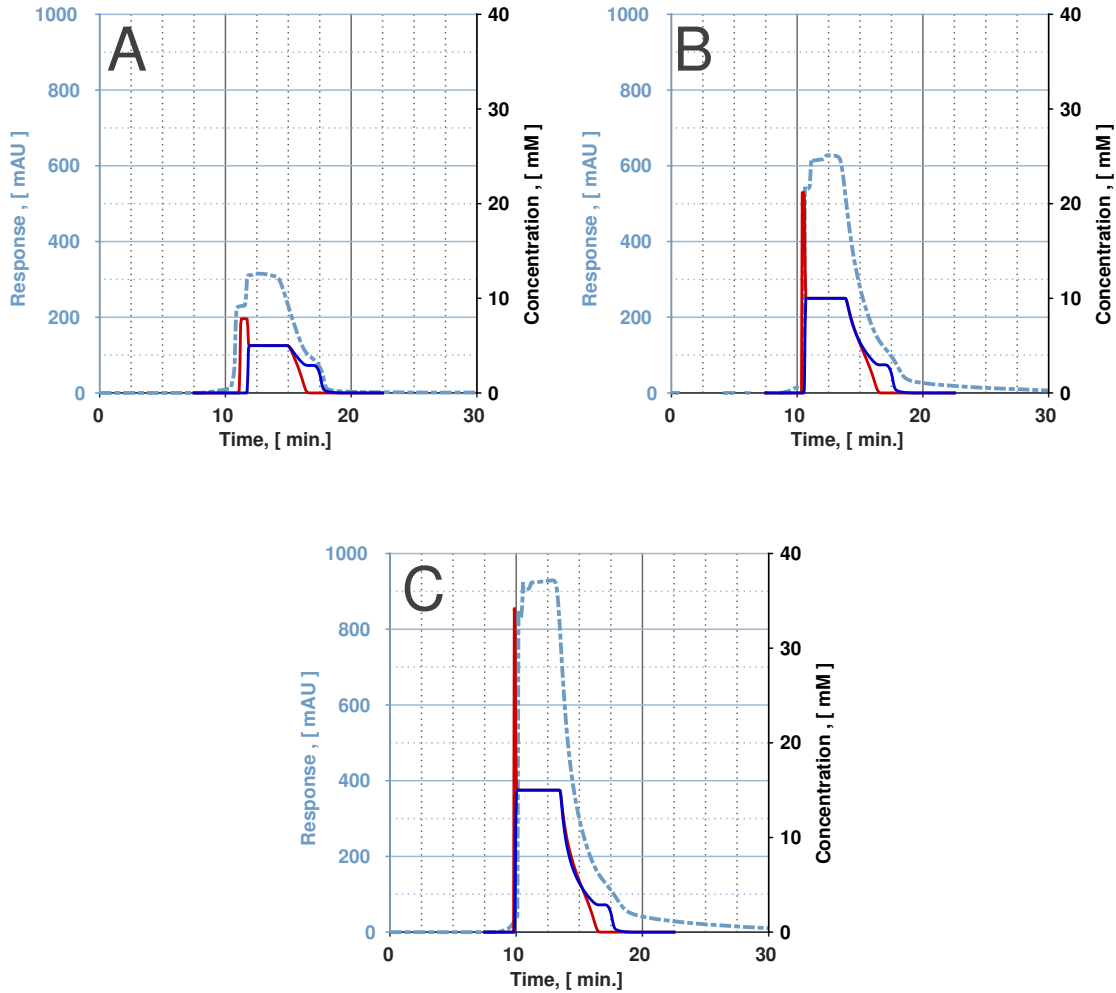
Figure 10.1: Total detector responses for overloaded injections of *equimolar* mixtures of C10 and C11 recorded at $\lambda_{\mathsf{UV}} = 235\,[\,\mathsf{nm}\,]$. (A): 5 $[\,\mathsf{mM}\,]$; (B): 10 $[\,\mathsf{mM}\,]$; & (C): 15 $[\,\mathsf{mM}\,]$. Experimental conditions: $T = 323\,\mathsf{K}$; $Q = 1.0\,[\,\mathsf{ml/min.}\,]$ (setpoint). Measurements performed with the Hypercarb$^{\mathrm{TM}}$ column described in Section 9.3, p. 121. Concentration profiles predicted by numerical simulation are shown for comparison. (−): C10; (−): C11. Single component isotherm parameters applied in numerical simulations are listed in Table A14, Appendix A10.5, p. 187.

In these preliminary experiments, a sharp step in the signal was registered, in particular for the 15 $[\,\mathsf{mM}\,]$ injections. The large injected volume allows a full equilibration of the stationary phase in the column, as can be observed from the plateau of the signal at the highest recorded values, which lasts approximately 2.5 $[\,\mathsf{min.}\,]$. Afterwards, the

column was regenerated with pure ACN, thus performing complete cycles in all three measurements—in analogous way as done for the numerical simulations in Section 8.3, p. 110.

Individual signal *reconstruction* by fraction collection & analysis

A commonly applied alternative to identify the signals of individual compounds under overloaded conditions, as those depicted in Figure 10.1, consists of recording these at different wavelengths, λ_{UV}. This usually works well to *isolate* each signal if the absorption responses of the solutes are substantially different; a good example of a system where this was exploited was investigated by Lisec [136]. In the case of the alkylbenzenes/ACN system adsorbing on PGC, as might be inferred from observation of the molecular structures of C10 and C11—Figure 9.1, p. 118, the adsorption responses are rather similar in the available UV range $200 - 400\,[\,\mathsf{nm}\,]$ recorded by the HPLC detector. This fact was confirmed by measuring the UV spectra, which are documented in Figures A5, A6 and A7 of Appendix A11, p. 188, so the possibility to obtain individual elution profiles under competitive conditions by analyzing the profiles at different wavelengths alone, can not be applied for this system.

An alternative to deal with this problem consists of collecting continuously a series of fractions during elution, throughout the time span of the measurement and subsequently analyze the collected fractions, in order to quantify the concentrations of each adsorbate. With the resulting concentration values, consequently, it is possible to *reconstruct* the corresponding elution profiles of each compound. Since the elution bands display fast changes in the concentration, particularly at the time when the breakthrough shock layers elute, fractions should be collected as quickly and precisely as possible, e.g., with a programmable fraction collector.

Table 10.1: Details of the preparation of employed solutions for mixture experiments and number of fractions, $N_{fr.}$, collected for each measurement. Solutions prepared with volumetric flasks of 250 $[\,\mathsf{ml}\,]$ for precise dilution; a standard, adjustable air displacement micropipette (Rainin Instrument, LLC; Mettler-Toledo, LLC); and chemicals listed in Table 9.2, p. 122.

Case	Applied volumes $[\,\mu l\,]$ C10 : $[\,\mu l\,]$ C11 : $[\,\mathsf{ml}\,]$ sln.	No. fractions, $N_{fr.}$	Fraction *size* $[\,\mathsf{min.}\,]$
CASE 1	320 $[\,\mu l\,]$: 340 $[\,\mu l\,]$: 250 $[\,\mathsf{ml}\,]$	100	0.2
CASE 2	320 $[\,\mu l\,]$: 680 $[\,\mu l\,]$: 250 $[\,\mathsf{ml}\,]$	100	0.1
CASE 3	640 $[\,\mu l\,]$: 340 $[\,\mu l\,]$: 250 $[\,\mathsf{ml}\,]$	100	0.1

A second set of measurements, identified as CASE 1, CASE 2 and CASE 3, was executed,

whereby a large number of samples were collected for further analysis. These measurements are explained in Table 10.1. Details of each of the overloaded injections are provided in Table 10.2, including measured concentrations of the fed solutions, $c_{i,\,\text{feed}}$. The *molar balances* calculated with

$$n_{i,\,\text{out}} \overset{!}{=} n_{i,\,\text{inj.}} \tag{10.1a}$$

where

$$n_{i,\,\text{out}} \equiv n_i \mid_{z=L} = \overline{Q} \int_0^\infty c_i(t, z = L) \, \mathrm{d}t \quad \text{and} \tag{10.1b}$$

$$n_{i,\,\text{inj.}} = \overline{Q} \, c_{i,\,\text{feed}} \, t_{\text{inj.}}, \quad i = 1, 2, \tag{10.1c}$$

were used in order to verify the accuracy of the reconstructed elution profiles.

Table 10.2: Molar balance verification of reconstructed elution profiles from collected fractions of decylbenzene (C10) and undecylbenzene (C11), i.e., $n_{i,\,\text{out}} \overset{!}{=} n_{i,\,\text{inj.}}$, Equations (10.1).

Case	Flow rate $\overline{Q}$	Feed conc. $c_{i,\,\text{feed}}$		Inj. time $t_{\text{inj.}}$	Inj. amount $n_{i,\,\text{inj.}}$		Eluted amount $n_{i,\,\text{out}}$	
		C10	C11		C10	C11	C10	C11
	[ml/min.]	[mM]	[mM]	[min.]	[mmol]	[mmol]	[mmol]	[mmol]
Case 1	0.99	5.4	5.0	10	0.0532	0.0493	0.0528	0.0490
Case 2	0.99	5.4	10.8	5	0.0267	0.0535	0.0263	0.0529
Case 3	0.99	10.7	5.2	5	0.0530	0.0257	0.0525	0.0253

Figure 10.2 illustrates the recorded detector signals together with the *reconstructed* individual elution profiles of the compounds. The large number of fractions proved adequate to obtain this information, in particular for the correct identification of sharp breakthrough layers. For the feed state plateaux and desorption portions of the elution profiles a sufficient number of fractions was collected, yielding accurate reconstructions.

10.3 Analysis of experimental & simulation profiles

Predictions of elution profiles were computed with the equilibrium-dispersive model (6.4), applying IAST to obtain required competitive, multicomponent equilibria. These predictions were solved numerically with the third order upwind-biased discretization and
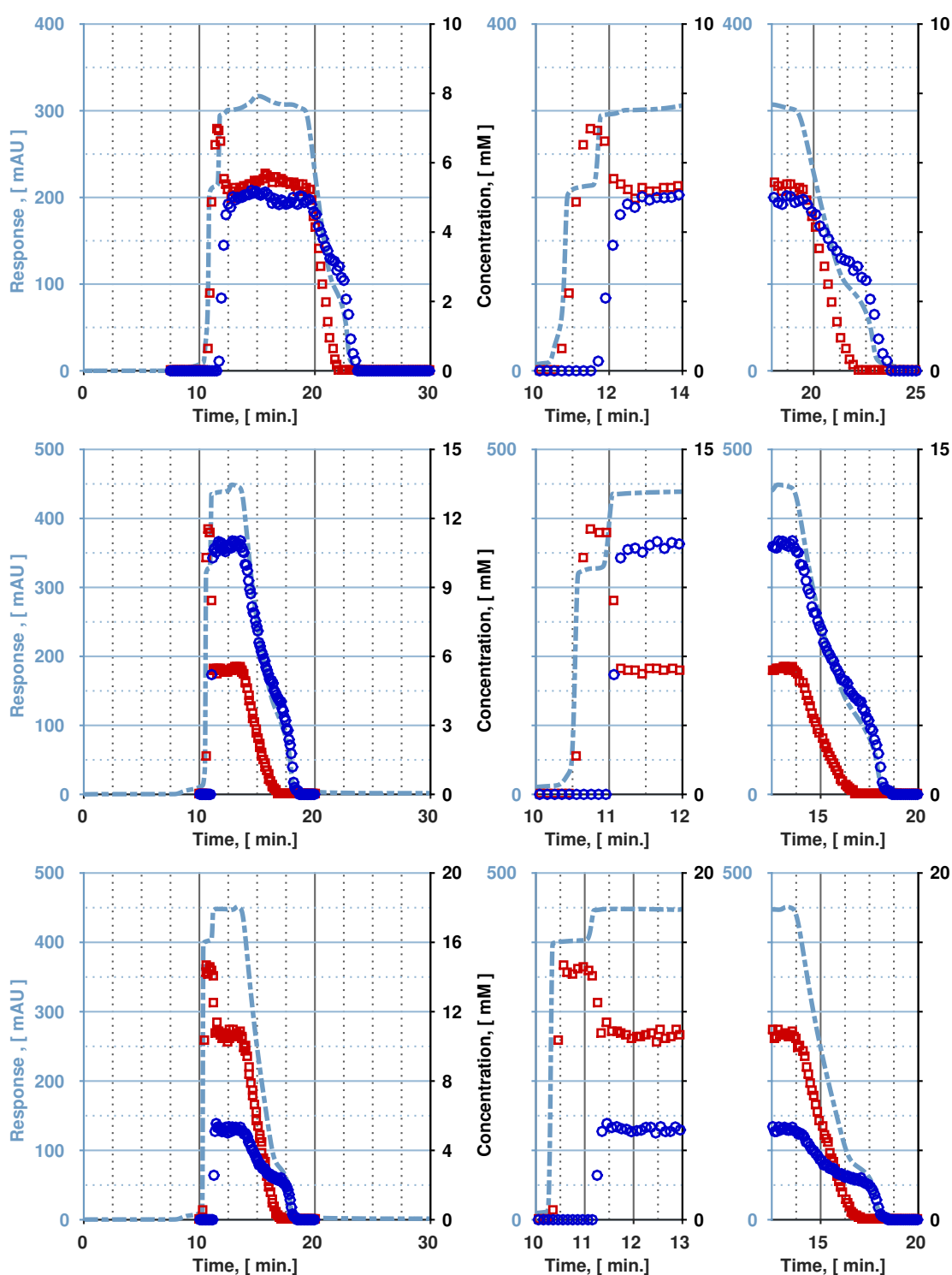
Figure 10.2: Measured elution profiles of overloaded injections for Case 1, Case 2 & Case 3. (−·): recorded response at $\lambda_{UV} = 235\,[\mathsf{nm}]$. (□): C10 fractions; (○): C11 fractions. Concentration values for all fractions are listed in Tables A15, p. 189 (Case 1), A16, p. 190 (Case 2) & A17, p. 191 (Case 3).

integrated with the SSP-RK method, explained in Chapter 7. The obtained profiles are illustrated in Figure 10.3 for CASE 1 and Figure 10.4 for CASES 2 and 3.
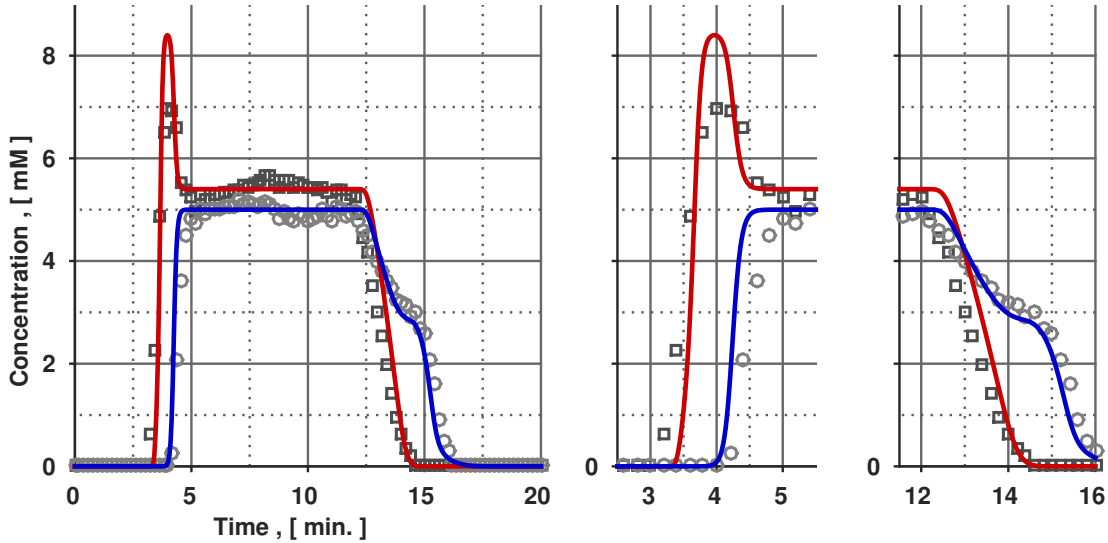
Figure 10.3: Estimated elution profiles of overloaded injections, computed with the 3$^{\text{rd}}$ order upwind-biased scheme described in Section 7.4 & integrated numerically with SSP-RK method (7.15). Numerical simulation parameters are listed in Table A18, p. 193. Applied adsorption isotherm parameters are listed in Table A14, p. 187. Symbols: experimental elution profiles, reconstructed from collected fractions. (□): decylbenzene (C10); (○): undecylbenzene (C11).

Since minor discrepancies between computed dynamic profiles and *reconstructed* profiles from collected fractions can be observed, a detailed quantification becomes necessary to perform a comparison between experimental and predicted profiles. This analysis was performed by considering *a*) mass balance calculations; & *b*) breakthrough times of *adsorption step* shock layers of both alkylbenzenes.

Estimation of competitive equilibria from adsorption-desorption cycles of overloaded experimental profiles

Adsorbed phase concentrations for binary mixtures, $q_i = f(c_1, c_2)$, $i = 1, 2$, can be obtained directly from experimental—i.e., measured—elution profiles by calculation of individual *capacities.* This is an analogous procedure to applying Equations (9.7), p. 129
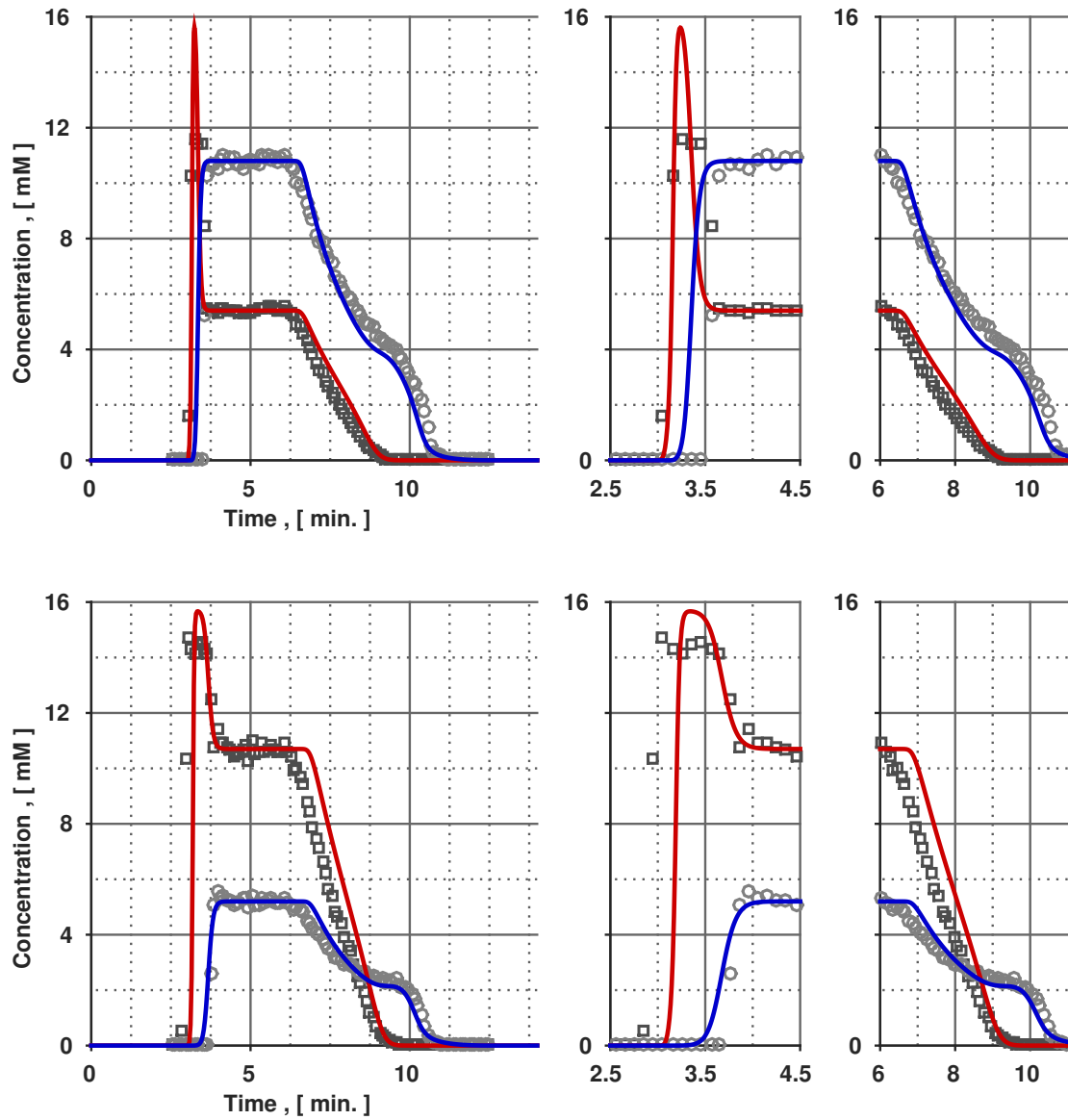
Figure 10.4: Estimated elution profiles of overloaded injections, computed with the 3rd order upwind-biased scheme described in Section 7.4 & integrated numerically with SSP-RK method (7.15). Simulation and applied adsorption isotherm parameters are listed in Tables A18, p. 193 & A14, p. 187, respectively. Symbols: experimental elution profiles, reconstructed from collected fractions. (□): decylbenzene (C10); (○): undecylbenzene (C11).

for a single adsorbate. The amounts of moles adsorbed are obtained from

$$n_1 = \overline{Q} \left[c_{1,\,\text{feed}}\, t_{\text{cut}} - \int_0^{t_{\text{cut}}} c_1(t, z = L)\ \mathrm{d}t - c_{1,\,\text{feed}}\, t_0 \right]$$

$$- \overline{Q} \left[\int_{t_{\text{cut}}}^{t_2} c_1(t, z = L)\ \mathrm{d}t - c_{1,\,\text{feed}}\,(t_2 - t_{\text{cut}}) \right] \quad (10.2a)$$

for the *less-adsorbed* decylbenzene (C10, compound 1) and

$$n_2 = \overline{Q} \left[c_{2,\,\text{feed}}\, t_2 - \int_0^{t_2} c_2(t, z = L)\ \mathrm{d}t - c_{2,\,\text{feed}}\, t_0 \right] \tag{10.2b}$$

for the *more-adsorbed* undecylbenzene (C11, compound 2). Adsorbed phase concentrations are given subsequently by

$$q_1 = \frac{n_1}{(1 - \epsilon)\, V_\text{c}} \quad \text{and} \quad q_2 = \frac{n_2}{(1 - \epsilon)\, V_\text{c}}. \tag{10.2c}$$

Figure 10.5 provides a graphical explanation of Equations (10.2). Since the adsorption
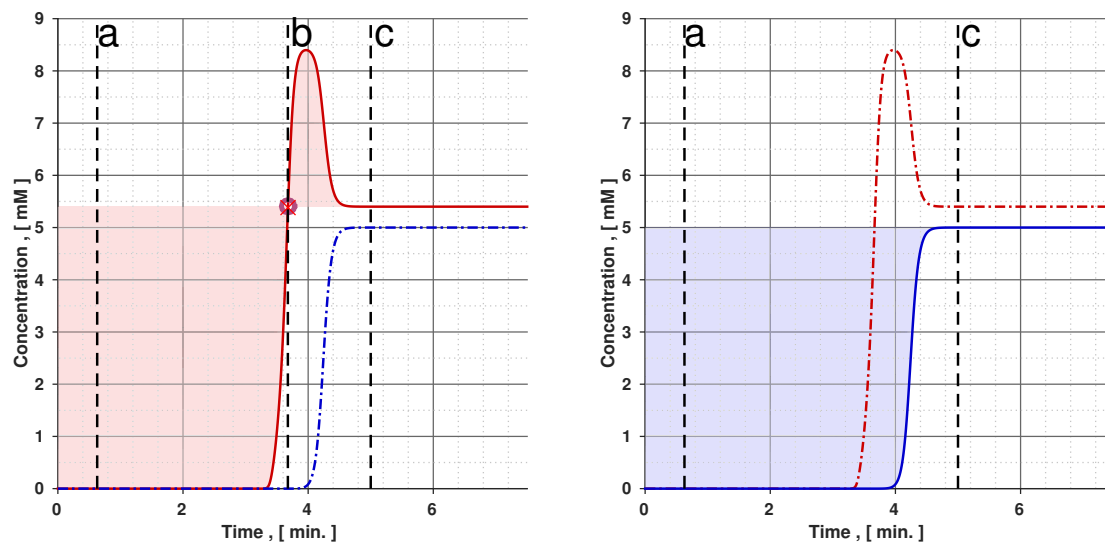
Figure 10.5: Graphical explanation of capacity equations for an adsorption step, Equations (10.2), for competitive binary adsorption, exemplified for the the dynamic simulation result of CASE 1. (a): hold-up time, t_0; (b): t_cut; & (c): t_2.

process is *reversible* and mass is conserved, adsorbate amounts n_i may be also calculated from the *desorption step* with:

$$n_i = \overline{Q} \left[\int_{t_{1,\text{des.}}}^{t_{2,\text{des.}}} c_i(t, z = L)\ \mathrm{d}t - c_{i,\,\text{feed}}\, t_0 \right], \quad i = \text{C10}, \text{C11}, \tag{10.3}$$

whereby, $t_{1,\text{des.}}$ indicates the time at which a step change is effected, going from the fed solution concentration value, $c_{i,\,\text{feed}}$, back to the initial concentration of i—the value prevailing before the application of the *adsorption step*. The upper limit, $t_{2,\text{des.}}$, is selected by detecting the point in time when the column has been regenerated completely, i.e., the chromatographic cycle has been completed.

Table 10.3 lists adsorbed phase concentrations obtained by applying the capacity equations (10.2) & (10.3) to: *a)* experimentally recorded, reconstructed, elution profiles; *b)* numerically simulated elution profiles; & *c)* direct prediction of IAST equilibria, $q = f(c)$, from given liquid phase concentrations, $c_{i,\text{feed}}$, *alone*—without dynamic experiments. Slight discrepancies between concentration values, q_i, of experimental adsorption and desorption steps are attributed to small errors in the fraction collection analyses and *small* experimental measurement errors, in general.

The predicted adsorbed phase concentration values, obtained by dynamic simulation and by direct application of IAST at the feed concentrations, $c_{i,\text{feed}}$, for the three cases, are practically identical. The small deviations between these values originated from numerical integration of the simulation profiles.

Calculation of relative errors by

$$e_i^{\text{rel.}} = \frac{q_i - \hat{q}_i}{q_i} \times 100\,\%, \quad i = \mathsf{C10}, \mathsf{C11}, \tag{10.4}$$

for the predicted values of adsorbed phase concentrations, $\hat{q}_i$, obtained with the simulations, yielded the results reported in Table 10.4. These differences are not negligible, which means that IAST was unable to predict the behavior of the experimental system with high accuracy at the investigated solution concentrations and experimental conditions. The qualitative behavior was well reproduced and it is of value as a preliminary estimation. Given the fact that a complete study of competitive equilibria in the alkylbenzenes/ACN/PGC system was outside of the scope of this work, it is not possible to state further conclusions regarding the suitability of IAST to completely describe the system.

Values of selectivity at equilibrium

Values of selectivity were obtained directly from the computed concentrations at equilibrium, using Equation (2.10), p. 19. These values are listed in Table 10.5. Although small differences in obtained values suggest a dependence in concentration, they vary in an estimated range of $1.49 - 1.56$, roughly 1.5, which confirms that separations at these concentration ranges for the investigated substances are feasible in the ACN/PGC system at the reported operating conditions with the employed PGC commercial stationary phase.

The values obtained by the equilibrium and dynamic simulation predict a slightly more difficult separation task. Therefore, these results indicate once more that IAST was not

able to estimate the system's behavior satisfactorily. Further optimization of the chromatographic separation was not further pursued, as the selected operating conditions permitted already the analysis of competitive equilibria in the alkylbenzenes/ACN/PGC system.

Comparison of breakthrough times during adsorption step

Table 10.6 lists breakthrough times, $t_{b,i}$, obtained from experimental and numerical simulation profiles. The reconstructed elution profiles were fit to sigmoidal functions in order to estimate $t_{b,i}$ more precisely. The calculated values of breakthrough times were found to be in accord with the tendencies observed for adsorbed phase concentration values estimated by capacity equations and reported in Table 10.3.

The retention times of decylbenzene (C10) are *overestimated*, whereas times of undecylbenzene (C11) are *underestimated*. As discussed before, these differences suggest that IAST is unable to predict the retention behavior with high accuracy, albeit providing a good qualitative description of competitive elution behavior among the measured alkylbenzenes.

Table 10.3: Results of computed equilibrium values obtained from competitive dynamic experiments, as well as predictions obtained from dynamic simulations using IAST as competitive equilibria model, via Equations (10.2) and *directly* applying IAST equilibrium calculations for applied feed concentrations, $c_{i,\text{feed}}$, using the IVP approach of Chapter 4 and single component isotherm parameters listed in Table A14, p. 187.

| Case | Experimental | | | | Dyn. simulation w/ IAST [a] | | | | IAST, *directly* (equil.) [b] | |
| | Ads. step | | Des. step | | Ads. step | | Des. step | | | |
	q_1 [mM]	q_2 [mM]	q_1 [mM]	q_2 [mM]	q_1 [mM]	q_2 [mM]	q_1 [mM]	q_2 [mM]	q_1 [mM]	q_2 [mM]
Case 1	64.9	89.4	62.7	88.5	66.6	82.9	66.6	82.9	66.7	84.2
Case 2	48.9	147.3	47.5	145.6	53.0	137.1	53.0	137.1	53.1	137.2
Case 3	100.6	76.3	97.7	73.0	115.7	73.8	115.7	73.8	115.8	73.8

a. Numerical approximation of EDM1D, using IAST as competitive equilibria model.
b. Calculated with the IVP approach using `ode45` integrator.

Table 10.4: Calculation of relative errors, $e_i^{\text{rel.}}$, in predicted equilibrium values reported in Table 10.3, using Equation (10.4).

Case	Ads. step		Des. step	
	$e_{\text{C10}}^{\text{rel.}}$ %	$e_{\text{C11}}^{\text{rel.}}$ %	$e_{\text{C10}}^{\text{rel.}}$ %	$e_{\text{C11}}^{\text{rel.}}$ %
Case 1	−2.62	7.27	−6.22	6.33
Case 2	−8.38	6.93	−11.58	5.84
Case 3	−15.01	3.28	−18.42	−1.10

Table 10.5: Computed selectivity values at equilibrium, α_{ij}, obtained from experimental, *reconstructed* elution profiles, predicted elution profiles and direct application of IAST from feed concentration values, $c_{i,\text{feed}}$, alone. Values at equilibrium taken from Table 10.3, using Equation (2.10), p. 19.

Case	Experimental		Dyn. Simulation		IAST, *directly*
	Ads. step	Des. step	Ads. step	Des. step	
Case 1	1.49	1.52	1.34	1.34	1.36
Case 2	1.51	1.53	1.29	1.29	1.29
Case 3	1.56	1.54	1.31	1.31	1.31

Table 10.6: Breakthrough times, $t_{b,i}$, of adsorption step shock layers for experimental, *reconstructed* elution profiles and predictions computed by numerical simulations of EDM1D applying IAST in describing competitive adsorption equilibria.

Case	Experimental		Dyn. Simulation w/ IAST	
	decylbenzene $t_{b,\text{C10}}$ [min.]	*undecylbenzene* $t_{b,\text{C11}}$ [min.]	*decylbenzene* $t_{b,\text{C10}}$ [min.]	*undecylbenzene* $t_{b,\text{C11}}$ [min.]
Case 1	3.50	4.47	3.64	4.25
Case 2	3.10	3.56	3.16	3.36
Case 3	2.93	3.75	3.19	3.68

Summary

Competitive equilibria, $q = f(c)$ of overloaded injections of binary mixtures of `C10` and `C11` at three different concentration values were determined from capacity equations. The reconstructed dynamic profiles from these measurements were compared to numerical approximations computed with EDM1D, employing IAST to describe competitive adsorption equilibria. In turn, IAST was solved with the IVP approach described in Chapter 4, using the formulation described in Chapter 7. In order to assess the adequacy of IAST, equilibrium values from the predicted simulation profiles were calculated using once again the capacity equations. Finally, direct competitive equilibrium values were obtained from IAST alone, at liquid phase concentration values, $c_{i,\,\mathrm{feed}}$, corresponding to each measured case. This complete set of results has been listed in Table 10.3.

Although only *three* equilibrium points are probably not sufficient to assess the suitability of IAST to describe completely the alkylbenzenes/ACN/PGC system, the dynamic predictions were able to reproduce the elution behavior of the three cases with relatively good accuracy. Unavoidable experimental measurement errors contribute to some extent to the discrepancies observed in the listed equilibrium values. It was found that IAST *overestimated* the equilibrium values of decylbenzene (`C10`) and *underestimated* the values of undecylbenzene (`C11`). Nonetheless, the methodology described at the beginning of this chapter was implemented successfully.

An activity coefficient model—cf. Chapter 3—might help to *repair* the discrepancies described, by providing a more accurate description of the adsorbed phase. In turn, additional experiments to reliably apply an activity coefficient model would become necessary, thus *substantially increasing* the experimental complexity—see e.g., [122].

Part IV

Concluding remarks

Chapter 11

Conclusion

"In the future, everyone will be famous for 15 minutes."

– Andy Warhol

The principal objective of this dissertation has been to develop a method for application of the Ideal Adsorbed Solution Theory (IAST). Important properties of a solution approach for IAST, including its flexibility to be applied with a large number of common single component adsorption isotherm equations, were analyzed.

A natural extension of the solution method was investigated, giving as a result, direct formulæ for the Jacobian matrix of adsorbed phase concentrations, $\mathcal{J}(q)$. These expressions can find direct and efficient application in numerical simulation of simple fixed-bed adsorber models.

Lastly, in order to apply the theoretically developed approach and computationally efficient calculation tools, a challenging experimental two-component system of liquid chromatography, wherein the adsorbates feature inflection points along their adsorption isotherm courses, was measured and analyzed.

In the first part of the experimental work, single component adsorption isotherms for two compounds were measured. IAST can be applied with this information to predict the competitive isotherms. Several binary mixture column effluent measurements of the same compounds were performed. Finally, a comparison between experiments and numerical simulations obtained by applying IAST and a standard fixed-bed model, was completed.

The main contribution of this work concentrated on IAST and the development of a new solution approach for its constitutive equations, rather than critically evaluating

the general suitability of IAST to describe competitive equilibria of the investigated experimental system. This task would require substantially more experimental work and analysis. In the following, the main outcome and conclusions of the performed investigation is provided in detail.

Key results of this investigation

Part I: Adsorption equilibria

This starting part of the work introduced basic concepts, including the theoretical basis for IAST and relevant details for its implementation. The two main highlights of this part are:

1. A new method to solve the equations of IAST was *developed, implemented and validated.* From this part of the investigation the following is concluded:

    (a) The method can be applied with a broad number of technically relevant single component adsorption isotherms. In practical cases, IAST provides preliminary insight for process understanding and conceptual design.

    (b) The tools described in Chapter 4 allow for a robust, straightforward implementation of IAST as an attractive competitive equilibria model.

2. In collaboration with others, formulæ were developed that express analytically the Jacobian, $\mathcal{J}(q(c))$, in the context of IAST, provided that the vector of fictitious liquid phase concentrations, c^0, is known *a priori* as explained in Chapter 4. Several important applications for these expressions exist—see e.g., Kvaalen & Tondeur [157] and Kvaalen *et al.* [158].

Part II: Adsorber dynamics

1. An application of formulæ for the Jacobian, $\mathcal{J}(q(c))$, derived in Part I, was illustrated for equilibrium-based, fixed-bed adsorber dynamics. A specific matrix $\mathcal{K}(\lambda)$ was derived to be directly applied in these dynamic models, thus providing an accurate, efficient and easy to implement tool.

2. A strategy to embed IAST equilibrium calculations—applicable also to other type of competitive adsorption equilibria models—was explained and illustrated; particular

emphasis was set upon mathematical properties of implemented numerical methods for simulation, as described in Chapter 7.

3. Several examples that illustrate the use of these numerical methods were given, in particular addressing systems where adsorbates possess inflection points along their courses, the subject of the experimental study described in Part III.

Part III: Experimental demonstration performing a High-Performance Liquid Chromatography investigation

1. A detailed experimental study to understand competitive equilibria of compounds that display inflection points along their courses was conducted; practical recommendations for the measurement of such type of systems were discussed.

2. Suitability of IAST with a simple, equilibrium-based, fixed-bed dynamic model to describe the measured experimental system was tested by using the solution methods of Parts I & II. The results were interpreted and discussed. The outcome of this part of the study seems to suggest that IAST is unable to predict the observed system behavior with *high accuracy*; it rather provides useful preliminary calculations, perhaps of interest for first design of this type of systems.

   Implementation of a more detailed competitive equilibria model, going beyond IAST, should take into account two aspects:

   (a) complexity of the experimental program needed to satisfactorily parametrize the model; &

   (b) increased effort to perform numerical computations.

   The first aspect is particularly challenging and, as mentioned before, up to date no *unified* model nor theory has been developed that can comprehensively describe nonideal behavior of compounds in an adsorbed phase. The second aspect is easily overcome and is nowadays becoming less important, inasmuch as computer performance is constantly improving, with complex calculation tasks everly being solved faster.

   As mentioned in Chapter 1, robotic platforms are gaining in importance to provide an approach that may better suit the needs of adsorption equipment designers, whilst assisting researchers to validate potential candidate models and hypotheses. Molecular simulation studies are in this respect gaining in popularity as well and are expected to play a role of increasing importance in the future.

Final comments

As the reader can conclude now, this field of research remains to be *exciting, vivid & dynamic*, with significant challenges to be addressed—mentioned earlier in Chapter 1. Despite of the complexity of the selected experimental system, this investigation has illustrated a systematic application of an *elegant* multicomponent adsorption equilibria model, characterized by its simplicity and capability to describe complex processes by applying fundamental thermodynamic knowledge.

Suggestions and recommendations for future studies

Going beyond IAST A *natural* extension of IAST is e.g., Real Adsorbed Solution Theory (RAST) [110, 111], as well as the more sophisticated approaches listed in Table 2.5, Chapter 2. The application of different *energy excess* models to obtain activity coefficients that properly describe the non-ideality of the adsorbed phase continues to be of interest to the research and industrial communities, since up to now, there seems to be no unified approach to provide activity coefficients for the adsorbed phase, which should be dependent on the surface potential, π.

Treatment of fluid phase as *nonideal* An even more ambitious approach, albeit necessary, includes also treating eventually the fluid-phase—gas or liquid—as non-ideal, for which well-established methods for their description are available; see e.g., [4, 48, 57]. This is an important area, since, for example, a second fluid phase could originate at specific process conditions as recently reported by Wegmann & Kerkhof [263].

Appendix

A1 Applied software

Mathematica

The CAS MATHEMATICA® [141] was used to verify and symbolically calculate & manipulate when required.

Matlab

Table A1 lists details of the MATLAB [168] PSE used to perform a major portion of numerical calculations presented in this dissertation.

It is important to stress that MATLAB is adequate for *script prototyping & debugging* and by no means should be thought of as a substitute for *true* scientific computing languages such as C++ or FORTRAN—this might change in the future, since this PSE has now an important focus for improved running performance on computer systems with *parallel architecture*, including GPU-based computing *clusters*. The books by Higham [264] and Quarteroni *et al.* [152] are recommended to the reader for a quick introduction to MATLAB.

Table A1: List of MATLAB toolboxes used for calculations. [a]

Toolbox	Version
MATLAB	8.4
Simulink	8.4
Bioinformatics Toolbox	4.5
Control System Toolbox	9.8
Curve Fitting Toolbox	3.5
Global Optimization Toolbox	3.3
Image Processing Toolbox	9.1
MATLAB Coder	2.7
MATLAB Compiler	5.2
Neural Network Toolbox	8.2.1
Optimization Toolbox	7.1
Parallel Computing Toolbox	6.5
Partial Differential Equation Toolbox	1.5
Robust Control Toolbox	5.2
Signal Processing Toolbox	6.22
SimBiology	5.1
Simulink Coder	8.7
Simulink Control Design	4.1
Stateflow	8.4
Statistics Toolbox	9.1
Symbolic Math Toolbox	6.1
System Identification Toolbox	9.1

a. MATLAB Version: 8.4.0.150421 (R2014b); License No.: 137842.

A2 Parameters applied in figures of Part I

A2.1 Parameters of Figure 2.2

Table A2: Parameters used to generate the adsorption isotherms, $q_i = f(c_i)$, illustrated in Figure 2.2.

Isotherm model	Parameter values
Langmuir (**Type I**) [65]	$q_i^{\text{sat}} = 1 \, [\text{mol/l}]; \; b_i = 1 \, [\text{l/mol}]$
BET (**Type II**) [66]	$q_i^{\text{sat}} = 1.0 \, [\text{mol/l}]; \; b_{i\text{S}} = 0.6 \, [\text{l/mol}]; \; b_{i\text{L}} = 0.12 \, [\text{l/mol}]$
Anti-Langmuir (**Type III**)	$q_i^{\text{sat}} = 1 \, [\text{mol/l}]; \; b_i = 1.5 \, [\text{l/mol}]$
Quadratic + Langmuir	$q_{i1}^{\text{sat}} = 100 \, [\text{mM}]; \; b_{i1} = 0.4 \, [\text{mM}^{-1}]; \; b_{i2} = 0.3 \, [\text{l}^2/\text{mol}^2];$
(**Type IV**) [51, 52]	$q_{i2}^{\text{sat}} = 7 \, [\text{mM}]; \; b_{i3} = 5 \, [\text{mM}^{-1}]$
Quadratic (**Type V**) [43]	$q_i^{\text{sat}} = 0.5 \, [\text{mol/l}]; \; b_{i1} = 0.2 \, [\text{l/mol}]; \; b_{i2} = 1 \, [\text{l}^2/\text{mol}^2]$

A2.2 Parameters of Figures 2.3 & 4.3.

Table A3: Parameters used to generate the adsorption isotherms, $q_i = f(c_i)$, illustrated in Figure 2.3.

Isotherm model	Parameter values
Competitive Langmuir [104]	$q_1^{\text{sat}} = 1 \, [\text{mol/l}]; \; b_1 = 1 \, [\text{l/mol}];$
	$q_2^{\text{sat}} = 1 \, [\text{mol/l}]; \; b_2 = 2 \, [\text{l/mol}]$

A3 Euler's Theorem for homogeneous functions[*]

In order to complete the formalism introduced in Section 2.3, it is necessary to demonstrate that Gibbs' free energy for adsorbed phase, G^a, is *homogeneous* of order $\mathfrak{n} = 1$.

Proposition 1. *The integral form of* Fundamental Relation (2.16d) *is valid, insofar as G^a is homogeneous of order $\mathfrak{n} = 1$ in the arguments T, π, n_1, ..., n_N.*

Proof. Let λ be an *arbitrary* parameter such that

$$G^a = f(\lambda T, \lambda \pi, \lambda n_1, \ldots, \lambda n_N) \overset{!}{=} \lambda^{\mathfrak{n}} f(T, \pi, n_1, \ldots, n_N)$$

$$= \lambda f(T, \pi, n_1, \ldots, n_N). \quad \text{(A3.1)}$$

Differentiation of Equation (A3.1) with respect to λ, by application of the Chain Rule, yields for its leftmost term:

$$\frac{\partial f}{\partial (\lambda T)} \frac{\partial (\lambda T)}{\partial \lambda} + \frac{\partial f}{\partial (\lambda \pi)} \frac{\partial (\lambda \pi)}{\partial \lambda} + \frac{\partial f}{\partial (\lambda n_1)} \frac{\partial (\lambda n_1)}{\partial \lambda} + \cdots + \frac{\partial f}{\partial (\lambda n_N)} \frac{\partial (\lambda n_N)}{\partial \lambda}, \quad \text{(A3.2)}$$

which further simplifies to

$$\frac{\partial f}{\partial (\lambda T)} T + \frac{\partial f}{\partial (\lambda \pi)} \pi + \frac{\partial f}{\partial (\lambda n_1)} n_1 + \cdots + \frac{\partial f}{\partial (\lambda n_N)} n_N. \quad \text{(A3.3)}$$

Now, specifying $\lambda = 1$, Equation (A3.3) becomes

$$\frac{\partial f}{\partial T} T + \frac{\partial f}{\partial \pi} \pi + \frac{\partial f}{\partial n_1} n_1 + \cdots + \frac{\partial f}{\partial n_N} n_N. \quad \text{(A3.4)}$$

On the other hand, the total differential of $G^a = f(T, \pi, n_1, \cdots, n_N)$ is given by

$$\mathrm{d}G^a = \frac{\partial f}{\partial T} \mathrm{d}T + \frac{\partial f}{\partial \pi} \mathrm{d}\pi + \frac{\partial f}{\partial n_1} \mathrm{d}n_1 + \cdots + \frac{\partial f}{\partial n_N} \mathrm{d}n_N. \quad \text{(A3.5)}$$

A *term-by-term* comparison of the right-hand side of (A3.5) with *Fundamental Relation*

$$\mathrm{d}G^a = -S^a \,\mathrm{d}T + \mathfrak{A}\,\mathrm{d}\pi + \sum_{i=1}^{N} \mu_i^a \,\mathrm{d}n_i^a \quad \text{(2.16d)}$$

—p. 25, permits a direct identification of

$$-S^a \equiv \frac{\partial f}{\partial T}; \quad \mathfrak{A} \equiv \frac{\partial f}{\partial \pi}; \quad \mu_1^a \equiv \frac{\partial f}{\partial n_1}; \quad \cdots; \quad \mu_N^a \equiv \frac{\partial f}{\partial n_N}. \quad \text{(A3.6)}$$

---

[*]Consult e.g., [265] for a formal definition of the theorem.

Henceforth, substitution of these terms in Equation (A3.4) yields

$$- S^a T + \mathfrak{A}\pi + \mu_1^a n_1^a + \cdots + \mu_N^a n_N^a = G^a. \tag{A3.7}$$

Now, restricting Equation (2.16d) to constant temperature, T, and spreading pressure, π, holds

$$\mu_1^a n_1^a + \cdots + \mu_N^a n_N^a = \sum_{i=1}^{N} \mu_i^a n_i^a = G^a, \tag{A3.8}$$

thus recovering Equation (2.18). $\qquad\qquad\square$

A4 Algebraic expressions for invariant adsorption

The goal is to express experimentally measured quantities as functions of adsorbed quantities, a, to obtain *invariant* adsorbed molar quantities, n_i^{ς}—i.e., *independent* of the location of Gibbs' dividing surface. This is done to correctly account for surface potential, π, in Gibbs' adsorption isotherm, Equation (2.26a). The following mass balance equation can be written [50]:

$$V_{\text{sln.}}\Delta c_i = n_i^{\text{tot}} - c_i V_{\text{sln.}}, \tag{A4.1}$$

where the total volume of liquid solution is

$$V_{\text{sln.}} = \sum_{i=1}^{N} n_i^{\text{tot}} \, \bar{v}_i + n_{\text{solv.}}^{\text{tot}} \, \bar{v}_{\text{solv.}}, \tag{A4.2}$$

expressed with the partial molar volumes, $\bar{v}_i$ & $\bar{v}_{\text{solv.}}$, of solutes i & solvent, respectively. It is therefore assumed that the liquid bulk mixture behaves *ideally*, which is a reasonable assumption under *dilute conditions*. With

$$n_i^{\text{tot}} = n_i^a + n_i^{\ell} \quad \text{and} \quad n_{\text{solv.}}^{\text{tot}} = n_{\text{solv.}}^a + n_{\text{solv.}}^{\ell} \tag{A4.3}$$

holds

$$V_{\text{sln.}}\Delta c_i = \left(n_i^a + n_i^{\ell}\right) - c_i V_{\text{sln.}}. \tag{A4.4}$$

Substituting (A4.3) into (A4.2) and inserting this result in (A4.4) leads to

$$
\begin{aligned}
c_i V_{\text{sln.}} &= c_i \left[\sum_{i=1}^{N} \left(n_i^a + n_i^{\ell}\right) \bar{v}_i + \left(n_{\text{solv.}}^a + n_{\text{solv.}}^{\ell}\right) \bar{v}_{\text{solv.}} \right] \\
&= c_i \left[\sum_{i=1}^{N} n_i^a \, \bar{v}_i + \sum_{i=1}^{N} n_i^{\ell} \, \bar{v}_i + n_{\text{solv.}}^a \, \bar{v}_{\text{solv.}} + n_{\text{solv.}}^{\ell} \, \bar{v}_{\text{solv.}} \right]
\end{aligned}
$$

where a simple factorization yields

$$
= c_i \left[\sum_{i=1}^{N} n_i^a \, \bar{v}_i + n_{\text{solv.}}^a \, \bar{v}_{\text{solv.}} \right] + c_i \left[\sum_{i=1}^{N} n_i^{\ell} \, \bar{v}_i + n_{\text{solv.}}^{\ell} \, \bar{v}_{\text{solv.}} \right]. \tag{A4.5}
$$

If it is assumed that c_i can be written as

$$c_i \equiv \frac{n_i^{\ell}}{\sum\limits_{i=1}^{N} n_i^{\ell} \, \bar{v}_i + n_{\text{solv.}}^{\ell} \, \bar{v}_{\text{solv.}}}; \tag{A4.6}$$

then, upon substitution in Equation (A4.4), yields the invariant amount $n_i^{\mathfrak{c}}$ define as

$$V_{\text{sln.}} \Delta c_i = n_i^a - c_i \left[\sum_{i=1}^{N} n_i^a \, \bar{v}_i + n_{\text{solv.}}^a \, \bar{v}_{\text{solv.}} \right] =: n_i^{\mathfrak{c}}, \tag{A4.7}$$

which is written only in terms of the *adsorbed phase moles* of solutes i & solvent and the final—i.e., measured—c_i. Finally,

$$n_i^m \approx V_{\text{sln.}} \Delta c_i = n_i^{\mathfrak{c}}. \tag{A4.8}$$

Now, n_i^m is defined formally as:

$$n_i^m := n_i^a - \frac{c_i}{c_{\text{solv.}}} n_{\text{solv.}}^a. \tag{2.27}$$

This result is easily proven from the restricted Gibbs-Duhem form for the bulk liquid phase:

$$\sum_{i=1}^{N} c_i \, \mathrm{d}\mu_i^a + c_{\text{solv.}} \, \mathrm{d}\mu_{\text{solv.}}^a = 0, \tag{A4.9}$$

so that

$$\mathrm{d}\mu_{\text{solv.}}^a = -\sum_{i=1}^{N} \frac{c_i}{c_{\text{solv.}}} \, \mathrm{d}\mu_i^a \tag{A4.10}$$

and substituting this result in Equation (2.26a) to arrive at

$$\mathfrak{A}\mathrm{d}\pi = \sum_{i=1}^{N} n_i^a \, \mathrm{d}\mu_i^a + n_{\text{solv.}}^a \, \mathrm{d}\mu_{\text{solv.}}^a = \sum_{i=1}^{N} n_i^a \, \mathrm{d}\mu_i^a + n_{\text{solv.}}^a \left[-\sum_{i=1}^{N} \frac{c_i}{c_{\text{solv.}}} \, \mathrm{d}\mu_i^a \right]$$

$$= \sum_{i=1}^{N} \underbrace{\left[n_i^a - \frac{c_i}{c_{\text{solv.}}} n_{\text{solv.}}^a \right]}_{=: \, n_i^m} \mathrm{d}\mu_i^a. \tag{A4.11}$$

This completes the definition of n_i^m.

∎

A5   Analytical solution of binary competitive Langmuir isotherm

Let $q^{\mathrm{sat}} = q_1^{\mathrm{sat}} = q_2^{\mathrm{sat}} = 1\,[\mathsf{mol/l}]$, with substitutions $X_i \equiv c_i^0$ and $x_i \equiv c_i$ to simplify the notation; henceforth,

$$q_i^0 = f(X_i) = \frac{b_i X_i}{1 + b_i X_i}, \quad i = 1, 2. \tag{A5.1}$$

Substitution of (A5.1) in Equation (3.9) and applying equilibrium condition (3.6) yields

$$\int\limits_0^{X_1} \frac{b_1}{1 + b_1 \xi}\,\mathrm{d}\xi = \int\limits_0^{X_2} \frac{b_2}{1 + b_2 \xi}\,\mathrm{d}\xi. \tag{A5.2}$$

Upon integration,

$$\ln\left[\,1 + b_1 X_1\,\right] = \ln\left[\,1 + b_2 X_2\,\right] \;\therefore\; 1 + b_1 X_1 = 1 + b_2 X_2, \tag{A5.3}$$

$$\text{thus obtaining the simple } \textit{orbit} \quad X_2 = f(X_1) = \frac{b_1}{b_2} X_1. \tag{A5.4}$$

Substitution in

$$\frac{x_1}{X_1} + \frac{x_2}{X_2} = 1 \quad \text{yields} \quad \frac{x_1}{X_1} + \frac{x_2}{\frac{b_1}{b_2} X_1} = 1; \tag{A5.5}$$

solving for X_1

$$X_1 = f(x_1, x_2) = x_1 + \frac{b_2}{b_1} x_2, \tag{A5.6}$$

and likewise subtituting in (A5.4)

$$X_2 = f(x_1, x_2) = \frac{b_1}{b_2} x_1 + x_2. \tag{A5.7}$$

From the total adsorbed concentration, Equation (3.11),

$$q_{\mathrm{tot}} = \left[\frac{x_1}{X_1 q_1^0} + \frac{x_2}{X_2 q_2^0}\right]^{-1}; \text{ substituting (A5.6) \& (A5.7) produces}$$

$$= \frac{1}{\dfrac{x_1}{\left[x_1 + \frac{b_2}{b_1} x_2\right]\left[\frac{b_1 X_1}{1 + b_1 X_1}\right]} + \dfrac{x_2}{\left[\frac{b_1}{b_2} x_1 + x_2\right]\left[\frac{b_2 X_2}{1 + b_2 X_2}\right]}}. \tag{A5.8}$$

Alternatively holds

$$q_1^0 = \frac{b_1 X_1}{1 + b_1 X_1} = \frac{b_1 \left[x_1 + \frac{b_2}{b_1} x_2 \right]}{1 + b_1 \left[x_1 + \frac{b_2}{b_1} x_2 \right]} = \frac{b_1 x_1 + b_2 x_2}{1 + b_1 x_1 + b_2 x_2} \qquad (A5.9)$$

and '*symmetrically*'

$$q_2^0 = \frac{b_2 X_2}{1 + b_2 X_2} = \frac{b_2 \left[\frac{b_1}{b_2} x_1 + x_2 \right]}{1 + b_2 \left[\frac{b_1}{b_2} x_1 + x_2 \right]} = \frac{b_1 x_1 + b_2 x_2}{1 + b_1 x_1 + b_2 x_2}. \qquad (A5.10)$$

Substitutions yield $\quad \dfrac{x_1}{X_1 q_1^0} = \dfrac{b_1 x_1}{(b_1 x_1 + b_2 x_2) \left[\dfrac{b_1 x_1 + b_2 x_2}{1 + b_1 x_1 + b_2 x_2} \right]}, \quad$ and $\qquad (A5.11)$

$$\frac{x_2}{X_2 q_2^0} = \frac{b_2 x_2}{(b_1 x_1 + b_2 x_2) \left[\dfrac{b_1 x_1 + b_2 x_2}{1 + b_1 x_1 + b_2 x_2} \right]}.$$

Upon summation of terms in (A5.11)

$$\frac{x_1}{X_1 q_1^0} + \frac{x_2}{X_2 q_2^0} = \frac{b_1 x_1 + b_2 x_2}{(b_1 x_1 + b_2 x_2) \left[\dfrac{b_1 x_1 + b_2 x_2}{1 + b_1 x_1 + b_2 x_2} \right]} = \frac{1}{\dfrac{b_1 x_1 + b_2 x_2}{1 + b_1 x_1 + b_2 x_2}} \qquad (A5.12)$$

is obtained, so that $\quad \dfrac{1}{q_{\text{tot}}} = \dfrac{1 + b_1 x_1 + b_2 x_2}{b_1 x_1 + b_2 x_2} \quad \therefore \quad q_{\text{tot}} = \dfrac{b_1 x_1 + b_2 x_2}{1 + b_1 x_1 + b_2 x_2}, \qquad (A5.13)$

thus leading to individual adsorbed phase concentrations

$$q_1 = q_{\text{tot}} \frac{x_1}{X_1} = \frac{b_1 x_1 + b_2 x_2}{1 + b_1 x_1 + b_2 x_2} \frac{x_1}{\dfrac{b_1 x_1 + b_2 x_2}{b_1}} = \frac{b_1 x_1}{1 + b_1 x_1 + b_2 x_2}, \qquad (A5.14)$$

$$q_2 = q_{\text{tot}} \frac{x_2}{X_2} = \frac{b_1 x_1 + b_2 x_2}{1 + b_1 x_1 + b_2 x_2} \frac{x_2}{\dfrac{b_1 x_1 + b_2 x_2}{b_2}} = \frac{b_2 x_2}{1 + b_1 x_1 + b_2 x_2}. \qquad (A5.15)$$

This simple algebraic exercise proves that: *a*) binary competitive Langmuir model is thermodynamically consistent; and *b*) its IAST counterpart is, in this particular case, *equivalent.*   ∎

A6   The generating functions v_k.

An important mathematical construct that helps to develop the solution principle explained in Chapter 4 consists of exploiting the form of GENERALIZED, INCREASING ISOTHERMS

$$q_k^0 = f(\xi) = \xi \, \frac{v_k'(\xi)}{v_k(\xi)}. \tag{2.2}$$

The *original system*, Equation 4.1, p. 46, can be formulated in terms of v_k as follows. From the integral form of Gibbs' adsorption isotherm, Equation (3.9), p. 34, and using (2.2) above,

$$\Pi_k = f(\xi) = \int^\xi \frac{v_k'(\xi)}{v_k(\xi)} \, \mathrm{d}\xi, \; \text{with the usual substitution,} \; \mathfrak{u} = v_k(\xi),$$

$$= \int^\xi \frac{\mathrm{d}\mathfrak{u}}{\mathfrak{u}} = \ln v_k(\xi), \quad k = 1, \ldots, N. \tag{A6.1}$$

It is clear therefore that v_k play an analogous role of '*spreading pressures*', where Π *maps* to v; in simpler words, if the sought solution, c^0, holds for Π-*equalities*, it does for v-*equalities*, too. Therefore, the equivalent system

$$v_1(X_1) - v_2(X_2) = 0,$$
$$v_1(X_1) - v_3(X_3) = 0,$$
$$\vdots \tag{4.13h}$$
$$v_1(X_1) - v_N(X_N) = 0,$$
$$\frac{x_1}{X_1} + \cdots + \frac{x_N}{X_N} - 1 = 0,$$

can be written; and—very importantly—in analogy to Π_k in Equation (3.6),

$$v_1 \overset{!}{=} v_2 \overset{!}{=} \cdots \overset{!}{=} v_N \quad \text{at EQUILIBRIUM.} \tag{A6.2}$$

∎

A7 Implementation example for limited κ-scheme

Application of the method of lines with the spatial discretization discussed in Section 7.4, p. 89, yields the following ODE system for the linear advection equation (8.1), p. 102:

$$
\begin{aligned}
\frac{\mathrm{d}}{\mathrm{d}t} w_1(t) &= -\frac{1}{h} u \left(w_{\frac{3}{2}} - w_{\frac{1}{2}} \right), & \text{(A7.1)}\\
\frac{\mathrm{d}}{\mathrm{d}t} w_2(t) &= -\frac{1}{h} u \left(w_{\frac{5}{2}} - w_{\frac{3}{2}} \right), \\
&\ \ \vdots \\
\frac{\mathrm{d}}{\mathrm{d}t} w_{J-1}(t) &= -\frac{1}{h} u \left(w_{J-\frac{1}{2}} - w_{J-\frac{3}{2}} \right), \\
\frac{\mathrm{d}}{\mathrm{d}t} w_J(t) &= -\frac{1}{h} u \left(w_{J+\frac{1}{2}} - w_{J-\frac{1}{2}} \right),
\end{aligned}
$$

with equally-spaced interval $h := \Delta x$. The numerical flux at the *inlet* is expressed with the boundary condition

$$
w_{\frac{1}{2}} = w_{\text{in}}(t). \qquad\qquad \text{(A7.2a)}
$$

The numerical fluxes for the interior cells, $j = 2, \cdots, J - 1$, are computed with

$$
\begin{aligned}
w_{\frac{3}{2}} &= \frac{1}{2} \left(w_1 + w_2 \right), \\
w_{\frac{5}{2}} &= w_2 + \frac{1}{2} \phi \left(r_{\frac{5}{2}} \right) \left(w_2 - w_1 \right), \\
&\ \ \vdots \\
w_{J-1+\frac{1}{2}} &= w_{J-1} + \frac{1}{2} \phi \left(r_{J-1+\frac{1}{2}} \right) \left(w_{J-1} - w_{J-2} \right)
\end{aligned}
\qquad \text{(A7.2b)}
$$

with flux function monitor, $\phi(r)$ (7.10a) and its argument given by

$$
r_{j+\frac{1}{2}} = \frac{w_{j+1} - w_j + \varepsilon_d}{w_j - w_{j-1} + \varepsilon_d}, \quad j = 2, \ldots, J - 1. \qquad \text{(A7.2c)}
$$

The numerical flux at the *outlet* is obtained with

$$
w_{J+\frac{1}{2}} = w_J + \frac{1}{2} \left(w_J - w_{J-1} \right). \qquad\qquad \text{(A7.2d)}
$$

The integration of ODE system (A7.1) can be performed directly with e.g., the SSP-RK method described in Section 7.5, p. 92.

A8   Parameters for examples of Chapter 8

A8.1   Parameters for the Quadratic plus Langmuir isotherm reported by Diack & Guiochon

Table A4: Single component adsorption isotherm parameters for Quadratic plus Langmuir model—cf. Eq. (2.3e), p. 17—of five phenyl-n-alkanes in ACN/PGC system at 323.15 K (50 °C) reported by Diack & Guiochon [51, 52].

Compound	Parameters				
	q_{i1}^{sat} $\left[\dfrac{\mathsf{mmol}}{\mathsf{l}}\right]$	b_{i2} $\left[\dfrac{\mathsf{mmol}}{\mathsf{l}}\right]$	b_{i1} $\left[\dfrac{\mathsf{L}}{\mathsf{mmol}}\right]$	q_{i2}^{sat} $\left[\dfrac{\mathsf{L}^2}{\mathsf{mmol}^2}\right]$	b_{i3} $\left[\dfrac{\mathsf{L}}{\mathsf{mmol}}\right]$
octylbenzene (C8)	219.4	2.5	0.030	0.0006	0.51
decylbenzene (C10)	147.2	6.0	0.087	0.010	1.69
undecylbenzene (C11)	122.4	17.0	0.103	0.032	1.78
dodecylbenzene (C12)	24.450	0.149	0.238	0.059	26.790
tridecylbenzene (C13)	102.9	7.0	0.363	0.309	4.66

A8.2   Process parameters and operation conditions

Table A5: Sets of parameter values applied in numerical simulations displayed in figures of Chapter 8.

Parameter		Values					
		Fig. 8.1	Fig. 8.2	Fig. 8.3	Fig. 8.4	Fig. 8.5	Fig. 8.6
u	[cm/min.]	7.9962	7.9962	7.8145	7.9556	7.956	7.9556
ϵ	[−]	0.745	0.745	0.770	0.745	0.745	0.745
$D_{\mathrm{app},k}$ [a]	[cm²/min.]	eps	eps	0.0117	0.0796	0.002	various
L_{c},	[mm]	50	50	30	50	50	50
Integrator [b] [c]	n/a	ssprk3	ode45	ssprk3	ssprk3	ssprk3	ssprk3
J	[−]	various	1000	100	500	1000	500
Δt	[min.]	2×10^{-4}	n/a	5×10^{-4}	4×10^{-4}	5×10^{-4}	4×10^{-4}
$c_{i,\,\mathrm{inj.}}$ [d]	[mM]	5.712	5.712	80.0 / 80.0	5.4 / 5.0	2.0 / 5.0	15 / 15
$V_{\mathrm{inj.}}$	[μl]	n/a	n/a	200	n/a	n/a	n/a

a. Same value applied for both components. eps $= 2.2204 \times 10^{-16}$ denotes the machine epsilon.
b. ode45: one-step, adaptive time-stepping Runge-Kutta pair by Dormand & Prince [173].
c. ssprk3: third order Strong Stability Preserving Runge-Kutta method, Equation (7.15), p. 93.
d. component 1 / component 2 / ⋯ .

A9   Supplementary information: laboratory equipment

A9.1   Agilent 1260 HPLC station
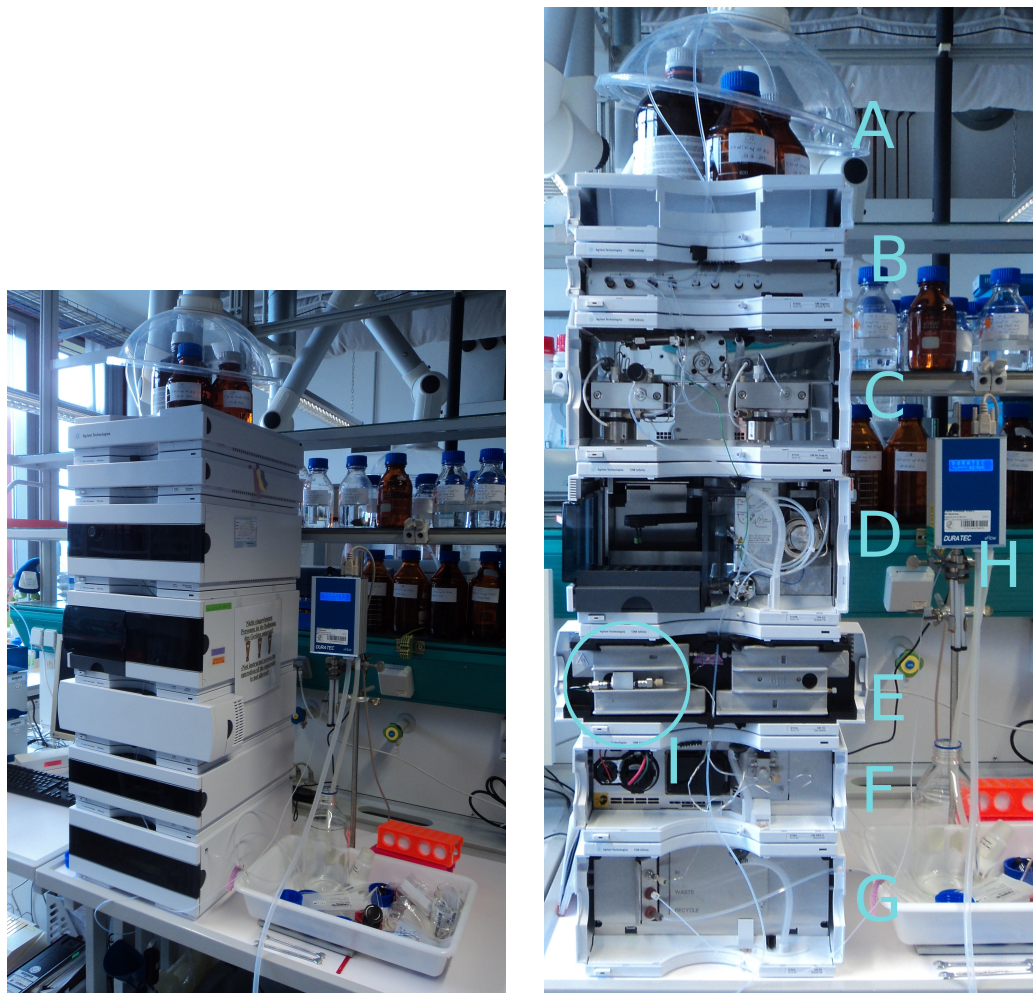
Figure A1: Agilent 1260 HPLC station used for experimental investigation of Part III. Components and part numbers: A: liquids & solvents; B: degasser (G1322A); C: dual pump module (G1312C); D: sampler & injection loop (G1329B); E: column compartment & oven (G1316A); F: multiple wavelength detector (G1365D); G: refractive index detector & waste outlet (G1362A); H: flowmeter; and Hypercarb^{TM} column (I). Courtesy of *Physicochemical Fundamentals Group*, MPI Magdeburg.

A9.2   Copy of manufacturer's certificate for Hypercarb^{TM} column
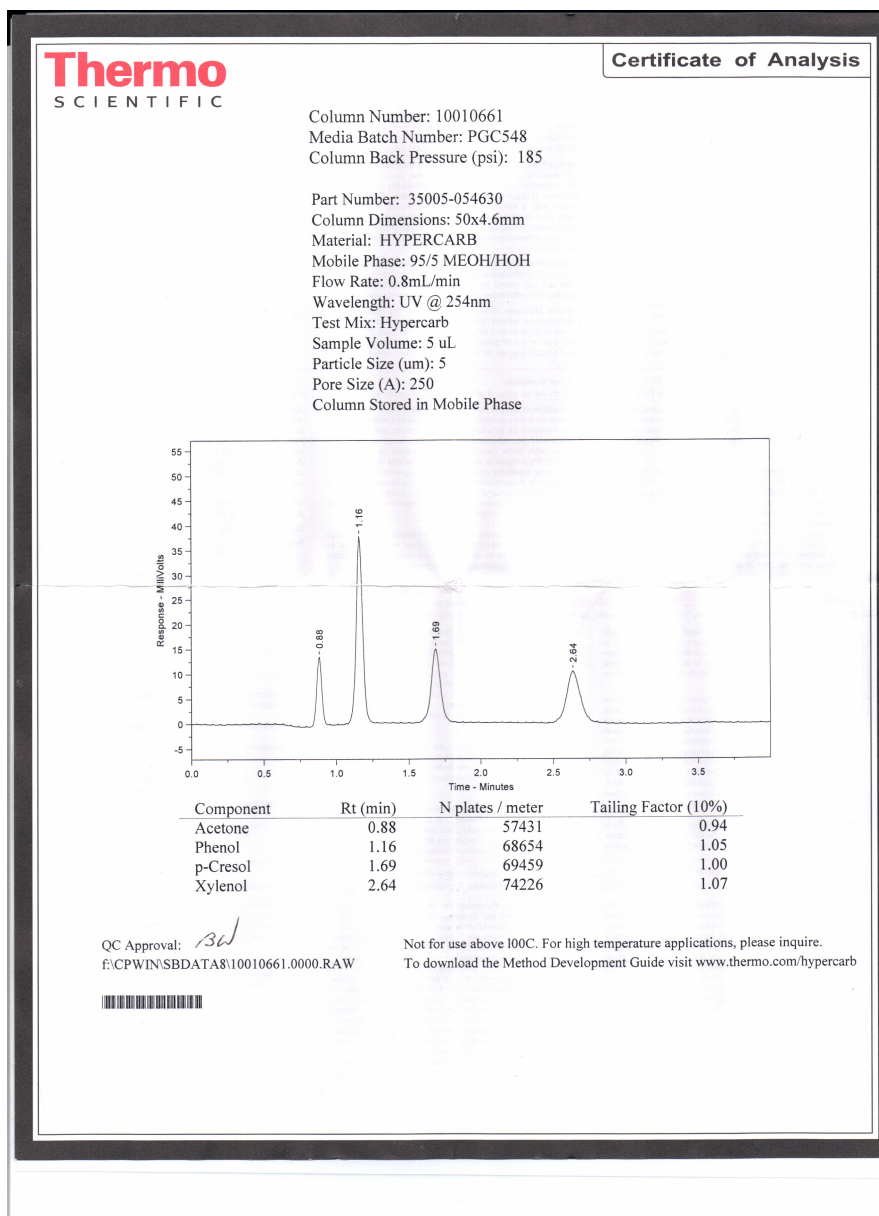
Figure A2: Calibration certificate for employed Hypercarb^{TM} column. [Part No.: **35005-054630**. Column No.: **10010661**.]. Courtesy of *Physicochemical Fundamentals Group*, MPI Magdeburg.

A9.3   Copy of manufacturer's certificate for DURATEC flowmeter

Figure A3: Calibration certificate for employed flow rate meter. Courtesy of *Physicochemical Fundamentals Group*, MPI Magdeburg.

A10 Some experimental results for Chapter 9

A10.1 Calibration curves for sample analysis

Table A6: Values of the peak areas for $1\,[\,\mu\text{l}\,]$ injections at $\lambda_{UV} = 220\,[\,\text{nm}\,]$ for listed concentrations of alkylbenzenes, represented graphically in Figure 9.5.

decylbenzene (C10)		undecylbenzene (C11)	
Peak area $[\,\text{mAU}\cdot\text{s}\,]$	Concentration $[\,\text{mM}\,]$	Peak area $[\,\text{mAU}\cdot\text{s}\,]$	Concentration $[\,\text{mM}\,]$
28.95	0.20	–	–
38.30	0.31	–	–
66.16	0.47	44.07	0.44
108.01	0.78	90.15	0.74
229.50	1.57	198.33	1.47
458.32	3.13	413.27	2.94
685.42	4.70	583.39	4.42
1161.90	7.83	1028.53	7.36
1841.72	12.54	1650.03	11.78
2421.83	16.14	2343.46	16.05
3033.73	20.06	2902.08	20.02
3353.00	22.09	3315.69	22.08
3638.65	25.072	3457.44	25.03
4106.50	28.049	4065.17	28.12

Table A7: Prepared solutions of decylbenzene (C10) and undecylbenzene (C11) for calibration curves displayed in Figure 9.5.

decylbenzene (C10)						undecylbenzene (C11)					
V_{C10} [ml]	V_{ACN} [ml]	ρ_{C10} [g/ml] [a]	MW_{C10} [g/mol]	n_{C10} [mmol]	$c_{C10,sln.}$ [mM]	V_{C11} [ml]	V_{ACN} [ml]	ρ_{C11} [g/ml] [b]	MW_{C11} [g/mol]	n_{C11} [mmol]	$c_{C11,sln.}$ [mM]
0.010	199.99 [c]	0.8555	218.38	0.0392	0.1959	0.010	249.990	0.8553	232.40	0.0368	0.1472
0.020	249.98	0.8555	218.38	0.0783	0.3134	0.020	249.980	0.8553	232.40	0.0736	0.2944
0.030	249.97	0.8555	218.38	0.1175	0.4701	0.030	249.970	0.8553	232.40	0.1104	0.4416
0.050	249.95	0.8555	218.38	0.1959	0.7835	0.050	249.950	0.8553	232.40	0.1840	0.7360
0.100	249.9	0.8555	218.38	0.3917	1.5670	0.100	249.900	0.8553	232.40	0.3680	1.4721
0.200	249.8	0.8555	218.38	0.7835	3.1340	0.200	249.800	0.8553	232.40	0.7360	2.9442
0.300	249.7	0.8555	218.38	1.1752	4.7010	0.300	249.700	0.8553	232.40	1.1041	4.4163
0.500	249.5	0.8555	218.38	1.9587	7.8350	0.500	249.500	0.8553	232.40	1.8401	7.3605
0.800	249.2	0.8555	218.38	3.1340	12.5359	0.800	249.200	0.8553	232.40	2.9442	11.7767
1.030	248.97	0.8555	218.38	4.0350	16.1400	1.090	248.910	0.8553	232.40	4.0114	16.0458
1.280	248.72	0.8555	218.38	5.0144	20.0575	1.360	248.640	0.8553	232.40	5.0051	20.0204
1.410	248.59	0.8555	218.38	5.5237	22.0946	1.500	248.500	0.8553	232.40	5.5203	22.0814
1.600	248.4	0.8555	218.38	6.2680	25.0719	1.700	248.300	0.8553	232.40	6.2564	25.0255
1.790	248.21	0.8555	218.38	7.0123	28.0492	1.910	248.090	0.8553	232.40	7.0292	28.1169

a. Reported at 20 °C.
b. Reported at 20 °C.
c. Solution prepared with 200 [ml] volumetric flask; the rest were prepared with 250 [ml] volumetric flask.

A10.2   Plate number and van Deemter curve for Hypercarb^{TM} column

Table A8: Estimation of plate number, N_{plate}, and axial diffusion coefficient, D_{ax}, for Hypercarb column.

Flow rate set-point	Avg. flow rate $\overline{Q}$	Linear velocity u	Peak maxima t_{peak}	Plate number N_{plate}	Plate height h_{plate}	Diffusion coefficient D_{ax}
[ml/min.]	[ml/min.]	$\cdot 10^{-4}$ [m/s]	[min.]	[−]	$\cdot 10^{-5}$ [m]	$\cdot 10^{-12}$ [m^2/s]
0.2	0.197	2.64	3.397	1812	2.759	2.01
0.4	0.391	5.25	1.704	2836	1.763	1.63
0.5	0.487	6.53	1.371	3123	1.601	1.67
0.6	0.586	7.81	1.152	3220	1.553	1.88
0.8	0.768	10.35	0.874	3333	1.5	2.33
1.0	0.9762	13.1	0.69	3219	1.553	3.16

A fit to van Deemter equation [266]

$$h_{plate} = f(u) = \frac{A}{u} + Bu + D \tag{A10.1}$$

yields the curve of the data in Table A8 with resulting parameters as illustrated in Figure A4.
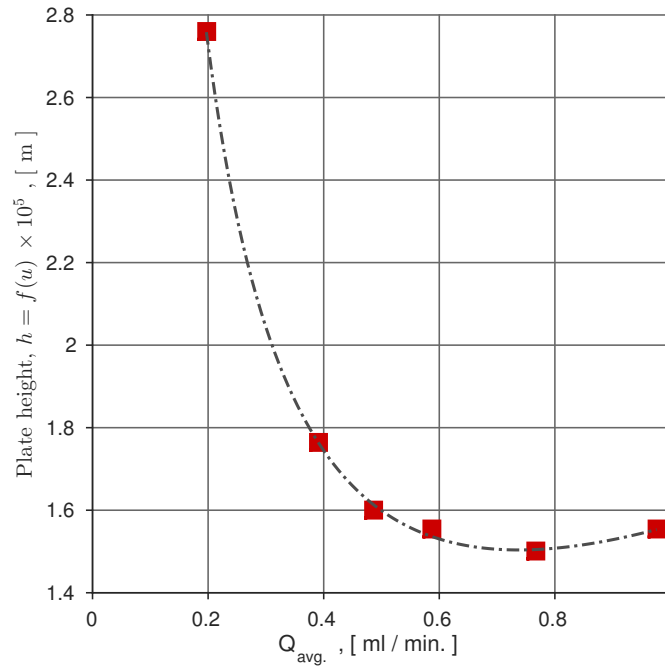
Figure A4: Estimated van Deemter curve for employed Hypercarb^{TM} column, using the data points listed in Table A8, measured by Kusian [255]. Obtained parameters for Equation (A10.1): $A = 0.4603$; $B = 0.8469$; & $D = 0.2550$.

A10.3 FA results of decylbenzene and undecylbenzene at $323\,\mathrm{K}$

Concentration range $0 - 20\,[\,\mathrm{mM}\,]$

Table A9: Frontal Analysis result for decylbenzene ($\mathsf{C10}$) & undecylbenzene ($\mathsf{C11}$) at $323.15\,\mathrm{K}$ ($50\,^{\circ}\mathrm{C}$). $20\,[\,\mathrm{mM}\,]$ solutions prepared with the chemicals' amounts listed in Table A7. A graphical illustration of listed values is depicted in Figures 9.8 and 9.9.

decylbenzene ($\mathsf{C10}$)		undecylbenzene ($\mathsf{C11}$)	
c	q	c	q
$[\,\mathrm{mM}\,]$	$[\,\mathrm{mM}\,]$	$[\,\mathrm{mM}\,]$	$[\,\mathrm{mM}\,]$
0.12	2.33	0.12	3.48
0.32	5.48	0.33	7.98
0.52	8.52	0.53	11.96
0.72	11.45	0.73	16.40
0.92	14.51	0.93	20.67
1.11	17.48	1.13	24.82
1.31	20.56	1.33	28.98
1.50	23.54	1.53	33.14
1.71	26.71	1.73	37.57
1.90	29.78	1.93	41.91
2.19	34.19	2.99	63.38
2.59	40.26	3.41	72.95
2.98	46.39	3.80	80.11
3.38	52.36	5.00	100.57
3.77	58.09	6.99	127.59
4.97	75.75	9.02	149.10
6.95	102.27	11.02	165.45
8.96	126.24	13.06	178.65
10.95	147.91	15.07	189.35
12.98	167.55	17.08	198.33
15.02	185.16	19.06	206.70
17.08	201.80	20.03	210.54
19.14	216.50	-	-
20.15	223.37	-	-

Concentration range $0 - 5\,[\,\text{mM}\,]$

Table A10: Frontal Analysis result for phenyl-*n*-decane (C10) & phenyl-*n*-undecane (C11) at 323.15 K (50 °C). 5 [mM] solutions prepared with the chemicals' amounts listed in Table A7.

decylbenzene (C10)		undecylbenzene (C11)	
c	q	c	q
[mM]	[mM]	[mM]	[mM]
0.26	3.65	0.25	5.26
0.52	7.3	0.48	10.1
0.78	10.53	0.73	15.02
1.04	13.7	9.98	19.98
1.25	16.31	1.21	24.53
1.49	19.39	1.46	29.64
1.73	22.43	1.7	34.67
1.98	25.59	1.94	39.68
2.23	28.78	2.18	44.69
2.47	31.87	2.42	49.66
2.71	34.93	2.66	54.45
2.96	38.06	2.91	59.2
3.21	41.24	3.14	63.9
3.45	44.29	3.38	68.41
3.69	47.32	3.62	72.84
3.94	50.36	3.86	77.16
4.18	53.4	4.1	81.32
4.42	56.36	4.34	85.32
4.67	59.24	4.57	89.21
4.91	62.15	4.81	92.98

Concentration range $0 - 20\,[\,\mathsf{mM}\,]$, five equilibrium points only

Table A11: Frontal Analysis result for phenyl-*n*-decane (C10) & phenyl-*n*-undecane (C11) at 323.15 K (50 °C). 5 [mM] solutions prepared with the chemicals' amounts listed in Table A7.

decylbenzene (C10)		undecylbenzene (C11)	
c	q	c	q
$[\,\mathsf{mM}\,]$	$[\,\mathsf{mM}\,]$	$[\,\mathsf{mM}\,]$	$[\,\mathsf{mM}\,]$
4.11	68.88	3.97	83.97
8.20	123.71	7.96	138.34
11.98	165.52	11.97	172.48
16.01	200.31	15.97	193.85
20.00	229.19	19.95	208.92

A10.4 FA results of decylbenzene and undecylbenzene at different temperatures

Table A12: Equilibrium points of decylbenzene (C10) and undecylbenzene (C11) in ACN/PCG system measured with FA method at different temperatures, illustrated in Figure 9.11. Measurement range: $0 - 20\,[\text{mM}]$.

| decylbenzene (C10) | | | | | | undecylbenzene (C11) | | | | | |
| 323.15 K (50 °C) | | 333.15 K (60 °C) | | 343.15 K (70 °C) | | 323.15 K (50 °C) | | 333.15 K (60 °C) | | 343.15 K (70 °C) | |
c [mM]	q [mM]	c [mM]	q [mM]	c [mM]	q [mM]	c [mM]	q [mM]	c [mM]	q [mM]	c [mM]	q [mM]
0.12	2.30	0.13	2.47	0.13	2.35	0.12	3.45	0.13	3.52	0.12	2.48
0.32	5.38	0.34	4.73	0.34	4.20	0.33	7.64	0.34	6.91	0.33	5.15
0.52	8.40	0.55	6.78	0.55	5.96	0.53	11.61	0.54	10.06	0.54	7.77
0.72	11.33	0.76	9.22	0.75	7.89	0.73	15.87	0.74	13.55	0.74	10.47
0.92	14.35	0.97	11.36	0.96	9.65	0.93	19.96	0.95	16.81	0.95	13.03
1.11	17.27	1.17	13.50	1.16	11.36	1.13	23.93	1.14	20.01	1.14	15.53
1.31	20.29	1.38	15.68	1.38	13.12	1.33	28.02	1.34	23.26	1.35	18.06
1.51	23.25	1.59	17.67	1.58	14.83	1.52	32.07	1.54	26.46	1.55	20.51
1.71	26.33	1.80	19.92	1.79	16.59	1.73	36.33	1.75	29.72	1.75	23.05
1.90	29.27	2.00	21.79	1.99	18.27	1.92	40.49	1.94	32.88	1.95	25.44
2.19	33.55	3.09	33.06	3.08	26.95	2.99	61.95	3.03	51.30	3.01	38.54
2.59	39.49	3.49	36.98	3.49	30.20	3.41	71.10	3.43	56.40	3.40	43.15
2.98	45.48	3.89	41.02	3.89	33.37	3.80	78.20	3.81	61.98	3.79	47.69
3.38	51.43	5.11	52.88	5.11	42.99	5.00	98.11	4.99	78.13	4.98	61.06
3.78	57.24	7.15	71.34	7.15	58.24	6.99	124.46	6.96	101.17	6.97	81.17
4.97	74.54	9.18	88.09	9.19	72.52	9.01	144.54	8.94	119.77	8.96	98.07
6.95	100.98	11.22	102.73	11.22	85.52	11.02	160.08	10.92	134.60	10.95	112.45
8.96	124.78	13.28	116.00	13.27	97.38	13.06	172.44	12.91	147.00	12.96	124.96
10.95	145.58	15.36	127.57	15.34	108.27	15.07	182.37	14.90	157.19	14.97	135.83
12.98	164.60	17.45	135.41	17.41	118.34	17.08	190.70	16.90	166.02	16.98	145.23
15.02	181.91	19.54	144.55	19.52	127.65	19.05	197.73	18.91	173.63	19.00	153.37
17.08	197.73	20.61	149.05	20.60	132.26	20.02	200.97	19.92	177.05	20.00	157.05
19.14	211.96	-	-	-	-	-	-	-	-	-	-
20.15	218.64	-	-	-	-	-	-	-	-	-	-

Table A13: Equilibrium points of decylbenzene (C10) and undecylbenzene (C11) in ACN/PCG system measured with FA method at different temperatures, illustrated in Figure 9.12. Measurement range: $0 - 5\,[\text{mM}]$.

| decylbenzene (C10) | | | | | | undecylbenzene (C11) | | | |
| 323.15 K (50 °C) | | 333.15 K (60 °C) | | 343.15 K (70 °C) | | 323.15 K (50 °C) | | 343.15 K (70 °C) | |
c [mM]	q [mM]	c [mM]	q [mM]	c [mM]	q [mM]	c [mM]	q [mM]	c [mM]	q [mM]
0.28	4.15	0.30	3.28	0.28	2.50	0.28	6.07	0.29	4.04
0.54	7.81	0.55	6.14	0.53	4.62	0.53	10.74	0.54	7.28
0.79	10.80	0.79	8.66	0.77	6.79	0.77	15.33	0.79	10.44
1.04	13.92	1.04	11.00	1.01	8.94	1.01	20.02	1.04	13.61
1.26	17.33	1.25	12.89	1.24	10.67	1.28	26.09	1.26	16.44
1.47	20.09	1.49	15.19	1.47	12.54	1.50	30.61	1.50	19.43
1.71	22.88	1.72	17.49	1.71	14.33	1.73	35.27	1.73	22.36
1.95	26.00	1.96	19.83	1.94	16.20	1.97	40.05	1.97	25.37
2.19	29.32	2.20	22.24	2.18	18.22	2.20	44.81	2.21	28.34
2.42	32.30	2.44	24.66	2.42	20.27	2.44	49.52	2.45	31.21
2.66	35.10	2.68	27.13	2.65	22.34	2.67	54.09	2.68	34.13
2.90	38.19	2.91	29.66	2.89	24.27	2.91	58.64	2.92	37.09
3.14	41.48	3.15	32.22	3.13	26.03	3.14	63.13	3.16	39.97
3.37	44.44	3.39	34.75	3.37	27.86	3.38	67.39	3.40	42.75
3.61	47.25	3.63	37.17	3.61	29.83	3.61	71.61	3.64	45.59
3.85	50.25	3.87	39.45	3.84	31.90	3.85	75.72	3.87	48.41
4.09	53.40	4.11	41.64	4.08	33.96	4.09	79.68	4.11	51.11
4.32	56.38	4.35	43.88	4.32	35.84	4.32	83.49	4.35	53.87
4.56	59.00	4.59	46.18	4.56	37.54	4.56	87.15	4.59	56.55
4.80	61.79	4.82	48.57	4.80	39.43	4.79	90.74	4.82	59.16

A10.5 Estimated single component isotherm parameters of Quadratic plus Langmuir model from FA results

Table A14: Single component adsorption isotherm parameters for Quadratic plus Langmuir model—Eq. (2.3e), p. 17—estimated for investigated alkylbenzenes in ACN/PGC system at 323.15 K (50 °C).

Compound	Parameters				
	q_{i1}^{sat} $\left[\dfrac{\text{mmol}}{\text{l}}\right]$	b_{i1} $\left[\dfrac{\text{L}}{\text{mmol}}\right]$	b_{i2} $\left[\dfrac{\text{L}^2}{\text{mmol}^2}\right]$	q_{i2}^{sat} $\left[\dfrac{\text{mmol}}{\text{l}}\right]$	b_{i3} $\left[\dfrac{\text{L}}{\text{mmol}}\right]$
decylbenzene (C10)	186.6	0.07415	0.003983	1.328	4.43
undecylbenzene (C11)	121.4	0.1311	0.02027	4.667	2.226

A11   UV spectral curves for decylbenzene (C10) and unde-cylbenzene (C11) dissolved in ACN

The following figures document the UV response of an Agilent MWD detector, similar to the one installed in the employed HPLC instrument.
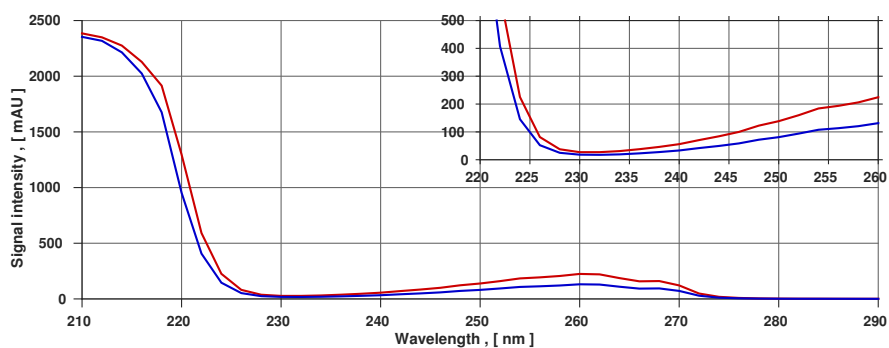

Figure A5: UV spectra of peak apex of investigated alkylbenzenes (C10 & C11), recorded with an Agilent 1100 HPLC station.
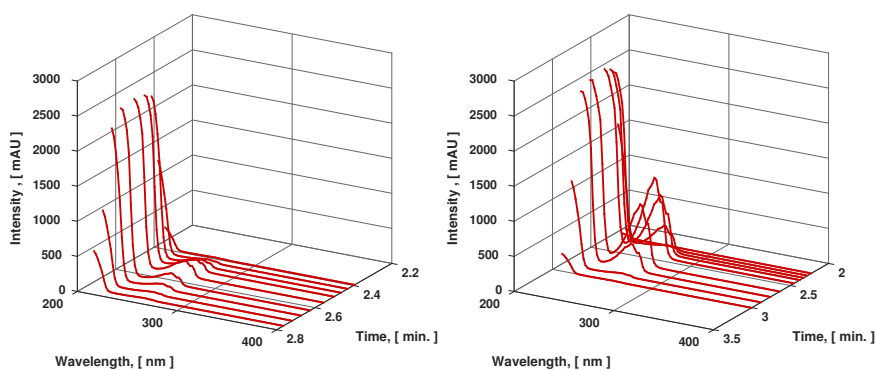

Figure A6: UV spectra of an analytical peak of C10 dissolved in ACN. $V_{\text{inj.}} = 1\,[\mu\text{l}]$.
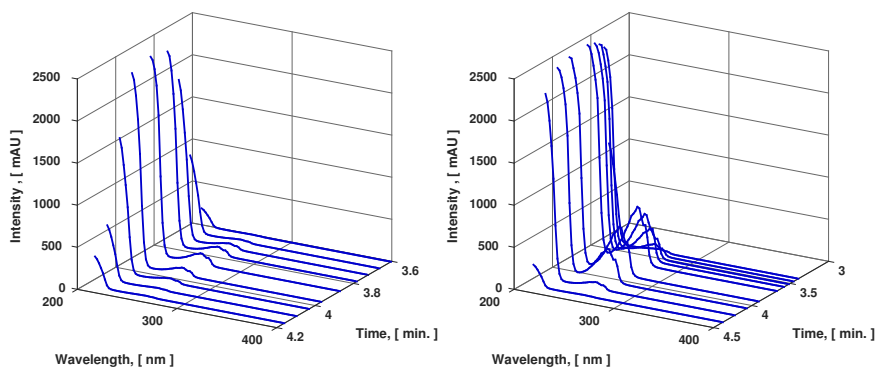
Figure A7: UV spectra of a analytical peak of C11 dissolved in ACN. $V_{\text{inj.}} = 1\,[\mu\text{l}]$.

A12   Collected fractions' data employed in Chapter 10

Table A15: Collected fractions to reconstruct elution profiles for CASE 1. Fraction collector used: '**FoxyJr.**'—cf. Section 9.2. Fraction *size*: 0.2 [min.]. Applied calibration factors (9.4) as reported in Section 9.4, p. 125.

Time	decylbenzene (C10)		undecylbenzene (C11)		Time	decylbenzene (C10)		undecylbenzene (C11)	
[min.]	[mAU · s]	[mM]	[mAU · s]	[mM]	[min.]	[mAU · s]	[mM]	[mAU · s]	[mM]
7.5	0	0	0	0	17.5	833.3	5.4143	711.1	4.8017
7.7	0	0	0	0	17.7	834.2	5.4203	715.0	4.8279
7.9	0	0	0	0	17.9	830.4	5.3955	720.5	4.8652
8.1	0	0	0	0	18.1	833.3	5.4143	740.5	4.9997
8.3	0	0	0	0	18.3	821.6	5.3386	718.6	4.8521
8.5	0	0	0	0	18.5	796.2	5.1737	710.9	4.8003
8.7	0	0	0	0	18.7	826.4	5.3694	747.1	5.0446
8.9	0	0	0	0	18.9	827.4	5.3761	744.5	5.0273
9.1	0	0	0	0	19.1	798.1	5.1858	719.0	4.8548
9.3	0	0	0	0	19.3	813.9	5.2883	726.1	4.9031
9.5	0	0	0	0	19.5	807.3	5.2454	732.5	4.9459
9.7	0	0	0	0	19.7	760.3	4.9399	709.7	4.7920
9.9	0	0	0	0	19.9	688.3	4.4722	679.9	4.5906
10.1	0	0	0	0	20.1	639.6	4.1560	667.8	4.5091
10.3	0	0	0	0	20.3	540.4	3.5115	618.8	4.1780
10.5	0	0	0	0	20.5	460.5	2.9922	592.6	4.0013
10.7	95.3	0.6191	0	0	20.7	388.1	2.5219	564.1	3.8088
10.9	348.2	2.2626	0	0	20.9	306.1	1.9892	531.8	3.5908
11.1	749.4	4.8696	0	0	21.1	220.0	1.4298	512.2	3.4583
11.3	1004.3	6.5258	0	0	21.3	149.8	0.9735	481.0	3.2478
11.5	1076.0	6.9915	0	0	21.5	96.0	0.6238	472.4	3.1899
11.7	1067.0	6.9332	41.1	0.2774	21.7	53.4	0.3471	467.5	3.1568
11.9	1018.1	6.6156	310.7	2.0976	21.9	29.7	0.1930	428.7	2.8946
12.1	850.5	5.5262	536.3	3.6211	22.1	0	0	446.0	3.0118
12.3	831.5	5.4029	666.8	4.5023	22.3	0	0	399.0	2.6944
12.5	805.2	5.2320	712.3	4.8093	22.5	0	0	386.3	2.6082
12.7	767.8	4.9888	698.2	4.7141	22.7	0	0	306.0	2.0665
12.9	814.4	5.2917	743.4	5.0198	22.9	0	0	240.8	1.6256
13.1	799.7	5.1965	729.4	4.9252	23.1	0	0	136.1	0.9191
13.3	799.8	5.1972	740.3	4.9984	23.3	0	0	73.6	0.4968
13.5	813.7	5.2870	739.0	4.9901	23.5	0	0	42.8	0.2891
13.7	815.9	5.3017	741.2	5.0046	23.7	0	0	0	0
13.9	824.1	5.3546	750.9	5.0701	23.9	0	0	0	0
14.1	820.6	5.3319	751.2	5.0722	24.1	0	0	0	0
14.3	825.9	5.3667	752.5	5.0812	24.3	0	0	0	0
14.5	827.8	5.3788	770.7	5.2040	24.5	0	0	0	0
14.7	844.8	5.4893	759.5	5.1281	24.7	0	0	0	0
14.9	839.5	5.4551	766.3	5.1743	24.9	0	0	0	0
15.1	842.0	5.4712	756.3	5.1067	25.1	0	0	0	0
15.3	848.7	5.5148	750.0	5.0639	25.3	0	0	0	0
15.5	856.6	5.5657	757.0	5.1115	25.5	0	0	0	0
15.7	874.1	5.6796	763.6	5.1557	25.7	0	0	0	0
15.9	871.1	5.6602	754.3	5.0929	25.9	0	0	0	0
16.1	858.0	5.5751	742.9	5.0163	26.1	0	0	0	0
16.3	834.3	5.4210	715.7	4.8328	26.3	0	0	0	0
16.5	861.1	5.5952	735.6	4.9666	26.5	0	0	0	0
16.7	859.8	5.5865	717.6	4.8452	26.7	0	0	0	0
16.9	834.8	5.4243	709.8	4.7927	26.9	0	0	0	0
17.1	850.1	5.5235	729.6	4.9266	27.1	0	0	0	0
17.3	845.6	5.4947	722.6	4.8790	27.3	0	0	0	0

Table A16: Collected fractions to reconstruct elution profiles for CASE 2. Fraction collector used: Agilent Technologies G1364C—cf. Section 9.2. Fraction *size*: 0.1 [min.]. Applied calibration factors (9.4) as reported in Section 9.4, p. 125.

Time	decylbenzene (C10)		undecylbenzene (C11)		Time	decylbenzene (C10)		undecylbenzene (C11)	
[min.]	[mAU · s]	[mM]	[mAU · s]	[mM]	[min.]	[mAU · s]	[mM]	[mAU · s]	[mM]
10.05	0	0	0	0	15.06	380.7	2.4737	1052.6	7.1074
10.16	0	0	0	0	15.15	342.8	2.2274	977.9	6.6030
10.26	0	0	0	0	15.25	311.7	2.0253	954.1	6.4423
10.35	0	0	0	0	15.35	284.4	1.8480	921.1	6.2194
10.45	0	0	0	0	15.45	256.9	1.6693	901.6	6.0878
10.55	251.9	1.6368	0	0	15.55	238.9	1.5523	873.1	5.8953
10.65	1579.2	10.2612	0	0	15.65	210.8	1.3697	859.0	5.8001
10.75	1782.1	11.5796	0	0	15.75	184.2	1.1969	819.6	5.5341
10.86	1753.3	11.3925	0	0	15.85	159.8	1.0383	800.7	5.4065
10.96	1757.4	11.4191	0	0	15.96	134.0	0.8707	776.0	5.2397
11.07	1298.4	8.4366	771.2	5.2073	16.07	107.6	0.6992	743.1	5.0176
11.16	844.5	5.4873	1522.7	10.2816	16.16	88.3	0.5737	732.1	4.9433
11.25	836.0	5.4321	1576.6	10.6455	16.25	71.4	0.4639	732.4	4.9453
11.35	826.9	5.3730	1585.6	10.7063	16.37	57.6	0.3743	715.1	4.8285
11.45	813.1	5.2833	1559.7	10.5314	16.45	41.6	0.2703	671.1	4.5314
11.55	845.3	5.4925	1605.1	10.8379	16.55	32.6	0.2118	657.3	4.4382
11.65	843.0	5.4776	1628.0	10.9926	16.66	24.0	0.1559	639.9	4.3207
11.75	832.2	5.4074	1584.1	10.6962	16.75	0	0	623.7	4.2113
11.85	837.3	5.4405	1621.5	10.9487	16.85	0	0	613.5	4.1425
11.96	833.2	5.4139	1612.8	10.8899	16.95	0	0	599.1	4.0452
12.07	827.8	5.3788	1582.8	10.6874	17.06	0	0	597.1	4.0317
12.15	823.3	5.3496	1577.7	10.6529	17.15	0	0	553.5	3.7373
12.25	813.4	5.2853	1563.1	10.5544	17.25	0	0	537.5	3.6293
12.35	818.6	5.3190	1592.1	10.7502	17.35	0	0	496.6	3.3531
12.45	824.2	5.3554	1604.8	10.8359	17.46	0	0	475.7	3.2120
12.55	830.2	5.3944	1596.9	10.7826	17.56	0	0	425.0	2.8697
12.65	827.0	5.3736	1590.1	10.7367	17.66	0	0	411.9	2.7812
12.75	837.9	5.4444	1586.8	10.7144	17.75	0	0	352.6	2.3808
12.85	843.3	5.4795	1632.5	11.0230	17.85	0	0	317.9	2.1465
12.95	848.5	5.5133	1619.1	10.9325	17.96	0	0	262.5	1.7725
13.06	855.7	5.5601	1630.2	11.0074	18.06	0	0	176.6	1.1924
13.16	850.8	5.5283	1608.3	10.8596	18.15	0	0	77.5	0.5233
13.25	838.7	5.4496	1613.4	10.8940	18.25	0	0	44.8	0.3025
13.35	831.2	5.4009	1597.5	10.7866	18.35	0	0	29.5	0.1992
13.45	837.7	5.4431	1614.4	10.9007	18.46	0	0	26.6	0.1796
13.55	857.5	5.5718	1633.7	11.0311	18.55	0	0	20.7	0.1398
13.65	833.9	5.4185	1590.8	10.7414	18.66	0	0		0
13.75	817.8	5.3138	1564.7	10.5652	18.75	0	0	0	0
13.85	810.5	5.2664	1557.2	10.5145	18.85	0	0	0	0
13.96	756.2	4.9136	1481.4	10.0027	18.95	0	0	0	0
14.06	744.0	4.8343	1475.9	9.9656	19.06	0	0	0	0
14.16	706.6	4.5913	1440.5	9.7265	19.15	0	0	0	0
14.25	660.3	4.2904	1376.4	9.2937	19.25	0	0	0	0
14.35	628.0	4.0806	1320.9	8.9190	19.35	0	0	0	0
14.45	591.1	3.8408	1292.3	8.7259	19.46	0	0	0	0
14.55	544.3	3.5367	1208.3	8.1587	19.56	0	0	0	0
14.65	504.8	3.2801	1170.0	7.9001	19.66	0	0	0	0
14.75	482.4	3.1345	1167.4	7.8825	19.75	0	0	0	0
14.85	439.5	2.8558	1117.2	7.5436	19.85	0	0	0	0
14.96	411.8	2.6758	1082.6	7.3099	19.96	0	0	0	0

Table A17: Collected fractions to reconstruct elution profiles for Case 3. Fraction collector used: Agilent Technologies G1364C—cf. Section 9.2. Fraction *size*: 0.1 [min.]. Applied calibration factors (9.4) as reported in Section 9.4, p. 125.

Time	*decylbenzene* (C10)		*undecylbenzene* (C11)		Time	*decylbenzene* (C10)		*undecylbenzene* (C11)	
[min.]	[mAU·s]	[mM]	[mAU·s]	[mM]	[min.]	[mAU·s]	[mM]	[mAU·s]	[mM]
10.05	0	0	0	0	15.06	831.8	5.4048	504.1	3.4038
10.16	0	0	0	0	15.15	748.3	4.8622	468.1	3.1607
10.25	0	0	0	0	15.25	723.3	4.6998	476.3	3.2161
10.35	83.1	0.5400	0	0	15.35	682.8	4.4366	461.0	3.1128
10.45	1589.9	10.3307	0	0	15.45	601.1	3.9058	439.3	2.9662
10.55	2260.7	14.6894	0	0	15.55	553.2	3.5945	433.1	2.9244
10.65	2202.3	14.3099	0	0	15.65	523.3	3.4003	439.7	2.9689
10.75	2179.6	14.1624	0	0	15.75	453.0	2.9435	416.3	2.8109
10.85	2231.8	14.5016	0	0	15.85	392.2	2.5484	394.6	2.6644
10.96	2245.6	14.5913	0	0	15.95	346.4	2.2508	388.0	2.6199
11.07	2206.1	14.3346	0	0	16.06	301.3	1.9578	392.9	2.6529
11.15	2171.3	14.1085	0	0	16.15	248.2	1.6127	376.3	2.5409
11.25	1924.5	12.5049	379.7	2.5638	16.25	190.1	1.2352	362.4	2.4470
11.35	1655.0	10.7537	754.6	5.0952	16.37	154.5	1.0039	375.3	2.5341
11.45	1751.7	11.3821	822.0	5.5503	16.45	112.2	0.7290	365.2	2.4659
11.55	1681.2	10.9240	787.8	5.3194	16.55	74.9	0.4867	348.4	2.3525
11.65	1678.9	10.9090	794.6	5.3653	16.66	56.5	0.3671	359.8	2.4294
11.75	1656.7	10.7648	777.6	5.2505	16.75	40.6	0.2638	339.6	2.2930
11.86	1642.8	10.6745	772.6	5.2167	16.85	32.6	0.2118	350.2	2.3646
11.96	1607.3	10.4438	752.3	5.0797	16.95	23.5	0.1527	333.7	2.2532
12.07	1619.2	10.5211	760.3	5.1337	17.06	16.1	0.1046	358.3	2.4193
12.15	1633.9	10.6166	765.5	5.1688	17.15	11.5	0.0747	324.8	2.1931
12.25	1649.3	10.7167	789.2	5.3288	17.25	8.8	0.0572	315.8	2.1323
12.35	1663.0	10.8057	789.9	5.3336	17.35	8.3	0.0539	306.3	2.0682
12.45	1579.8	10.2651	741.3	5.0054	17.45	7.0	0.0455	300.0	2.0257
12.55	1688.3	10.9701	795.0	5.3680	17.55	0	0	280.4	1.8933
12.65	1612.0	10.4743	753.0	5.0844	17.65	0	0	255.3	1.7238
12.75	1631.3	10.5997	754.3	5.0932	17.75	0	0	216.0	1.4585
12.85	1688.1	10.9688	792.3	5.3498	17.85	0	0	169.4	1.1438
12.95	1636.5	10.6335	767.2	5.1803	17.95	0	0	106.1	0.7164
13.06	1648.9	10.7141	780.5	5.2701	18.06	0	0	48.9	0.3302
13.15	1664.5	10.8155	790.0	5.3342	18.15	0	0	31.3	0.2113
13.25	1640.1	10.6569	768.1	5.1864	18.25	0	0	23.4	0.1580
13.35	1631.0	10.5978	764.7	5.1634	18.35	0	0	17.7	0.1195
13.45	1635.7	10.6283	767.0	5.1789	18.45	0	0	0	0
13.55	1676.3	10.8921	790.5	5.3376	18.55	0	0	0	0
13.65	1627.0	10.5718	759.9	5.1310	18.66	0	0	0	0
13.75	1602.7	10.4139	754.3	5.0932	18.75	0	0	0	0
13.86	1533.2	9.9623	732.2	4.9440	18.85	0	0	0	0
13.95	1544.8	10.0377	739.6	4.9939	18.95	0	0	0	0
14.06	1496.1	9.7212	727.0	4.9088	19.06	0	0	0	0
14.15	1452.6	9.4386	709.4	4.7900	19.15	0	0	0	0
14.25	1350.4	8.7745	664.8	4.4889	19.25	0	0	0	0
14.35	1299.7	8.4451	655.3	4.4247	19.35	0	0	0	0
14.45	1210.7	7.8668	627.2	4.2350	19.45	0	0	0	0
14.55	1145.6	7.4438	599.0	4.0446	19.55	0	0	0	0
14.65	1097.3	7.1300	588.2	3.9716	19.65	0	0	0	0
14.75	1025.6	6.6641	564.8	3.8136	19.75	0	0	0	0
14.85	957.5	6.2216	546.2	3.6880	19.85	0	0	0	0
14.95	875.5	5.6888	516.1	3.4848	19.95	0	0	0	0

A13   Parameters for numerical simulations of Chapter 10

Table A18: Sets of parameter values applied in numerical simulations displayed in figures of Chapter 10.

Parameter		Values					
		Fig. 10.1, A	Fig. 10.1, B	Fig. 10.1, C	CASE 1, Fig. 10.3	CASE 2, Fig. 10.4	CASE 3, Fig. 10.4
u	[cm/min.]	7.9556	7.9556	7.9556	7.9556	7.9556	7.9556
ϵ	[−]	0.745	0.745	0.745	0.745	0.745	0.745
$D_{\mathrm{app},k}$ [a]	[cm²/min.]	0.0199	0.0199	0.0199	0.0796	0.0796	0.0796
L_{c},	[mm]	50	50	50	50	50	50
Integrator [b] [c]	n/a	ssprk3	ssprk3	ssprk3	ssprk3	ssprk3	ssprk3
J	[−]	500	500	500	500	500	500
Δt	[min.]	4×10^{-4}	4×10^{-4}	4×10^{-4}	4×10^{-4}	4×10^{-4}	4×10^{-4}
$c_{i,\mathrm{inj.}}$ [d]	[mM]	5.0 / 5.0	10.0 / 10.0	15.0 / 15.0	5.4 / 5.0	5.4 / 10.8	10.7 / 5.2
$V_{\mathrm{inj.}}$	[μl]	5000	5000	5000	10000	5000	5000

a. Same value applied for both components. eps $= 2.2204 \times 10^{-16}$ denotes the machine epsilon.

b. ode45: one-step, adaptive time-stepping Runge-Kutta pair by Dormand & Prince [173].

c. ssprk3: third order Strong Stability Preserving Runge-Kutta method, Equation (7.15), p. 93.

d. component 1 / component 2 / ⋯.

This page intentionally left blank.

Bibliography

[1] Alírio E. Rodrigues, M. Douglas LeVan, and Daniel Tondeur, editors. *Adsorption: Science and Technology*, volume 158 of *NATO ASI Series. Advanced Science Institutes Series E: Applied Sciences*. Kluwer Academic Publishers, 1988. ISBN 978-94-009-2263-1 (online). http://dx.doi.org/10.1007/978-94-009-2263-1.

[2] Phillip C. Wankat. *Rate-controlled separations*. Elsevier Applied Science. Elsevier Science Publishers Ltd., 1990. ISBN 1-85166-521-8.

[3] J. D. Seader and Ernest J. Henley. *Separation Process Principles*. John Wiley & Sons, Inc., 2nd edition, 2006. ISBN 978-0-471-46480-8.

[4] Robert H. Perry and Don W. Green, editors. *Perry's Chemical Engineers' Handbook*. McGraw-Hill, 8th edition, 2008. ISBN 0-071-42294-3.

[5] William F. Banholzer and Mark E. Jones. Chemical Engineers Must Focus on Practical Solutions. *AIChE Journal*, 59(8):2708–2720, 2013. http://dx.doi.org/10.1002/aic.14172.

[6] Motoyuki Suzuki. *Adsorption Engineering*. Chemical engineering monographs, vol. 25. Elsevier, 1990. ISBN 0-444-98802-5.

[7] Ralph T. Yang. *Gas separation by adsorption processes*. Imperial College Press, 1997. ISBN 978-1-86094-047-7 (pbk.).

[8] Douglas M. Ruthven. Adsorption, Fundamentals. In *Kirk-Othmer Encyclopedia of Chemical Technology*. John Wiley & Sons, Inc., 2000. ISBN 978-0-47-123896-6. http://dx.doi.org/10.1002/0471238961.0104191518212008.a01.pub2.

[9] Carmen M. Yon and John D. Sherman. Adsorption, Gas Separation. In *Kirk-Othmer Encyclopedia of Chemical Technology*. John Wiley & Sons, Inc., 2000. ISBN 978-0-47-123896-6. http://dx.doi.org/10.1002/0471238961.0104191519080518.a01.pub2.

[10] Stanley A. Gembicki and James Rekoske and Anil Oroskar and James Johnson. Adsorption, Liquid Separation. In *Kirk-Othmer Encyclopedia of Chemical Technology*. John Wiley & Sons, Inc., 2000. ISBN 978-0-47-123896-6. http://dx.doi.org/10.1002/0471238961.0104191507051302.a01.pub2.

[11] Alfons Mersmann. Adsorption. In *Ullmann's Encyclopedia of Industrial Chemistry, Vol. 1*. WILEY-VCH Verlag GmbH & Co. KGaA, Weinheim, 2003. ISBN 3-527-30385-5. http://dx.doi.org/10.1002/14356007.

[12] Hans-Jörg Bart and Ulrich von Gemmingen. Adsorption. In *Ullmann's Encyclopedia of Industrial Chemistry*. WILEY-VCH Verlag GmbH & Co. KGaA, Weinheim, 2012. ISBN 9783527306732. http://dx.doi.org/10.1002/14356007.b03_09.pub2.

[13] Georges Guiochon. Basic Principles of Chromatography. In *Ullmann's Encyclopedia of Industrial Chemistry, Vol. 4*. WILEY-VCH Verlag GmbH & Co. KGaA, Weinheim, 2003. ISBN 3-527-30385-5. http://dx.doi.org/10.1002/14356007.

[14] Georges Guiochon, Attila Felinger, Dean G. Shirazi, and Anita M. Katti. *Fundamentals of Preparative and Nonlinear Chromatography*. Elsevier Academic Press, 2nd edition, 2006. ISBN 978-0-12-370537-2.

[15] Georges Guiochon and Oliver Trapp. Basic Principles of Chromatography. In *Ullmann's Encyclopedia of Industrial Chemistry*. WILEY-VCH Verlag GmbH & Co. KGaA, Weinheim, 2012. ISBN 9783527306732. http://dx.doi.org/10.1002/14356007.b05_155.pub2.

[16] Salvatore Fanali, Paul R. Haddad, Colin F. Poole, Peter Schoenmakers, and David Lloyd. *Liquid Chromatography: Applications*. Elsevier Science, 2013. ISBN 978-0-12-415806-1.

[17] Salvatore Fanali, Paul R. Haddad, Colin F. Poole, Peter Schoenmakers, and David Lloyd. *Liquid Chromatography: Fundamentals and Instrumentation*. Elsevier Science, 2013. ISBN 978-0-12-415807-8.

[18] F. Rezaei and P. Webley. Structured adsorbents in gas separation processes. *Separation and Purification Technology*, 70(3):243–256, 2010. http://dx.doi.org/10.1016/j.seppur.2009.10.004.

[19] Ralph T. Yang. *Adsorbents: Fundamentals and Applications*. Wiley-Interscience, 2003. ISBN 978-0-471-29741-3. http:/dx.doi.org/10.1002/047144409X.

[20] K. Ishizaki, S. Komarneni, and M. Nanko. *Porous Materials. Process technology and applications.* Springer Science+Business Media, 2008. ISBN 978-1-4615-5811-8 (eBook).

[21] Berend Smit and Theo L. M. Maesen. Towards a molecular understanding of shape selectivity. *Nature*, 451:671–678, 2008. http://dx.doi.org/10.1038/nature06552.

[22] Berend Smit and Theo L. M. Maesen. Molecular Simulations of Zeolites: Adsorption, Diffusion, and Shape Selectivity. *Chemical Reviews*, 108(10): 4125–4184, 2008. http://dx.doi.org/10.1021/cr8002642.

[23] Jian-Rong Li, Julian Sculley, and Hong-Cai Zhou. Metal-Organic Frameworks for Separations. *Chemical Reviews*, 112:869–932, 2012. http://dx.doi.org/10.1021/cr200190s.

[24] Timothy Van Heest, Stephanie L. Teich-McGoldrick, Jeffery A. Greathouse, Mark D. Allendorf, and David S. Sholl. Identification of Metal-Organic Framework Materials for Adsorption Separation of Rare Gases: Applicability of Ideal Adsorbed Solution Theory (IAST) and Effects of Inaccessible Framework Regions. *The Journal of Physical Chemistry C*, 116(24):13183–13195, 2012. http://dx.doi.org/10.1021/jp302808j.

[25] Ganapathy Subramanian, editor. *Chiral Separation Techniques. A Practical Approach.* Wiley-VCH, 3rd edition, 2007. ISBN 978-3-527-31509-3. http://dx.doi.org/10.1002/9783527611737.

[26] David S. Sholl and Andrew J. Gellman. Developing Chiral Surfaces for Enantioselective Chemical Processing. *AIChE Journal*, 55(10):2484–2490, 2009. http://dx.doi.org/10.1002/aic.12036.

[27] Michael Lämmerhofer. Chiral recognition by enantioselective liquid chromatography: Mechanisms and modern chiral stationary phases. *Journal of Chromatography A*, 1217(6):814–856, 2010. http://dx.doi.org/10.1016/j.chroma.2009.10.022.

[28] Johanna Schell, Nathalie Casas, Ronny Pini, and Marco Mazzotti. Pure and binary adsorption of CO_2, H_2, and N_2 on activated carbon. *Adsorption*, 18(1): 49–65, 2012. http://dx.doi.org/10.1007/s10450-011-9382-y.

[29] Nathalie Casas, Johanna Schell, Ronny Pini, and Marco Mazzotti. Fixed bed adsorption of CO_2/H_2 mixtures on activated carbon: experiments and modeling. *Adsorption*, 18(2):143–161, 2012. http://dx.doi.org/10.1007/s10450-012-9389-z.

[30] Paul A. Webley. Adsorption technology for CO_2 separation and capture: a perspective. *Adsorption*, 20(2-3):225–231, 2014. http://dx.doi.org/10.1007/s10450-014-9603-2.

[31] Jennifer Wilcox, Reza Haghpanah, Erik C. Rupp, Jiajun He, and Kyoungjin Lee. Advancing Adsorption and Membrane Separation Processes for the Gigaton Carbon Capture Challenge. *Annual Review of Chemical and Biomolecular Engineering*, 5:479–505, 2014. http://dx.doi.org/10.1146/annurev-chembioeng-060713-040100.

[32] M.S. Ray. Adsorption principles, design data and adsorbent materials for industrial applications: A Bibliography (1967-1997). In A. Dąbrowski, editor, *Adsorption and its Applications in Industry and Environmental Protection Vol.I: Applications in Industry*, volume 120, Part A of *Studies in Surface Science and Catalysis*, pages 977–1049. Elsevier, 1999. http://dx.doi.org/10.1016/S0167-2991(99)80578-3.

[33] S. Sircar. Publications on Adsorption Science and Technology. *Adsorption*, 6(4): 359–365, 2000. http://dx.doi.org/10.1023/A:1026521201309.

[34] Darren P. Broom and K. Mark Thomas. Gas adsorption by nanoporous materials: Future applications and experimental challenges. *Materials Research Society Bulletin (MRS Bulletin)*, 38:412–421, 2013. http://dx.doi.org/10.1557/mrs.2013.105.

[35] David Peralta, Karin Barthelet, Javier Pérez-Pellitero, Celine Chizallet, Gérald Chaplais, Angélique Simon-Masseron, and Gerhard D. Pirngruber. Adsorption and Separation of Xylene Isomers: CPO-27-Ni vs HKUST-1 vs NaY. *The Journal of Physical Chemistry C*, 116(41):21844–21855, 2012. http://dx.doi.org/10.1021/jp306828x.

[36] Duong D. Do. *Adsorption Analysis: Equilibria and Kinetics*. Series on Chemical Engineering Vol. 2. Imperial College Press, 1998. ISBN 1-86-094130-3.

[37] Fabrice Gritti and Georges Guiochon. Adsorption Mechanism in RPLC. Effect of the Nature of the Organic Modifier. *Analytical Chemistry*, 77:4257–4272, 2005. http://dx.doi.org/10.1021/ac0580058.

[38] A. L. Myers and J. M. Prausnitz. Thermodynamics of Mixed-Gas Adsorption. *AIChE Journal*, 11:121–127, 1965. http://dx.doi.org/10.1002/aic.690110125.

[39] R. Krishna, S. Calero, and B. Smit. Investigation of entropy effects during sorption of mixtures of alkanes in MFI zeolite. *Chemical Engineering Journal*, 88 (1-3):81–94, 2002. http://dx.doi.org/10.1016/S1385-8947(01)00253-4.

[40] Sofie Bartholdy, Martin G. Bjørner, Even Solbraa, Alexander Shapiro, and Georgios M. Kontogeorgis. Capabilities and Limitations of Predictive Engineering Theories for Multicomponent Adsorption. *Industrial & Engineering Chemistry Research*, 52:11552–11563, 2013. http://dx.doi.org/10.1021/ie400593b.

[41] J. A. Swisher, L.-C. Lin, J. Kim, and B. Smit. Evaluating Mixture Adsorption Models Using Molecular Simulation. *AIChE Journal*, 59(8):3054–3064, 2013. http://dx.doi.org/10.1002/aic.14058.

[42] Krista S. Walton and David S. Sholl. Predicting Multicomponent Adsorption: 50 Years of the Ideal Adsorbed Solution Theory. *AIChE Journal*, 61(9):2757–2762, 2015. http://dx.doi.org/10.1002/aic.14878.

[43] M. Ilić, D. Flockerzi, and A. Seidel-Morgenstern. A thermodynamically consistent explicit competitive adsorption isotherm model based on second-order single component behaviour. *Journal of Chromatography A*, 1217(1):2132–2137, 2010. http://dx.doi.org/10.1016/j.chroma.2010.02.006.

[44] A. Tarafder and M. Mazzotti. A Method for Deriving Explicit Binary Isotherms Obeying the Ideal Adsorbed Solution Theory. *Chemical Engineering and Technology*, 35(1):102–108, 2012. http://dx.doi.org/10.1002/ceat.201100274.

[45] Aspen Technology, Inc. *Aspen Plus*. Bedford, Massachusetts, USA, 2015.

[46] D. M. Ruthven. *Principles of adsorption and adsorption processes*. Wiley-Interscience, 1984. ISBN 0-471-86606-7.

[47] Willem Hundsdorfer and Jan G. Verwer. *Numerical solution of time-dependent advection-diffusion-reaction equations*. Springer, 2003. ISBN 3-540-03440-4.

[48] J. M. Smith, H. C. Van Ness, and M. M. Abbott. *Introduction to Chemical Engineering Thermodynamics*. The McGraw-Hill Companies Inc., Series in Chemical Engineering. McGraw-Hill, 7th edition, 2005. ISBN 0-07-124708-4.

[49] Noel de Nevers. *Physical and chemical equilibrium for chemical engineers.* John Wiley & Sons, Inc., 2012. ISBN 978-0-470-92710-6.

[50] C. J. Radke and J. M. Prausnitz. Thermodynamics of Multi-Solute Adsorption from Dilute Liquid Solutions. *AIChE Journal*, 18(4):761–768, 1972. http://dx.doi.org/10.1002/aic.690180417.

[51] M. Diack and G. Guiochon. Adsorption Isotherm and Overloaded Elution Profiles of Phenyldodecane on Porous Carbon in Liquid Chromatography. *Analytical Chemistry*, 63:2608–2613, 1991. http://dx.doi.org/10.1021/ac00022a014.

[52] M. Diack and G. Guiochon. Adsorption Isotherms and Overloaded Elution Profiles of Phenyl-*n*-alkanes on Porous Carbon in Liquid Chromatography. *Langmuir*, 8:1587–1593, 1992. http://dx.doi.org/10.1021/la00042a016.

[53] H. O. Rubiera Landa, D. Flockerzi, and A. Seidel-Morgenstern. A Method for Efficiently Solving the IAST Equations with an Application to Adsorber Dynamics. *AIChE Journal*, 59(4):1263–1277, 2013. http://dx.doi.org/10.1002/aic.13894.

[54] J. Heinonen, H. O. Rubiera Landa, T. Sainio, and A. Seidel-Morgenstern. Use of Adsorbed Solution theory to model competitive and co-operative sorption on elastic ion exchange resins. *Separation and Purification Technology*, 95:235–247, 2012. http://dx.doi.org/10.1016/j.seppur.2012.05.003.

[55] H. O. Rubiera Landa, A. Rajendran, and A. Seidel-Morgenstern. Evaluating the application of discrete adsorption data to predict competitive equilibria and fixed-bed dynamics using Ideal Adsorbed Solution Theory. *Industrial & Engineering Chemistry Research*, 2016, *submitted.* .

[56] J. W. Gibbs. *The Scientific Papers Of J. Willard Gibbs V1: Thermodynamics.* Kessinger Publishing's Legacy Reprints. Kessinger Publishing, 1906. ISBN 1-432-63194-2. www.kessinger.net.

[57] Stanley I. Sandler. *Chemical and Engineering Thermodynamics.* John Wiley & Sons, Inc., 3$^{\mathrm{rd}}$ edition, 1999. ISBN 0-471-18210-9.

[58] A. L. Myers. Thermodynamics of adsorption in porous materials. *AIChE Journal*, 48:145–160, 2002. http://dx.doi.org/10.1002/aic.690480115.

[59] Alan L. Myers and Peter A. Monson. Physical adsorption of gases: the case for absolute adsorption as the basis for thermodynamic analysis. *Adsorption*, 20: 591–622, 2014. http://dx.doi.org/10.1007/s10450-014-9604-1.

[60] K. Y. Foo and B. H. Hameed. Insights into the modeling of adsorption isotherm systems. *Chemical Engineering Journal*, 156:2–10, 2010. http://dx.doi.org/10.1016/j.cej.2009.09.013.

[61] Stephen Brunauer, Lola S. Deming, W. Edwards Deming, and Edward Teller. On a Theory of the van der Waals Adsorption of Gases. *Journal of the American Chemical Society*, 62:1723–1732, 1940. http://dx.doi.org/10.1021/ja01864a025.

[62] C. H. Giles, T. H. MacEwan, S. N. Nakhwa, and D. Smith. Studies in Adsorption. Part XI. A System of Classification of Solution Adsorption Isotherms, and its Use in Diagnosis of Adsorption Mechanisms and in Measurement of Specific Surface Areas of Solids. *Journal of the Chemical Society*, pages 3973–3993, 1960. http://dx.doi.org/10.1039/JR9600003973.

[63] D. H. Everett. Manual of Symbols and Terminology for Physicochemical Quantities and Units, Appendix II: Definitions, Terminology and Symbols in Colloid and Surface Chemistry. *Pure & Applied Chemistry*, 31(4):577–638, 1972. IUPAC. Physical Chemistry Division. Commission on colloid and surface chemistry including catalysis. http://dx.doi.org/10.1351/pac197231040577.

[64] D. H. Everett. Reporting data on adsorption from solution at the solid/solution interface (Recommendations 1986). *Pure & Applied Chemistry*, 58(7):967–984, 1986. IUPAC. Physical Chemistry Division. Commission on colloid and surface chemistry including catalysis. http://dx.doi.org/10.1351/pac198658070967.

[65] I. Langmuir. The adsorption of gases on plane surfaces of glass, mica and platinum. *Journal of the American Chemical Society*, 40(9):1361–1403, 1918. http://dx.doi.org/10.1021/ja02242a004.

[66] Stephen Brunauer, P.H. Emmett, and Edward Teller. Adsorption of Gases in Multimolecular Layers. *Journal of the American Chemical Society*, 60:309–319, 1938. http://dx.doi.org/10.1021/ja01269a023.

[67] M. Polanyi. Section III.— Theories of the adsorption of gases. A general survey and some additional remarks. Introductory paper to section III. *Transactions of the Faraday Society*, 28:316–333, 1932. http://dx.doi.org/10.1039/TF9322800316.

[68] Mietek Jaroniec. Fifty Years of the Theory of the Volume Filling of Micropores. *Adsorption*, 3(3):187–188, 1997. http://dx.doi.org/10.1007/BF01650129.

[69] O. Redlich and D. L. Peterson. A useful adsorption isotherm. *The Journal of Physical Chemistry*, 63(6):1024, 1959. http://dx.doi.org/10.1021/j150576a611.

[70] S. E. Hoory and J. M. Prausnitz. Monolayer adsorption of gas mixtures on homogeneous and heterogeneous solids. *Chemical Engineering Science*, 22(7): 1025–1033, 1967. http://dx.doi.org/10.1016/0009-2509(67)80166-0.

[71] Grigoriy L. Aranovich and Marc D. Donohue. An Equation of State for Multilayer Adsorption. *Journal of Colloid and Interface Science*, 175(2):492–496, 1995. http://dx.doi.org/10.1006/jcis.1995.1480.

[72] W. Scot Appel, M. Douglas LeVan, and John E. Finn. Nonideal Adsorption Equilibria Described by Pure Component Isotherms and Virial Mixture Coefficients. *Industrial & Engineering Chemistry Research*, 37(12):4774–4782, 1998. http://dx.doi.org/10.1021/ie980257u.

[73] Nan Qi, W. Scot Appel, M. Douglas LeVan, and John E. Finn. Adsorption Dynamics of Organic Compounds and Water Vapor in Activated Carbon Beds. *Industrial & Engineering Chemistry Research*, 45(7):2303–2314, 2006. http://dx.doi.org/10.1021/ie050758x.

[74] Douglas M. Ruthven and Francis Wong. Generalized Statistical Model for the Prediction of Binary Adsorption Equilibria in Zeolites. *Industrial & Engineering Chemistry Fundamentals*, 24(1):27–32, 1985. http://dx.doi.org/10.1021/i100017a005.

[75] François James, Mauricio Sepúlveda, and Patrick Valentin. Statistical Thermodynamics Models for Multicomponent Isothermal Diphasic Equilibria, 1995.

[76] F. Gritti, A. Felinger, and G. Guiochon. Properties of the Adsorption Equilibrium Isotherms Used and Measured in RPLC. *Chromatographia*, 60(1): S3–S12, 2004. http://dx.doi.org/10.1365/s10337-004-0273-1.

[77] James A. O'Brien and Alan L. Myers. Rapid Calculations of Multicomponent Adsorption Equilibria from Pure Isotherm Data. *Industrial & Engineering Chemistry Process Design and Development*, 24:1188–1191, 1985. http://dx.doi.org/10.1021/i200031a049.

[78] A. L. Myers and D. Valenzuela. Computer algorithm and graphical method for calculating adsorption equilibria of gas mixtures. *Journal of Chemical Engineering of Japan*, 19(5):392–396, 1986. http://dx.doi.org/10.1252/jcej.19.392.

[79] Diego P. Valenzuela and Alan L. Myers. *Adsorption Equilibrium Data Handbook*. Prentice Hall Advanced Reference Series - Physical and Life Sciences. Prentice Hall, Inc., 1989. ISBN 0-13-008815-3.

[80] A. Seidel, G. Reschke, S. Friedrich, and D. Gelbin. Equilibrium adsorption of two-component organic solutes from aqueous solutions on activated carbon. *Adsorption Science and Technology*, 3:189–199, 1986.

[81] Terrell L. Hill. Theory of Multimolecular Adsorption from a Mixture of Gases. *The Journal of Chemical Physics*, 14:46–47, 1946. http://dx.doi.org/10.1063/1.1724061.

[82] James R. Arnold. Adsorption of Gas Mixtures. Nitrogen-Oxygen on Anatase. *Journal of the American Chemical Society*, 71(1):104–110, 1949. http://dx.doi.org/10.1021/ja01169a029.

[83] Nick D. Hutson and Ralph T. Yang. Theoretical Basis for the Dubinin-Radushkevich (D-R) Adsorption Isotherm Equation. *Adsorption*, 3(3): 189–195, 1997. http://dx.doi.org/10.1007/BF01650130.

[84] M. J. G. Linders. *Prediction of breakthrough curves of activated carbon based sorption systems - from elementary steps to process design*. PhD thesis, Technische Universiteit Delft, 1999. ISBN 90-6464-512-4.

[85] Robert S. Hansen, Ying Fu, and F. E. Bartell. Adsorption of Nitrogen, Oxygen and Argon on Rutile at Low Temperatures; Applicability of the Concept of Surface Heterogeneity. *The Journal of Physical Chemistry*, 56(1):140–144, 1952. http://dx.doi.org/10.1021/j150493a027.

[86] Robert Sips. On the Structure of a Catalyst Surface. *The Journal of Chemical Physics*, 16:490–495, 1948. http://dx.doi.org/10.1063/1.17466922.

[87] Péter Vajda and Attila Felinger. Multilayer adsorption on fractal surfaces. *Journal of Chromatography A*, 1324:121–127, 2014. http://dx.doi.org/10.1016/j.chroma.2013.11.028.

[88] O. Talu and A. L. Myers. Rigorous Thermodynamic Treatment of Gas Adsorption. *AIChE Journal*, 34:1887–1893, 1988. http://dx.doi.org/10.1002/aic.690341114.

[89] Jószef Tóth. Thermodynamical Correctness of Gas/Solid Adsorption Isotherm Equations. *Journal of Colloid and Interface Science*, 163:299–302, 1994. http://dx.doi.org/10.1006/jcis.1994.1107.

[90] Ekkehard Richter, Wilfried Schütz, and Alan L. Myers. Effect of adsorption equation on prediction of multicomponent adsorption equilibria by the Ideal Adsorbed Solution Theory. *Chemical Engineering Science*, 44(8):1609–1616, 1989. http://dx.doi.org/10.1016/0009-2509(89)80003-X.

[91] Ekkehard Richter. Zur Berechnung von Adsorptionsgleichgewichten an Kohlenstoff-Molekularsieben. *Chemie Ingenieur Technik*, 61(1):63–66, 1989. http://dx.doi.org/10.1002/cite.330610114.

[92] M. J. G. Linders, L. J. P. van den Broeke, F. Kapteijn, J. A. Moulijn, and J. J. G. M. van Bokhoven. Binary Adsorption Equilibrium of Organics and Water on Activated Carbon. *AIChE Journal*, 47(8):1885–1892, 2001. http://dx.doi.org/10.1002/aic.690470818.

[93] Renato Rota, Guiseppe Gamba, and Massimo Morbidelli. On the use of the adsorbed solution theory for designing adsorption separation units. *Separations Technology*, 3(4):230–237, 1993. http://dx.doi.org/10.1016/0956-9618(93)80022-J.

[94] A. Seidel-Morgenstern. Experimental determination of single solute and competitive adsorption isotherms. *Journal of Chromatography A*, 1037:255–272, 2004. http://dx.doi.org/10.1016/j.chroma.2003.11.108.

[95] Orhan Talu. Measurement and Analysis of Mixture Adsorption Equilibrium in Porous Solids. *Chemie Ingenieur Technik*, 83(1-2):67–82, 2011. http://dx.doi.org/10.1002/cite.201000164.

[96] A. L. Myers. Activity Coefficients of Mixtures Adsorbed on Heterogeneous Surfaces. *AIChE Journal*, 29(4):691–693, 1983. http://dx.doi.org/10.1002/aic.690290428.

[97] M. Jaroniec and R. Madey. *Physical Adsorption on Heterogeneous Solids*. Elsevier Science Publishers, Amsterdam - New York, 1988.

[98] W. Rudzinski and D. H. Everett. *Adsorption of Gases on Heterogeneous Surfaces*. Academic Press Ltd., 1992. ISBN 0-12-601690-9.

[99] Jonathan L. Coffman, Jack F. Kramarczyk, and Brian D. Kelley. High-Throughput Screening of Chromatographic Separations: I. Method Development and Column Modeling. *Biotechnology and Bioengineering*, 100(4): 605–618, 2008. http://dx.doi.org/10.1002/bit.21904.

[100] Jack F. Kramarczyk, Brian D. Kelley, and Jonathan L. Coffman. High-Throughput Screening of Chromatographic Separations: II. Hydrophobic Interaction. *Biotechnology and Bioengineering*, 100(4):707–720, 2008. http://dx.doi.org/10.1002/bit.21907.

[101] David L. Wensel, Brian D. Kelley, and Jon L. Coffman. High-Throughput Screening of Chromatographic Separations: III. Monoclonal Antibodies on Ceramic Hydroxyapatite. *Biotechnology and Bioengineering*, 100(5):839–854, 2008. http://dx.doi.org/10.1002/bit.21906.

[102] Brian D. Kelley, Mary Switzer, Patrick Bastek, Jack F. Kramarczyk, Kathleen Molnar, Tianning Yu, and Jon Coffman. High-Throughput Screening of Chromatographic Separations: IV. Ion-Exchange. *Biotechnology and Bioengineering*, 100(5):950–963, 2008. http://dx.doi.org/10.1002/bit.21905.

[103] Beckley K. Nfor, Marc Noverraz, Sreekanth Chilamkurthi, Peter D. E. M. Verhaert, Luuk A. M. van der Wielen, and Marcel Ottens. High-throughput isotherm determination and thermodynamic modeling of protein adsorption on mixed mode adsorbents. *Journal of Chromatography A*, 1217(44):6829–6850, 2010. http://dx.doi.org/10.1016/j.chroma.2010.07.069.

[104] E. C. Markham and Arthur F. Benton. The adsorption of gas mixtures by silica. *Journal of the American Chemical Society*, 53:497–507, 1931. http://dx.doi.org/10.1021/ja01353a013.

[105] J. C. Bellot and J. S. Condoret. Modelling of Liquid Chromatography Equilibria. *Process Biochemistry*, 28:365–376, 1993. http://dx.doi.org/10.1016/0032-9592(93)80023-A.

[106] Igor Quiñones and Georges Guiochon. Application of different adsorption isotherm models to the description of single-component and competitive adsorption data. *Journal of Chromatography A*, 734:83–96, 1996. http://dx.doi.org/10.1016/0021-9673(95)01162-5.

[107] Henning Kaemmerer, Zoltan Horvath, Ju Weon Lee, Malte Kaspereit, Robert Arnell, Martin Hedberg, Björn Herschend, Matthew J. Jones, Kerstin Larson, Heike Lorenz, and Andreas Seidel-Morgenstern. Separation of Racemic Bicalutamide by an Optimized Combination of Continuous Chromatography and Selective Crystallization. *Organic Process Research & Development*, 16:331–342, 2012. Special Issue: INTENANT. http://dx.doi.org/10.1021/op200136z.

[108] Krzysztof Kaczmarski, Alberto Cavazzini, Paweł Szabelski, Dongmei Zhou, Xiaoda Liu, and Georges Guiochon. Application of the general rate model and the generalized Maxwell-Stefan equation to the study of the mass transfer kinetics of a pair of enantiomers. *Journal of Chromatography A*, 962(1-2):57–67, 2002. http://dx.doi.org/10.1016/S0021-9673(02)00585-X.

[109] S. Suwanayuen and R. P. Danner. Vacancy Solution Theory of Adsorption From Gas Mixtures. *AIChE Journal*, 26(1):76–83, 1980. http://dx.doi.org/10.1002/aic.690260113.

[110] E. Costa, J. L. Sotelo, G. Calleja, and C. Marrón. Adsorption Of Binary And Ternary Hydrocarbon Gas Mixtures On Activated Carbon: Experimental Determination And Theoretical Prediction Of The Ternary Equilibrium Data. *AIChE Journal*, 27(1):5–12, 1981. http://dx.doi.org/10.1002/aic.690270103.

[111] Guiseppe Gamba, Renato Rota, Guiseppe Storti, Sergio Carrà, and Massimo Morbidelli. Adsorbed Solution Theory Models for Multicomponent Adsorption Equilibria. *AIChE Journal*, 35(6):959–966, 1989. http://dx.doi.org/10.1002/aic.690350609.

[112] Orhan Talu and Imre Zwiebel. Multicomponent Adsorption Equilibria of Nonideal Mixtures. *AIChE Journal*, 32(8):1263–1276, 1986. http://dx.doi.org/10.1002/aic.690320805.

[113] M. Sakuth, J. Meyer, and J. Gmehling. Measurement and prediction of binary adsorption equilibria of vapors on dealuminated Y-zeolites (DAY). *Chemical Engineering and Processing*, 37(4):267–277, 1998. http://dx.doi.org/10.1016/S0255-2701(98)00038-5.

[114] Alexander A. Shapiro and Erling H. Stenby. Potential Theory of Multicomponent Adsorption. *Journal of Colloid and Interface Science*, 201: 146–157, 1998. http://dx.doi.org/10.1006/jcis.1998.5424.

[115] Matias A. Monsalvo and Alexander A. Shapiro. Modeling adsorption of binary and ternary mixtures on microporous media. *Fluid Phase Equilibria*, 254(1-2): 91–100, 2007. http://dx.doi.org/10.1016/j.fluid.2007.02.006.

[116] Matias A. Monsalvo and Alexander A. Shapiro. Modeling adsorption of liquid mixtures on porous materials. *Journal of Colloid and Interface Science*, 333(1): 310–316, 2009. http://dx.doi.org/10.1016/j.jcis.2009.01.055.

[117] Austin Ladshaw, Sotira Yiacoumi, and Costas Tsouris. A Generalized Procedure for the Prediction of Multicomponent Adsorption Equilibria. *AIChE Journal*, 61 (8):2600–2610, 2015. http://dx.doi.org/10.1002/aic.14826.

[118] Gilbert W. Castellan. *Physical Chemistry.* World Student Series Edition - 3rd printing - 1973. Addison-Wesley Publishing Company, 2nd edition, 1971. Library of Congress Catalog Card Number: 75-133375.

[119] Terrell L. Hill. Statistical Mechanics of Adsorption. V. Thermodynamics and Heat of Adsorption. *The Journal of Chemical Physics*, 17(6):520–535, 1949. http://dx.doi.org/10.1063/1.1747314.

[120] Terrell L. Hill. Statistical Mechanics of Adsorption. IX. Adsorption Thermodynamics and Solution Thermodynamics. *The Journal of Chemical Physics*, 18(3):246–256, 1950. http://dx.doi.org/10.1063/1.1747615.

[121] Terrell L. Hill. Theory of Physical Adsorption. In W.G. Frankenburg, V.I. Komarewsky, and E.K. Rideal, editors, *Advances in Catalysis*, volume 4, pages 211–258. Elsevier, 1952. ISBN 978-0-12-007804-2.

[122] John M. Prausnitz, Rüdiger N. Lichtenthaler, and Edmundo Gomes de Azevedo. *Molecular Thermodynamics of Fluid-Phase Equilibria.* Prentice Hall International Series in the Physical and Chemical Engineering Sciences. Prentice Hall PTR, 3rd edition, 1999. ISBN 0-13-977745-8.

[123] Wolfgang Ostwald and Ramón de Izaguirre. Ueber eine allgemeinere Theorie der Adsorption von Lösungen. *Kolloid-Zeitschrift*, 30(5):279–306, 1922. http://dx.doi.org/10.1007/BF01422997.

[124] J. J. Kipling. *Adsorption from Solutions of Non-electrolytes.* Academic Press, Inc. (London) Ltd., 1965. ISBN 978-1-4832-3106-8 (e-book). Library of Congress Catalog Card Number: 65-26421.

[125] H. H. Rowley and W. B. Innes. Equilibria of Two-dimensional Systems. I. *The Journal of Physical Chemistry*, 46(5):537–548, 1942. http://dx.doi.org/10.1021/j150419a001.

[126] W. B. Innes and H. H. Rowley. Surface Fugacity and the Heat of Free Expansion on a Surface for a Single-component Film. *The Journal of Physical Chemistry*, 46(5):548–554, 1942. http://dx.doi.org/10.1021/j150419a002.

[127] W. B. Innes and H. H. Rowley. Equilibria of Two-dimensional Systems. II. *The Journal of Physical Chemistry*, 49(5):411–417, 1945. http://dx.doi.org/10.1021/j150443a001.

[128] Françoise Rouquerol, Jean Rouquerol, and Kenneth Sing. *Adsorption by Powders and Porous Solids. Principles, Methodology and Applications*. Academic Press, 1999. ISBN 0-12-598920-2.

[129] H. L. Wang, J. L. Duda, and C. J. Radke. Solution Adsorption from Liquid Chromatography. *Journal of Colloid and Interface Science*, 66(1):153–165, 1978. http://dx.doi.org/10.1016/0021-9797(78)90196-0.

[130] François Riedo and Ervin sz. Kováts. Adsorption from liquid mixtures and liquid chromatography. *Journal of Chromatography*, 239:1–28, 1982. http://dx.doi.org/10.1016/S0021-9673(00)81964-0.

[131] Yu. A. Eltekov, Yu. V. Kazakevich, A. V. Kiselev, and A. A. Zhuchkov. Study of Adsorption from Solutions by Frontal Chromatography. *Chromatographia*, 20(9): 525–528, 1985. http://dx.doi.org/10.1007/BF02312170.

[132] Yu V. Kazakevich and H. M. McNair. Study of the Excess Adsorption of the Eluent Components on Different Reversed-Phase Adsorbents. *Journal of Chromatographic Science*, 33(6):321–327, 1995. http://dx.doi.org/10.1093/chromsci/33.6.321.

[133] Torgny Fornstedt. Characterization of adsorption processes in analytical liquid-solid chromatography. *Journal of Chromatography A*, 1217(6):792–812, 2010. http://dx.doi.org/10.1016/j.chroma.2009.12.044.

[134] Péter Vajda, Attila Felinger, and Georges Guiochon. Evaluation of surface excess isotherms in liquid chromatography. *Journal of Chromatography A*, 1291: 41–47, 2013. http://dx.doi.org/10.1016/j.chroma.2013.03.023.

[135] Orhan Talu, Jianmin Li, and Alan L. Myers. Activity Coefficients of Adsorbed Mixtures. *Adsorption*, 1:103–112, 1995. http://dx.doi.org/10.1007/BF00704999.

[136] Oksana Lisec. *Frontalanalyse zur Bestimmung von Adsorptionsisothermen für die Berechnung der präparativen Chromatographie.* PhD thesis, Technische Universität Berlin, Fachbereich 5 - Chemie, 1999.

[137] Sabine Sochard, Nuno Fernandes, and Jean-Michel Reneaume. Modeling of Adsorption Isotherm of a Binary Mixture with Real Adsorbed Solution Theory and Nonrandom Two-Liquid Model. *AIChE Journal*, 56(12):3109–3119, 2010. http://dx.doi.org/10.1002/aic.12220.

[138] Cristiano Migliorini, Marco Mazzotti, Gianmarco Zenoni, MariaPia Pedeferri, and Massimo Morbidelli. Modeling Chromatographic Chiral Separations under Nonlinear Competitive Conditions. *AIChE Journal*, 46(8):1530–1540, 2000. http://dx.doi.org/10.1002/aic.690460806.

[139] Edgar N. Rudisill and M. Douglas LeVan. Standard states for the adsorbed-solution theory. *Chemical Engineering Science*, 47(5):1239–1245, 1992. http://dx.doi.org/10.1016/0009-2509(92)80245-8.

[140] Flor R. Siperstein and Alan L. Myers. Mixed-Gas Adsorption. *AIChE Journal*, 47(5):1141–1159, 2001. http://dx.doi.org/10.1002/aic.690470520.

[141] Wolfram Research, Inc. *Mathematica. Version 10.0.* Champaign, Illinois, USA, 2014.

[142] M. Douglas LeVan and T. Vermeulen. Binary Langmuir and Freundlich Isotherms for Ideal Adsorbed Solutions. *The Journal of Physical Chemistry*, 85: 3247–3250, 1981. http://dx.doi.org/10.1021/j150622a009.

[143] Douglas D. Frey and Alírio E. Rodrigues. Explicit Calculation of Multicomponent Equilibria for Ideal Adsorbed Solutions. *AIChE Journal*, 40: 182–186, 1994. http://dx.doi.org/10.1002/aic.690400121.

[144] R. W. D. Nickalls. A new approach to solving the cubic: Cardano's solution revealed. *The Mathematical Gazette*, 77:354–359, 2003. http://dx.doi.org/10.2307/3619777.

[145] Milton Abramowitz and Irene Stegun, editors. *Handbook of Mathematical Functions with Formulas, Graphs, and Mathematical Tables.* Dover Publications, Inc., 1972. ISBN 978-0-486-61272-0.

[146] Enzo Mangano, Daniel Friedrich, and Stefano Brandani. Robust algorithms for the Solution of the Ideal Adsorbed Solution Theory Equations. *AIChE Journal*, 2014. http://dx.doi.org/10.1002/aic.14684.

[147] João C. Santos, Yiyu Cheng, Madalena M. Dias, and Alírio E. Rodrigues. Surface B-splines fitting for speeding up the simulation of adsorption processes with IAS model. *Computers & Chemical Engineering*, 35:1186–1191, 2011. http://dx.doi.org/10.1016/j.compchemeng.2010.08.003.

[148] Giulio Santori, Mauro Luberti, and Hyungwoong Ahn. Ideal adsorbed solution theory solved with direct search minimisation. *Computers & Chemical Engineering*, 71:235–240, 2014. http://dx.doi.org/10.1016/j.compchemeng.2014.07.027.

[149] David Kahaner, Cleve Moler, and Stephen Nash. *Numerical Methods and Software.* Prentice Hall Series in Computational Mathematics. Prentice Hall, Inc., 1989. ISBN 0-13-627258-4.

[150] Shoichiro Nakamura. *Applied numerical methods with software.* Prentice Hall, Inc., 1991. ISBN 0-13-041047-0.

[151] William H. Press, Saul A. Teukolsky, William T. Vetterling, and Brian P. Flannery. *Numerical Recipes in Fortran 77: The Art of Scientific Computing (Vol. 1 of Fortran Numerical Recipes).* 2nd edition, 1996. ISBN 0-521-43064-X.

[152] Alfio Quarteroni, Fausto Saleri, and Paola Gervasio. *Scientific Computing with MATLAB and Octave.* Texts in Computational Science and Engineering. Springer, 3rd edition, 2010. ISBN 978-3-642-12429-7. http://www.springer.com/series/5151.

[153] James A. O'Brien and Alan L. Myers. A Comprehensive Technique for Equilibrium Calculations in Adsorbed Mixtures: The Generalized FastIAS Method. *Industrial & Engineering Chemistry Research*, 27:2085–2092, 1988. http://dx.doi.org/10.1021/ie00083a021.

[154] James Stewart. *Calculus: Early Trascendentals.* Brooks/Cole Publishing Co., 7th edition, 2012. ISBN 978-0-538-49790-9.

[155] Dennis G. Zill and Michael R. Cullen. *Differential Equations: with Boundary-Value Problems.* Brooks/Cole Publishing Co., 4th edition, 1996. ISBN 978-0-53-495580-9.

[156] Uri M. Ascher and Linda R. Petzold. *Computer Methods for Ordinary Differential Equations and Differential-Algebraic Equations.* Society for Industrial and Applied Mathematics, 1998. ISBN 978-0-898714-12-8 (pbk.).

[157] Eric Kvaalen, Laurent Neel, and Daniel Tondeur. Directions of quasi-static mass and energy transfer between phases in multicomponent open systems: Implications in separation science. *Chemical Engineering Science*, 40(7): 1191–1204, 1985. http://dx.doi.org/10.1016/0009-2509(85)85077-6.

[158] Eric Kvaalen and Daniel Tondeur. Constraints on phase equilibrium equations. *Chemical Engineering Science*, 43(4):803–810, 1988. http://dx.doi.org/10.1016/0009-2509(88)80075-7.

[159] Hyun-Ku Rhee, Rutherford Aris, and Neal R. Amundson. *First-Order Partial Differential Equations. Volume 1: Theory and Application of Single Equations.* Dover Publications, Inc., 1986. ISBN 0-486-41993-2 (pbk.).

[160] Hyun-Ku Rhee, Rutherford Aris, and Neal R. Amundson. *First-Order Partial Differential Equations. Volume 2: Theory and Application of Hyperbolic Systems of Quasilinear Equations.* Dover Publications, Inc., 1989. ISBN 0-486-41994-0 (pbk.).

[161] John E. Tolsma and Paul I. Barton. On computational differentiation. *Computers & Chemical Engineering*, 22(4-5):475–490, 1997. http://dx.doi.org/10.1016/S0098-1354(97)00264-0.

[162] Dietrich Flockerzi. Internal communication. 2011.

[163] A. Seidel and D. Gelbin. On applying the Ideal Adsorbed Solution Theory to multicomponent adsorption equilibria of dissolved organic components on activated carbon. *Chemical Engineering Science*, 43(1):79–89, 1988. http://dx.doi.org/10.1016/0009-2509(88)87128-8.

[164] E. Hairer, S. P. Nørsett, and G. Wanner. *Solving Ordinary Differential Equations I. Nonstiff Problems.* Springer Series in Computational Mathematics, Vol. 8. Springer-Verlag, 2nd edition, 1993. ISBN 3-540-56670-8.

[165] Lawrence F. Shampine. *Numerical solution of ordinary differential equations.* Chapman & Hall Mathematics. Chapman & Hall, Inc., 1994. ISBN 0-412-05151-6.

[166] E. Hairer, S. P. Nørsett, and G. Wanner. *Solving Ordinary Differential Equations II. Stiff and Differential-Algebraic Problems.* Springer Series in Computational Mathematics, Vol. 14. Springer-Verlag, 2nd rev. edition, 1996. ISBN 3-540-53775-9.

[167] Andreas Seidel, Erika Tzscheutschler, Karl-Heinz Radeke, and David Gelbin. Adsorption equilibria of aqueous phenol and indol solutions on activated carbons. *Chemical Engineering Science*, 40(2):215–222, 1985.

[168] The MathWorks, Inc. *MATLAB. Version 8.4.0.150421 (R2014b).* Natick, Massachusetts, USA, 2014.

[169] Hee Moon and Chi Tien. Further Work on Multicomponent Adsorption Equilibria Calculations Based on the Ideal Adsorbed Solution Theory. *Industrial & Engineering Chemistry Research*, 26:2042–2047, 1987. http://dx.doi.org/10.1021/ie00070a019.

[170] R. P. Brent. An algorithm with guaranteed convergence for finding a zero of a function. *Computer Journal*, 14(4):422–425, 1971. http://dx.doi.org/10.1093/comjnl/14.4.422.

[171] William H. Press, Saul A. Teukolsky, William T. Vetterling, and Brian P. Flannery. *Numerical Recipes in Fortran 90: The Art of Scientific Computing (Vol. 2 of Fortran Numerical Recipes).* 2nd edition, 1996. ISBN 0-521-57439-0 (hardcover).

[172] L. F. Shampine. Vectorized Solution of ODEs in MATLAB with Control of Residual and Error. In T. E. Simos, editor, *Recent Advances in Computational and Applied Mathematics*, pages 259–271. Springer, 2011. http://dx.doi.org/10.1007/978-90-481-9981-5_11.

[173] J. R. Dormand and P. J. Prince. A family of embedded Runge-Kutta formulae. *Journal of Computational and Applied Mathematics*, 6:19–26, 1980. http://dx.doi.org/10.1016/0771-050X(80)90013-3.

[174] Charles William Gear. *Numerical initial value problems in ordinary differential equations.* Prentice Hall Series in Automatic Computation. Prentice Hall PTR, 1971. ISBN 0-136-26606-1.

[175] Leôncio Diógenes T. Câmara and Antônio J. Silva Neto. Network modeling of chromatography by stochastic phenomena of adsorption, diffusion and

convection. *Applied Mathematical Modelling*, 33:2491–2501, 2009.
http://dx.doi.org/10.1016/j.apm.2008.07.013.

[176] H. Schmidt-Traub, M. Schulte, and A. Seidel-Morgenstern, editors. *Preparative Chromatography*. WILEY-VCH Verlag GmbH & Co. KgaA, 2$^{\text{nd}}$ edition, 2012. ISBN 978-3-527-32898-7.

[177] Hong Gao and Bingchang Lin. A simplified numerical method for the General Rate model. *Computers and Chemical Engineering*, 34:277–285, 2010. http://dx.doi.org/10.1016/j.compchemeng.2009.10.014.

[178] Eric von Lieres and Joel Andersson. A fast and accurate solver for the general rate model of column liquid chromatography. *Computers & Chemical Engineering*, 34(8):1180–1191, 2010. http://dx.doi.org/10.1016/j.compchemeng.2010.03.008.

[179] Zheng Liu, Jonas Roininen, Iiro Pulkkinen, Tuomo Sainio, and Ville Alopaeus. Moment based weighted residual method - new numerical tool for a nonlinear multicomponent chromatographic general rate model. *Computers & Chemical Engineering*, 53:153–163, 2013. http://dx.doi.org/10.1016/j.compchemeng.2013.02.008.

[180] Zheng Liu, Jonas Roininen, Iiro Pulkkinen, Pia Saari, Tuomo Sainio, and Ville Alopaeus. A new moment analysis method to estimate the characteristic parameters in chromatographic general rate model. *Computers & Chemical Engineering*, 55:50–60, 2013. http://dx.doi.org/10.1016/j.compchemeng.2013.04.015.

[181] Z. Ma, R. D. Whitley, and N.-H. L. Wang. Pore and Surface Diffusion in Multicomponent Adsorption and Liquid Chromatography Systems. *AIChE Journal*, 42(5):1244–1262, 1996. http://dx.doi.org/10.1002/aic.690420507.

[182] J. A. Berninger, R. D. Whitley, X. Zhang, and N.-H. L. Wang. A versatile model for simulation of reaction and nonequilibrium dynamics in multicomponent fixed-bed adsorption processes. *Computers & Chemical Engineering*, 15(11): 749–768, 1991. http://dx.doi.org/10.1016/0098-1354(91)85020-U.

[183] Fabrice Gritti and Georges Guiochon. A revisit of the concept of external film mass transfer resistance in the packed beds used in high-performance liquid chromatography. *Chemical Engineering Science*, 72:108–114, 2012. http://dx.doi.org/10.1016/j.ces.2012.01.028.

[184] J. C. Bellot and J. S. Condoret. Liquid Chromatography Modelling: A Review. *Process Biochemistry*, 26:363–376, 1991. http://dx.doi.org/10.1016/0032-9592(91)85027-L.

[185] Giorgio Carta and Alois Jungbauer. *Protein Chromatography*. WILEY-VCH Verlag GmbH & Co. KGaA, 2010. ISBN 978-3-527-31819-3.

[186] R. Byron Bird, Warren E. Stewart, and Edwin N. Lightfoot. *Transport Phenomena*. John Wiley & Sons, Inc., 2nd edition, 2002. ISBN 978-0-470-11539-8.

[187] P. V. Danckwerts. Continuous flow systems — Distribution of Residence Times. *Chemical Engineering Science*, 2(1):1–13, 1953. http://dx.doi.org/10.1016/0009-2509(53)80001-1.

[188] Richard A. Marra and David O. Cooney. Multicomponent sorption operations: Bed shrinking and swelling in an ion-exclusion case. *Chemical Engineering Science*, 33:1597–1601, 1978. http://dx.doi.org/10.1016/0009-2509(78)85135-5.

[189] Tong Yun and Georges Guiochon. Modeling of radial heterogeneity in chromatographic columns. Columns with cylindrical symmetry and ideal model. *Journal of Chromatography A*, 672:1–10, 1994. http://dx.doi.org/10.1016/0021-9673(94)80589-X.

[190] Karin C. E. Östergren and Christian Trägårdh. Numerical study of two-dimensional compaction, flow, and dispersion in a chromatographic column. *Numerical Heat Transfer, Part A: Applications*, 32(3):247–265, 1997. http://dx.doi.org/10.1080/10407789708913890.

[191] Karin C. E. Östergren, A. Christian Trägårdh, Gisle G. Enstad, and Jostein Mosby. Deformation of a Chromatographic Bed during Steady-State Liquid Flow. *AIChE Journal*, 44(1):2–12, 1998. http://dx.doi.org/10.1002/aic.690440103.

[192] R. N. Keener, J. E. Maneval, K. C. E. Östergren, and E. J. Fernandez. Mechanical Deformation of Compressible Chromatographic Columns. *Biotechnology Progress*, 18:587–596, 2002. http://dx.doi.org/10.1021/bp020051v.

[193] Dariusch Hekmat, Michael Kuhn, Verena Meinhardt, and Dirk Weuster-Botz. Modeling of transient flow through a viscoelastic preparative chromatography packing. *Biotechnology Progress*, 29(4):958–967, 2013. http://dx.doi.org/10.1002/btpr.1768.

[194] Tivadar Farkas, Michael J. Sepaniak, and Georges Guiochon. Radial Distribution of the Flow Velocity, Efficiency and Concentration in a Wide HPLC Column. *AIChE Journal*, 43(8):1964–1974, 2004. http://dx.doi.org/10.1002/aic.690430806.

[195] S. F. Chung and C. Y. Wen. Longitudinal Dispersion of Liquid Flowing Through Fixed and Fluidized Beds. *AIChE Journal*, 14(6):857–866, 1968. http://dx.doi.org/10.1002/aic.690140608.

[196] Georges Guiochon and Bingchang Lin. *Modeling for preparative chromatography.* Academic Press, 2003. ISBN 0-12-044983-8.

[197] Veronika R. Meyer. *Practical High-Performance Liquid Chromatography.* John Wiley & Sons, Ltd., 5th edition, 2010. ISBN 978-0-470-68217-3 (pbk.). http://dx.doi.org/10.1002/0470032677.

[198] Bruce A. Finlayson. *Nonlinear Analysis in Chemical Engineering.* Chemical Engineering Series. McGraw-Hill, 1980. ISBN 0-07-020915-4.

[199] Bruce A. Finlayson. *Numerical methods for problems with moving fronts.* Ravenna Park Publishing, 1992. ISBN 0-96-317650-1.

[200] Arvind Varma and Massimo Morbidelli. *Mathematical Methods in Chemical Engineering.* Oxford University Press, Inc., 1997. ISBN 0-19-509821-8.

[201] J. Norton Wilson. A Theory of Chromatography. *Journal of the American Chemical Society*, 62(6):1583–1591, 1940. http://dx.doi.org/10.1021/ja01863a071.

[202] Don DeVault. The Theory of Chromatography. *Journal of the American Chemical Society*, 65(4):532–540, 1943. http://dx.doi.org/10.1021/ja01244a011.

[203] A. P. Tudge. Studies in chromatographic transport. I. A simplified theory. *Canadian Journal of Physics*, 39:1600–1610, 1961. http://dx.doi.org/10.1139/p61-190.

[204] A. P. Tudge. Studies in chromatographic transport. II. The effect of adsorption isotherm shape. *Canadian Journal of Physics*, 39:1611–1618, 1961. http://dx.doi.org/10.1139/p61-191.

[205] A. P. Tudge. Studies in chromatographic transport. III. Chromathermography. *Canadian Journal of Physics*, 40:557–572, 1962. http://dx.doi.org/10.1139/p62-058.

[206] Daniel Tondeur and Michel Bailly. Design methods for ion-exchange processes based on the Equilibrium Theory. In Alírio Rodrigues, editor, *Ion-Exchange: Science and Technology*, NATO-ASI Series E107, pages 147–197. Martinus Nijhoff Publishers, Dordrecht, 1986.

[207] Xin Wang and Chi Bun Ching. Determination of the Competitive Adsorption Isotherms of Nadolol Enantiomers by an Improved *h*-Root Method. *Industrial & Engineering Chemistry Research*, 42(24):6171–6180, 2003. http://dx.doi.org/10.1021/ie0303698.

[208] J. Nowak, K. Gedicke, D. Antos, W. Piątkowski, and A. Seidel-Morgenstern. Synergistic effects in competitive adsorption of carbohydrates on an ion-exchange resin. *Journal of Chromatography A*, 1164(1-2):224–234, 2007. http://dx.doi.org/10.1016/j.chroma.2007.07.022.

[209] Jani Siitonen and Tuomo Sainio. Explicit equations for the height and position of the first component shock for binary mixtures with competitive Langmuir isotherms under ideal conditions. *Journal of Chromatography A*, 1218: 6379–6387, 2011. http://dx.doi.org/10.1016/j.chroma.2011.07.004.

[210] Peter D. Lax. *Hyperbolic Systems of Conservation Laws and the Mathematical Theory of Shock Waves.* CBMS-NSF regional conference series in applied mathematics. Society for Industrial and Applied Mathematics, 1973. ISBN 978-0-898711-77-6. http://dx.doi.org/10.1137/1.9781611970562.

[211] Pierre Rouchon, Marc Schoenauer, Patrick Valentin, Claire Vidal-Madjar, and Georges Guiochon. Theory of the Propagation of Finite Concentration Bands in Gas Chromatography. A Numerical Solution of the Ideal Problem. *The Journal of Physical Chemistry*, 89(10):2076–2082, 1985. http://dx.doi.org/10.1021/j100256a055.

[212] Pierre Rouchon, Marc Schonauer, Patrick Valentin, and Georges Guiochon. Numerical Simulation of Band Propagation in Nonlinear Chromatography. *Separation Science and Technology*, 22(8-10):1793–1833, 1987. http://dx.doi.org/10.1080/01496398708057614.

[213] Randall J. LeVeque. *Finite Volume Methods for Hyperbolic Problems.* Cambridge Texts in Applied Mathematics. Cambridge University Press, 2002. ISBN 0-521-81087-6.

[214] Eleuterio F. Toro. *Riemann Solvers and Numerical Methods for Fluid Dynamics.* Springer, 3rd edition, 2009. ISBN 978-3-540-49834-6 (online). http://dx.doi.org/10.1007/b79761.

[215] M. Remešíková. Solution of convection-diffusion problems with nonequilibrium adsorption. *Journal of Computational and Applied Mathematics*, 169:101–116, 2004. http://dx.doi.org/10.1016/j.cam.2003.11.005.

[216] J. Kačur, B. Malengier, and M. Remešíková. Solution of contaminant transport with equilibrium and non-equilibrium adsorption. *Computer Methods in Applied Mechanics and Engineering*, 194:479–489, 2005. http://dx.doi.org/10.1016/j.cma.2004.05.017.

[217] Uri M. Ascher. *Numerical Methods for Evolutionary Differential Equations.* Computational science and engineering; 5. Society for Industrial and Applied Mathematics, 2008. ISBN 978-0-898716-52-8 (pbk.).

[218] Graham W. Griffiths and William E. Schiesser. *Traveling Wave Analysis of Partial Differential Equations.* Elsevier, 2012. ISBN 978-0-12-384652-5.

[219] William E. Schiesser. *The numerical method of lines: integration of partial differential equations.* Academic Press, 1991. ISBN 0-12-624130-9.

[220] Philippe Saucez, W.E. Schiesser, and Alain Vande Wouwer. Upwinding in the method of lines. *Mathematics and Computers in Simulation*, 56(2):171–185, 2001. http://dx.doi.org/10.1016/S0378-4754(01)00288-9.

[221] M. Czok and G. Guiochon. The Physical Sense of Simulation Models of Liquid Chromatography: Propagation through a Grid or Solution of the Mass Balance Equation? *Analytical Chemistry*, 62(2):189–200, 1990. http://dx.doi.org/10.1021/ac00201a020.

[222] B. Koren. A robust upwind discretization method for advection, diffusion and source terms. Technical Report NM-R9308, Centrum voor Wiskunde en Informatica - Department of Numerical Mathematics, April 1993.

[223] W. Hundsdorfer, B. Koren, M. van Loon, and J. G. Verwer. A Positive Finite-Difference Advection Scheme. *Journal of Computational Physics*, 117(1): 35–46, 1995. http://dx.doi.org/10.1006/jcph.1995.1042.

[224] Celina P. Leão and Alírio Rodrigues. Transient and steady-state models for simulated moving bed processes: numerical solutions. *Computers & Chemical*

Engineering, 28(9):1725–1741, 2004.
http://dx.doi.org/10.1016/j.compchemeng.2004.01.007.

[225] Friedemann Kemm. A comparative study of TVD-limiters—well-known limiters and an introduction of new ones. *International Journal for Numerical Methods in Fluids*, 67(4):404–440, 2011. http://dx.doi.org/10.1002/fld.2357.

[226] P. K. Sweby. High Resolution Schemes Using Flux Limiters for Hyperbolic Conservation Laws. *SIAM Journal on Numerical Analysis*, 21(5):995–1011, 1984. http://dx.doi.org/10.1137/0721062.

[227] L. F. Shampine, S. Thompson, J. A. Kierzenka, and G. D. Byrne. Non-negative solutions of ODEs. *Applied Mathematics and Computation*, 170:556–569, 2005. http://dx.doi.org/10.1016/j.amc.2004.12.011.

[228] Chi-Wang Shu. Total variation diminishing time discretizations. *SIAM Journal on Scientific and Statistical Computing*, 9(6):1073–1084, 1988. http://dx.doi.org/10.1137/0909073.

[229] Sigal Gottlieb and Chi-Wang Shu. Total variation diminishing Runge-Kutta schemes. *Mathematics of Computation*, 67(221):73–85, 1998. http://dx.doi.org/10.1090/S0025-5718-98-00913-2.

[230] Sigal Gottlieb, David I. Ketcheson, and Chi-Wang Shu. High Order Strong Stability Preserving Time Discretizations. *Journal of Scientific Computing*, 38 (3):251–289, 2009. http://dx.doi.org/10.1007/s10915-008-9239-z.

[231] P. Bogacki and L. F. Shampine. A (3)2 Pair of Runge-Kutta Formulas. *Applied Mathematics Letters*, 2:321–325, 1989. http://dx.doi.org/10.1016/0893-9659(89)90079-7.

[232] Cleve Moler. *Numerical Computing with* MATLAB. Society for Industrial and Applied Mathematics, 2004. ISBN 978-0-898716-60-3. http://dx.doi.org/10.1137/1.9780898717952.

[233] Barbara Lee Keyfitz and Herbert C. Kranzer. The Riemann Problem for a Class of Hyperbolic Conservation Laws Exhibiting a Parabolic Degeneracy. *Journal of Differential Equations*, 47(1):35–65, 1983. http://dx.doi.org/10.1016/0022-0396(83)90027-X.

[234] Barbara Lee Keyfitz. A survey of nonstrictly hyperbolic conservation laws. In Claude Carasso, Denis Serre, and Pierre-Arnaud Raviart, editors, *Nonlinear*

Hyperbolic Problems, Lecture Notes in Mathematics, pages 152–162. Springer Berlin Heidelberg, 1987.

[235] William W. Hager. Updating the Inverse of a Matrix. *SIAM Review*, 31(2): 221–239, 1989. http://dx.doi.org/10.1137/1031049.

[236] Gene H. Golub and Charles F. Van Loan. *Matrix Computations*. The Johns Hopkins University Press, 3$^{\text{rd}}$ edition, 1996. ISBN 0-8018-5414-8 (pbk.).

[237] PubChem Compound Database. *1-Phenyldecane*. National Center for Biotechnology Information, https://pubchem.ncbi.nlm.nih.gov/compound/7716 (accessed Sept. 23, 2015), 2015.

[238] PubChem Compound Database. *UNDECYLBENZENE*. National Center for Biotechnology Information, https://pubchem.ncbi.nlm.nih.gov/compound/23194 (accessed Sept. 23, 2015), 2015.

[239] Vratislav Svoboda. Multi-component elution overload chromatography of compounds with S-shaped isotherms. *Journal of Chromatography A*, 518:77–97, 1990. http://dx.doi.org/10.1016/S0021-9673(01)93164-4.

[240] Andreas Seidel-Morgenstern and Georges Guiochon. Modelling of the competitive isotherms and the chromatographic separation of two enantiomers. *Chemical Engineering Science*, 48(15):2787–2797, 1993. http://dx.doi.org/10.1016/0009-2509(93)80189-W.

[241] A. Kurganov, V. Davankov, K. Unger, F. Eisenbeiss, and J. Kinkel. Unusual peak distortion in ligand-exchange chromatography of enantiomers under overloaded conditions. *Journal of Chromatography A*, 666(1-2):99–110, 1994. http://dx.doi.org/10.1016/0021-9673(94)80373-0.

[242] Tarab Ahmad and Georges Guiochon. Effect of the mobile phase composition on the adsorption behavior of tryptophan in reversed-phase liquid chromatography. *Journal of Chromatography A*, 1114(1):111–122, 2006. http://dx.doi.org/10.1016/j.chroma.2006.02.046.

[243] Tarab Ahmad and Georges Guiochon. Numerical determination of the adsorption isotherms of tryptophan at different temperatures and mobile phase compositions. *Journal of Chromatography A*, 1142(2):148–163, 2007. http://dx.doi.org/10.1016/j.chroma.2006.12.087.

[244] Péter Vajda, Szymon Bocian, Bogusław Buszewski, and Attila Felinger. Effect of polar interactions on the nonlinear behavior of phenol and aniline in reversed phase liquid chromatography. *Journal of Chromatography A*, 1228:155–164, 2012. http://dx.doi.org/10.1016/j.chroma.2011.12.024.

[245] C. West, C. Elfakir, and M. Lafosse. Porous graphitic carbon: A versatile stationary phase for liquid chromatography. *Journal of Chromatography A*, 1217 (19):3201–3216, 2010. http://dx.doi.org/10.1016/j.chroma.2009.09.052.

[246] Cristina I. De Matteis, David A Simpson, Stephen W. Doughty, Melvin R. Euerby, P. Nicholas Shaw, and David A. Barrett. Chromatographic retention behaviour of n-alkylbenzenes and pentylbenzene structural isomers on porous graphitic carbon and octadecyl-bonded silica studied using molecular modelling and QSRR. *Journal of Chromatography A*, 1217:6987–6993, 2010. http://dx.doi.org/10.1016/j.chroma.2010.08.023.

[247] Cristina I. De Matteis, David A. Simpson, Melvin R. Euerby, P. Nicholas Shaw, and David A. Barrett. Chromatographic retention behaviour of monosubstituted benzene derivatives on porous graphitic carbon and octadecyl-bonded silica studied using molecular modelling and quantitative structure-retention relationships. *Journal of Chromatography A*, 1229:95–106, 2012. http://dx.doi.org/10.1016/j.chroma.2011.12.090.

[248] Agilent Technologies, Inc. *Agilent OpenLAB CDS ChemStation Edition*. Waldbronn, Germany, 2011.

[249] Luisa Pereira. Porous Graphitic Carbon as a Stationary Phase in HPLC: Theory and Applications. *Journal of Liquid Chromatography & Related Technologies*, 31: 1687–1731, 2008. http://dx.doi.org/10.1080/10826070802126429.

[250] John H. Knox, Bulvinder Kaur, and G.R. Millward. Structure and performance of porous graphitic carbon in liquid chromatography. *Journal of Chromatography A*, 352:3–25, 1986. http://dx.doi.org/10.1016/S0021-9673(01)83368-9.

[251] A. A. Isirikyan and A. V. Kiselev. The absolute adsorption isotherms of vapors of nitrogen, benzene and n-hexane, and the heats of adsorption of benzene and n-hexane on graphitized carbon blacks. I. Graphitized thermal blacks. *The Journal of Physical Chemistry*, 65(4):601–607, 1961. http://dx.doi.org/10.1021/j100822a004.

[252] H. J. Möckel, A. Braedikow, H. Melzer, and Gaby Aced. A Comparison of the Retention of Homologous Series and Other Test Solutes on an ODS Column and a Hypercarb Carbon Column. *Journal of Liquid Chromatography*, 14(13): 2477–2498, 1991. http://dx.doi.org/10.1080/01483919108049334.

[253] Toshihiko Hanai. Separation of polar compounds using carbon columns. *Journal of Chromatography A*, 989(2):183–196, 2003. http://dx.doi.org/10.1016/S0021-9673(02)02017-4.

[254] Cristian Gobbo, Isabelle Beurroies, David de Ridder, Rienk Eelkema, Siewert J. Marrink, Steven De Feyter, Jan H. van Esch, and Alex H. de Vries. MARTINI Model for Physisorption of Organic Molecules on Graphite. *The Journal of Physical Chemistry C*, 117(30):15623–15631, 2013. http://dx.doi.org/10.1021/jp402615p.

[255] Anja Kusian. *Adsorptionsisothermen von Phenylalkanen auf porösem graphitischen Kohlenstoff*. Studienarbeit (B.Sc. Thesis), Otto-von-Guericke-Universität Magdeburg, Fakultät für Verfahrens- und Systemtechnik, August 2013.

[256] Jana Jacobson, John Frenz, and Csaba Horváth. Measurement of adsorption isotherms by liquid chromatography. *Journal of Chromatography A*, 316:53–68, 1984. http://dx.doi.org/10.1016/S0021-9673(00)96140-5.

[257] Jana M. Jacobson, John H. Frenz, and Csaba G. Horváth. Measurement of Competitive Adsorption Isotherms by Frontal Chromatography. *Industrial & Engineering Chemistry Research*, 26(1):43–50, 1987. http://dx.doi.org/10.1021/ie00061a009.

[258] K. Lenz, Y. A. Beste, and W. Arlt. Comparison of static and dynamic measurements of adsorption isotherms. *Separation Science and Technology*, 37 (7):1611–1629, 2002. http://dx.doi.org/10.1081/SS-120002739.

[259] Satish C. Sharma and Tomlinson Fort Jr. Adsorption from Solution via Continuous Flow Frontal Analysis Solid-Liquid Chromatography. *Journal of Colloid and Interface Science*, 43(1):36–42, 1973. http://dx.doi.org/10.1016/0021-9797(73)90344-5.

[260] Anna Andrzejewska, Krzysztof Kaczmarski, and Georges Guiochon. Theoretical study of the accuracy of the pulse method, frontal analysis, and frontal analysis by characteristic points for the determination of single component adsorption

isotherms. *Journal of Chromatography A*, 1216:1067–1083, 2009. http://dx.doi.org/10.1016/j.chroma.2008.12.021.

[261] O. Lisec, P. Hugo, and A. Seidel-Morgenstern. Frontal analysis method to determine competitive adsorption isotherms. *Journal of Chromatography A*, 908: 19–34, 2001. http://dx.doi.org/10.1016/S0021-9673(00)00966-3.

[262] Attila Felinger. *Data analysis and signal processing in chromatography.* Data Handling in Science and Technology, 21. Elsevier, 1998. ISBN 978-0-444-82066-2.

[263] Christine Wegmann and Piet J. A. M. Kerkhof. Application of the Minka and Myers Theory of Liquid Adsorption to Systems with Two Liquid Phases. *Industrial & Engineering Chemistry Research*, 51(21):7340–7348, 2012. http://dx.doi.org/10.1021/ie300273x.

[264] Desmond J. Higham and Nicholas J. Higham. *MATLAB Guide.* Society for Industrial and Applied Mathematics, 2$^{\text{nd}}$ edition, 2005. ISBN 978-0-898715-78-1.

[265] Eric W. Weisstein. *CRC Concise Encyclopedia of MATHEMATICS.* CRC Press, 1999. ISBN 0-8493-9640-9.

[266] J. J. van Deemter, F. J. Zuiderweg, and A. Klinkenberg. Longitudinal diffusion and resistance to mass transfer as causes of nonideality in chromatography. *Chemical Engineering Science*, 50(24):3869–3882, 1995. http://dx.doi.org/10.1016/0009-2509(96)81813-6.

List of publications*

Articles in peer-reviewed journals

1. A Method for Efficiently Solving the IAST Equations with an Application to
   Adsorber Dynamics [53].
   `http://hdl.handle.net/11858/00-001M-0000-0013-87CE-3`

2. Use of Adsorbed Solution theory to model competitive and co-operative sorption on
   elastic ion exchange resins [54].
   `http://hdl.handle.net/11858/00-001M-0000-0013-8A1E-6`

Scientific posters

1. A. Seidel-Morgenstern, H. O. Rubiera Landa and D. Flockerzi. Application of a
   thermodynamically consistent explicit competitive adsorption isotherm model based
   on second-order single component behavior. 13 thInternational Symposium on
   Preparative & Industrial Chromatography & Allied Techniques, Stockholm,
   Sweden, 2010 (SPICA 2010).
   `http://hdl.handle.net/11858/00-001M-0000-0013-8F0B-4`.

2. H. O. Rubiera Landa, D. Flockerzi, and A. Seidel-Morgenstern. Efficient solution of
   the ideal adsorbed solution theory equations for single component adsorption
   isotherms with inflection points. 8 th European Congress of Chemical Engineering
   together with ProcessNet Annual Meeting / 1 st European Congress of Applied
   Biotechnology together with 29 th DECHEMA's Biotechnology Annual Meeting,
   Berlin, Germany, 2011 (ECCE-8).
   `http://hdl.handle.net/11858/00-001M-0000-0013-8B42-C`.

---

3. H. O. Rubiera Landa, D. Flockerzi, and A. Seidel-Morgenstern. Efficient ideal adsorbed solution theory calculation applied to simulated countercurrent chromatography. 14$^{\text{th}}$ International Symposium on Preparative & Industrial Chromatography & Allied Techniques, Brussels, Belgium, 2012 (SPICA 2012).
   http://hdl.handle.net/11858/00-001M-0000-0013-886C-8.

4. H. O. Rubiera Landa and A. Seidel-Morgenstern. Adsorption Equilibria of Phenyl-*n*-alkanes on Porous Graphitic Carbon. 26$^{\text{th}}$ International Symposium, Exhibit & Workshops on Preparative and Process Chromatography, Ion Exchange, Adsorption Processes & Related Separation Techniques, Boston, MA, USA, 2013 (PREP 2013).
   http://hdl.handle.net/11858/00-001M-0000-0015-0CEA-E.

5. H. O. Rubiera Landa, A. Rajendran and A. Seidel-Morgenstern. Application of Discrete Data Isotherms to Predict Multicomponent Adsorption Equilibria and Packed Column Dynamics [Actual poster title: Discrete Data Isotherms for Multicomponent Adsorption Equilibria & Packed Column Dynamics]. 15$^{\text{th}}$ International Symposium on Preparative & Industrial Chromatography & Allied Techniques, Basel, Switzerland, 2014 (SPICA 2014).
   http://hdl.handle.net/11858/00-001M-0000-0023-F961-C.

6. H. O. Rubiera Landa, A. Rajendran and A. Seidel-Morgenstern. Describing Competitive Equilibria and Fixed-Bed Dynamics Using Discrete Equilibrium Data. 28$^{\text{th}}$ International Symposium, Exhibit & Workshops on Preparative and Process Chromatography, Ion Exchange, Adsorption Processes & Related Separation Techniques, Philadelphia, PA, USA, 2015 (PREP 2015).
   http://hdl.handle.net/11858/00-001M-0000-0028-3878-3.

Talks at technical conferences and meetings

1. H. O. Rubiera Landa. Numerical formulation of elution chromatography techniques. *6. Doktorandenseminar "Präparative Chromatographie"*, Muggendorf, Germany, 2010.
   http://hdl.handle.net/11858/00-001M-0000-0013-8FE7-5.

2. H. O. Rubiera Landa, D. Flockerzi, and A. Seidel-Morgenstern. Efficient Solution of the Ideal Adsorbed Solution Theory (IAST) Equations for General Single Component Adsorption Isotherms, 2010 (2010 AIChE Annual Meeting).
   http://hdl.handle.net/11858/00-001M-0000-0013-8E91-F.

3. H. O. Rubiera Landa, D. Flockerzi, and A. Seidel-Morgenstern. Prediction of Competitive Adsorption Equilibria for General Single Component Adsorption Isotherm Shapes using the Ideal Adsorbed Solution Theory. 24th International Symposium, Exhibit & Workshops on Preparative and Process Chromatography, Ion Exchange, Adsorption Processes & Related Separation Techniques, Boston, MA, USA, 2011 (PREP 2011).
`http://hdl.handle.net/11858/00-001M-0000-0013-8BBF-3`.

4. H. O. Rubiera Landa. Efficient Solution of the Ideal Adsorbed Solution Theory (IAST) Equations for General Single Component Adsorption Isotherms. *7. Doktorandenseminar "Chromatographische Trennprozesse"*, 2011.
`http://hdl.handle.net/11858/00-001M-0000-0013-8C69-C`.

5. H. O. Rubiera Landa, D. Flockerzi, and A. Seidel-Morgenstern. A new approach to calculate multicomponent adsorption equilibrium using ideal adsorbed solution theory. *Jahrestreffen der ProcessNet-Fachgruppe Adsorption*, Magdeburg, Germany, 2012.
`http://hdl.handle.net/11858/00-001M-0000-0013-8937-3`.

6. H. O. Rubiera Landa, A. Rajendran, D. Flockerzi, and A. Seidel-Morgenstern. Ideal Adsorbed Solution Theory (IAST) calculations using directly discrete single component adsorption equilibrium data. *Jahrestreffen der ProcessNet-Fachgruppe Adsorption*, Bad Wildungen, Germany, 2013.
`http://hdl.handle.net/11858/00-001M-0000-0015-0CE2-D`.

7. H. O. Rubiera Landa and A. Seidel-Morgenstern. Evaluation of Ideal Adsorbed Solution Theory to Predict the Elution Behavior of Mixtures of Dissolved Phenyl-*n*-alkanes on Carbon. 11th International Symposium on the Fundamentals of Adsorption, Baltimore, MD, USA, 2013 (FOA 11).
`http://hdl.handle.net/11858/00-001M-0000-0015-0CF8-0`.

This page intentionally left blank.

About the author

Héctor Octavio RUBIERA LANDA, MSc.

■ Born in *México, Distrito Federal* (Mexico City) on January 4th, 1977.

Professional experience

■ **Research Associate & Doctoral Candidate (*Dr.-Ing.*)**: Max Planck Institute for Dynamics of Complex Technical Systems, Magdeburg, Germany. (2010 - present).

■ **Gas Turbine Controls Field Engineer**: General Electric International, Inc. (GE Power & Water), Latin America Region. (2001 - 2006).

■ **Field Engineering Program (FEP)**: General Electric Company, Niskayuna, NY, USA. (2001 - 2002).

Education

■ Otto-von-Guericke-Universität Magdeburg. Magdeburg, Germany. M.Sc., Chemical & Process Engineering, (2007-2009).

■ Instituto Tecnológico y de Estudios Superiores de Monterrey. Monterrey, N. L., México, B.Sc., Chemical & Systems Engineering, *Ingeniero Químico y de Sistemas, (Licenciatura)*, (1996-2001).

■ **Languages**: English (bilingual proficiency); German (professional working proficiency); & Spanish (mother language).